Characteristics and potential inhalation exposure risks of environmentally persistent free radicals and potentially toxic metal in atmospheric particulate matter and solid fuel combustion particles, China

（中国固形燃料燃焼由来または都市浮遊粒子状物質中の環境持続性フリーラジカルと毒性金属の特徴と健康リスクの評価）

2022 年 3 月

埼玉大学 大学院理工学研究科（博士後期課程）

理工学専攻　環境科学・社会基盤コース

主指導教員　王　青躍

XIAO KAI

SAITAMA UNIVERSITY

Doctoral Thesis

Characteristics and potential inhalation exposure risks of environmentally persistent free radicals and potentially toxic metal in atmospheric particulate matter and solid fuel combustion particles, China

中国固形燃料燃焼由来または都市浮遊粒子状物質中の環境持続性フリーラジカルと毒性金属の特徴と健康リスクの評価

Submitted by:

XIAO KAI

ID: 19DE063

Supervisor:

Professor Qingyue Wang

March, 2021

Abstract

Lung cancer has unique epidemiological characteristics due to the toxicity of indoor residential coal combustion (RCC) particles in Xuanwei, which suggests that there may be unique molecular mechanisms for the development of lung cancer in Xuanwei. However, mechanism of the high lung incidence is still not clear. After an extensive literature survey, we found that the risks posed by PM have been extensively researched, but the risk attribution of specific components of atmospheric particulate matters (APMs) is far from being fully understood. Observations of EPFRs in PM may provide the key to understanding the carcinogenic behaviour of these particles. To our knowledge, RCC and residential biomass combustion (RBC), and APMs are considered an important sources of EPFRs and HULIS, furthermore, there is few information available for personal exposure levels to inhaled EPFRs and HULIS in high lung cancer incidence areas of Xuanwei, China. Therefore there is a need to assess exposure to EPFRs and HULIS. In this study, we selected six kinds of coal and three kinds of biomass in Xuanwei, then conducted simulated combustion experiments, and six group of APMs using an Andersen high volume air sampler to explore the content and particle size distribution pattern of EPFRs and HULIS and health risk assessment of EPFRs and HULIS in particulate matter produced by different sources, providing new perspectives and evidence to reveal the high incidence of lung cancer in Xuanwei.

Comparing the different type particulate matter, we found that the mass concentration of particulate matter emitted from solid fuel combustion was mainly concentrated in particle size < 2.0 μm (58.17 ± 3.59 % for RBC particles, 67.02 ± 9.06 % for RCC particles), while the mass concentrations of atmospheric particulate matter were mainly concentrated in the particle size < 2.0 μm (49.74 ± 2.15 %) and >7.0 μm (20.28 ± 3.29 %). It indicates that the emission of fine particulate matter from raw coal combustion is more than that from biomass combustion, and the health risk is not negligible as the ambient atmosphere is dominated by fine particulate matter. We found that the mass of atmospheric particles showed a bimodal distribution, with the major peak in the range of particle size <1.1 μm and the minor peak in the range of size >7 μm. In contrast, the concentration of particulate matter emitted from solid fuel combustion is mainly concentrated in the range of particle size <1.1 μm. Xuanwei area, there are no large sources of pollution in the vicinity of the sampling site, and its pollution may be caused by solid fuel combustion, road transport, dust from construction sites, exhaust emissions from cars or mining in the county, and long-distance transport of pollution from surrounding cities. Beijing area, it is generally acknowledged that primary source like road dust and soil as the main emission source of coarse particulate matter, while fine atmospheric particulate matters are emitted from both primary source and secondary formation due to complex chemical processes in the atmosphere. Predominantly, high PM in the winter in Beijing was mainly attributed to the adverse meteorological conditions like low temperature

and lower boundary layer height, less precipitation and weaker wind and solid fuel (coal) combustion for indoor heating. another reason may be that probably due to the transport of polluted air masses from urban areas. The results show that the particulate matter pollution in Xuanwei is not serious and is at a medium level in the country, indicating that the mass concentration of particulate matter is not the main factor of lung cancer in Xuanwei, which may be due to the possibility that the local particulate matter in Xuanwei contains some special components or the content of certain pollutants exceeds the standard.

The result are follows:

APMs in Xuanwei: The average ratio of NO_3^-/SO_4^{2-} in all particulate were 0.22, 0.18, 0.15, 0.34 and 0.36, it indicating that stationary industrial and combustion sources contributed to PM were more significant. The ANE / CAE < 1 in all particulate indicate that the APMs was alkaline. SO_4^{2-} prefers to combine with NH_4^+ to form $(NH_4)_2SO_4$, which hinders the formation of NH_4NO_3, the remaining SO_4^{2-} and NO_3^- to neutralize the K^+, KNO_3 was formed at all particulate. However, K_2SO_4 can only be formed in the particle size less than 3.3 μm. As and Se were identified as the most enriched (EF >10) WSPTMs in all PM sizes, were predominantly from anthropogenic emissions, suggesting that coal combustion could be the important contributor of PM-bound WSPTMs in this study area. Total WSPTMs exhibited high TCR values (9.98×10^{-6}, 1.06×10^{-5}, and 1.19×10^{-5} for girls, boys and adults, respectively) in the smaller particles (<1.1 μm). Se make a major contribution (63.60%) CR in $PM_{2.0}$, furthermore decreased with the PM size increase and should be of more concern.

RCC particulate matter： (1) HULIS-C to the PM were 2.09 %~5.65 % for $PM_{2.0}$ and 2.68 %~5.62 % for $PM_{2.0\sim7.0}$, respectively. HULIS-C emitted from RCC is mainly concentrated in $PM_{2.0}$ (68.48 %~79.30 %). (2) During our measurements, the concentrations of HULIS-C and WSOC were significantly correlated with SO_4^{2-}, NO_3^-, and NH_4^+ in RCC particles. (3) HULIS-Cx to HULIS-Ct (%) values in RCC particles are 68.48 %–79.30 % (average 73.95 ± 5.13%) for $PM_{2.0}$ and 20.70 %~34.27 (average 26.05 ± 5.13%) for $PM_{2.0\text{-}7.0}$, respectively. The HULIS-Cx to WSOCx (%) values in RCC particles are 32.73 %–63.76 % (average 53.85 ± 12.12%) for $PM_{2.0}$ and 33.91%~82.67% (average 57.06 ± 17.32%) for $PM_{2.0\sim7.0}$, respectively. (4) Our result show that all PMs, the TCR was higher than 1 for adults and lower than 1 for children, except for $PM_{1.1}$. TCR values for As, Cd and Co decreased with increasing PM particle size (for adults and children), indicating that As, Cd and Co had the highest in $PM_{1.1}$. Interestingly, the TCR values for Cr (VI) were stable across PM particle sizes with no variability (for adults and children), and the TCR for lead was negligible. Notably, the TCR values for V showed a bimodal distribution, with the major peak in the particle size <1.1 μm while the minor peak in the size range of > 7 μm. The noncancer risk of Ba account for 91.28 %, 71.39 %, 78.74 %, 82.38 %, and 84.95 % within $PM_{1.1}$, $PM_{1.1\text{–}2.0}$, $PM_{2.0\text{–}3.3}$, $PM_{3.3\text{–}7.0}$, and $PM_{>7.0}$. It indicates that the non-carcinogenic risk of WSPTMs in RCC particles, mainly Ba, followed by As and the non-carcinogenic risk is highest within $PM_{1.1}$ in

Xuanwei. (5) The mean g factors were ranged from 2.0016 to 2.0043, 2.0039 to 2.0043 and 2.0039 to 2.0046 for biomass combustion, coal combustion and APMs, respectively, indicating that the samples were mainly oxygen-centered radicals (phenoxyl and semiquinone radicals) in Xuanwei. (6) The potential health risks of EPFRs for adult and child in $PM_{1.1}$ were equivalent to 130.31 ± 35.06, 49.52 ± 13.32 cigarettes in coal combustion particles, 53.11 ± 6.65, 20.18 ± 2.53 cigarettes in biomass combustion particles, and 80.02 ± 37.37, 30.41 ± 14.20 cigarettes in APMs, respectively. The results suggest that the health risk of EPFRs is significantly increased when the particle size distribution of EPFRs is taken into account, and RCC particulate matter is more hazardous to humans than APMs, followed by RBC particulate matter.

Our results can help stakeholders and policy makers recognize the characteristics of anthropogenic particles and their impact on air quality in the region, and initiate strategies to further control emissions to improve public health. We recommend continuing efforts in controlling coal burning throughout the year and also to include the surrounding areas.

In the future, a comprehensive investigation of coal combustion HULIS-C and EPFRs emissions under different stove types, combustion conditions and combustion stages are necessary to better understand HULIS-C. we should pay more attention to mechanism on the ROS generated by the HULIS and EPFRs through the cellular matrices and tissue. Some attempts should be done in cell-free and cell-based experiments to obtain well-characterized information about the ROS generated by the HULIS and EPFRs combination and to better address the health effects of HULIS and EPFRs.

CONCENT

Chapter 1 Introduction

1.1 Purpose and significance of the study

The ambient particulate matter pollution and household air pollution from solid fuels from 1990 to 2017 contributed to global premature deaths of about 2.94 and 1.64 million, respectively (Stanaway et al., 2018). In recent decades, with the rapid economic growth and urbanization of China, air pollutants have rapidly increase to become an environmental issue of public health concern in most metropolitan areas in China (X. Wu et al., 2020) (Lv et al., 2019). World Health Organization (WHO) estimated that air pollution was associated with approximately 300,000 premature deaths per year in China (J. Duan et al., 2014). Solid fuels such as wood, crop residues and coal are still the main sources of energy for cooking and heating in some rural areas of China (G. Shen et al., 2013)(F. Wu et al., 2015). China is the biggest coal consumer country in the world, with 4 billion tons of coal consumed each year, which accounted for about 60% of Chinese total primary energy or half of global coal consumption (National Bureau of Statistics of China (National Bureau of Statistics, 2016)).(X. Zhu et al., 2019)(Ming Zhang & Su, 2016)(Delmastro et al., 2015). In 2019, about 2.7 billion tons of coal were consumed in China, which contributed about 68.6% of the national primary energy source (http://www.stats.gov.cn/tjsj/ndsj/; accessed on 18 October 2021). Solid fuels are important anthropogenic sources of particulate and toxic and hazardous pollutants in the atmosphere (Wenhua Wang et al., 2019).

According to the records in the scientific literature, the significant risks posed to human health by the inhalation of particulate matter (PM) are strongly associated with their size and physic-chemical characteristics (Rohra et al., 2018)(Fomba et al., 2018)(Zanobetti et al., 2014). The inefficient combustion of these solid fuels leads to high emissions of various air pollutants, such as CO, SO_2, particulate matter (PM), black carbon (BC), polycyclic aromatic hydrocarbons (PAHs), Environmental Persistent Free Radicals (EPFRs) (Barry Dellinger et al., 2007)(Ruan et al., 2019)(Y. Huang et al., 2020), and potentially toxic metals (PTMs) (Jin Zhang et al., 2017), which have serious air quality impacts (Clark et al., 2013). The particles generated from solid fuels produce reactive oxygen species (ROS), especially once it enters the human body. Oxidative stress in the airways and alveoli leads to stimulation of alveolar macrophages and injury to the epithelial lining, which in turn attracts inflammatory cells from the circulation (Mehra et al., 2012). This mechanism is considered to be related to highly redox-active components in the particulate matter. There were evidence that exposure to $PM_{2.5}$ (particulate matter with aerodynamic size less than 2.5 μm) and other pollutants in indoor air causes cardiovascular and respiratory diseases, lung cancer, premature births, neural tube defects, and many other problems

(Lelieveld et al., 2015)(B. Wang et al., 2015)(Pope & Dockery, 2006).Although rural residents in China are gradually transitioning to cleaner fuels such as natural gas, most residents cook with bituminous coal (bituminous coal), anthracite coal, or wood in poorly ventilated rooms in rural Xuanwei City, Yunnan Province, in southwestern China. Therefore, it can lead to health risks (W. Meng et al., 2019) and it is still one of the most important concerned by atmospheric scientists (An et al., 2019).

Lung cancer remains the most prevalent cancer (11.6% of all cases) and the leading cause of cancer deaths worldwide (18.4% of all cancer deaths)(Bray et al., 2018). Smoking is the largest preventable cause of lung cancer and contributes to more than 80% of cases of this disease on a global scale (Kulhánová et al., 2020). Xuanwei has the highest incidence and mortality rate of lung cancer in China (Figure 1)(Seow et al., 2014)(Vermeulen et al., 2019) (Wenhua Wang et al., 2019). Specially, the women have the highest incidence of lung cancer among non-smokers in Xuanwei, China (W. Chen et al., 2015). According to the "2012 Chinese Cancer Registry Annual Report," the average incidence rate of lung cancer in Xuanwei was 92 per 100,000, which is four–five times higher than the national rate (Mengyuan Zhang et al., 2021). The incidence of lung cancer among non-smokers is 400/100,000 (Mumford et al., 1987)(G. Li et al., 2021), which is 20 times higher than the national average, especially among women in rural areas (R. Li, Liu, et al., 2019) (Y. Xiao et al., 2012) (Kim et al., 2014). The mortality of lung cancer in Xuanwei rural areas are 27.7/100,000 for men and 25.3/100,000 for women, almost five times that of China's national average (4.97/100,000 for both sexes) (Jinhui Li, Guo, et al., 2019), it ranks among the top in the world for female lung cancer mortality (Hosgood et al., 2014). However, the etiology of lung cancer in the region remains unclear and known or suspected risk factors (such as tobacco (Sheng et al., 2018), potentially toxic metals (S. Lu et al., 2014)(X. Feng et al., 2020)(K. Xiao, Qin, et al., 2021), polycyclic aromatic hydrocarbons (PAHs) (R. Wang et al., 2021), and SiO_2 (L. Tian et al., 2008) (S. Lu et al., 2016)) may account for only a small fraction of lung cancer cases, necessitating further study.

Our research was divided into two parts:

Part one: Xuanwei in southern China

Xuanwei, Yunnan Province, is rich in coal resources and is an important coal energy base in Yunnan Province. After field investigation and data search, we found that wild pine and poplar trees are widely distributed, and 1.78 million hectares of corn was planted in Yunnan, accounting for 25.61% of the crop area in 2019 (http://stats.yn.gov.cn/; accessed on 22 September 2021). Most residents live in poorly ventilated houses and use coal and biomass as daily fuels. This indicates that in Xuanwei, residential coal combustion (RCC) and residential biomass combustion (RBC) may be the main source of indoor air pollution. Due to the abnormally high levels of lung cancer and mortality in Xuanwei City, Yunnan

Province, it has attracted much attention. A large number of studies have shown that smoking is not enough to explain the high incidence of lung cancer in Xuanwei. On the contrary, solid fuel combustion is closely related to this lung cancer.

After an extensive literature survey, we found that the risks posed by PM have been extensively researched (K. Xiao, Wang, et al., 2021) (S. Lu et al., 2017), but the risk attribution of specific components of atmospheric particulate matters (APMs) is far from being fully understood. Observations of EPFRs in PM may provide the key to understanding the carcinogenic behaviour of these particles (Lubick, 2008)(Gehling & Dellinger, 2013)(Gehling et al., 2014). To our knowledge, RCC particles, RBC particles, and APMs are considered an important sources of EPFRs (Yuqin Wang et al., 2019)(J. Zhao et al., 2021), furthermore, there is few information available for personal exposure levels to inhaled EPFRs in high lung cancer incidence areas of Xuanwei, China. Therefore there is a need to assess exposure to EPFRs (Y. Xu et al., 2021). In this study, we selected six kinds of coal and three kinds of biomass in Xuanwei, then conducted simulated combustion experiments, and six group of APMs using an Andersen high volume air sampler to explore the content and particle size distribution pattern of EPFRs and health risk assessment of EPFRs in particulate matter produced by different sources, providing new perspectives and evidence to reveal the high incidence of lung cancer in Xuanwei.

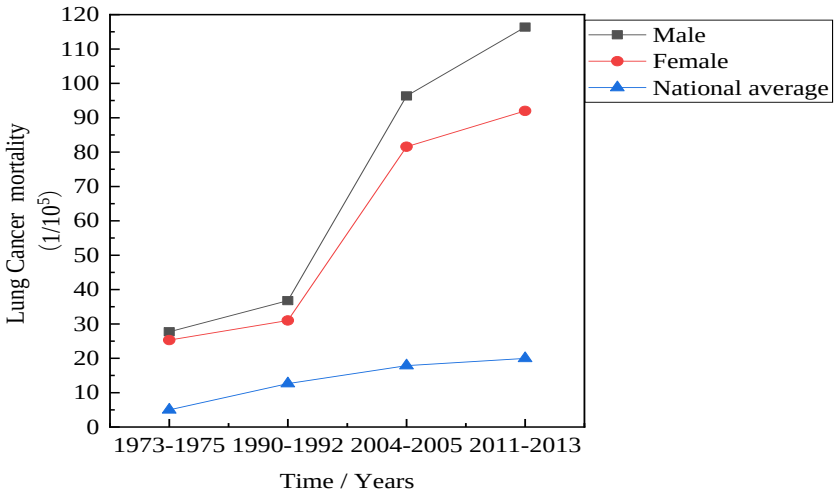

Fig. 1. The lung cancer mortality rates in 1973~2013(Mumford et al., 1987)(G. Chen et al., 2015)

Part two: Beijing in northern, China

Beijing is the capital city of China with a population of approximately 21.54 million and annual coal consumption of 17.62 million tons in 2018 (National Bureau of Statistics (NBS), 2019) (Beijing Bureau of Statistics (NBS)2018). Beijing as one of the core cities in Beijing-Tianjin-Hebei (BTH) (high

elements emission areas) (C. Zhu et al., 2018), it has been troubled by air pollution. Due to heating and meteorological conditions, air pollution in the wintertime is typically more serious than in other seasons in Beijing (Yele Sun et al., 2013). In the past few decades, many studies have investigated the characteristics and sources of atmospheric PM in Beijing. In $PM_{2.5}$ and PM_{10} samples from Beijing, different elements showed different size distributions during summer and winter (Lv et al., 2019). 13 elements in $PM_{2.5}$ in urban Beijing were measured were to investigate the concentration of elements, illustrate their temporal variations, and estimate the health risks (Cui et al., 2020). The concentrations of metals and ions, their characteristics and comparison in hazy and non-hazy days of PM_{10} were discussed (X. Wu et al., 2020). There are few studies on sources analysis and health risks of metal elements in size-segregated PM in Beijing, many studies have assessed human health risk caused by individual sizes (often for either PM_{10} or $PM_{2.5}$) (J. Duan et al., 2014) (Jianwei Liu et al., 2019) (Lv et al., 2019) (X. Wu et al., 2020). The compounds of PM are complex and have obvious seasonal and regional differences (Che et al., 2021). In addition, due to changes in physical and chemical composition, the toxic effects of particulate matter vary greatly with geographic location. Therefore, it is very important to quantify the chemical composition of aerosols to determine the potential deleterious effects on human health, especially in higher population residential area.

Given the background discussion above, in this study, we collected atmospheric samples with a high-volume air sampler (Anderson Sampler, HV-RW, Shibata Science Co., Ltd., Japan) in a high population residential area of Beijing during the winter (December 26, 2018 to January 11, 2019). Nine water soluble inorganic ions (Cl^-, NO_3^-, NO_2^- , SO_4^{2-}, NH_4^+, Na^+, K^+, Ca^{2+} and Mg^{2+}) were analyzed by Ion Chromatography (IC, ICS1600, Dionex Aquion, Thermo Fisher Scientific CO, Waltham, MA, USA), the mass concentration of 21 metal elements was measured by inductively coupled plasma mass spectrometry (ICP-MS, Agilent 7700, Agilent Technologies, Inc., Santa Clara, CA, USA). The main objectives of this study were :1) to investigate the occurrence levels of metals elements, water soluble inorganic ions and their size distributions, 2) to identify the potential sources contributing to the enrichment of metals, 3) estimate the health risk to child and adults of several toxic trace elements (As, Cd, Cr (VI), V, Ni, Co and Pb).

1.2 Current Status of Lung Cancer Research in Xuanwei Region

Since the 1960s, lung cancer in Xuanwei Township has increasingly attracted many researchers and many epidemiologic and etiologic studies have been conducted. Previous etiologic and epidemiologic

studies have confirmed that lung cancer in Xuanwei County has its own unique characteristics (Jinhui Li, Guo, et al., 2019)("Lung Cancer in Radon-Exposed Miners and Estimation of Risk from Indoor Exposure," 1995)(R. Li, Liu, et al., 2019). First, the high incidence of lung cancer in the Xuanwei region is regional in nature, manifesting itself in higher incidence rates in rural areas than in cities. The incidence of human lung cancer in the region differs from other economically developed and highly developed areas. The high incidence of lung cancer in the Xuanwei region is mainly in rural areas, and the mortality rate is the highest in the country. Second, the incidence of tumors in the Xuanwei population is much higher in women than in men. Rural women have the highest lung cancer incidence rate in the country, 20 times higher than in the rest of China, and their female lung cancer mortality rate is among the highest in the world. Most notably, lung cancer mortality rates for men and women are four and eight times higher than the national average, respectively (H. Lin et al., 2015). In general, men have a higher lung cancer mortality rate than women because smoking is more prevalent in men than in women. However, in the Xuanwei region, local female residents tend to be non-smokers, yet they have a much higher lung cancer mortality rate than men (Yang Chen et al., 2015). Third, lung cancer patients in Xuanwei County tend to develop and die at a younger age than in other cities and have a shorter time to onset. The incubation period for normal lung cancer is about 15 years, while locally, the incubation period is only about 10 years. The number of deaths increases sharply by age 30. The age of the sick and dying population is high, and the type of lung cancer is mainly adenocarcinoma, with a high degree of malignancy and an extremely poor prognosis (Ka Hei Lui et al., 2017). Fourth, the prevalence of lung cancer has significant familial aggregation, and genetic variants may play an important role in the development of human lung cancer (R. Li, Liu, et al., 2019). Lung cancer in Xuanwei has unique epidemiological characteristics due to severe air pollution and toxicity of indoor coal combustion particles, suggesting that there may be unique molecular mechanisms for the development of lung cancer in Xuanwei.

While smoking is the most common cause of lung cancer (S. Sun et al., 2007), however, the etiology of lung cancer among never-smokers remains unclear and known or suspected risk factors likely account for only a modest proportion of lung cancer cases (Silverman et al., 2012) (Samet et al., 2009)(Barone-Adesi et al., 2012).There was an etiologic link between domestic smoky coal burning and lung cancer in Xuan Wei (Mumford et al., 1987)(Kim et al., 2014)(Jinhui Li, Ran, et al., 2019). A retrospective cohort study (Barone-Adesi et al., 2012) showed that domestic use of bituminous coal would increase lung cancer mortality by up to 100-fold (hazard ratio for women: 98.8, 95% CI 36.8-276.6) compared to anthracite coal (stony anthracite coal available in some parts of the region) (Barone-Adesi et al., 2012). Recent studies suggest that Hulis in particulate matter emissions from coal combustion may also contribute to the high incidence of lung cancer in Xuanwei (K. Xiao, Wang, et al., 2021). Some studies

suspect that exposure to respirable silica from coal combustion emissions is a possible cause of the high lung cancer mortality rate in Xuanwei (S. Dai et al., 2008) (Large et al., 2009) (Jinhui Li, Ran, et al., 2019). Previous studies have shown that long-term exposure to PAHs is strongly associated with the development and progression of various cancers (Hofmann et al., 2013), especially lung cancer (Downward et al., 2014) (Vermeulen et al., 2019). Yan Chen et al. demonstrated that overexpression of miR-34a could inhibit both tumor growth and metastasis and play an important role in tumorigenesis and progression of NSCLC by increasing the expression of PTEN and YY1 (Yan Chen et al., 2021).

Although many lungs cancer-related influencing factors have been identified, the mechanisms underlying the high incidence of lung cancer in Xuanwei County are quite complex and still not fully elucidated. There is few information available for personal exposure levels to inhaled EPFRs in high lung cancer incidence areas of Xuanwei, China. Therefore there is a need to assess exposure to EPFRs (Y. Xu et al., 2021).

1.3 The overview of air pollution

Air pollution is the contamination of the indoor or outdoor environment by any chemical, physical or biological agent that alters the natural characteristics of the atmosphere. Household combustion devices, motor vehicles, industrial facilities, and forest fires are common sources of air pollution. The major pollutants of public health concern include particulate matter, carbon monoxide, ozone, nitrogen dioxide, and sulfur dioxide. Outdoor and indoor air pollution contributes to respiratory and other diseases and is a significant source of morbidity and mortality. From the smog that hangs over cities to the smog inside homes, air pollution poses a major threat to health and climate. The combined effects of environmental (outdoor) and household air pollution cause millions of premature deaths each year, primarily due to increased mortality from stroke, heart disease, chronic obstructive pulmonary disease, lung cancer, and acute respiratory infections (https://www.who.int/; accessed on 18 October 2021).

Some key facts about environmental pollution are listed below:

(1) Around 2.6 billion people cook using polluting open fires or simple stoves fueled by kerosene, biomass (wood, animal dung and crop waste) and coal.

(2) Each year, close to 4 million people die prematurely from illness attributable to household air pollution from inefficient cooking practices using polluting stoves paired with solid fuels and kerosene.

(3) Household air pollution causes noncommunicable diseases including stroke, ischaemic heart disease, chronic obstructive pulmonary disease (COPD) and lung cancer.

(4) Close to half of deaths due to pneumonia among children under 5 years of age are caused by particulate matter (soot) inhaled from household air pollution.

1.3.1 Particulate Matter

There are many different types of particles that can be found in the atmosphere. Particulate matter can be divided into two categories according to the process of their formation. One category is primary respirable particulate matter, which are emitted directly into the atmosphere, and the other category is secondary particulate matter, who are primary particulate matter formed through a series of atmospheric physicochemical processes. On the other hand, according to aerodynamic diameter, PM can be classified as total suspended particulate matter (TSP with an aerodynamic diameter less than 100 μm) coarse particles (PM_{10} with an aerodynamic diameter less than 10 μm), fine particles ($PM_{2.5}$ with an aerodynamic diameter less than 2.5 μm), and especially sub-micrometer (PM_1 with an aerodynamic diameter less than 1 μm) and ultrafine particles (UFPs, $PM_{0.1}$ with an aerodynamic diameter less than 0.1 μm)(K. Xiao, Qin, et al., 2021). As shown in Figure 2.

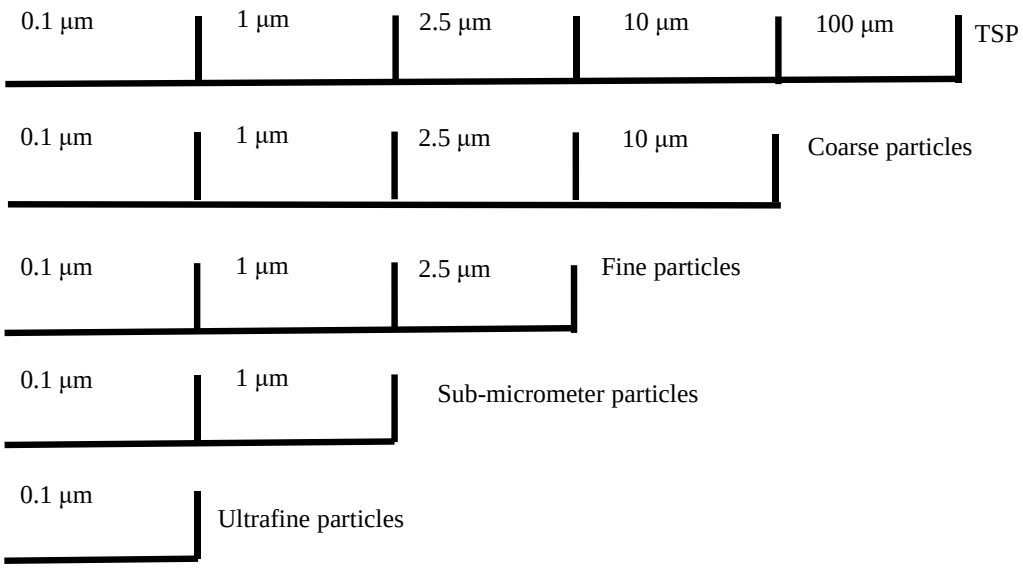

Fig. 2. Size distribution of Particulate Matter

1.3.2 Sources of Particulate Matter

PM can be derived from both primary sources, in which they are directly produced by a series of human activities (e.g., fossil fuel combustion (K. Xiao, Wang, et al., 2021), industrial metallurgical

processes (Dunea et al., 2016), vehicle emissions (Edgerton et al., 1999)(Agarwal et al., 2015) and waste incineration (F. Yan et al., 2016)) into the atmosphere, and secondary aerosol formation(Manalis et al., 2005) (Onder & Dursun, 2006) (Yele Sun et al., 2006), released from natural sources (e.g., sea sprays (Steinfeld, 1998), soil dust (Vega et al., 2011), volcanism, erosion, surface winds and forest fires (Johnston et al., 2021)).

1.3.3 Composition of Particulate Matter

Particulate matter (PM) mixtures have different physical and chemical characteristics, which are associated with an array of adverse effects on human health (Radulescu et al., 2015) (Querol et al., 2007)(Mölter et al., 2015)(Amodio et al., 2013). Understanding the spatial and temporal and qualitative characteristics of $PM_{2.5}$ data is therefore essential to support epidemiological studies to consolidate knowledge about the effects of particle size and chemical composition on human health. (Baltrenaite et al., 2014)(Neuberger et al., 2004)(Olsen et al., 2014). The complex mix of PM can produce different changes in the tissues, depending on its composition, which includes a water-soluble or a water-insoluble fraction (Dongbin Wang et al., 2013). The smaller the particle size of the particles, the larger the specific surface area, the more harmful substances, viruses and fine bacteria adsorbed, etc (Smith et al., 2001) (Oberdörster, 2000) (Georgakakou et al., 2016) (Cao et al., 2014) (Y. R. Li et al., 2016)(K. Xiao, Wang, et al., 2021)(K. Xiao, Qin, et al., 2021).

1.3.3.1 Water-Soluble Inorganic Ionic Species (WSIIs)

Water-Soluble Inorganic Ionic Species are the major components of PM, occupied by 33% or more of fine particles (S. Kong et al., 2014)(P. S. Zhao et al., 2013), and can compose up to 50–60% of the mass of $PM_{2.5}$ during haze period (Xingru Li et al., 2013). WSIIs can directly change the radiation balance by scattering or absorbing both incoming solar radiation and thermal radiation emitted from the Earth's surface (Bellouin et al., 2005). WSIIs also play important roles in atmospheric chemistry. SO_4^{2-}, NO_3^- and NH_4^+, which were always regarded as secondary species in $PM_{2.5}$ (Dexiang Wang et al., 2014)(Q. Yan et al., 2020). During regional haze events, SO_4^{2-}, NO_3^-, and NH_4^+ in respirable particulate matter significantly contribute to the acidity and visibility reduction of aerosols (Xinghua Li et al., 2013) (Guenther et al., 2012)(Pathak et al., 2009). In addition, WSIIs may pose a threat to human health (Spengler et al., 1990). Previous researchers found a large increase in WSIIs during the winter heating

period in northern China (Sudheer et al., 2014). and the secondary formation of SO_4^{2-}, NO_3^-, and NH_4^+ (SNA) have been considered as the main contributors (R. Zhang et al., 2013)(S. Kong et al., 2014).

Thus, the observation of the chemical composition of size-separated water-soluble ions is valuable for understanding their physical/chemical characteristics, their origin, and their behavior and formation mechanisms.

1.3.3.2 Potentially toxic metals (PTMs)

Potentially toxic metals (PTMs), which are cytotoxic, concealed, persistent, and biologically accumulated, play a decisive role in the assessment of atmospheric pollution and the hazards to human health (Jin Zhang et al., 2017). After breathing into the human body, they may cause various human dysfunctions or cause a variety of diseases: As, Cr, Ni, Pb, and Cd have certain carcinogenic ability, while As and Cd have potential teratogenic effects on the human body, and Pb and Hg are toxic to the fetus (X. Hu et al., 2012)(Z. Hu et al., 2012). Cr, Ni, Cu, Fe, Co, Mn, As, V, and Zn could support electron exchange (Sen et al., 2016) and induce the formation of reactive oxygen species (ROS) in the lungs (Verma et al., 2014), causing damage of oxidative DNA and inflammation of respiratory tracts (Distefano et al., 2009). Lead (Pb) is a well-known toxic element that may be harmful to the nervous and hematopoietic system, leading to impaired growth and mental function (Shunqin Wang & Zhang, 2006). Relevant literature shows that about 70–80% of the metal elements in the atmosphere are adsorbed on fine particles (Mohanraj et al., 2004). Consequently, the presence of different PM-bound toxic compounds may pose severe health concerns and information about their size-distribution is of primary relevance to determine and quantify the potential deleterious effects on human health.

1.3.3.3 Humic-like substances (HULIS)

RCC are important anthropogenic sources of particulate and toxic and hazardous pollutants in the atmosphere (Wenhua Wang et al., 2019). The particles generated from RCC produce reactive oxygen species (ROS), once it enters the human body. Oxidative stress in the airways and alveoli leads to stimulation of alveolar macrophages and injury to the epithelial lining, which in turn attracts inflammatory cells from the circulation.(Mehra et al., 2012). Xuanwei has the highest incidence and mortality rate of lung cancer in China, (Wenhua Wang et al., 2019) which is characterized by high mortality, especially among women in rural areas. (R. Li, Liu, et al., 2019), (Y. Xiao et al., 2012), (Kim et al., 2014). Residential coal combustion have been accepted as the main cause of human lung cancer

(R. Li, Liu, et al., 2019) (K. H. Lui et al., 2017) (Finkelman & Tian, 2018) (X. Feng et al., 2020).

Humic substances (HULIS) are large molecules of unresolved water-soluble organic carbon (WSOC) with a polycyclic ring or carboxyl, carbonyl, and hydroxyl group structure (H. Sun et al., 2021), consisting of 9–72% of WSOC (Tan et al., 2016). They have been widely reported in atmospheric aerosols in urban (Song et al., 2012), rural, forested (Zheng et al., 2013), and marine environments, (X. Fan, Song, et al., 2016), rain water (Santos et al., 2012), cloud water (Kristensen et al., 2014), and fog (Birdwell & Valsaraj, 2010). HULIS was found to enhance catalytically the generation of ROS under simulated physiological conditions, thereby likely may contribute to PM caused health problems (S. Lu et al., 2019) (X. Xu et al., 2020)(Win et al., 2018). Many studies have shown that biomass combustion and secondary formation in the atmosphere are considered to be important sources of HULIS (Zheng et al., 2013), (Kuang et al., 2015), (Ma et al., 2018), (Srivastava et al., 2018). However, it has recently been suggested that RCC is a significant and major source of HULIS (H. Sun et al., 2021).

1.3.3.4 Environmental Persistent Free Radicals (EPFRs)

Environmental Persistent Free Radicals (EPFRs) are a novel class of emerging contaminants, which are similar to carcinogenic tar paramagnetic species in cigarettes that can damage normal cells in the body, induce DNA mutations, accelerate the rate of ageing and increase the risk of disease(Y. Xu et al., 2021). EPFRs are widespread in the environment due to the easy formation in the post-flame and cool-zone regions of combustion systems and other thermal conversion processes (Cruz et al., 2012). In addition to PM, EPFRs are also found in contaminated soil (Cruz et al., 2012), waste incineration, automobile exhaust, Biomass combustion, coal combustion, thermal treatments of plastic and hazardous waste (Valavanidis et al., 2008), tar balls and pyrolysis of biodiesel at high temperatures (Mosonik et al., 2018). Several studies have shown that the concentration of EPFRs in atmosphere were spatially and temporally inhomogeneous, which is mainly caused by different contributions of emission sources, such as residential fuel, vehicles, and industrial activities (Q. Chen, Sun, Wang, et al., 2019) (C. Wang et al., 2020). They are more environmentally persistent than short-lived radicals and can persist in the medium for long periods of time without even disappearing(Qian et al., 2020).

The g-factor and peak width (referred to as ΔHp-p, Gauss) were important parameter for identifying the type of free radicals (Shaltout et al., 2015) (Arangio et al., 2016), the average ΔHp-p is calculated was finding the distance between the maximum and minimum y-axis values on the x-axis (Runberg et al., 2020). According to previous reports, carbon-centered radicals is generally less than 2.003, oxygen-centered radicals is generally greater than 2.0040, and *g* factors in the range of 2.0030–2.0040 are

believed to correspond to a mixture of carbon- and oxygen-centered radicals (Barry Dellinger et al., 2007)(Ruan et al., 2019)(Y. Huang et al., 2020). The most possible mechanisms of EPFRs are formed at transition metal centers that can be easily reduced when an organic compound chemisorbs (Ruan et al., 2019), can be seen in Figure 3. Subsequently, an elimination of water or hydrogen chloride results in chemisorption of the organic molecular adsorbate, and then a single electron transfer from the organic molecule to the transition metal (such as Al_2O_3, Fe_2O_3, Fe_3O_4, CuO, ZnO, MnO, and NiO) center, which leads to the simultaneous reduction of metal and the formation of EPFRs (Barry Dellinger et al., 2007).

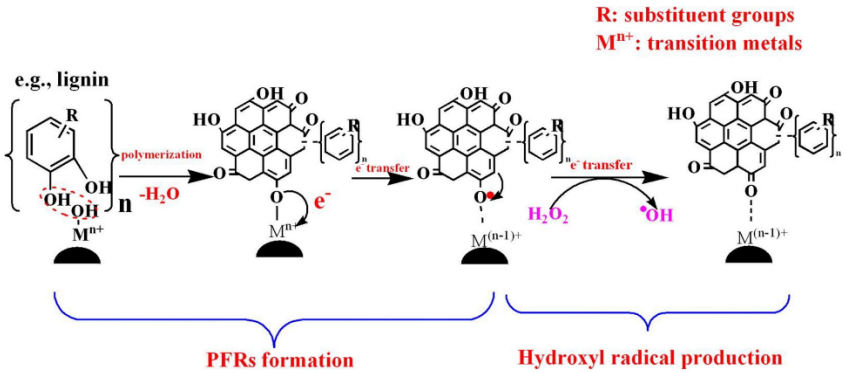

Fig. 3. Proposed mechanisms of EPFR formation (Ruan et al., 2019)

Scientists have recently begun to assume that environmentally persistent free radicals within PM, which are a class of strongly oxidizing substances, are possible factors that may be responsible for human acute or chronic pneumonia and lung cancer (Pöschl & Shiraiwa, 2015) (Balakrishna et al., 2011). The toxicity of EPFRs stems from their persistence in the environment coupled with their ability to generate •OH, which may lead to the downstream generation of other reactive oxygen species (ROS) (Kelley et al., 2013) including peroxyl (RO_2•) and alkoxyl (RO•) radicals. APM–bound EPFRs may directly result in oxidative stress in the lung when exposed to APMs (Guo et al., 2020). One possible mechanism for this type of health damage is the continuous conversion of O_2 molecules into reactive oxygen species (ROS) by EPFRs (Gehling et al., 2014).

1.3.3.5 Humic-like substances (HULIS)

RCC are important anthropogenic sources of particulate and toxic and hazardous pollutants in the atmosphere (Wenhua Wang et al., 2019). The particles generated from RCC produce reactive oxygen species (ROS), once it enters the human body. Oxidative stress in the airways and alveoli leads to stimulation of alveolar macrophages and injury to the epithelial lining, which in turn attracts inflammatory cells from the circulation.(Mehra et al., 2012). Xuanwei has the highest incidence and

mortality rate of lung cancer in China, (Wenhua Wang et al., 2019) which is characterized by high mortality, especially among women in rural areas. (R. Li, Liu, et al., 2019), (Y. Xiao et al., 2012), (Kim et al., 2014). Residential coal combustion have been accepted as the main cause of human lung cancer (R. Li, Liu, et al., 2019) (K. H. Lui et al., 2017) (Finkelman & Tian, 2018) (X. Feng et al., 2020).

Humic substances (HULIS) are large molecules of unresolved water-soluble organic carbon (WSOC) with a polycyclic ring or carboxyl, carbonyl, and hydroxyl group structure (H. Sun et al., 2021), consisting of 9–72% of WSOC (Tan et al., 2016). They have been widely reported in atmospheric aerosols in urban (Song et al., 2012), rural, forested (Zheng et al., 2013), and marine environments, (X. Fan, Song, et al., 2016), rain water (Santos et al., 2012), cloud water (Kristensen et al., 2014), and fog (Birdwell & Valsaraj, 2010). HULIS was found to enhance catalytically the generation of ROS under simulated physiological conditions, thereby likely may contribute to PM caused health problems (S. Lu et al., 2019) (X. Xu et al., 2020)(Win et al., 2018). Many studies have shown that biomass combustion and secondary formation in the atmosphere are considered to be important sources of HULIS (Zheng et al., 2013), (Kuang et al., 2015), (Ma et al., 2018), (Srivastava et al., 2018). However, it has recently been suggested that RCC is a significant and major source of HULIS (H. Sun et al., 2021).

1.3.4 Health Effects of Oxidative Stress Generated by Particulate Matter

PM has been identified as group I carcinogen by the International Agency for Research on Cancer (Gou et al., 2016). Epidemiological and experimental studies have shown that coarse particles, in general, remain in the upper respiratory system and stay there for a long time whereas fine particles penetrate deep respiratory system and deposit in the alveolar region, entering the blood circulation system more easily, and translocating to extrapulmonary organs including the liver, spleen, heart, and even brain threatening human health (Y. C. Lin et al., 2020). In the last decade, many residential areas throughout the world have been affected by fine particulate matter with an aerodynamic diameter below 2.5 μm, which disturbs air quality and favors the propagation of higher respiratory morbidity levels and numerous clinical symptoms, especially in infants and small children (Henschel et al., 2012) (Pope & Dockery, 2006)(Ward & Ayres, 2004). Exposure to haze consisting of high concentrations of PM leads to increased morbidity and mortality from cardiovascular disease, respiratory disease, and lung cancer (Cao et al., 2014)(C. Xu et al., 2017). Among the most significant effects on humans are fine and ultrafine particulate matter, as it adsorbs toxic and carcinogenic substances and can be deposited in the lungs and cross the alveoli into the blood system. Exposure to fine or ultrafine particles induces reactive oxygen species

(ROS) -mediated oxidative stress, altering cellular permeability in epithelial cells due to their organic or inorganic content (Bodlet et al., 2013). A primary form of ROS is the hydroxyl radical formed by hydrogen peroxide after exposure to PM (T. Shi et al., 2003). Also, $PM_{2.5}$ can produce superoxide leading to the formation of hydrogen peroxide (B. Dellinger et al., 2001). H_2O_2 is a main free radical in the lung; it can produce cell damage by oxidant stress. Alveolar macrophages and epithelial cells generate oxidants (Bonner, 2007). The water-soluble fraction can produce cell signaling, expression of inflammatory mediators, oxidative stress (Ghio et al., 1999) that generates DNA damage via a transition metal-dependent OH formation, implicating an important role of H_2O_2 (Knaapen et al., 2002). Oxidative stress in the airways and alveoli leads to stimulation of alveolar macrophages and injury to the epithelial lining, which in turn attracts inflammatory cells from the circulation (Mehra et al., 2012).

1.4 Main Research Content and Technical Route

The research in this thesis focuses on the following aspects, the technical route is shown in Figure 4.

(1) The selection of sampling sites and the collection of samples.

Xuanei, northern of China: Three kinds of raw biomass (Pine, Corncob, Poplar) from Zhongan Town, and six kinds of residential raw coal from Bole Town (Luomu coal [LM] and Bole coal [BL]), Houshou Town (Lijiawu coal [LJW]), Laochang Town (Shunfa coal [SF]), Laibin Town (Guangming coal [GM] and Zongfan coal [ZF]), and six group of APMs (Houshou Town) were collected. In addition to the above, six sample groups of APMs (A-H) were conducted by a high-volume air sampler (Shibata Science Co., Ltd., Saitama., Japan) at a flow rate of 566 L/min in Xuanwei local rural residents on February and March in 2017.

Beijing, southern of China: The aerosol sampling was conducted by a high-volume air sampler at a flow rate of 566 L/min in Beijing from 26 December 2018 to 11 January 2019.

(2) Collection of simulated combustion particulate matter

Collection and mass concentration detection of coal combustion emissions of particulate matter. The combustion conditions of coal and biomass used by local residents were simulated in the laboratory, and the particulate matter emitted from coal combustion and biomass was collected by particle size and the mass concentration of different particle sizes was calculated.

(3) Main work

Xuanei, northern of China: Electron spin resonance (ESR) spectroscopy was used to determine

EPFRs. The concentrations of four anions (Chlorine ion, Cl^-; Nitrate ion, NO_3^-; Nitrite ion, NO_2^-; Sulfate ion, SO_4^{2-}) and five cations (Ammonium ion, NH_4^+; Sodium ion, Na^+; Potassium ion, K^+; Calcium ion, Ca^{2+}; and Magnesium ion, Mg^{2+}) were analyzed by ion chromatography (IC). Meanwhile, WSPTMs was analyzed by inductively coupled plasma mass spectrometer (ICP-MS). HULIS and WSOC were analyzed by a total organic carbon analyzer.

Beijing, southern of China:

The concentrations of four anions (Chlorine ion, Cl^-; Nitrate ion, NO_3^-; Nitrite ion, NO_2^-; Sulfate ion, SO_4^{2-}) and five cations (Ammonium ion, NH_4^+; Sodium ion, Na^+; Potassium ion, K^+; Calcium ion, Ca^{2+}; and Magnesium ion, Mg^{2+}) were analyzed by ion chromatography (IC). Meanwhile, WSPTMs was analyzed by inductively coupled plasma mass spectrometer (ICP-MS).

(4) To study and compare the occurrence levels of metal elements, water-soluble inorganic ions and their size distribution in atmospheric particulate matter in Beijing, China.

(5) To estimate and compare the health risk to child and adults of several toxic trace elements (As, Cd, Cr (VI), V, Ni, Co and Pb) in northern and southern, China.

(6) To explore the content and particle size distribution pattern of EPFRs, HULIS and health risk assessment of EPFRs in particulate matter produced by different sources, providing new perspectives and evidence to reveal the high incidence of lung cancer in Xuanwei.

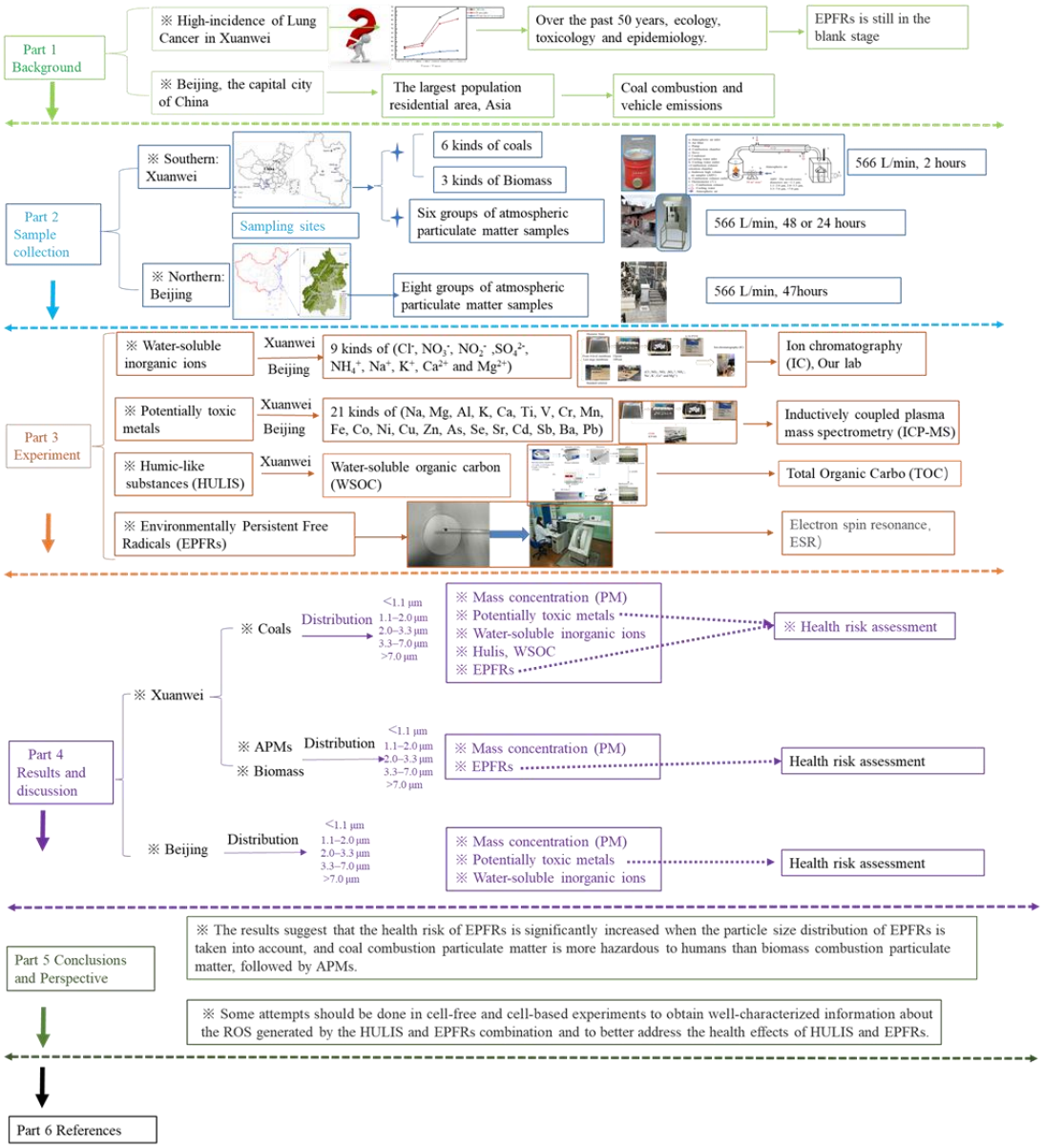

Fig. 4. The technical route

Chapter 2 Study area and sample collection

2.1 Location and Weather condition of the sampling site

Xuanwei, located in the northeastern part of Yunnan Province, is a county-level city under the jurisdiction of Qujing City, Yunnan Province. Geographic location between E103°35'30"-104°40'50", N25°53'30"-26°44'50", adjacent to Panzhou City in Guizhou Province in the east, adjacent to Zanyi District in this city in the south, looking at Huizhe County across the Niuguan River in the west, bordering with Weining County in Guizhou in the north, 260 km from the provincial capital Kunming City. The land area is 6069.88 km^2, with the highest altitude of 2868 m and the lowest altitude of 920 m. At the end of 2015, there were 28 townships (towns and streets) under the jurisdiction of Xuanwei, and the total household population of Xuanwei reached 1,528,500, with a sex ratio of 111.96 (with women as 100).

Xuanwei is mainly influenced by oceanic air masses in summer and autumn and continental air masses in winter and spring, forming a low-latitude plateau monsoon climate with multiple climate zones in the northern subtropical, southern temperate, and middle temperate zones coexisting. The main characteristics of the climate are no cool summer, no severe winter, large daily temperature difference, however, the annual temperature difference is small, the four seasons are not very distinct; winter and spring are relatively dry, while summer and autumn are relatively wet, precipitation is relatively concentrated, the rate of change of the four seasons is relatively large; the multi-year average temperature is about 13.4 ℃, the highest annual average temperature is 14.6 ℃, the lowest annual average temperature is 12.7 ℃, and the interannual average temperature difference is 1.9 ℃.

As the capital of China, Beijing is the political, economic, and cultural center of China. Beijing is located at the northwestern edge (39.4-41.6 N。,115.7-117.4 E。) of the North China Plain, adjacent to Tianjin to the east, and the other adjacent to Hebei Province, surrounded by the Taihang and Yanshan Mountains in the west, north and northeast. Moreover, it is one of the most crowded cities in the world (Men et al., 2018). The resident population of Beijing city is 21.54 million and car ownership of 6.36 million vehicles in 2018 (National Bureau of Statistics (NBS), 2019) (Beijing Bureau of Statistics (NBS)2018). This area experiences a monsoon-influenced humid continental climate, which is

characterized by hot, humid summers, and cold, dry winters (L. Yao et al., 2020). The mean temperature over the year is -2.18 ± -2.55 °C, with annual precipitation of 400-500 mm (W. Xu et al., 2020).

2.2 Civil houses and solid fuels at sampling sites

Xuanwei residents living fuel is mainly bituminous coal and wood (pine, poplar, etc.) or straw (corn cobs, etc.), especially in remote mountainous areas of the township, due to the inconvenience of transportation, more near the habit of taking materials, according to the characteristics of the geographical distribution of small coal kilns, the natural formation of the central part of the city, including the nearby Hu Tou Village to burn bituminous coal, remote areas, including Xize Township burn wood more, a small number of areas have anthracite coal kilns to burn anthracite coal is the main.

Rural houses in the Xuanwei area are mainly two-story civil structures (Figure 5a). The first half of the first floor of this type of house is the living room or kitchen, which is the place where the family often stays. Due to the small windows installed, the air circulation is not smooth. As a result, smoke is generated when residents use local coal for heating or cooking. As shown in Figure 5b, the stove is directly discharged indoors without any treatment, so the concentration of particulate matter is very high. The link between the high incidence of lung cancer and harmful pollutants emitted from local solid fuel combustion has been a hot topic and focus of research since the 1980s in Xuanwei, Yunnan Province, China (Mumford et al., 1987).

Fig. 5. The stove (a) and building structure (b) in rural Xuanwei, China.

2.3 Sample collection

2.3.1 Sample Collection in Xuanwei

2.3.1.1 Collection of Raw Coal and Biomass

After the field investigation, three kinds of raw biomass (Pine, Corncob, Poplar) from Zhongan Town, and six kinds of residential raw coal from Bole Town (Luomu coal [LM] and Bole coal [BL]), Houshou Town (Lijiawu coal [LJW]), Laochang Town (Shunfa coal [SF]), Laibin Town (Guangming coal [GM] and Zongfan coal [ZF]), and six group of APMs (Houshou Town) were collected. The detail information of raw coal, and biomass as shown in Table 1 and Figure 7.

2.3.1.2 Collection of Atmospheric Particulate Matters in Xuanwei

Six sample groups of APMs (A-F) were conducted by a high-volume air sampler (Shibata Science Co., Ltd., Saitama., Japan) at a flow rate of 566 L/min in Xuanwei local rural residents on February and March in 2017, and the aerodynamic diameters were <1.1 μm, 1.1–2.0 μm, 2.0–3.3 μm, 3.3–7.0 μm, and >7.0 μm, respectively. The detail information of raw coal, biomass, and APMs, as shown in Figure 6 and Table 1. The records of APMs collected in Yunnan residential areas in 2017 was list in Table 2.

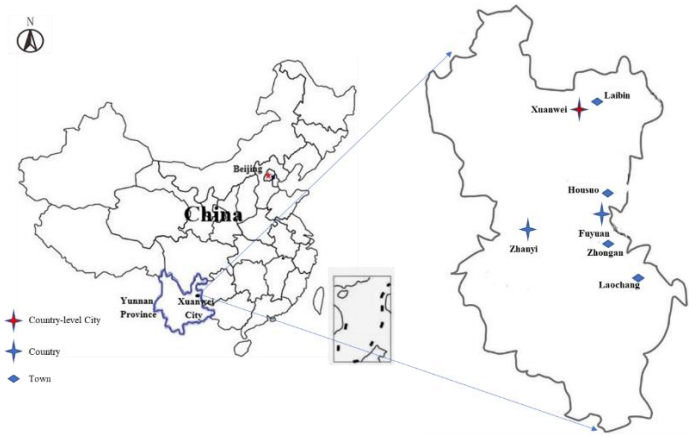

Fig. 6. Sampling sites in Xuanwei

Table 1. The detail information of Raw coal, biomass and APMs from Xuanwei

Types	Mine	Sample groups	Location	Altitude / m	Latitude	Longitude
Coal	Luomu	LM	Bole Town	1793	26°29′34.09″	103°46′9.17″
	Bole	BL	Bole Town	2104	25°47′15.32″	104°07′32.32″
	Zongfan	ZF	Laibin Town	2024	26°17′58.25″	104°05′42.49″
	Guangming	GM	Laibin Town	1987	26°19′46.55″	104°09′36.43″
	Shunfa	SF	Laochang Town	1994	25°13′31.13″	104°31′22.42″
	Lijiawu	LJW	Housuo Town	2078	25°79′99.21″	104°28′60.06″
Biomass		Corncob	Zhongan Town	1831	25°39′58.85″	104°15′8.20″
		Pine	Zhongan Town	1831	25°39′58.85″	104°15′8.20″
		Poplar	Zhongan Town	1812	25°40′38.06″	104°15′9.59″
APMs		A~D	Housuo Town	2023	25°50′59″	104°23′22″
		E~F	Housuo Town	2267	25°49′37″	104°14′15″

Table 2. The records of APMs collected in Yunnan residential areas in 2017

Group	Date	Period	Duration /h	Volume L/min	Weather	Temperature
A	2.18	9:40	48	566	Sunny	9-17℃
	2.19				Sunny	9-22℃
	2.20	9:40			Cloudy-Sunny	9-21℃
B	2.20	10:20	48	566	Cloudy-Sunny	9-21℃
	2.21				Cloudy-Sunny	8-20℃
	2.22	10:20			Cloudy	9-20℃
C	2.22	11:30	48	566	Cloudy	9-20℃
	2.23				Light rain	8-19℃
	2.24	11:30			Light rain	3-6℃
D	2.24	11:50	24	566	Light rain	3-6℃
	2.25	11:50			Light rain	-1-2℃
E	2.25	13:40	48	566	Light rain	-1-2℃
	2.26	13:40			Light rain	0-2℃
F	2.27	14:20	43	566	Light rain	3-8℃
	2.28	Power outage for 5 hours			Light rain	3-14℃
	3.01	14:20			Light rain	1-8℃

2.3.2 Collection of Atmospheric Particulate Matters in Beijing

Our sampling site is in a high population residential area (Fig.7), with about 600,000 people, and the traffic volume is very heavy in the morning and evening rush hours. Residents living in this area are

potential receptors for metals in the air.

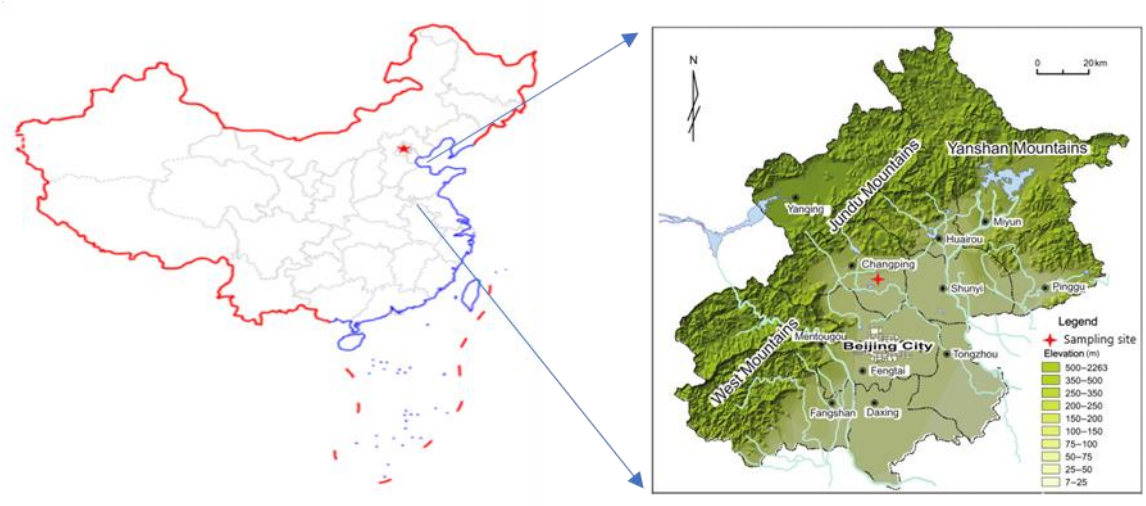

Fig. 7. Map of the sampling area (left), the map (right) indicates the sampling site in Beijing.

The aerosol sampling was conducted by a high-volume air sampler at a flow rate of 566 L/min in Beijing from 26 December 2018 to 11 January 2019. The sampler (Anderson Sampler, equipped with 5 cut size :1.1, 1.1- 2.0, 2.0-3.3, 3.3-7.0, 7.0 μm) can collect the particulate matter in the flue gas on five quartz filter membranes according to the aerodynamic diameter. The quartz filter used for collecting PM was baked in a muffle furnace (450 ℃) for 6 hours before sampling and placed in a constant temperature and humidity chamber at 25 ℃ and 45 % humidity for 24 hours and then wrapped in clean aluminum foil paper and placed in a refrigerator at −45 ° C until use. After sampling, the membranes were equilibrated and weighed again using the same procedure. To ensure accuracy, each filter was weighed at least three times before and after sampling, and the results were averaged. After weighing, store the filter at −45 ° C until analysis. The sampling duration was 47 h and were changed new quartz filter at about 12:00 am. During the sampling period, the temperature (T; ℃), relative humidity (RH; %), wind speed (WS; km/h) and wind direction (WD) and other atmospheric pollutants (SO_2, CO, NO_2 and O_3) were collected from the website of Air quality online monitoring and analysis platform (https://www.aqistudy.cn; accessed on 20 August 2020) and Ventusky-Weather Maps (https://www.ventusky.com; accessed on 20 August 2020). The details information about the meteorological parameters during the sapling period as shown in Table 3. Each group about time series of average ambient temperature (AT; ℃), relative humidity (RH; %), wind speed (WS; km/h) and wind direction (WD) in Beijing as shown in Table 4.

Table 3. The meteorological parameters during the sapling period

Date	Weather	$PM_{2.5}$ μg/m^3	PM_{10} μg/m^3	SO_2 μg/m^3	CO mg/m^3	NO_2 μg/m^3	O_3_8h μg/m^3
2018/12/26	Sunny~cloudy	9	26	4	0.4	26	50
2018/12/27	Sunny~cloudy	7	52	4	0.3	10	54
2018/12/28	Sunny	9	39	4	0.4	19	50
2018/12/29	Sunny	10	28	5	0.4	26	52
2018/12/30	Sunny~cloudy	15	32	4	0.5	37	42
2018/12/31	Cloudy	38	59	10	0.9	56	20
2019/1/1	Sunny~cloudy	28	45	8	0.7	34	47
2019/1/2	Cloudy	57	75	12	1	56	28
2019/1/3	Haze	123	136	21	1.9	82	12
2019/1/4	Sunny	18	40	5	0.5	26	61
2019/1/5	Cloudy	17	34	7	0.5	37	49
2019/1/6	Cloudy	64	95	12	1.4	70	13
2019/1/7	Cloudy	34	54	9	0.9	44	52
2019/1/8	Sunny	10	29	4	0.5	28	62
2019/1/9	Sunny	41	66	12	0.9	59	26
2019/1/10	Sunny~cloudy	75	113	14	1.5	79	17
2019/1/11	Haze	103	130	15	1.7	80	21
Average	-	38.71	61.94	8.82	0.85	45.24	38.59
SD	-	33.91	34.87	4.82	0.49	22.14	16.89

Table 4. Each group about time series of average ambient temperature (AT; ℃), relative humidity (RH; %), wind speed (WS; km/h) and wind direction (WD) in Beijing

Date	T℃	RH%	WS km/h	Wind direction
12/26-12/28	-5.33	13.33	6.00	Northwest
12/28-12/30	-5.00	10.00	5.00	Northwest, Northeast
12/30-12/1	-5.33	13.33	6.00	Northwest, Northeast
1/1-1/3	-1.33	26.67	3.00	Northwest, Northeast
1/3-1/5	-1.67	20.00	2.33	Northwest, Northeast
1/5-1/7	-0.67	16.67	3.33	Southeast, Northwest
1/7-1/9	-0.67	16.67	4.00	Southeast, Northwest
1/9-1/11	-0.67	16.67	3.33	Southeast, Northwest

2.4 Sample processing and collection of simulated combustion particulate matter

2.4.1 Instrument and materials

Instrument: Muffle furnace, Thermometer, Electronic balance (LA130 S-F), Blower, Yunnan civil coal furnace, Combustion device, Andersen high-flow five-stage sampler (Shibata Science Co., Ltd., Japan).

Materials: Raw coal, Biomass, Solid alcohol.

Others: Tweezers, Nitrile Sterile, Dust-free gloves, Tin foil, Self-sealing bags, Lighter.

2.4.2 Combustion devices

Sampling is performed in a closed and ventilated laboratory with ventilation fans. The flue gas collection system consists of a laboratory-designed flue unit and sampler. The flue unit consists of an enclosed flared fume hood, two bends (1 m long, 20 cm diameter), a long straight pipe (5 m long, 20 cm

diameter), and a cooling water sleeve (2 m long, 30 cm diameter). In addition, a closed flue gas holding chamber is connected at the end of the flue, where an Andersen high-flow five-stage sampler (Shibata Science Co., Ltd., Japan) is placed. Several parts of the sampling system are removable for easy cleaning and are connected by flanges. To avoid contamination of the flue gas by the flue material, the complete flue unit is made of stainless steel and the gaskets used in the connections are made of Teflon (Figure 8). The entire unit can be considered as a completely closed and pure system, which minimizes background contamination during sampling and facilitates experimental analysis. The experimental process ensures that there are no flue gas leaks throughout the coal combustion process and no visible particle deposits in the piping.

The Andersen sampler (Figure 9) is placed horizontally in the flue gas holding chamber. The particles in five sizes were collected, with a flow rate at 566 L/min, and the aerodynamic diameter are <1.1 μm, 1.1-2.0 μm, 2.0-3.3 μm, 3.3-7.0 μm, and >7.0 μm, respectively.

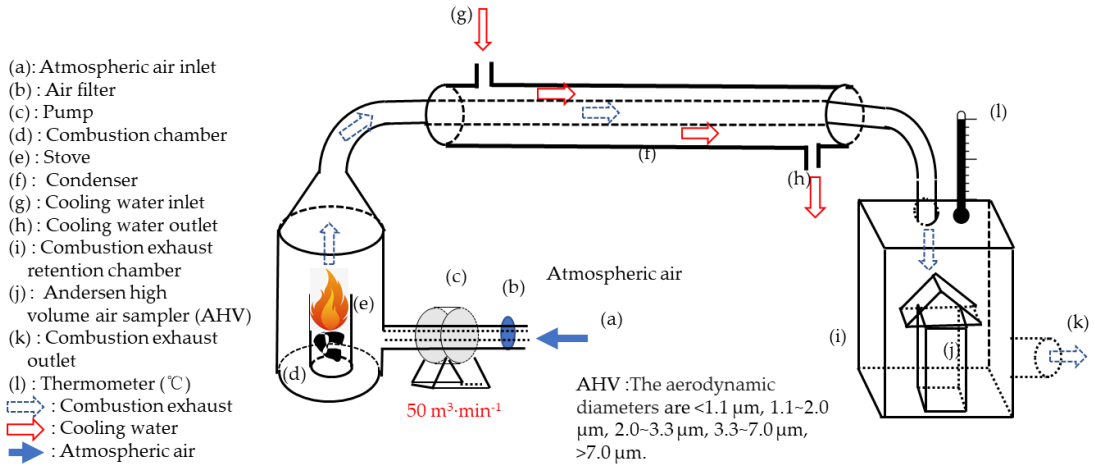

Fig. 8. Sketch of sampling system.

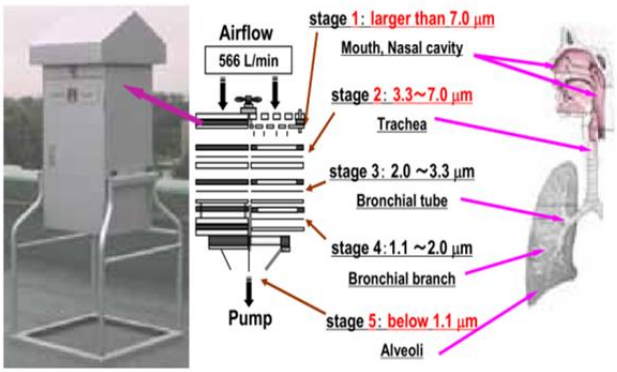

Fig. 9. The Andersen high volume five-stage sampler

2.4.3 Sampling experiments

Before simulating coal combustion, all parts of the sampling system were carefully cleaned (the quartz film used for solid fuel combustion particulate collection was roasted in a muffle furnace (450 °C) for 6 hr before sampling), placed in a constant temperature and humidity chamber at 25 ℃ and 45 % humidity for 48 hr, weighed accurately with an electronic balance (LA130 S-F) and numbered, then wrapped tightly in clean aluminum foil and placed in a - 4 °C refrigerator for storage. The 500 g raw coal or biomass was ignited using solid alcohol, and to avoid the effect of alcohol combustion on particulate matter emissions, the coal stove was moved outdoors during the ignition stage, and when the fuel was seen to begin to glow red and have a slight flame, the stove was then carefully placed in a closed flared fume hood directly below the flared fume hood, and clean air was introduced through the blower (50 m^3/min^{-1}), and the flue gas was passed through the sampler's pump as well as The flue gas is fully mixed through the flue device by the action of the blower and cooled at the cooling water casing before entering the flue gas retention chamber, where the flue gas temperature at the chamber is around 40 °C. This experiment uses the actual air as the oxygen source, and the corresponding background concentration in the atmosphere may cause errors in the final actual results. To ensure the reliability of the experimental data, the particulate matter in the air is filtered with a 200-purpose filter cloth at the inlet of the blower, which can minimize the background pollution during sampling. The whole sampling process of coal combustion lasts for 2 hr, including the ignition stage, combustion stage and combustion stage. However, the combustion rate of biomass varies greatly depending on the material, with poplar and pine sampled for 1 hr and corn cob sampled for 30 min.

2.5 Calculation of particulate matter concentration

After sampling, the quartz filter membrane was carefully removed and wrapped with the original aluminum foil, and the filter membrane samples were weighed after 48 hr of constant temperature and humidity (25 °C, 45 % humidity). The mass concentration of different particle sizes was calculated based on the sample weight, sampling time and flow rate. The mass concentration of particulate matter was calculated according to the following equation (1).

$$C = \frac{(W_2 - W_1)}{L \times T} \qquad (1)$$

Where: C -mass concentration ($\mu g/m^{-3}$)

W1 -mass of the filter membrane before sampling (μg)

W2 - the mass of the filter membrane before sampling (μg)

L -sampling flow rate (m^3/h^{-1})

T--sampling time (hr)

2.6 Mass concentration of size-segregated particulate matters

Respirable particulate matter is a common proxy indicator of air pollution. It affects more people than any other pollutant. The main components of PM are sulfate, nitrate, ammonia, sodium chloride, black carbon, mineral dust and water. It consists of a complex mixture of solid and liquid particles of organic and inorganic substances suspended in the air. Routine air quality measurements typically describe such PM concentrations in terms of micrograms per cubic meter ($\mu g/m^3$). WHO Air quality guideline (AQG) values (24-hour mean) are 15 $\mu g/m^3$ and 45 $\mu g/m^3$ for $PM_{2.5}$ and PM_{10}, respectively (https://www.who.int/news-room/fact-sheets/detail/ambient-(outdoor)-air-quality-and-health; accessed on 22 September 2021). Chinese national ambient air quality standards (CNAAQS) Grade I(GB3095-2012), in which the Grade I standard (24-hour mean) for $PM_{2.5}$ of 35 $\mu g\ m^{-3}$, and PM_{10} of 50 $\mu g\ m^{-3}$ (https://www. transportpolicy.net/standard/china-air-quality-standards/ ; accessed on 22 September 2021).

Generally, PM can be classified as coarse particles (PM_{10} with an aerodynamic diameter less than 10 μm), fine particles ($PM_{2.5}$) (Jingjing Zhang et al., 2018)(Do et al., 2021). In our research, Anderson sampler used that does not have cut-off sizes of 2.5 and 10 μm, in order to facilitate statistical analysis, we regard particles <1.1 μm and 1.1 - 2.0 μm as fine particles (with an aerodynamic diameter less than 2.0 μm), and others as coarse particles PM>2.0 including (2.0 - 3.0 μm, 3.3 - 7.0 μm, >7.0 μm). The sum of all particles is called total suspended particles (TSP).

2.6.1 Mass concentration of size-segregated in APMs in Xuanwei

The mass concentration of size-segregated in APMs of Xuanwei residential area were show in Figure 10 and Table 5. The mass concentrations of atmospheric particulate matter in groups A, and B were higher than those in the other four groups, probably due to light rainfall during the sampling period in the other groups. The mean concentration of $PM_{1.1}$, $PM_{1.1\text{-}2.0}$, $PM_{2.0\text{-}3.3}$, $PM_{3.3\text{-}7.0}$, $PM_{>7.0}$ and TSP were

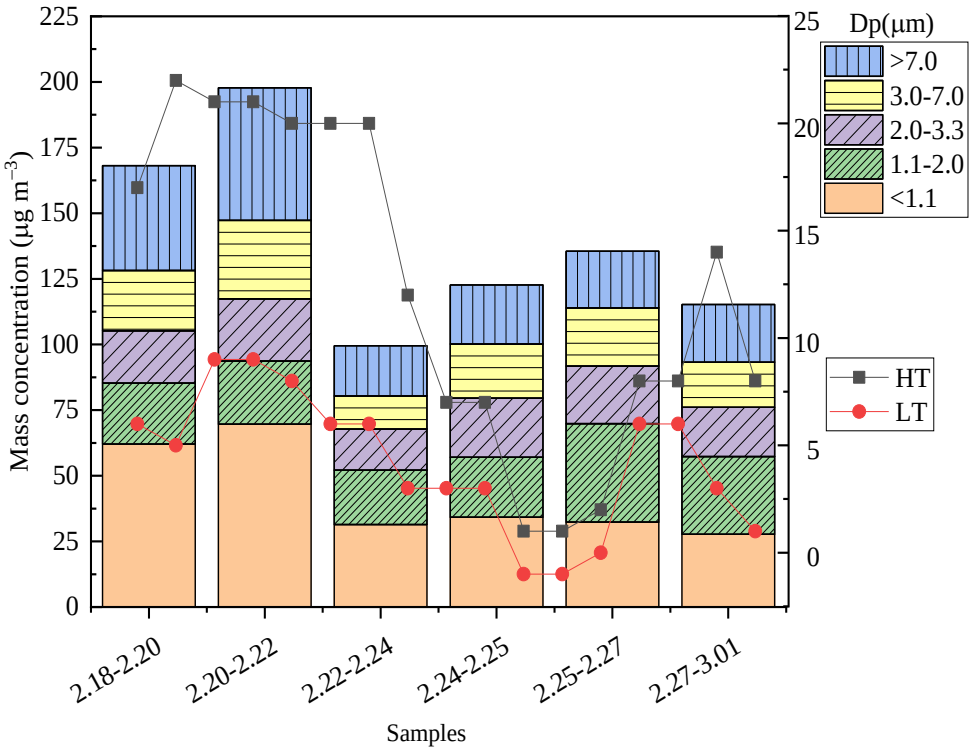

Fig. 10. The average mass concentration of PM within $PM_{1.1}$, $PM_{1.1\text{-}2.0}$, $PM_{2.0\text{-}3.3}$, $PM_{3.3\text{-}7.0}$, and $PM_{>7.0}$ during the sampling. (HT and LT represent the highest temperature and lowest temperature on the sampling day, respectively)

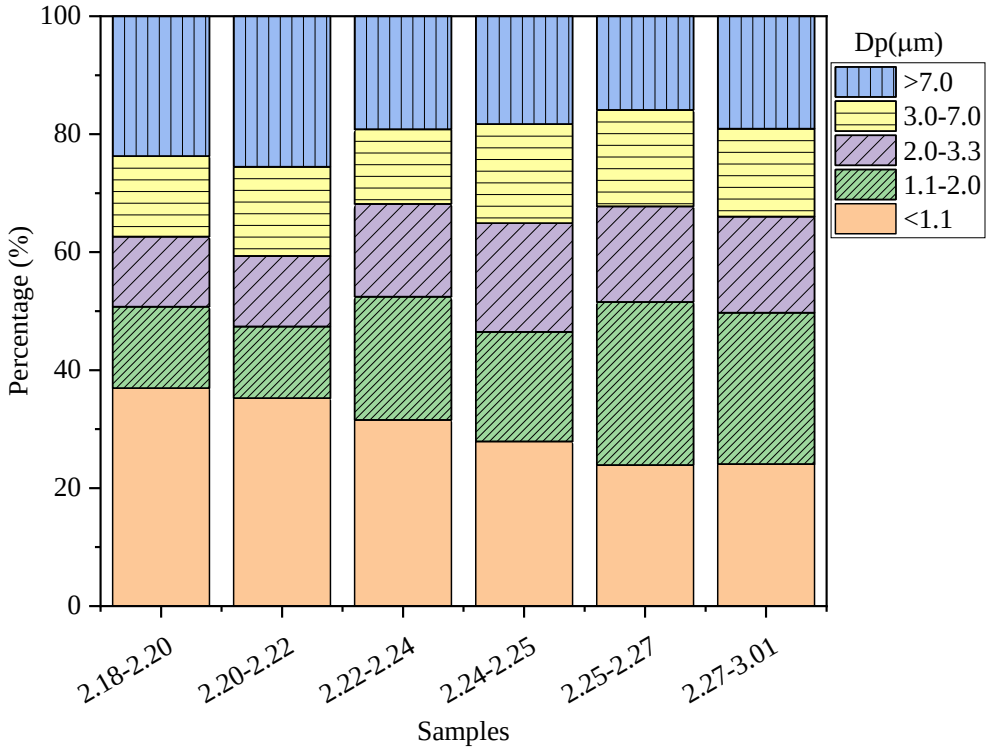

Fig. 11. The relative portions of average mass concentration within $PM_{1.1}$, $PM_{1.1\text{-}2.0}$, $PM_{2.0\text{-}3.3}$, $PM_{3.3\text{-}7.0}$, and $PM_{>7.0}$ during the sampling period.

ranged from 27.73 to 69.69 μg/m^3 with an average value of 42.92 ± 16.50 μg/m^3, from 26.33 to 37.48 μg/m^3 with an average value of 26.33 ± 5.66 μg/m^3, from 15.64 to 23.62 μg/m^3 with an average value of 20.42 ± 2.68 μg/m^3, from 12.58 to 29.95 μg/m^3 with an average value of 20.90 ± 5.34 μg/m^3, from 19.08 to 50.43 μg/m^3 with an average value of 29.22 ± 11.72 μg/m^3, and from 99.50 to 197.75 μg/m^3 with an average value of 139.79 ± 33.41 μg/m^3, respectively.

Table 5. Mass concentration of size-segregated in APMs in Xuanwei (μg/m^3)

Groups	<1.1 μm	1.1-2.0 μm	<2.0 μm	2.0-3.3 μm	3.0-7.0 μm	<7.0 μm	>7.0 μm	TSP
A	62.08	23.25	85.33	19.94	22.94	128.21	39.88	168.09
B	69.69	24.06	93.75	23.62	29.95	147.32	50.43	197.75
C	31.41	20.80	52.21	15.64	12.58	80.43	19.08	99.50
D	34.23	22.82	57.05	22.58	20.61	100.24	22.45	122.69
E	32.39	37.48	69.87	21.96	22.15	113.98	21.53	135.51
F	27.73	29.57	57.30	18.77	17.18	93.25	21.96	115.21
Mean	42.92	26.33	69.25	20.42	20.90	110.57	29.22	139.79
Max	69.69	37.48	93.75	23.62	29.95	147.32	50.43	197.75
Min	27.73	20.80	52.21	15.64	12.58	80.43	19.08	99.50
STD	16.50	5.66	15.50	2.68	5.34	22.32	11.72	33.41

STD: Standard Deviation, Max: Maximum, Min: minimum

Table 6. Percentage distribution of mass concentration to TSP (%) and international standard ratio for APMs in Xuanwei

Percentage distribution of mass concentration (%)								International standard ratio			
								CNAAQS	CNAAQS	AQG	AQG
Groups	$PM_{1.1}$	$PM_{1.1-2.0}$	$PM_{2.0}$	$PM_{2.0-3.3}$	$PM_{3.3-7.0}$	$PM_{7.0}$	$PM_{>7.0}$	$PM_{2.0}$/ $PM_{2.5}$	$PM_{7.0}$/ PM_{10}	$PM_{2.0}$/ $PM_{2.5}$	$PM_{7.0}$/ PM_{10}
A	36.93	13.83	50.77	11.86	13.65	76.28	23.72	2.44	2.56	5.69	2.85
B	35.24	12.17	47.41	11.94	15.14	74.50	25.50	2.68	2.95	6.25	3.27
C	31.57	20.90	52.47	15.72	12.64	80.83	19.17	1.49	1.61	3.48	1.79
D	27.90	18.60	46.50	18.40	16.80	81.70	18.30	1.63	2.00	3.80	2.23
E	23.90	27.66	51.56	16.21	16.34	84.11	15.89	2.00	2.28	4.66	2.53
F	24.07	25.66	49.74	16.29	14.91	80.94	19.06	1.64	1.87	3.82	2.07
Mean	29.94	19.80	49.74	15.07	14.91	79.72	20.28	1.98	2.21	4.62	2.46
Max	36.93	27.66	52.47	18.40	16.80	84.11	25.50	2.68	2.95	6.25	3.27
Min	23.90	12.17	46.50	11.86	12.64	74.50	15.89	1.49	1.61	3.48	1.79
STD	5.08	5.67	2.15	2.39	1.44	3.29	3.29	0.44	0.45	1.03	0.50

STD: Standard Deviation, Max: Maximum, Min: minimum

The $PM_{2.0}$ mean concentration were ranged from 52.21 to 93.75 μg/m^3, which were 1.98 ± 044 times

of average limit of 35 μg/m^3 for $PM_{2.5}$ (24-hour mean) set by Chinese national ambient air quality standards (CNAAQS) Grade I (GB3095-2012), and 4.62 ± 1.03 times than the $PM_{2.5}$ concentration of 15 μg/m^3 in the air quality guidelines (AQG) standard put forth by the WHO. The $PM_{7.0}$ mean concentration were ranged from 80.40 to 147.32 μg/m^3, which were 2.21 ± 0.45 times of average limit of 50 μg/m^3 for PM_{10} (24-hour mean) set by Chinese national ambient air quality standards (CNAAQS) Grade I(GB3095-2012), and 2.46 ± 0.50 times than the PM_{10} concentration of 45 μg/m^3 in the air quality guidelines (AQG) standard put forth by the WHO (Table 5 and Table 6).

Percentage distribution of mass concentration (%) and international standard ratio for APMs are listed in Figure 11 and Table 6. Percentage distribution of mass concentration to TSP of $PM_{1.1}$, $PM_{1.1\text{-}2.0}$, $PM_{2.0\text{-}3.3}$, $PM_{3.3\text{-}7.0}$, and $PM_{>7.0}$ were ranged from 23.90 to 36.93 %, 12.17 to 27.66 %, 11.86 to 18.40 %, 12.64 to 16.80 % and 15.89 to 25.50 % in Xuanwei residential area, respectively. It is worth noting that the mass concentration of fine particulate matter with particle size < 2.0 μm to TSP mass concentration ranged from 46.50 to 52.47 %, indicating that the ambient atmosphere in the region is dominated by fine particulate matter. There is no large pollution source in the sampling site, the main source of pollution is residential solid fuel combustion.

Actually, there is no any large pollution source in the county. The reasons are attributed to scattered coal combustion for living and heating, dust pollution caused by the road transportation, construction site and uncovered ground, vehicle emissions and cook fume in the county, as well as air pollution transported from the surrounding cities.

2.6.2 Mass concentration of size-segregated in RBC particles

The mass concentration of size-segregated in RBC particles were show in Figure 12 and Table 7. The mean PM concentration were in the order of Corncob > Poplar > Pine. The mean concentration of $PM_{1.1}$, $PM_{1.1\text{-}2.0}$, $PM_{2.0\text{-}3.3}$, $PM_{3.3\text{-}7.0}$, $PM_{>7.0}$ and TSP were ranged from 1781.82 to 4975.61 μg/m^3 with an average value of 2948.77 ± 1438.66 μg/m^3, from 840.40 to 2420.05 μg/m^3 with an average value of 1415.44 ± 712.85 μg/m^3, from 648.84 to 1794.04 μg/m^3 with an average value of 1087.57 ± 504.44 μg/m^3, from 725.25 to 1486.45 μg/m^3 with an average value of 1085.38 ± 3121.10 μg/m^3, from 531.31 to 1178.86 μg/m^3 with an average value of 804.40 ± 273.91 μg/m^3, and from 500.06 to 11855.01 μg/m^3 with an average value of 7341.57 ± 3192.13 μg/m^3, respectively.

The $PM_{2.0}$ mean concentration were ranged from 2767.68 to 7395.66 μg/m^3, which were 124.69 ± 61.27 times of average limit of 35 μg/m^3 for $PM_{2.5}$ (24-hour mean) set by Chinese national ambient air quality standards (CNAAQS) Grade I(GB3095-2012), and 290.95 ± 142.97 times than the $PM_{2.5}$

concentration of 15 μg/m^3 in the air quality guidelines (AQG) standard put forth by the WHO. The $PM_{7.0}$

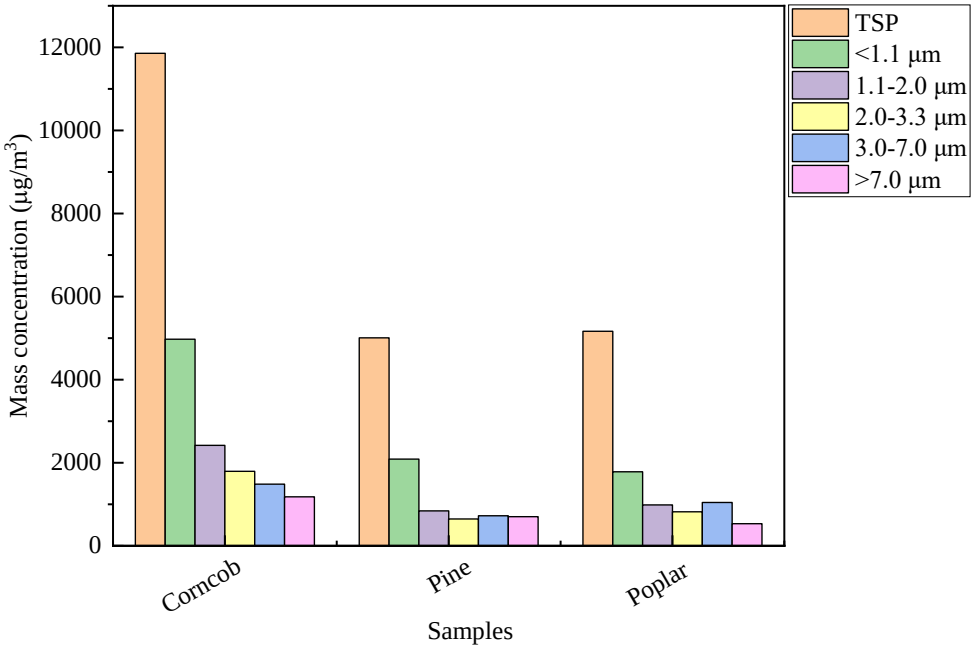

Fig. 12. Mass concentration of size-segregated in RBC particles

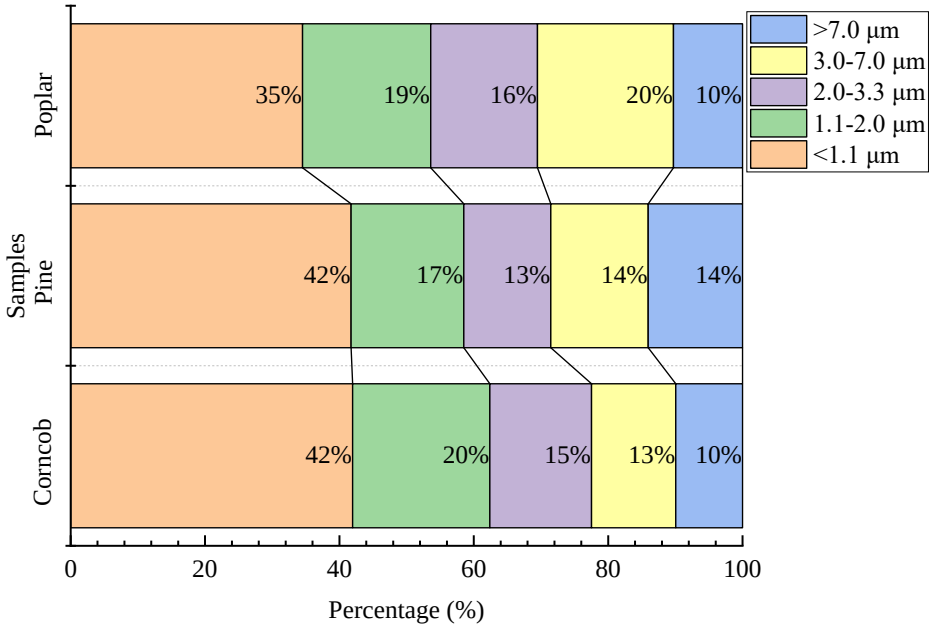

Fig. 13. Percentage of size-segregated in RBC particles

mean concentration were ranged from 4303.03 to 10676.15 μg/m^3, which were 130.74 ± 58.60 times of

average limit of 50 μg/m^3 for PM_{10} (24-hour mean) set by Chinese national ambient air quality standards (CNAAQS) Grade I (GB3095-2012), and 145.27 ± 65.11 times than the PM_{10} concentration of 45 μg/m^3 in the air quality guidelines (AQG) standard put forth by the WHO (Table 7 and Table 8).

Percentage distribution of mass concentration (%) and international standard ratio for RBC particles are listed in Figure 13 and Table 8. Percentage distribution of mass concentration to TSP of $PM_{1.1}$, $PM_{1.1\text{-}2.0}$, $PM_{2.0\text{-}3.3}$, $PM_{3.3\text{-}7.0}$, and $PM_{>7.0}$ were ranged from 34.51 to 41.97 %, 16.79 to 20.41 %, 12.95 to 15.88 %, 12.54 to 20.23 % and 9.94 to 14.04 % in Xuanwei residential area, respectively. Compared to APMs, the mass concentration of fine particulate matter with particle size < 2.0 μm to TSP mass concentration were higher, ranged from 53.60 to 62.38 % with an average value of 58.17 ± 3.59 %.In winter, strong correlations of $PM_{2.5}$ with PM_{10}, SO_2, and CO (r = 0.53–0.98, p < 0.001) were identified, most likely linked to fossil fuel combustion for domestic heating (Hao et al., 2020).

Table 7. Mass concentration of size-segregated in RBC particles (μg/m^3)

Groups	<1.1 μm	1.1-2.0 μm	<2.0 μm	2.0-3.3 μm	3.0-7.0 μm	<7.0 μm	>7.0 μm	TSP
Corncob	4975.61	2420.05	7395.66	1794.04	1486.45	10676.15	1178.86	11855.01
Pine	2088.89	840.40	2929.29	648.48	725.25	4303.03	703.03	5006.06
Poplar	1781.82	985.86	2767.68	820.20	1044.44	4632.32	531.31	5163.64
Average	2948.77	1415.44	4364.21	1087.57	1085.38	6537.17	804.40	7341.57
Max	4975.61	2420.05	7395.66	1794.04	1486.45	10676.15	1178.86	11855.01
Min	1781.82	840.40	2767.68	648.48	725.25	4303.03	531.31	5006.06
STD	1438.66	712.85	2144.58	504.44	312.10	2929.79	273.91	3192.13

STD: Standard Deviation, Max: Maximum, Min: minimum

Table 8. Percentage distribution of mass concentration to TSP (%) and international standard ratio for RBC particles

Percentage distribution of mass concentration (%)								International standard ratio			
								CNAAQS	CNAAQS	AQG	AQG
Groups	$PM_{1.1}$	$PM_{1.1\text{-}2.0}$	$PM_{2.0}$	$PM_{2.0\text{-}3.3}$	$PM_{3.3\text{-}7.0}$	$PM_{7.0}$	$PM_{>7.0}$	$PM_{2.0}$/ $PM_{2.5}$	$PM_{7.0}$/ PM_{10}	$PM_{2.0}$/ $PM_{2.5}$	$PM_{7.0}$/ PM_{10}
Corncob	41.97	20.41	62.38	15.13	12.54	90.06	9.94	211.30	213.52	493.04	237.25
Pine	41.73	16.79	58.51	12.95	14.49	85.96	14.04	83.69	86.06	195.29	95.62
Poplar	34.51	19.09	53.60	15.88	20.23	89.71	10.29	79.08	92.65	184.51	102.94
Average	39.40	18.76	58.17	14.66	15.75	88.57	11.43	124.69	130.74	290.95	145.27
Max	41.97	20.41	62.38	15.88	20.23	90.06	14.04	211.30	213.52	493.04	237.25
Min	34.51	16.79	53.60	12.95	12.54	85.96	9.94	79.08	86.06	184.51	95.62
STD	3.46	1.50	3.59	1.24	3.26	1.86	1.86	61.27	58.60	142.97	65.11

STD: Standard Deviation, Max: Maximum, Min: minimum

2.6.2 Mass concentration of size-segregated particles in RCC particles

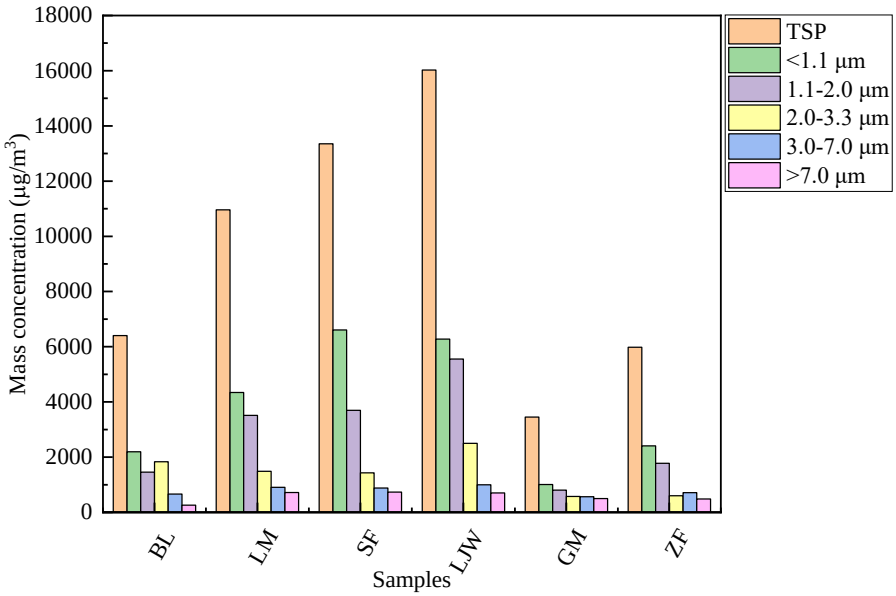

Fig. 14. Mass concentration of size-segregated in RCC particles

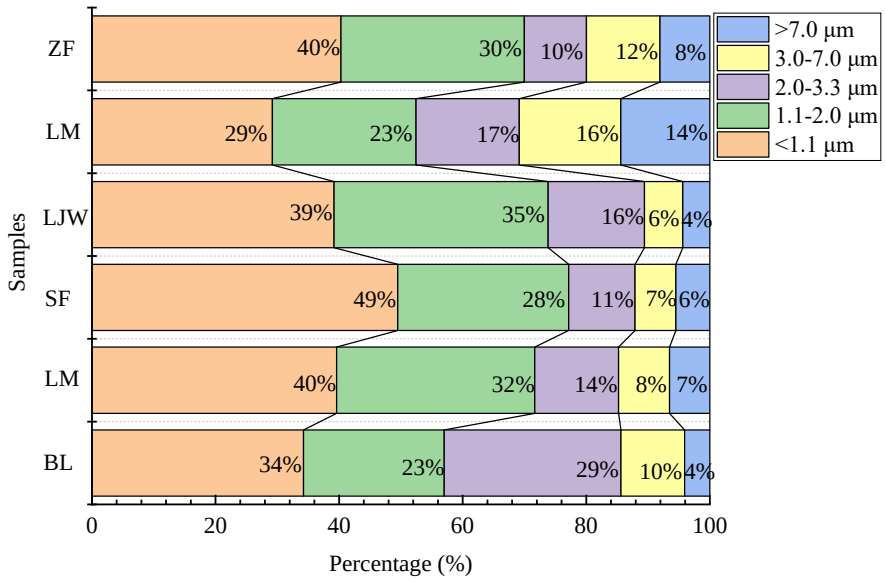

Fig. 15. Percentage of size-segregated in RCC particles

The mass concentration of size-segregated RCC particles was show in Figure 14 and Table 8. The

mean PM concentration were in the order of LJW > SF > LM > BL > ZF > GM. The mean concentration of $PM_{1.1}$, $PM_{1.1\text{-}2.0}$, $PM_{2.0\text{-}3.3}$, $PM_{3.3\text{-}7.0}$, $PM_{>7.0}$ and TSP were ranged from 1008.54 to 6606.30 μg/m^3 with an average value of 3575.85 ± 2106.00 μg/m^3, from 802.41 to 5555.06 μg/m^3 with an average value of 2608.53 ± 1620.04 μg/m^3, from 577.15 to 2497.06 μg/m^3 with an average value of 1465.08 ± 672.75 μg/m^3, from 566.84 to 995.29 μg/m^3 with an average value of 768.34 ± 150.85 μg/m^3, from 262.07 to 734.69 μg/m^3 with an average value of 522.25 ± 169.78 μg/m^3, and from 3452.59 to 16026.21 μg/m^3 with an average value of 9363.22 ± 4434.46 μg/m^3, respectively.

The $PM_{2.0}$ mean concentration were ranged from 1810.95 to 11833.04 μg/m^3, which were 188.76 ± 104.41 times of average limit of 35 μg/m^3 for $PM_{2.5}$ (24-hour mean) set by Chinese national ambient air quality standards (CNAAQS) Grade I(GB3095-2012), and 440.44 ± 243.63 times than the $PM_{2.5}$ concentration of 15 μg/m^3 in the air quality guidelines (AQG) standard put forth by the WHO. The $PM_{7.0}$ mean concentration were ranged from 2388.10 to 14330.09 μg/m^3, which were 132.13 ± 73.09 times of average limit of 50 μg/m^3 for PM_{10} (24-hour mean) set by Chinese national ambient air quality standards (CNAAQS) Grade I (GB3095-2012), and 178.03 ±92.51 times than the PM_{10} concentration of 45 μg/m^3 in the air quality guidelines (AQG) standard put forth by the WHO (Table 9 and Table 10).

Table 9. Mass concentration of size-segregated in RCC particles (μg/m^3)

Groups	<1.1 μm	1.1-2.0 μm	<2.0 μm	2.0-3.3 μm	3.0-7.0 μm	<7.0 μm	>7.0 μm	TSP
BL	2193.76	1457.60	3651.35	1833.04	659.60	5484.39	262.07	6406.07
LM	4340.40	3514.43	7854.83	1487.04	904.00	9341.87	715.55	10961.43
SF	6606.30	3697.00	10303.30	1432.57	881.92	11735.87	734.69	13352.47
LJW	6277.97	5555.06	11833.04	2497.06	995.29	14330.09	700.82	16026.21
GM	1008.54	802.41	1810.95	577.15	566.84	2388.10	497.64	3452.59
ZF	2410.19	1775.62	4185.81	600.71	711.13	4786.51	482.92	5980.57
Average	3575.85	2608.53	6184.38	1465.80	768.34	7650.18	522.25	9363.22
Max	6606.30	5555.06	11833.04	2497.06	995.29	14330.09	734.69	16026.21
Min	1008.54	802.41	1810.95	577.15	566.84	2388.10	262.07	3452.59
STD	2106.00	1620.04	3654.48	672.75	150.85	4162.83	169.78	4434.46

STD: Standard Deviation, Max: Maximum, Min: minimum

Percentage distribution of mass concentration (%) and international standard ratio for RCC particles are listed in Figure 15 and Table 9. Percentage distribution of mass concentration to TSP of $PM_{1.1}$, $PM_{1.1\text{-}2.0}$, $PM_{2.0\text{-}3.3}$, $PM_{3.3\text{-}7.0}$, and $PM_{>7.0}$ were ranged from 29.21 to 49.48 %, 22.75 to 34.66 %, 10.04 to 28.61 %,

6.21 to 16.42 % and 4.09 to 14.41% in Xuanwei residential area, respectively. Compared to APMs, the mass concentration of fine particulate matter with particle size < 2.0 μm to TSP mass concentration were higher, ranged from 52.45 to 77.16 % with an average value of 67.02 ± 9.06. Compared to the previous results (Q. Yan et al., 2020), the particulate matters emitted from RCC (Huaibei, Xinjiang, Inner Mongolia, and Guizhou in China) were major concentrated in the size range of 0.43–2.1μm, which accounted for 39.2%–62.8% of total particulate matter, indicating that fine particulate matters emitted from RCC in Xuanwei area is higher than other areas of China.

Table 10. Percentage distribution of mass concentration to TSP (%) and international standard ratio for RCC particles

Percentage distribution of mass concentration (%)								International standard ratio			
								CNAAQS	CNAAQS	AQG	AQG
Groups	$PM_{1.1}$	$PM_{1.1-2.0}$	$PM_{2.0}$	$PM_{2.0-3.3}$	$PM_{3.3-7.0}$	$PM_{7.0}$	$PM_{>7.0}$	$PM_{2.0}$/ $PM_{2.5}$	$PM_{7.0}$/ PM_{10}	$PM_{2.0}$/ $PM_{2.5}$	$PM_{7.0}$/ PM_{10}
BL	34.25	22.75	57.00	28.61	10.30	85.61	4.09	104.32	73.03	243.42	121.88
LM	39.60	32.06	71.66	13.57	8.25	85.22	6.53	224.42	157.10	523.66	207.60
SF	49.48	27.69	77.16	10.73	6.60	87.89	5.50	294.38	206.07	686.89	260.80
LJW	39.17	34.66	73.84	15.58	6.21	89.42	4.37	338.09	236.66	788.87	318.45
GM	29.21	23.24	52.45	16.72	16.42	69.17	14.41	51.74	36.22	120.73	53.07
ZF	40.30	29.69	69.99	10.04	11.89	80.03	8.07	119.59	83.72	279.05	106.37
Average	38.67	28.35	67.02	15.88	9.94	82.89	7.16	188.76	132.13	440.44	178.03
Max	49.48	34.66	77.16	28.61	16.42	89.42	14.41	338.09	236.66	788.87	318.45
Min	29.21	22.75	52.45	10.04	6.21	69.17	4.09	51.74	36.22	120.73	53.07
STD	6.19	4.35	9.06	6.18	3.51	6.79	3.51	104.41	73.09	243.63	92.51

STD: Standard Deviation, Max: Maximum, Min: minimum

2.6.3 Comparison of mass concentrations of particulate matter from different sources in Xuanwei

Comparing the different type particulate matter, we found that the mass concentration of particulate matter emitted from solid fuel combustion was mainly concentrated in particle size < 2.0 μm (58.17 ± 3.59 % for RBC particles, 67.02 ± 9.06 % for RCC particles), while the mass concentrations of atmospheric particulate matter were mainly concentrated in the particle size < 2.0 μm (49.74 ± 2.15 %) and >7.0 μm (20.28 ± 3.29 %). It indicates that the emission of fine particulate matter from raw coal

combustion is more than that from biomass combustion, and the health risk is not negligible as the ambient atmosphere is dominated by fine particulate matter.

From this study, it can be obtained that the concentrations of RCC particles and RBC particles are much higher than the APMs concentrations, not only because biomass and coal combustion are generated in a sealed environment for simulated combustion, without dilution of them and even less conditions for diffusion. In general, particulate matter released into the atmosphere from solid fuel combustion is diluted, transported over long distances, and subject to primary and secondary chemical reactions, so that the concentration of particulate matter in the atmosphere is much lower than the mass concentration of particulate matter produced by direct emission sources. Unlike general atmospheric particulate sampling, we collect high concentrations of RCC and RBC particulate matter directly with our sampling system. In the future, a comprehensive investigation different RCC and RBC under different stove types, combustion conditions and combustion stages are necessary to better understand the distribution pattern of PM.

2.6.4 Mass concentration of size-segregated particles in APMs in Beijing

2.6.4.1 Weather conditions during the Beijing sampling

Many studies have reported that the mass concentration of size distribution varies in different conditions (Q. Yao et al., 2020) (Do et al., 2021).The characteristics of atmospheric aerosols can be investigated based on the weather conditions (Do et al., 2021) （AT, RH, WS and WD and atmospheric pollutants (SO_2, CO, NO_2 and O_3) (Weiqian Wang et al., 2020).

The detailed information about the meteorological parameters, weather conditions and atmospheric pollutants was provided in Table 3, Table 4. During the sampling period, the temperature varied from -8 ℃ to 3 ℃ with a mean value of 2.18 ± 2.55 ℃; the ambient RH was in a range of 10 - 30 % and averaged at 18.24 ± 7.06 %; the average wind speed of 4.12 ± 2.40 km/h. Table 1 and Fig.2 show that the lowest $PM+_{2.0}$ and $PM_{>2.0}$ (38.52 and 111.41 μg/m^3, respectively), which was collected between 28-30 December, during this sampling period, the ambient temperature (-5 ℃) and relative humidity (10 %) was lower than other groups, and wind speed was higher than other sampling time. Meanwhile, $PM_{2.0}$ and $PM_{>2.0}$ was highest (75.95 and 207.23 μg/m^3, respectively), which was collected between 1- 3 January, during the sampling period, the ambient temperature (-1.33 ℃) and relative humidity (26.67 %)

are relatively higher, while the wind speed (3.00 km/h) is lower than most other sampling groups. Pearson correlation coefficients between the meteorological parameters and atmospheric pollutants in size-segregated PM was presented in Table 11. Pearson correlation coefficients show that the mass concentration $PM_{2.0}$ and $PM_{>2.0}$ both had an apparent correlation ($p<0.01$) with AT(r=0.55), RH(r=0.46) ,WS(r=-0.43) and AT(r=0.70), RH(r=0.80) ,WS(r=-0.61), respectively; in addition, the mass concentration PM2.0 and PM>2.0 also presented an apparent correlation with atmospheric pollutants ($PM_{2.0}$, SO_2, r = 0.68, CO, r = 0.71, NO_2, r = 0.66, O_3, r = -0.67, $p < 0.01$;$PM_{>2.0}$ SO_2, r = 0.86, CO, r = 0.85, NO_2, r = 0.76 $p < 0.01$, O_3, r = -0.76, $p < 0.01$). This result was consistent with the study (Weiqian Wang et al., 2020) .

Table 11. Pearson correlation coefficients between the meteorological parameters (temperature, wind speed and humidity) and atmospheric pollutants (SO_2, CO, NO_2 and O_3) in the different size range of particles

Size range	T ℃	RH %	WS km/h	SO_2 μg/m^3	CO mg/m^3	NO_2 μg/m^3	O_3-8h μg/m^3
< 1.1 μm	0.43	0.34	-0.37	0.58	0.63	0.58	-0.60
1.1-2.0 μm	0.64	0.58	-0.40	0.72	0.74	0.71	-0.67
2.0-3.3 μm	0.31	0.85	-0.37	0.58	0.49	0.36	-0.44
3.3-7.0 μm	0.85	0.52	-0.65	0.75	0.79	0.76	-0.61
>7.0 μm	0.59	0.32	-0.41	0.66	0.74	0.76	-0.74
<2.0 μm	0.55	0.46	-0.43	0.68	0.71	0.66	-0.67
>2.0μm	0.70	0.83	-0.61	0.86	0.85	0.76	-0.76

2.6.4.2 The size distribution of APMs in Beijing

The size distribution of APMs in Beijing was show in Figure 16 and Table 12. The mean concentration of $PM_{1.1}$, $PM_{1.1\text{-}2.0}$, $PM_{2.0\text{-}3.3}$, $PM_{3.3\text{-}7.0}$, $PM_{>7.0}$ and TSP were ranged from 21.61 to 57.87 μg/m^3 with an average value of 39.67 ± 10.66 μg/m^3, from 16.91 to 41.89 μg/m^3 with an average value of 32.25 ± 6.78 μg/m^3, from 38.52 to 99.75 μg/m^3 with an average value of 71.92 ± 16.47 μg/m^3, from 23.92 to 82.81 μg/m^3 with an average value of 36.54 ± 17.70 μg/m^3, from 47.63 to 79.34 μg/m^3 with an average value of 39.86 ± 77.51 μg/m^3, and from 149.93 to 289.84 μg/m^3 with an average value of 230.65 ± 42.29 μg/m^3, respectively.

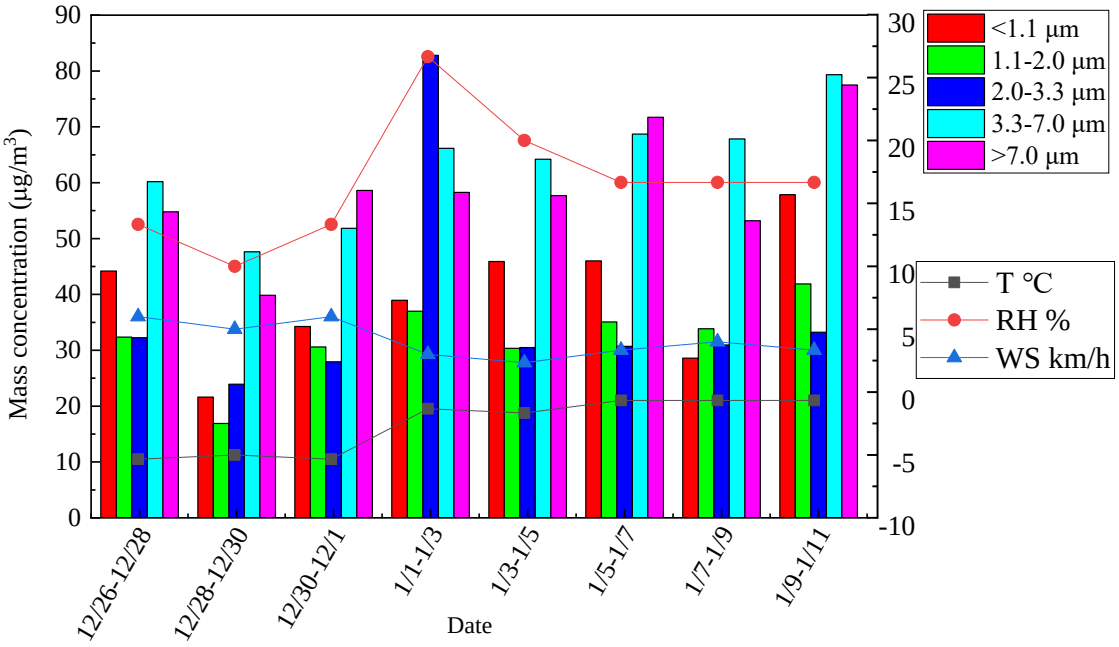

Fig. 16. The meteorological factors and mass concentrations in different size-resolved PM in Beijing

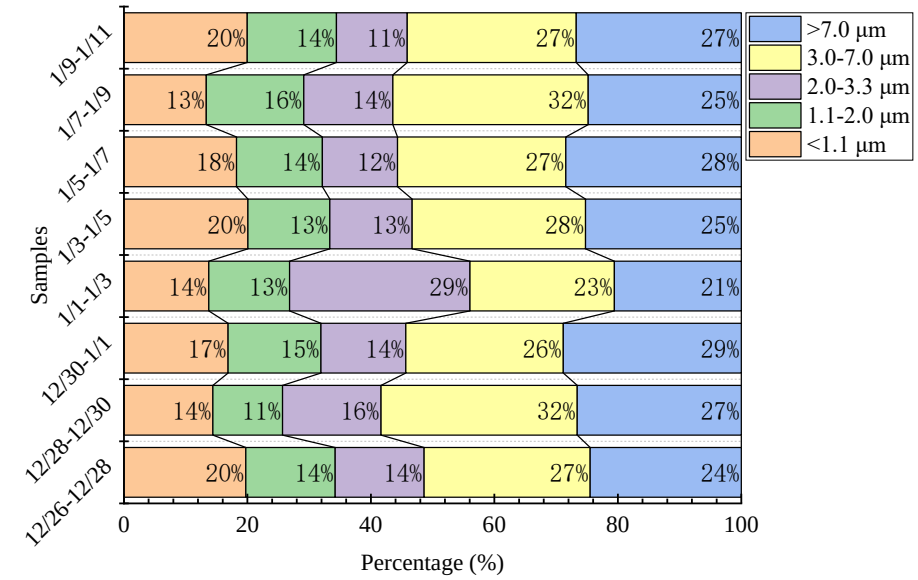

0

Fig. 17. Percentage of size-segregated in APMs particles in Beijing

The $PM_{2.0}$ mean concentration were ranged from 38.52 to 99.75 μg/m^3, which were 2.05 ± 0.47 times of average limit of 35 μg/m^3 for $PM_{2.5}$ (24-hour mean) set by Chinese national ambient air quality standards (CNAAQS) Grade I(GB3095-2012), and 4.79 ± 1.10 times than the $PM_{2.5}$ concentration of 15 μg/m^3 in the air quality guidelines (AQG) standard put forth by the WHO. The $PM_{7.0}$ mean concentration were ranged from 62.45 to 158.75 μg/m^3, which were 2.17 ± 0.54 times of average limit of 50 μg/m^3 for

PM_{10} (24-hour mean) set by Chinese national ambient air quality standards (CNAAQS) Grade I (GB3095-2012), and 2.41 ± 0.60 times than the PM_{10} concentration of 45 μg/m^3 in the air quality guidelines (AQG) standard put forth by the WHO (Table 12 and Table 13).

Percentage distribution of mass concentration (%) and international standard ratio for APMs are listed in Figure 17 and Table 13. Percentage distribution of mass concentration to TSP of $PM_{1.1}$, $PM_{1.1\text{-}2.0}$, $PM_{2.0\text{-}3.3}$, $PM_{3.3\text{-}7.0}$, and $PM_{>7.0}$ were ranged from 13.33 to 20.08 %, 11.28 to 15.79 %, 11.47 to 29.94 %, 23.37 to 31.77 % and 20.57 to 28.84 % in Beijing, respectively. which indicates that fine particles

Table 12. Mass concentration of size-segregated of APM in Beijing (μg/m^3)

Groups	<1.1 μm	1.1-2.0 μm	<2.0 μm	2.0-3.3 μm	3.0-7.0 μm	<7.0 μm	>7.0 μm	TSP
12/26-12/28	44.19	32.35	76.55	32.25	60.20	108.80	54.79	223.78
12/28-12/30	21.61	16.91	38.52	23.92	47.63	62.45	39.86	149.93
12/30-1/1	34.26	30.59	64.86	27.94	51.84	92.80	58.62	203.26
1/1-1/3	38.95	37.00	75.95	82.81	66.17	158.75	58.25	283.17
1/3-1/5	45.90	30.34	76.24	30.48	64.21	106.72	57.68	228.62
1/5-1/7	46.00	35.08	81.08	30.71	68.72	111.79	71.72	252.22
1/7-1/9	28.59	33.85	62.44	30.94	67.83	93.38	53.18	214.39
1/9-1/11	57.87	41.89	99.75	33.24	79.34	132.99	77.51	289.84
Average	39.67	32.25	71.92	36.54	63.24	108.46	58.95	230.65
Max	57.87	41.89	99.75	82.81	79.34	158.75	77.51	289.84
Min	21.61	16.91	38.52	23.92	47.63	62.45	39.86	149.93
STD	10.66	6.78	16.47	17.70	9.37	26.78	10.75	42.29

STD: Standard Deviation, Max: Maximum, Min: minimum

significantly contribute to atmospheric particulate matter pollution in winter in Beijing. It was also observed in previous studies (Yele Sun et al., 2006)(J. Duan et al., 2014). There is no large pollution source in the sampling site. But both $PM_{2.0}$ and $PM_{7.0}$ average concentrations in winter are similar to previous research in Beijing in winter($PM_{2.5}$ 85.47 μg/m^3 ,PM_{10} 107.20 μg/m^3) and higher in summer ($PM_{2.5}$ 60.20 μg/m^3 ,PM_{10} 46.3 μg/m^3) (Lv et al., 2019), which are attributable to the on transported from Tianjin-Hebei-Shandong province. These activities in the province are the frequent occurrence of unfavorable atmospheric diffusion conditions, resulting in increased air pollutant emissions (Lv et al., 2019) (Gao, Jiajia, et al., 2015).

It is generally acknowledged that primary source like road dust and soil as the main emission source of coarse particulate matter, while fine atmospheric particulate matters are emitted from both primary source and secondary formation due to complex chemical processes in the atmosphere (Lv et al., 2019).

Predominantly, high PM in the winter in Beijing was mainly attributed to the adverse meteorological conditions like low temperature and lower boundary layer height, less precipitation and weaker wind and solid fuel (coal) combustion for indoor heating (Z. Liu et al., 2019), Another reason may be that probably due to the transport of polluted air masses from urban areas (Hao et al., 2020).

Table 13. Percentage distribution of mass concentration to TSP (%) and international standard ratio for APM particles in Beijing

Percentage distribution of mass concentration (%)								International standard ratio			
								CAN AQS	CAN AQS	AQG	AQG
Groups	PM 1.1	PM 1.1-2.0	PM 2.0	PM 2.0-3.3	PM 3.3-7.0	PM 7.0	PM >7.0	$PM_{2.0}$/ $PM_{2.5}$	$PM_{7.0}$/ PM_{10}	$PM_{2.0}$/ $PM_{2.5}$	$PM_{7.0}$/ PM_{10}
12/26-12/28	19.75	14.46	34.21	14.41	26.90	48.62	24.48	2.19	2.18	5.10	2.42
12/28-12/30	14.42	11.28	25.69	15.95	31.77	41.65	26.58	1.10	1.25	2.57	1.39
12/30-1/1	16.86	15.05	31.91	13.75	25.51	45.66	28.84	1.85	1.86	4.32	2.06
1/1-1/3	13.76	13.06	26.82	29.24	23.37	56.06	20.57	2.17	3.18	5.06	3.53
1/3-1/5	20.08	13.27	33.35	13.33	28.09	46.68	25.23	2.18	2.13	5.08	2.37
1/5-1/7	18.24	13.91	32.15	12.18	27.24	44.32	28.43	2.32	2.24	5.41	2.48
1/7-1/9	13.33	15.79	29.12	14.43	31.64	43.55	24.80	1.78	1.87	4.16	2.08
1/9-1/11	19.96	14.45	34.42	11.47	27.37	45.88	26.74	2.85	2.66	6.65	2.96
Average	17.05	13.91	30.96	15.60	27.74	46.55	25.71	2.05	2.17	4.79	2.41
Max	20.08	15.79	34.42	29.24	31.77	56.06	28.84	2.85	3.18	6.65	3.53
Min	13.33	11.28	25.69	11.47	23.37	41.65	20.57	1.10	1.25	2.57	1.39
STD	2.69	1.30	3.14	5.32	2.66	4.09	2.45	0.47	0.54	1.10	0.60

STD: Standard Deviation, Max: Maximum, Min: minimum

2.6.5 Differences in atmospheric particulate matter between Xuanwei and Yunnan

According to the conclusions of 2.4.1 and 2.4.4.2 we find that the mass of atmospheric particles shows a bimodal distribution, with the major peak in the particle size <1.1 μm range while the minor peak in the size range of > 7 μm, respectively, it were consistent with previous studies (Q. Yan et al., 2020) (G. Shen et al., 2010).

The $PM_{2.0}$ mean concentration at Xuanwei and Beijing in winter were ranged from 52.21 to 93.75 μg/m^3 and ranged from 38.52 to 99.75 μg/m^3, respectively, which were 1.98 ± 044 times, 2.05 ± 0.47 times of average limit of 35 μg/m^3 for $PM_{2.5}$ (24-hour mean) set by Chinese national ambient air quality

standards (CNAAQS) Grade I(GB3095-2012). The levels of $PM_{2.0}$ in Xuanwei were lower than those in Chinese cities like Shijiazhuang (139 μg/m^3)(Y. Xie et al., 2019), Xi'an (108 μg/m^3)(Q. Dai et al., 2018), Xinxiang (94 μg/m^3)(K. Yang et al., 2019), and Beijing (83 μg/m^3)(Ji et al., 2019), while it was higher than Fuzhou (27 μg/m^3), Nanjing (55 μg/m^3)(Nie et al., 2018), and Chengdu (57 μg/m^3)(H. Qiu et al., 2019). The $PM_{7.0}$ mean concentration at Xuanwei and Beijing in winter were 2.21 ± 0.45 times and 2.17 ± 0.54 times of average limit of 50 μg/m^3 for PM_{10} (24-hour mean) set by Chinese national ambient air quality standards (CNAAQS) Grade I (GB3095-2012).

Numerous studies have been conducted to analyze the mass concentration, particle size distribution, and composition of atmospheric particulate matter. The annual mean concentrations of $PM_{2.5}$ at Luoyang and Pingdingshan sites were 128 ± 66 (range 43 to 315 μg/m^3) and 119 ± 71 μg/m^3 (range 27 to 448 μg/m^3), respectively, which were 3.6 and 3.4 times of annual average limit of 35 μg/m^3 set by Chinese National Ambient Air Quality Standard of grade 2 (NAAQS II) (Q. Wang et al., 2020). The average outdoor $PM_{2.5}$ mass concentration was 41.7 ± 25.1 μg/m^3 , which were collected from December 2018 to September 2020, a total of 171 indoor-outdoor pairs of samples in Nanjing (F. Yang et al., 2021).

The results show that the particulate matter pollution in Xuanwei is not serious and is at a medium level in the country, indicating that the mass concentration of particulate matter is not a major factor of lung cancer in Xuanwei, but it is possible that the local particulate matter in Xuanwei contains some special components or the content of certain pollutants exceeds the standard.

2.7. Brief summary

1) We collected six groups of atmospheric particulate matter, three types of biomasses, and six types of raw coal in Xuanwei, Yunnan, an area with a high incidence of lung cancer and eight sets of atmospheric particulate matter samples were collected in Beijing

2) Simulated combustion of biomass and raw coal.

3) Comparing the different type particulate matter, we found that the mass concentration of particulate matter emitted from solid fuel combustion was mainly concentrated in particle size < 2.0 μm (58.17 ± 3.59 % for RBC particles, 67.02 ± 9.06 % for RCC particles), while the mass concentrations of atmospheric particulate matter were mainly concentrated in the particle size < 2.0 μm (49.74 ± 2.15 %) and >7.0 μm (20.28 ± 3.29 %). It indicates that the emission of fine particulate matter from raw coal combustion is more than that from biomass combustion, and the health risk is not negligible as the ambient atmosphere is dominated by fine particulate matter.

4) We found that the mass of atmospheric particles showed a bimodal distribution, with the major peak in the range of particle size <1.1 μm and the minor peak in the range of size >7 μm. In contrast, the concentration of particulate matter emitted from solid fuel combustion is mainly concentrated in the range of particle size <1.1 μm.

5) Xuanwei area, there are no large sources of pollution in the vicinity of the sampling site, and its pollution may be caused by solid fuel combustion, road transport, dust from construction sites, exhaust emissions from cars or mining in the county, and long-distance transport of pollution from surrounding cities.

6) Beijing area, it is generally acknowledged that primary source like road dust and soil as the main emission source of coarse particulate matter, while fine atmospheric particulate matters are emitted from both primary source and secondary formation due to complex chemical processes in the atmosphere. Predominantly, high PM in the winter in Beijing was mainly attributed to the adverse meteorological conditions like low temperature and lower boundary layer height, less precipitation and weaker wind and solid fuel (coal) combustion for indoor heating. another reason may be that probably due to the transport of polluted air masses from urban areas.

7) The results show that the particulate matter pollution in Xuanwei is not serious and is at a medium level in the country, indicating that the mass concentration of particulate matter is not the main factor of lung cancer in Xuanwei, which may be due to the possibility that the local particulate matter in Xuanwei contains some special components or the content of certain pollutants exceeds the standard.

Chapter 3 Materials and methods

3.1 Ion Chromatography (IC)

3.1.1 Principle of IC

Ion chromatography (IC) is a liquid chromatography method used to analyze anions and cations. According to the principle of separation, ion chromatography can be grouped into ion exchange chromatography, ion exclusion chromatography, ion pair chromatography. Ion chromatography is capable of measuring concentrations of major anions, such as fluoride, chloride, nitrate, nitrite and sulfate, and major cations, such as lithium, sodium, ammonium, potassium, calcium and magnesium, in the parts per billion (ppb) range. Ion chromatography is a form of liquid chromatography in which ionic species are separated based on their interaction with a resin to measure their concentration. The ionic species are separated in different ways, depending on the type and size of the species. The sample solution is passed through a pressurized column and the ions are absorbed by the components on the column. The absorbed ions begin to separate from the column as the ion extract, called the eluent, flows through the column. The retention time of different species determines the concentration of ions in the sample.

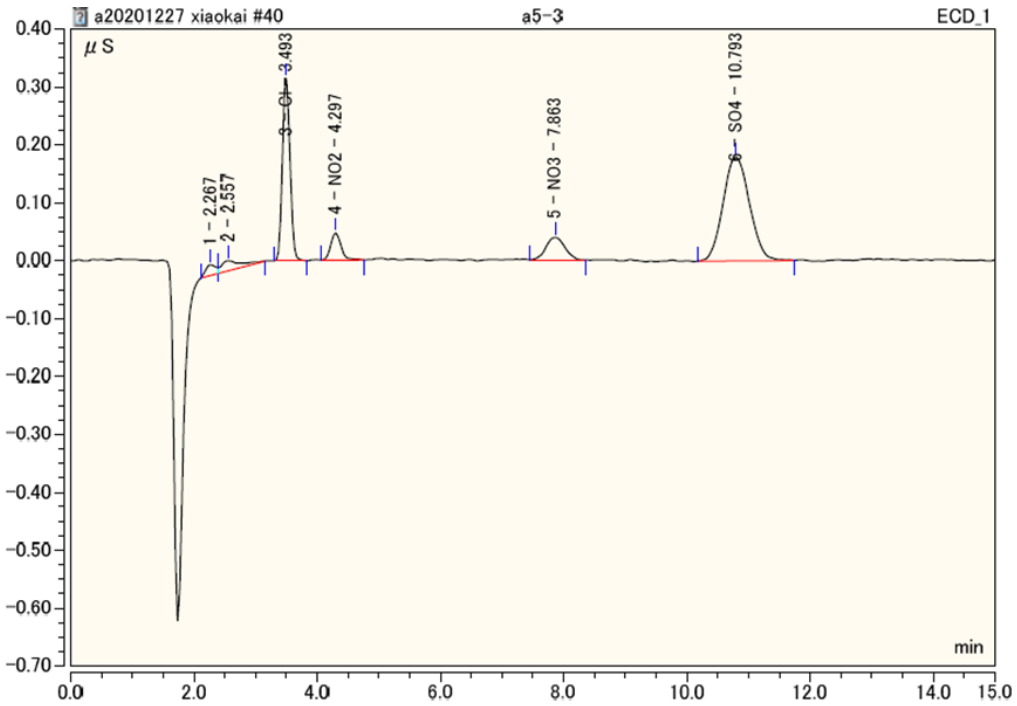

Fig. 18. The anion concentrations

Each peak represents an individual ion from the sample solution. The elution time, i.e., the time required for an ion to pass through the column, varies for each ionic species separately from the column as the pH and/or ionic strength of the eluent increases. The concentration of ions passing through the column at a particular time is indicated by the height and width of the peak and can be correlated with the concentration of a particular species in the sample solution (Fig 18 and Fig 19). Ion concentrations can be calculated using the area under each peak, where a larger area correlates with a higher concentration of a particular ion species. Most ion chromatography machines provide software that calculates this area, which users can convert to ppm or other quantity using calibration standard solutions.

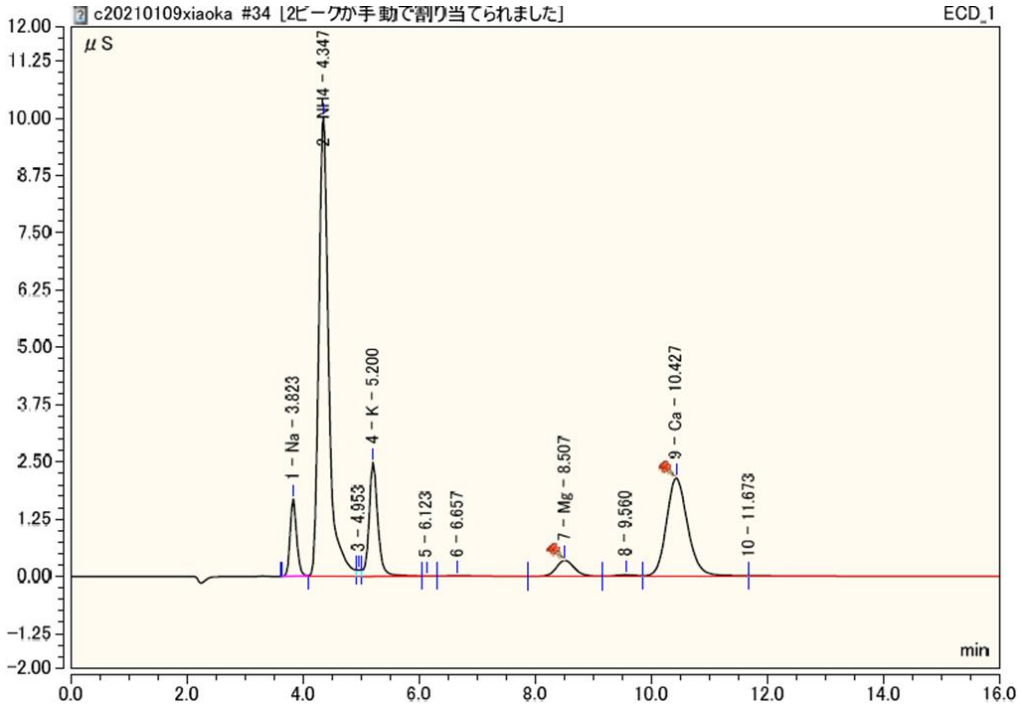

Fig. 19. The cation concentrations

Fig 18 shows anion concentrations and the Fig 19 depicts cation concentrations from this research samples.

3.1.2 The advantages of IC

The main impetus for the early development of ion chromatography was the analysis of anions, which became the first choice for anion analysis due to its ability to separate a wide range of inorganic anions in a short period of time. Currently, ion chromatography has many advantages in ion analysis, such as high sensitivity and selectivity, fast separation, simultaneous analysis of multiple ionic

compounds, good stability of separation columns, and high capacity. Compared with chemical analysis, chromatography is not limited by the chemical properties of compounds and can be used to separate and determine homologues and optical isomers with the same chemical properties (X. Liu et al., 2021).

3.1.3 Applications of IC

Currently, ion chromatography has been widely used in environmental monitoring (H. Feng et al., 2020), power and energy industry (Marocco et al., 2021), electronics industry (Y. Lu et al., 2019), food industry (Gasparini et al., 2020) and beverage industry (Ye et al., 2021), chemical industry (Cai et al., 2016), pharmaceutical industry (Jenke, 2011), and other fields (M. Shen et al., 2020). Meanwhile, due to the wide application of ion chromatography, the diversity and complexity of the samples to be measured have put higher demands on the separation performance of ion chromatography.

3.1.4 Ion balance calculation

The acidity of aerosols is an effective method for assessing the pH of atmospheric PM, which promotes heterogeneous reactions of particulate matter on surfaces and the formation of secondary inorganic ions (J. Fan et al., 2020). In this study, the acidity of PM, which is calculated by converting the concentrations of anions and cations (μg m^{-3}) into micro-equivalents (μeq·m^{-3}) by the following equations (C. C. Meng et al., 2016) (Qiao et al., 2019)(Zhan et al., 2021)(2-3):

$$ANE = [SO_4^{2-}]/48 + [NO_3^-]/62 + [Cl^-]/35.5 + [NO_2^-]/46 \quad (2)$$

$$CAE = [Na^{2-+}]/23 + [NH_4^+]/18 + [K^+]/39 + [Mg^{2+}]/12 + [Ca^{2+}]/20 \quad (3)$$

where $[SO_4^{2-}]$, $[NO_3^-]$, $[Cl^-]$, $[NO_2^-]$, $[Na^{2-+}]$, $[NH_4^+]$, $[K^+]$, $[Mg^{2+}]$, and $[Ca^{2+}]$ represent the mass concentration of detected WSIIs. Generally, the value of ANE / CAE = 1 indicates that the anions and cations are in equilibrium; ANE / CAE $>$ 1 indicates that PM is acidic; and ANE / CAE $<$ 1 indicates that PM is alkaline (Zhan et al., 2021)(Jingyi Li et al., 2020)(Qiao et al., 2019).

3.1.5 Pre-treatment and analysis of Water-Soluble Inorganic Ionic Species (WSIIs) of samples

An ultrasonic method was used to extract water-soluble inorganic ions from portions of the PM filter samples, and normally over 98 % of sulfate, nitrate, and ammonium can be extracted. The filter was submerged in a vial with 10 mL ultrapure water (resistivity > 18 $M\Omega cm^{-1}$), sealed and subjected to ultrasound for 10 min for each extraction. The extraction was repeated 3 times. Extract solution were filtered with a pore size of 0.20 μm polytetrafluoroethylene and then the concentration of water-soluble inorganic ions (Cl^-, NO_3^-, NO_2^- , SO_4^{2-}, NH_4^+, Na^+, K^+, Ca^{2+} and Mg^{2+}) were analyzed by Ion Chromatography to determine the concentrations of water-soluble inorganic ions. The analysis includes 6 groups of atmospheric samples, 3 groups of biomasses simulated combustion samples and 6 sets of raw coal simulated combustion samples in Xuanwei area, and 8 groups of atmospheric samples in Beijing area.

3.1.6 Required Instruments and Chemical Reagents in Experiment

The required experimental instruments include

(1) Ultrasonic cleaner (USD-3R, 1-4592-33, Monota RO Co., Ltd. Japan)

(2) 0.20 μm polytetrafluoroethylene (PTFE; DISMIC-13HP, Toyo Roshi Kaisha, Ltd. Japan)

(3) Ion Chromatography (IC, ICS1600, Dionex Aquion, Thermo Fisher Scientific CO, Waltham, MA, USA)

The main standard solutions and chemical reagents in the experiment are

(1) Multianion standard solution II for Iron chromatography (Wako pure chemical industries Co. Ltd. Japan)

(2) Multication standard solution II for Iron chromatography (Wako pure chemical industries Co. Ltd. Japan)

(3) Sodium carbonate (Wako pure chemical industries Co. Ltd. Japan)

(4) Sodium hydrogen carbonate (Wako pure chemical industries Co. Ltd. Japan)

(5) Methanesulfonic acid Sodium hydrogen carbonate (Wako Special Grade, Wako pure chemical industries Co. Ltd. Japan)

3.2 Inductively coupled plasma mass spectrometer (ICP-MS)

3.2.1 Principle of ICP-MS

Inductively coupled plasma mass spectrometry (ICP-MS) is a mass spectrometry method that uses an inductively coupled plasma to ionize the sample. It atomizes the sample and produces atoms and small polyatomic ions, which are then detected. It is known and used for its ability to detect metals and several non-metals in liquid samples at very low concentrations. It can detect different isotopes of the same element, which makes it a versatile tool for isotope labeling.

Plasma is the ionization source for ICP, while positively charged ions are the mass analyzer for mass spectrometry (MS). Generally, argon is used to generate plasma at high frequencies (30 MHz) with energies between 1000 and 2000 W, since most elements in the periodic table are excited and ionized in the plasma temperature range of 6000-10,000 K. The torch is made of quartz and consists of three concentric tubes through which the argon gas flows. When a sample is introduced into the plasma, it goes through desolation, vaporization, atomization and ionization before entering the mass analyzer (Thomas, 2002).

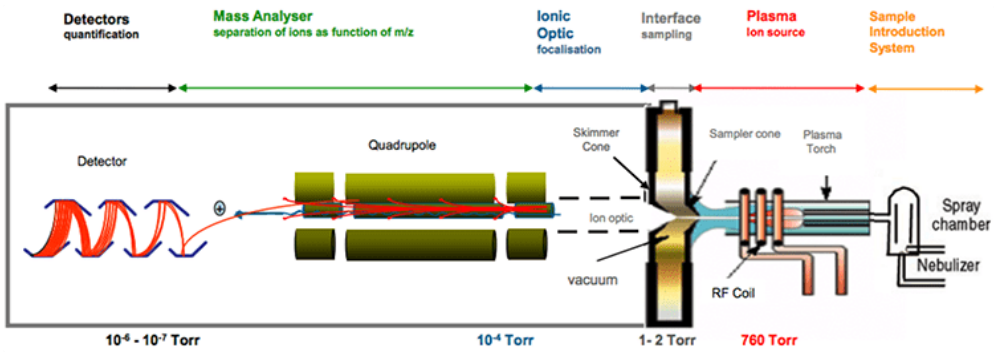

Fig. 20. A schematic diagram of the working functions of ICP-MS.

How ICP-MS works: The sample, which must usually be in liquid form, is pumped at a rate of 1 ml/min, usually with a peristaltic pump, into an atomizer where it is converted into fine aerosols with argon gas at a rate of about 1 l/min. The fine droplets of aerosol make up only 1-2% of the sample and are separated from the larger droplets by a spray chamber. The fine aerosol then exits the outlet tube of the spray chamber and is delivered to the plasma torch via a sample injector. The schematic diagram of the working functions of ICP-MS was shown in Fig 20.

3.2.2 The advantages of ICP-MS

CP-MS has some distinct advantages, including the ability to perform simultaneous multi-element measurements and very low detection limits; therefore, this technique is suitable for biomonitoring studies and occupational exposure monitoring. In addition, ICP-MS offers lower detection limits and simpler spectral interpretation than inductively coupled plasma atomic (optical) emission spectrometry (ICP-OES); it also provides isotopic information (Parsons & Barbosa, 2007).

3.2.3 Applications of ICP-MS

Inductively coupled plasma mass spectrometry (ICP-MS) is increasingly used for trace analysis in a number of industries and types of laboratories. developed in the late 1980s, ICP-MS combines the simple sample introduction and rapid analysis of ICP technology with the precision and low detection limits of mass spectrometry. The instrument can perform trace multi-element analysis, typically at the parts-per-trillion or parts-per-trillion level. ICP-MS is used in many different fields, including drinking water, wastewater, environmental chemistry (Hirner, 2006), geology and soil science, mining/metallurgy, food science, and medicine (J. Huang et al., 2006).

3.2.4 Analysis of Potentially Toxic Metals (PTMs) and Water-Soluble Potentially Toxic Metals (WSPTMs) by ICP-MS

Potentially Toxic Metals (PTMs): Inductively coupled plasma mass spectrometer was used to identify 21 elemental species (Na, Mg, Al, K, Ca, Ti, V, Cr, Mn, Fe, Co, Ni, Cu, Zn, As, Se, Sr, Cd, Sb, Ba, Pb) concentration For Beijing samples. After weighting, a certain amount of filter was cut and placed in polytetrafluoroethylene (PTFE) reaction tubes, then each filter was digested with a 5： 2： 1 mixture of HNO_3-H_2O_2-HF in PTFE vessels and heated in a microwave system (ETHOS UP, MAXI-44). There were six heating steps for microwave digestion of filter: 1) the temperature was increased from room temperature to 90 °C and was maintained for 3 mins; 2) the temperature was increased from 90 to 150 °C and was maintained for 5 mins; 3) the temperature was increased from 150 to 175 °C and was maintained for 17 mins; 4) the temperature was increased from 175 to 200 °C and was maintained for 30 mins; 5) after cooling for 30 minutes, remove the polypropylene reaction vessel from the microwave sample

pretreatment device, and put the decomposition solution in the PTFE reaction vessel into the polypropylene digestion tube ; 6) place the polypropylene digestion tube in the acid decomposition system and heat it at 100°C for about 5 hours to remove hydrofluoric acid until the solution is about 0.1 mL . The digested solution was then diluted to 10 mL with 2 % HNO_3 and stored at room temperature until analysis. Three blank filters were treated and analyzed with the same methods as for and metals to obtain background values. Potential toxic metals were analyzed by ICP-MS at the Center for Environmental Science in Saitama (CESS) in Japan (K. Xiao, Wang, et al., 2021)(K. Xiao, Qin, et al., 2021).

Water-Soluble Potentially Toxic Metals (WSPTMs): In brief, normally the extraction rate of sulfate, nitrate and ammonium can reach more than 98 %. After weighing, portions of the sample filters (include three blank filters) were submerged in a vial were ultrasonically extracted with 10 mL ultrapure water (resistivity > 18 MΩcm-1) and repeated three times, each time for 10 min. The aqueous extract solution was filtered with a pore size of 0.20 μm polytetrafluoroethylene (PTFE; DISMIC-13HP) membranes. Then, the solution after filtration, WSPTMs (V, Cr, Mn, Co, Ni, Zn, As, Cd, Ba, and Pb) were analyzed by inductively coupled plasma mass spectrometer (ICP-MS) to determine the concentrations at the Center for Environmental Science in Saitama (CESS) in Japan.

3.2.5 Required Instruments and Chemical Reagents in Experiment

The required instruments in the experiment are:

(1) Ultrasonic cleaner (USD-3R, 1-4592-33, Monota RO Co., Ltd. Japan)

(3) Microwave digester

(4) Inductively coupled plasma-mass spectrometry (ICP-MS, Agilent770, Agilent Co. Ltd., USA)

The main chemical reagents are:

(1) Nitric acid (Wako pure chemical industries Co. Ltd. Japan)

(2) Hydrofluoric acid (Wako pure chemical industries Co. Ltd. Japan)

(3) Hydrogen peroxide (Wako pure chemical industries Co. Ltd. Japan)

(4) Indium (Wako pure chemical industries Co. Ltd. Japan)

3.3 Total Organic Carbon Analyzer (TOC)

3.3.1 Principle of Total Organic Carbon Analyzer (TOC)

The TOC analyzer identifies total organic carbon by using non-dispersive methods of infrared absorption and high-temperature combustion, which are suitable for a wide variety of wastewater tests. Essentially, the TOC analyzer has a special low-temperature reaction tube and a high-temperature combustion tube in which high-purity oxygen is introduced into the wastewater sample. Under the strong influence of high-temperature oxidation, the wastewater sample is rapidly oxidized, which significantly converts carbon dioxide, inorganic carbonates and other organic substances. At the same time, the low temperature reaction tube can also be used to generate high purity carbon dioxide, using a mixture of inorganic carbonates and organics to achieve the above chemically generated treatment.

Total Organic Carbon TOC is a valuable analytical technique for measuring organic contamination levels or the organic content of an analyte matrix. The basic function of a TOC analyzer is to first oxidize organic carbon in an aqueous solution to carbon dioxide and then measure the resulting carbon dioxide. In the measurement principle, the organic carbon compounds present in the aqueous solution in question are first oxidized to carbon dioxide in a catalytic combustion at 680ºC. The carbon dioxide is then transported by a carrier gas, which is cooled and dehumidified, and finally passes through a halogen scrubber into the NDIR (non-dispersive infrared) unit, where the carbon dioxide is detected. The detection signal of the non-dispersive infrared will produce a peak. The peak region can be used for integration. The use of low combustion temperatures (680ºC) minimizes catalyst deactivation and combustion tube corrosion. By using a platinum catalyst, complete oxidation of all organic compounds can be obtained.

What is measured when calculating Total Organic Carbon?

When completing TOC analysis, the following is measured:

- TC – Total Carbon
- TIC – Total Inorganic Carbon
- POC – Purgeable Organic Carbon
- NPOC – Non-Purgeable Organic Carbon
- DOC – Dissolved Organic Carbon
- NDOC – Non-Dissolved Organic Carbon

To calculate TOC, you can subtract the total amount of inorganic carbon from total carbon found. Alternatively, you can add Purgeable and Non-Purgeable Organic Carbon, or Dissolved and Non-Dissolved Organic Carbon. As sums, they look like:

TOC = TC - TIC

TOC = POC + NPOC

TOC = DOC + NDOC

3.3.2 The advantages of TOC Analyzer

(1) Total organic carbon analyzers can objectively help to eliminate errors and avoid confusion about critical processes.

(2) TOC techniques should be among the most convenient and controllable types of detection measures. Specifically in the detection of TOC, this method allows for the rapid identification of toxic residues, which involves sample selection and online detection without significant contamination.

(3) The TOC method addresses avoid certain errors caused by human operations, and also better reproducibility and a higher level of sensitivity.

The combustion catalytic oxidation method with 680 °C achieves both high organic matter detection capacity and high measurement sensitivity. The ultrawide range from 4 µg/L to 30,000 mg/L permits measurements from purified water to highly-polluted water. The combustion catalytic oxidation method analyzes TOC by burning the sample and using an infrared gas analyzer to detect the carbon dioxide generated from the carbon contained in the organic matter. The high oxidation decomposition capacity permits the efficient detection of insoluble organic matter and covers a wide range from low concentrations to high concentrations.

3.3.3 Analysis of Humic Like Substances (HULIS) and Water-Soluble Organic Carbon (WSOC)

In this study, only coal-fired particulate matter was analyzed for HULIS and WSOC(Tiede et al., 2009). Many published studies have shown that HULIS is usually isolated by solid phase extraction (SPE) (X. Fan, Wei, et al., 2016)(Park & Yu, 2016)(Win et al., 2020)(Huo et al., 2021). The flow chart of

HULIS-C (black arow) and WSOC (blue arow) isolation and measurement are illustrated in Figure 21. In order to obtain the water-soluble fraction of PMs (a, b), as described in Section 2.3. The water extracts were filtered through a syringe PTFE filter with a 0.20 μm PTFE to avoid any interference (insoluble suspensions, filter debris) from residual quartz filters (S. Lu et al., 2019). Then, 10 mL of the aqueous extract was acidified to pH=2 with 1 M hydrochloric acid and loaded onto a pretreated C-18 solid phase extraction column (octadecyl carbon chain bonded silica gel; 200 mg, 3 mL) to separate into HULIS and hydrophilic fractions. Subsequently, C-18 was rinsed with two portions of 1 mL ultrapure water before elution with 4.5 mL of high-performance liquid chromatography grade methanol containing 2 % ammonia (w/w). Finally, the eluate was dried under a gentle nitrogen stream for 5~7 hours and re-redissolved in 10 mL of ultrapure water and then was analyzed by a total organic carbon analyzer (Multi N/C 3100 TOC, Analytik Jena, Germany). The details of WSOC were described in previous study (a ~ c, h) (Yanrong Yang et al., 2020)(Xiang et al., 2017). WSOC were measured by a by a total organic carbon analyzer. In this study, HULIS-C refers to HULIS with carbon content, and the OC/Organic Matter (OM) conversion factor was not used to convert the quality of HULIS due to the uncertainty of the OC/OM conversion factor method and the lack of OC/OM conversion factors for RCC particles. Therefore, the generic term "HULIS" is used to interpret some results and discussions (K. Xiao, Wang, et al., 2021)

.

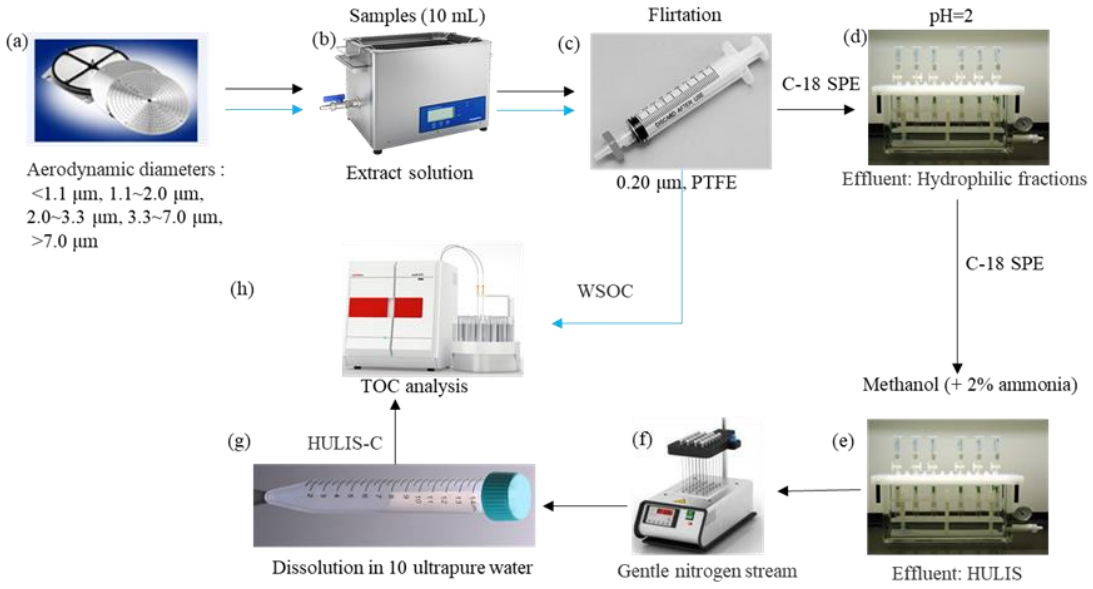

Fig. 21. The flow chart of HULIS-C (black arow) and WSOC (blue arow) isolation and measurement.

3.4 Electron Spin Resonance (ESR)

3.4.1 Principle of Electron Spin Resonance (ESR)

Electron spin resonance (ESR) is a powerful analytical method to detect, analyze and characterize unpaired electrons in matter. Electron spin resonance spectroscopy, it is a branch of absorption spectroscopy in which radiation having frequency in microwave region is absorbed by paramagnetic substance to induce transition between magnetic energy level of electron with unpaired spins. The composition of ESR is shown in the figure 22.

In ESR the energy levels are produced by the interaction of magnetic moment of an unpaired electron in a molecule or ion with an applied magnetic field. Required frequency of radiation dependent upon strength of magnetic field. The ESR spectrum results due to the transitions between these energy levels by absorbing radiations of microwave frequency (Tingming Shi et al., 2003).

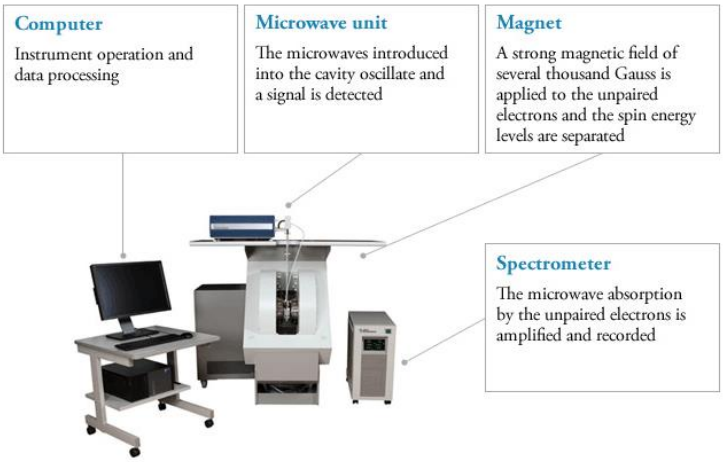

Fig. 22. The composition of ESR

3.4.2 Applications of ESR

Electron paramagnetic resonance is used in a wide range of applications in chemistry, physics, materials, semiconductors, organic chemistry, complex chemistry, radiation chemistry, chemical engineering, marine chemistry, catalysts, biology, biomedicine, environment, life sciences, etc., without destroying the structure of the object of study or affecting the ongoing chemical and physical processes.

3.4.3 Detection of EPFRs

Electron spin resonance (ESR) spectroscopy was used to determine EPFRs. To determine EPFRs, quartz fiber filters were cut into strips of 3-4 mm, then added to a quartz EPR tube and measured on the corresponding instrument. The relevant parameters were as follows: Sweep time,120 s; Center field 324.74 mT; sweep width, 25 mT; modulation frequency, 100 kHz; modulation Width, 0.05 mT; microwave frequency 9105.26 MHz; and microwave power, 0.998 mW.

3.4.4 Data processing and calculation of the absolute number of spins

ESR tests were performed on standards containing Mn (II) to calibrate the absolute number of spins and, then, characteristic parameters such as the g factor, and $\Delta Hp\text{-}p$ of the EPFRs were obtained. The formula used to calculate the spin numbers and g factors are shown in equation (2-3) (X. Tian et al., 2019) (P. Qiu et al., 2021) (Runberg et al., 2020):

$$g = 0.07145 \times \lambda\,(\mathrm{MHz}) / H\,(\mathrm{mT}) \quad (2)$$

$$\mathrm{Spins_{sample}}\,(\mathrm{spins/g}) = 3.02*10^{14}\,(\mathrm{spins/g}) \times \mathrm{Integral_{sample}} / \mathrm{Integral_{standard}} \quad (3)$$

Where g is the electron spin g-factor of the particle, λ (MHz) represents the microwave frequency, H (mT) is the resonance magnetic field strength during the measurements. $3.02*10^{14}$ is is the total spins of the standard Mn, $\mathrm{Spins_{sample}}$ is the spin concentration of the unknown sample, $\mathrm{Integral_{sample}}$ and $\mathrm{Integral_{standard}}$ represent the signal integration areas of the sample and Mn (II) standard, respectively (Runberg et al., 2020). The sample atmospheric spin concentrations of EPFRs (spins/m^3) were calculated as the total spin divided by the total sample volume. The EPFR spin concentrations in PM masses (spins/g) were determined as the total spin divided by the collected PM mass.

Chapter 4 Result and Discussions

4.1 Water-Soluble Inorganic Ionic Species (WSIIs)

4.1.1 The Levels of Water-Soluble Inorganic Ionic Species (WSIIs) in APMs

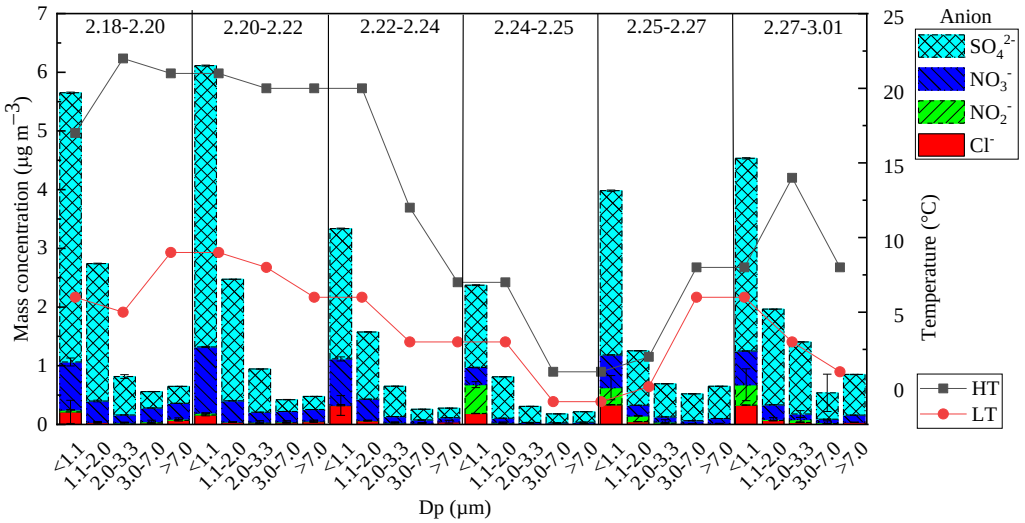

Fig.23. The anion and cation of average mass concentration within $PM_{1.1}$, $PM_{1.1\text{-}2.0}$, $PM_{2.0\text{-}3.3}$, $PM_{3.3\text{-}7.0}$, and $PM_{>7.0}$ during the sampling period. (HT and LT represent the highest temperature and lowest temperature on the sampling day, respectively)

Fig. 23 and Fig. 24 illustrates the intra-groups variations in particulate-bound ion concentration. The total WSIIs concentration mainly concentrated in $PM_{1.1}$. Fine particulates $PM_{2.0}$ were enriched in SO_4^{2-}, $NO_3^-$and NH_4^+ accounting 10.99 ± 2.48% of $PM_{2.0}$ mass concentration (Table.14), which was lower ($PM_{2.1}$, 16%) than in urban environment over central Indo-Gangetic Plain (Singh et al., 2021); while rest of the ions (like Cl^-, NO_2^-, Na^+, K^+, Ca^{2+}, and Mg^{2+}) altogether contribute 1.54 ± 0.60%. The mean mass concentration of SO_4^{2-}, $NO_3^-$and NH_4^+ were 2.13 ± 0.78 μg m^{-3}, 0.84 ± 0.240.36 ± 0.15 μg m^{-3} and 0.36 ± 0.15 μg m^{-3} in $PM_{2.0}$, respectively.

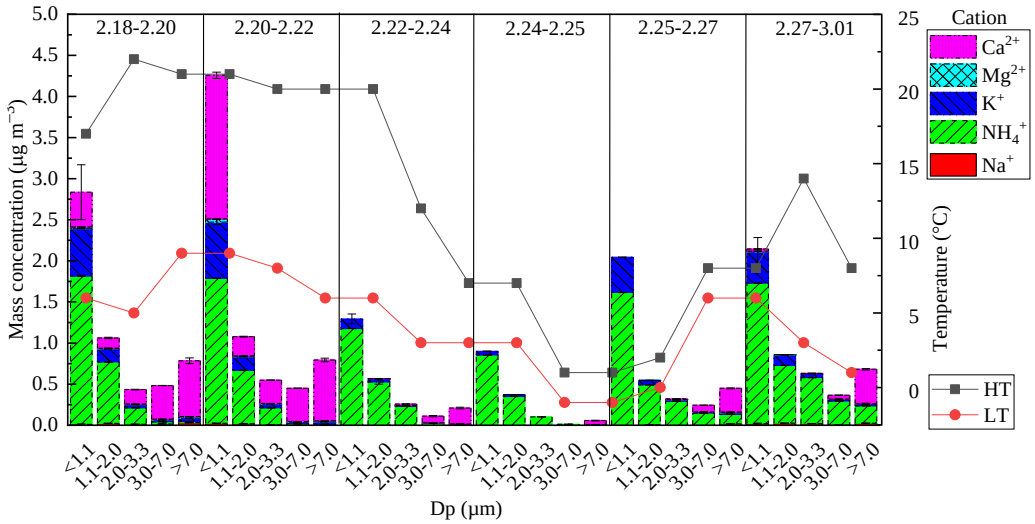

Fig.24. The cation average mass concentration within $PM_{1.1}$, $PM_{1.1\text{-}2.0}$, $PM_{2.0\text{-}3.3}$, $PM_{3.3\text{-}7.0}$, and $PM_{>7.0}$ during the sampling period. (HT and LT represent the highest temperature and lowest temperature on the sampling day, respectively)

Table 14. Contribution of ions to APMs mass concentration

Groups	Mass concentration (μg/m³)						Percentage (%)				
	TSP	$PM_{2.0}$	TSP		$PM_{2.0}$		TSP		$PM_{2.0}$		$PM_{2.0}$/TSP
			WSIIs	SNA	WSIIs	SNA	WSII/PM	SNA/PM	WSII/PM	SNA/PM	WSIIs/WSIIs
2.18-2.20	168.0899	85.33	16.02	12.75	12.29	10.66	9.53	7.59	14.40	12.49	66.56
2.20-2.22	197.7504	93.75	17.56	12.68	13.92	10.76	8.88	6.41	14.85	11.48	61.29
2.22-2.24	99.50432	52.21	8.54	7.57	6.77	6.22	8.58	7.60	12.98	11.92	72.84
2.24-2.25	122.6934	57.05	5.33	4.47	4.46	3.68	4.35	3.64	7.81	6.45	69.02
2.25-2.27	135.5148	69.87	10.71	8.91	7.83	6.56	7.90	6.58	11.20	9.40	61.32
2.27-3.01	115.2148	57.30	13.98	11.85	9.50	8.15	12.13	10.29	16.58	14.22	58.29
Mean	139.79	69.25	12.02	9.71	9.13	7.67	8.56	7.02	12.97	10.99	64.88
Max	197.75	93.75	17.56	12.75	13.92	10.76	12.13	10.29	16.58	14.22	72.84
Min	99.50	52.21	5.33	4.47	4.46	3.68	4.35	3.64	7.81	6.45	58.29
STD	33.41	15.50	4.26	3.04	3.22	2.52	2.31	1.97	2.84	2.48	5.04

The mass concentration of total WSIIs shows a strong correlation with the mass concentration of particulate matter (r = 0.76), HT (r = 0.79) and LT (r = 0.84) (Fig 25), indicates that temperature is an important factor affecting the mass concentration of atmospheric particulate matter and the mass concentration of ionic WSIIs. The concentration of WSIIs in the group of 2.18-2.20 and 2.20-2.22 were higher than the other group of samples, which can be explained the former has better weather conditions (sunny days) during the sampling period, where strong photochemical reactions occur in favor of aerosol formation, and the latter has light rain during the sampling period, resulting in wet deposition.

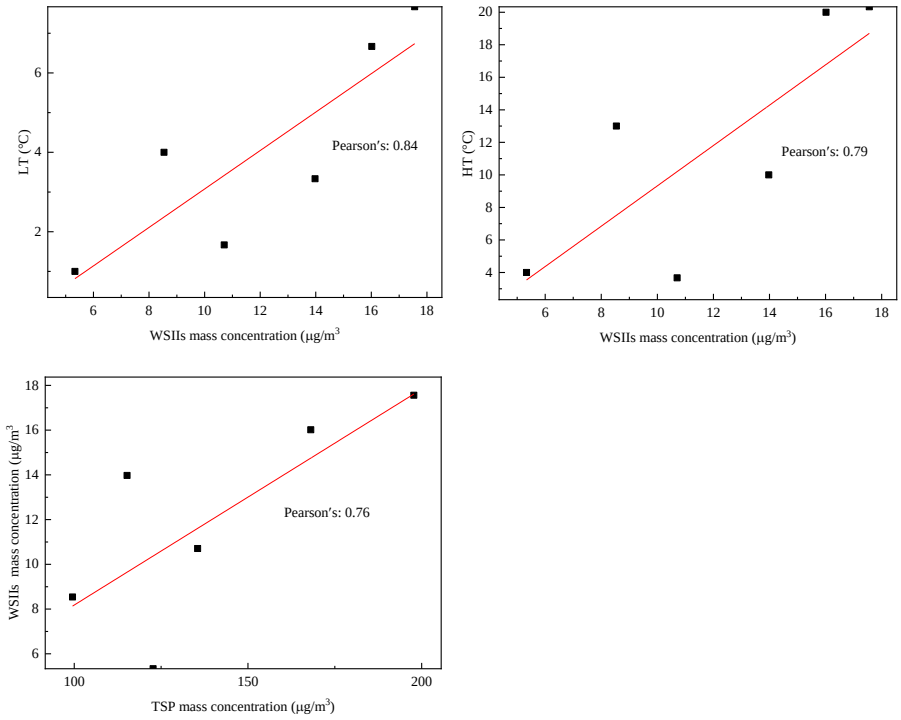

Fig. 25. The Pearson correlation coefficients between APMs average mass concentration and WSIIs average mass concentration, HT and LT.

4.1.2 The Levels of Water-Soluble Inorganic Ionic Species (WSIIs) in APMs

The size distribution of water-soluble inorganic ionic species can be used to infer the chemical properties and origin of aerosols ,which affect their transport through the atmosphere (X. Huang et al., 2016). Size distributions of the water-soluble inorganic ionic species within $PM_{1.1}$, $PM_{1.1\text{-}2.0}$, $PM_{2.0\text{-}3.3}$, $PM_{3.3\text{-}7.0}$, and $PM_{>7.0}$ are shown in Fig. 26. The average concentration of Cl^-, NO_2^-, SO_4^{2-}, and K^+ presented unimodal distributions with major peaks in the fine mode at $PM_{1.1}$, accounting for 67.12%, 78.33 %, 53.44 %, and 73.35% (Table 15), which is consistent with previous studies (X. Wu et al., 2020)(Jianwei Liu et al., 2018). As with SO_4^{2-}, the size distribution of NO_3^- and NH_4^+ were unimodal, peaking at <1.1 μm with 54.05% and 55.89 % found in $PM_{1.1}$, respectively. This suggests that gas-to-particle condensation reactions may be the dominant process in NH_4^+ formation. NO_x, SO_2, and NH_3 are the gaseous precursors of NO_3^-, SO_4^{2-}, and NH_4^+ , respectively (Xin Zhang et al., 2021), therefore, the ratio of NO_3^-/SO_4^{2-} could be used to judge the relative contributions of transportation (such as motor vehicle exhausts) and stationary sources (such as coal burning) (K. Xiao, Qin, et al., 2021). In developed countries, NO_3^-/SO_4^{2-} is between 1.33 and 2.20. Since coal accounts for more than 70% of total energy

in China and car ownership is lower than in developed countries, NO_3^-/SO_4^{2-} is usually less than 1, mainly 0.13-0.67 (X. Wu et al., 2020). The average ratio of NO_3^-/SO_4^{2-} within in $PM_{1.1}$, $PM_{1.1\text{-}2.0}$, $PM_{2.0\text{-}3.3}$, $PM_{3.3\text{-}7.0}$, and $PM_{>7.0}$ were 0.22, 0.18, 0.15, 0.34 and 0.36, it indicating that stationary industrial and combustion sources contributed to PM were more significant. In fine particles, NO_3^- exists mainly in the form of NH_4NO_3 (X. Huang et al., 2016). NH_4^+ and K^+ are important tracer of biomass burning emissions (Xin Zhang et al., 2021), was highly enriched in fine particulate ($PM_{2.0}$), both of them has also sources like agricultural practices and livestock emissions. Generally, Cl^- is also to be the marker for coal combustion and biomass burning (X. Wu et al., 2020). During the sampling period, coal, corn cobs, and pine wood were widely used by residents for heating and cooking. Therefore, Cl^-, NO_3^-, NO_2^-, SO_4^{2-}, and NH_4^+ mainly emitted from solid fuel combustion in our research. Na^+, Mg^{2+} and Ca^{2+} were bimodal, with major peaking at >7.0 μm and the minor peak at <1.1 μm. In our research, Ca^{2+}, Mg^{2+}were mainly from road dust, no construction dust during our sampling (K. Xiao, Qin, et al., 2021). The distribution patterns of Na^+, Mg^{2+}, Ca^{2+}, and K^+ are consistent with those of the corresponding WSPTMs and are explained in detail in section 4.2.1.

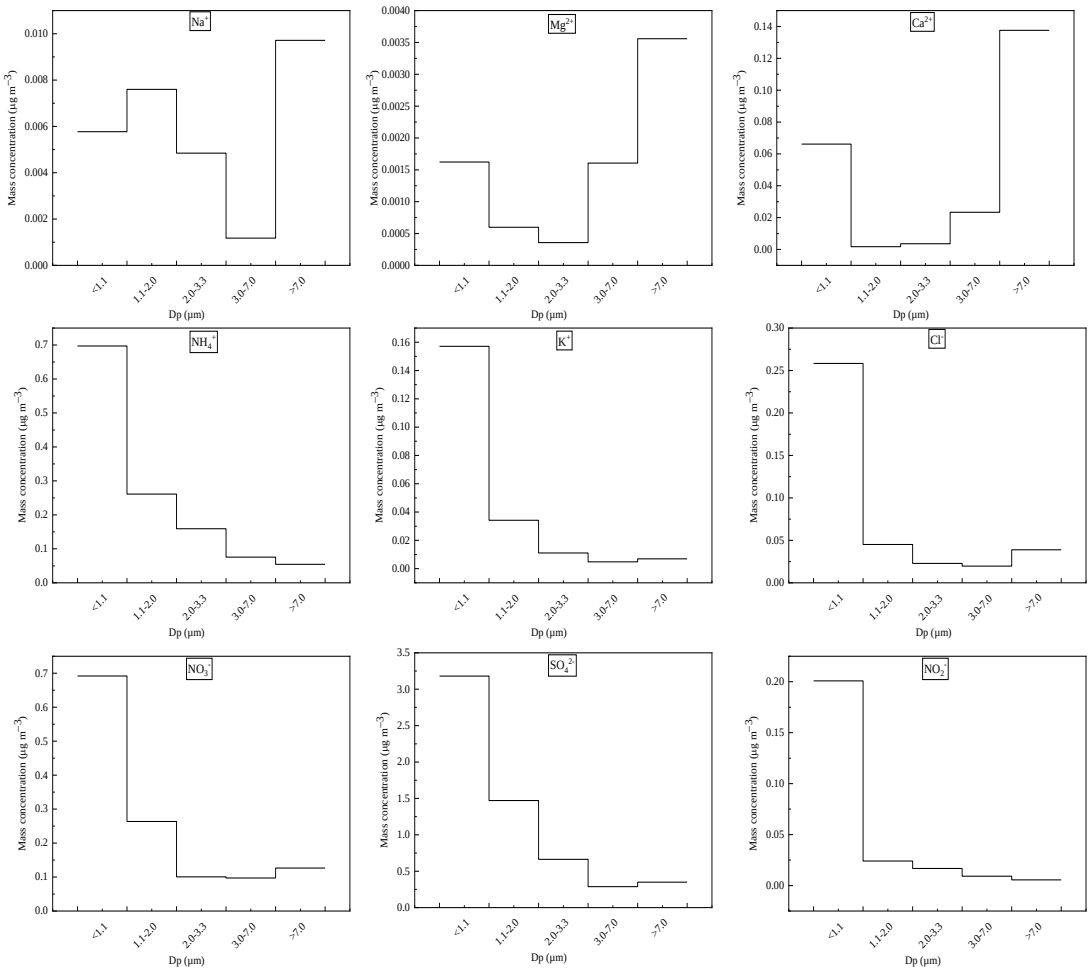

Fig.26. Size distribution of individual water-soluble inorganic ionic species during the sampling period

Table 15. Percentage (%) of individual water-soluble inorganic ionic species to WSIIs during the sampling period.

Ionic Species	Na^+	NH_4^+	K^+	Mg^{2+}	Ca^{2+}	Cl^-	NO_2^-	NO_3^-	SO_4^{2-}
$PM_{1.1}$	19.83	55.89	73.35	20.96	28.47	67.12	78.33	54.05	53.44
$PM_{1.1\text{-}2.0}$	26.10	20.93	15.97	7.72	0.75	11.73	9.38	20.60	24.71
$PM_{2.0}$	45.93	76.82	89.33	28.67	29.22	78.85	87.72	74.65	78.16
$PM_{2.0\text{-}3.3}$	16.65	12.76	5.19	4.62	1.53	5.94	6.54	7.87	11.14
$PM_{3.3\text{-}7.0}$	4.04	6.06	2.25	20.74	10.03	5.12	3.58	7.60	4.83
$PM_{>7.0}$	33.38	4.36	3.23	45.97	59.21	10.10	2.17	9.88	5.87

4.1.3 Ionic balance and neutralization of particulate acidity

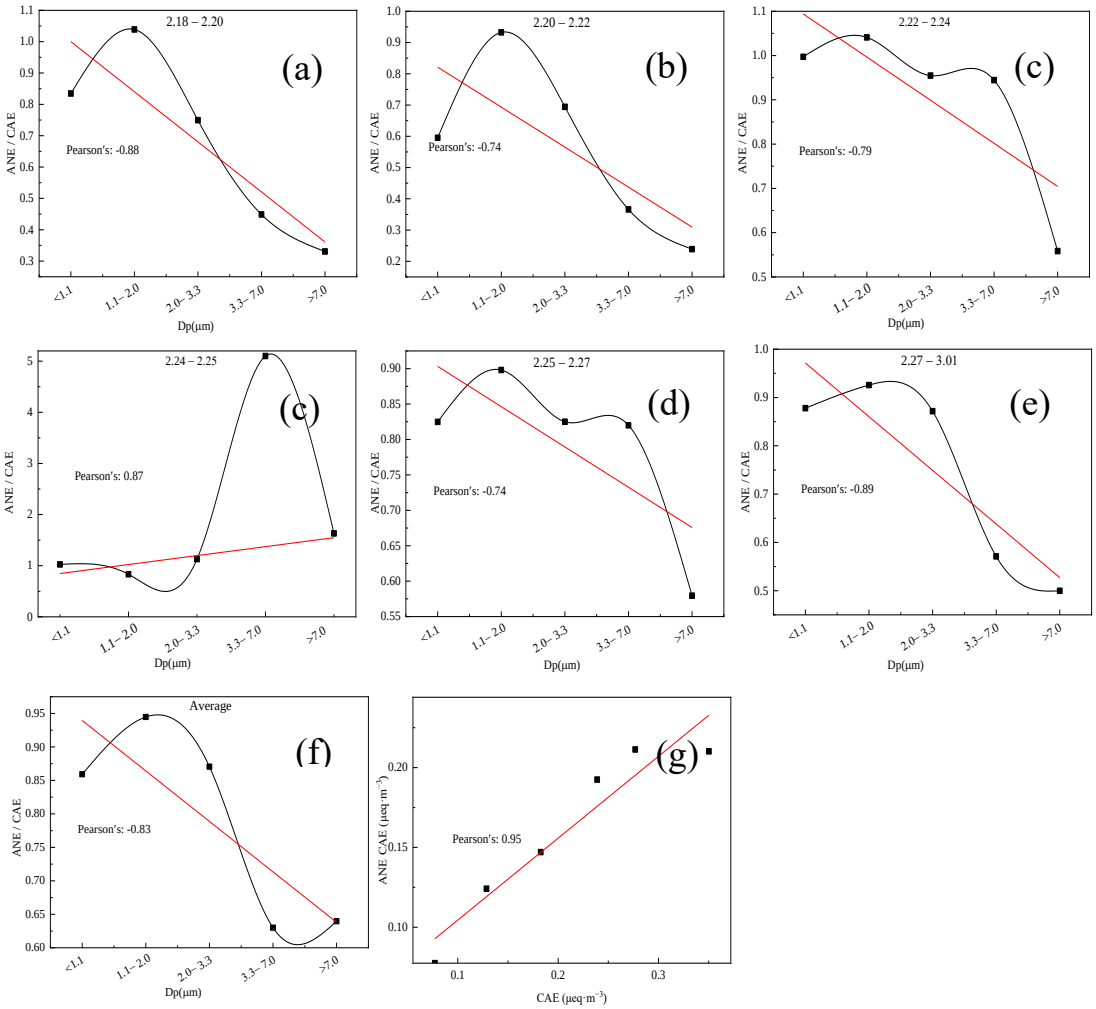

Fig. 27. Ionic balance and within $PM_{1.1}$, $PM_{1.1\text{-}2.0}$, $PM_{2.0\text{-}3.3}$, $PM_{3.3\text{-}7.0}$, and $PM_{>7.0}$ during the sampling period. ((a-e) are the ionic balance for different Group samples within $PM_{1.1}$, $PM_{1.1\text{-}2.0}$, $PM_{2.0\text{-}3.3}$, $PM_{3.3\text{-}7.0}$, and $PM_{>7.0}$, respectively; (f) is the average ionic balance within $PM_{1.1}$, $PM_{1.1\text{-}2.0}$, $PM_{2.0\text{-}3.3}$, $PM_{3.3\text{-}7.0}$, and $PM_{>7.0}$, respectively; (g) is the Ionic equivalence of total anions against total cations.)

Table 16 shows the Pearson correlation coefficients between the major cations and anions within $PM_{1.1}$, $PM_{1.1\text{-}2.0}$, $PM_{2.0\text{-}3.3}$, $PM_{3.3\text{-}7.0}$, and $PM_{>7.0}$ during the sampling period. NH_4^+ has a very strong correlation with SO_4^{2-}, higher than NO_3^-, suggesting that NH_4NO_3 and $(NH_4)_2SO_4$ were major chemical fraction of ions in $PM_{2.0}$. NH_4NO_3 is formed under high concentrations of NH_3 and gaseous nitric acid, high humidity and low temperature (Che et al., 2021). But at low NH_3 concentrations, the neutralization of acidic sulfate by NH_3 is favored over the formation of SO_4^{2-} (Squizzato et al., 2013). When SO_4^{2-}, NO_3^-, and Cl^- co-exist, NH_4^+ usually first combines with SO_4^{2-}, since $(NH_4)_2SO_4$ is more stable (Q. Yao et al., 2020). According to sections 3.2.2 and 3.2.1, the mass concentration of SO_4^{2-} are 4.5 and 4.0 times higher than the concentration of the NH_4^+ and NO_3^- in $PM_{>2.0}$, respectively, and there is no correlation between NH_4^+ and NO_3^-, which illustrated that SNA was in the form of $(NH_4)_2SO_4$. In addition, while fresh smoke from biomass burning contains more KCl particles, aged smoke had more KNO_3 and K_2SO_4 particles(Jia Li et al., 2003). During the aging process, Cl^- was replaced by NO_3^- and SO_4^{2-}, yielding KNO_3 particles and HCl gases (C. Li et al., 2015). Regardless, only K^+ and NO_3^- exhibited strong correlation ((r=0.72 for $PM_{1.1}$), (r=0.63 for $PM_{1.1\text{-}2.0}$), (r=0.77 for $PM_{2.0\text{-}3.3}$), (r=0.69 for $PM_{3.3\text{-}7.0}$), and (r=0.99 for $PM_{>7.0}$)) while those of K^+ and SO_4^{2-} were ((r=0.96 for $PM_{1.1}$), (r=0.96 for $PM_{1.1\text{-}2.0}$), (r=0.84 for $PM_{2.0\text{-}3.3}$), (r=0.31 $PM_{3.3\text{-}7.0}$), and (r=0.03 for $PM_{>7.0}$)). This means that KNO_3 was formed at all sizes, however, K_2SO_4 can only be formed in the particle size less than 3.3 μm.

Table 16. Pearson correlation coefficients between the major cations and anions within $PM_{1.1}$, $PM_{1.1\text{-}2.0}$, $PM_{2.0\text{-}3.3}$, $PM_{3.3\text{-}7.0}$, and $PM_{>7.0}$ during the sampling period.

Dp (μm)	Species	Na^+	NH_4^+	K^+	Mg^{2+}	Ca^{2+}
<1.1	Cl^-	-0.17	0.07	-0.27	-0.64	-0.67
	NO_3^-	0.74	0.72	0.72	0.82	0.81
	SO_4^{2-}	0.71	0.90	0.96	0.89	0.74
1.1-2.0	Cl^-	0.55	0.31	-0.02	-0.51	-0.42
	NO_3^-	0.81	0.75	0.63	0.55	0.58
	SO_4^{2-}	0.85	0.92	0.96	0.84	0.77
2.0-3.3	Cl^-	0.71	0.78	0.76	0.10	0.18
	NO_3^-	0.32	0.12	0.77	0.72	0.83
	SO_4^{2-}	0.86	0.92	0.84	0.10	0.09
3.0-7.0	Cl^-	0.57	-0.44	0.67	0.70	0.95
	NO_3^-	0.79	-0.44	0.69	0.89	0.97
	SO_4^{2-}	-0.08	0.86	0.31	0.09	-0.32
>7.0	Cl^-	0.71	-0.24	0.82	0.71	0.76
	NO_3^-	0.71	-0.10	0.99	0.91	0.94
	SO_4^{2-}	0.52	0.98	0.03	0.20	0.07

From the above discussions, SO_4^{2-} prefers to combine with NH_4^+ to form $(NH_4)_2SO_4$, which hinders

the formation of NH_4NO_3 (G. Wang et al., 2016)(He et al., 2014), the remaining SO_4^{2-} and NO_3^- to neutralize the K^+, Ca^{2+} and Mg^{2+} in $PM_{2.0}$. Based on the Pearson correlation coefficients between NO_3^- and Ca^{2+} and Mg^{2+}, it was suggested that K^+, Ca^{2+} and Mg^{2+} were mainly neutralized by NO_3^-. Our findings correspond well with the current situation in the rural areas of Xuanwei, Yunnan, where residents mainly use coal and biomass for heating and cooking, and where the economy is relatively backward and almost unaffected by mobile emission sources.

4.1.4 Water-Soluble Inorganic Ionic Species (WSIIs) in RCC particles

Sources and size distribution characteristics of ions species are better known and can serve as valuable references for the less known aerosol constituents.

Fig 28 shows the mass concentrations (μg m^{-3}) and standard deviation (SD) of ion species (coal, N=6). Five size-segregated PM filters in each RCC samples were analyzed for mass concentrations and therefore we showed the mass concentrations of ion species with five various size ranges. As can be seen from the Fig 28, coal combustion emits more NH_4^+ and SO_4^{2-} (Shuxiao Wang et al., 2010), the average concentrations of individual ions were in the order of $SO_4^{2-} > Cl^- > NO_3^- > NH_4^+ > NO_2^- > Na^+ > Mg^{2+} > K^+ > Ca^{2+}$, respectively. The size distribution of nine water-soluble inorganic ions (WSIIs) were major concentrated in fine particles. Secondary inorganic aerosol (SIA, SO_4^{2-}, NO_3^-, and NH_4^+) are the major components of water-soluble inorganic ions (WSIIs), contributed to 59.08 ± 9.48 % of total WSIIs, which was provided in the Table 17. Compared with previous studies, WSIIs/$PM_{2.0}$ is 2.22 ± 2.36 % lower than atmospheric particulate matter occupied by 33-41% or more of fine particles (Shuxiao Wang et al., 2010)(Zhou et al., 2016). SO_4^{2-} dominated SIA in the extremely high and RCC was a candidate of high SO_4^{2-} concentrations (Dao et al., 2019)(Y. C. Lin et al., 2020), which is consistent with our research (as Fig 6 a).On the other hand, the average charge of the anion in each particle size segment is 2.72 ± 1.17 times than the cation (Table 18), indicating that the aqueous solution of the particulate matter emitted by the residential coal burning is acidic in Xuanwei area.

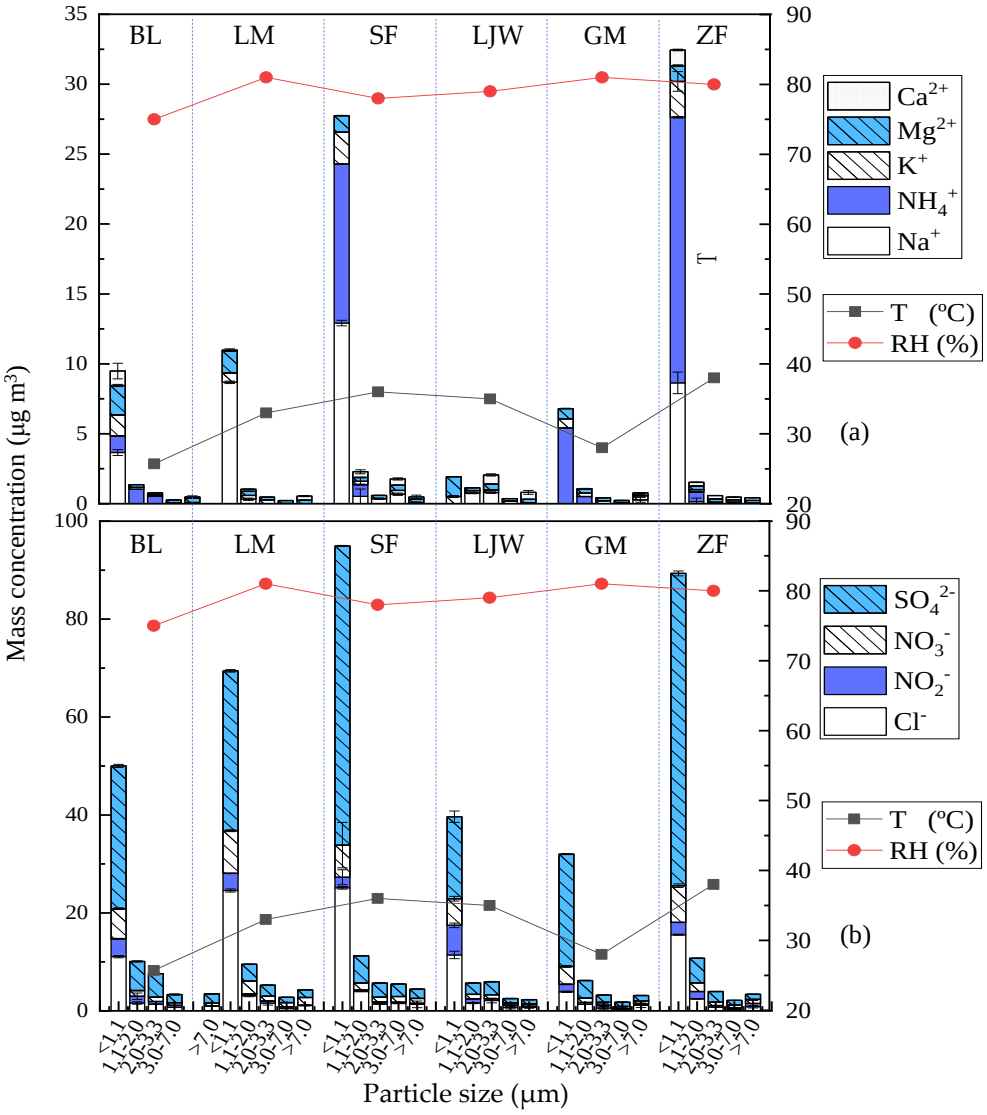

Fig. 28. Mass concentration (μg m^{-3}) and standard deviation (STD) of ion species (Coal, N=6, (a): cation mass concentration; (b): anion mass concentrations). (Bole coal [BL], Luomu coal [LM], Shunfa coal [SF], Lijiawu coal [LJW], Guangming coal [GM], and Zongfan coal [ZF]).

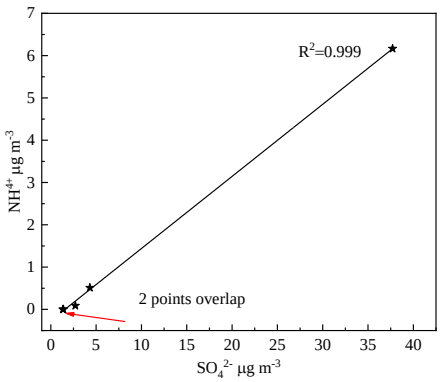

Fig. 29. The correlation coefficients between NH_4^+ and SO_4^{2-}

Table 17. The mass concentration of ion species (μg m^{-3}) and percentage of SIA/WSIIs (%)

Samples	Size (μm)	Cl^-	NO_2^-	NO_3^-	SO_4^{2-}	Na^+	NH_4^+	K^+	Mg^{2+}	Ca^{2+}	Total	SIA/WSIIs
	<1.1	11.07	3.65	6.14	29.16	3.66	1.20	1.50	2.10	1.03	59.52	0.61
	1.1-2.0	1.60	1.40	1.15	5.94	0.00	1.03	0.13	0.20	0.00	11.47	0.71
BL	2.0-3.3	1.37	0.56	0.86	4.83	0.00	0.53	0.10	0.15	0.00	8.39	0.74
	3.0-7.0	0.72	0.42	0.54	1.68	0.00	0.00	0.06	0.21	0.00	3.62	0.61
	>7.0	0.94	0.06	0.60	1.87	0.00	0.00	0.08	0.31	0.09	3.96	0.62
	<1.1	24.59	3.50	8.71	32.62	8.68	0.00	0.68	1.58	0.05	80.41	0.51
	1.1-2.0	3.09	0.37	2.62	3.45	0.32	0.00	0.27	0.30	0.15	10.56	0.57
LM	2.0-3.3	1.59	0.43	0.99	2.25	0.00	0.00	0.27	0.20	0.00	5.72	0.57
	3.0-7.0	0.47	0.36	0.85	1.09	0.00	0.00	0.02	0.21	0.00	3.00	0.65
	>7.0	1.09	0.07	1.57	1.58	0.00	0.00	0.00	0.26	0.28	4.85	0.65
	<1.1	25.13	2.17	6.56	61.07	12.92	11.38	2.28	1.17	0.00	122.67	0.64
	1.1-2.0	3.95	0.33	1.43	5.54	0.53	0.84	0.23	0.28	0.40	13.54	0.58
SF	2.0-3.3	1.41	0.42	0.96	2.91	0.36	0.00	0.00	0.24	0.00	6.29	0.61
	3.0-7.0	1.52	0.25	1.16	2.56	0.68	0.00	0.27	0.38	0.44	7.26	0.51
	>7.0	1.32	0.22	1.00	1.88	0.00	0.00	0.06	0.27	0.15	4.92	0.59
	<1.1	11.43	6.04	5.44	16.75	0.00	0.00	0.52	1.41	0.00	41.58	0.53
	1.1-2.0	1.59	0.87	0.92	2.32	0.77	0.00	0.17	0.20	0.00	6.84	0.47
LJW	2.0-3.3	2.12	0.35	0.84	2.63	0.80	0.00	0.19	0.42	0.65	8.01	0.43
	3.0-7.0	0.67	0.51	0.47	0.87	0.00	0.00	0.20	0.17	0.00	2.89	0.46
	>7.0	0.69	0.27	0.46	0.86	0.00	0.00	0.07	0.25	0.49	3.10	0.43
	<1.1	3.91	1.52	3.65	22.92	0.00	5.42	0.66	0.73	0.00	38.81	0.82
	1.1-2.0	1.34	0.39	0.87	3.61	0.00	0.51	0.24	0.30	0.03	7.29	0.69
GM	2.0-3.3	0.56	0.64	0.57	1.46	0.00	0.00	0.21	0.22	0.00	3.65	0.56
	3.0-7.0	0.39	0.07	0.44	0.89	0.00	0.00	0.09	0.15	0.00	2.03	0.65
	>7.0	1.15	0.22	0.69	1.09	0.28	0.00	0.30	0.20	0.00	3.92	0.45
	<1.1	15.55	2.52	7.51	63.76	8.64	19.00	2.56	1.13	1.13	121.78	0.74
	1.1-2.0	2.45	1.50	1.79	5.02	0.15	0.69	0.17	0.26	0.26	12.29	0.61
ZF	2.0-3.3	0.78	0.33	0.67	2.18	0.00	0.00	0.11	0.24	0.24	4.54	0.63
	3.0-7.0	0.34	0.30	0.57	0.93	0.00	0.00	0.10	0.19	0.19	2.62	0.58
	>7.0	0.84	0.70	0.82	1.04	0.00	0.00	0.04	0.19	0.19	3.82	0.49
AG												0.59
SD												0.09

AG: Average

This experiment was carried out in a laboratory. As we all know, there is a big difference between laboratory experiments and field measurements. In this study, there is no obvious relationship between temperature and humidity with WSIIs. Air supply and combustion conditions are parameters that affect

Table 18. Charge balance of ions

Sample	Size (μm)	cation	Anion	Anion/cation
BL	<1.1	0.49	1.11	2.25
	1.1-2.0	0.08	0.22	2.83
	2.0-3.3	0.04	0.17	3.74
	3.0-7.0	0.02	0.07	3.80
	>7.0	0.03	0.08	2.36
LM	<1.1	0.53	1.60	3.02
	1.1-2.0	0.05	0.21	3.99
	2.0-3.3	0.02	0.12	5.05
	3.0-7.0	0.02	0.06	3.26
	>7.0	0.04	0.09	2.58
SF	<1.1	1.35	2.14	1.59
	1.1-2.0	0.12	0.26	2.17
	2.0-3.3	0.04	0.13	3.57
	3.0-7.0	0.09	0.12	1.35
	>7.0	0.03	0.10	3.10
LJW	<1.1	0.13	0.90	6.85
	1.1-2.0	0.05	0.13	2.35
	2.0-3.3	0.11	0.14	1.28
	3.0-7.0	0.02	0.06	2.96
	>7.0	0.05	0.05	1.09
GM	<1.1	0.38	0.68	1.81
	1.1-2.0	0.06	0.14	2.24
	2.0-3.3	0.02	0.07	2.96
	3.0-7.0	0.02	0.04	2.58
	>7.0	0.04	0.07	1.97
ZF	<1.1	1.65	1.95	1.18
	1.1-2.0	0.08	0.24	2.82
	2.0-3.3	0.03	0.09	2.48
	3.0-7.0	0.03	0.05	1.66
	>7.0	0.03	0.07	2.79
AG				2.72
SD				1.18

AG: Average

the emission of pollutants from RCC (Oros & Simoneit, 2000). NH_4^+ is closely correlated with SO_4^{2-} was provided in the Fig 29, which may indicate the complete neutralization of SO_4^{2-} by NH_4^+ in particulate matter. It can be inferred that the combustion of residential coal can result in the formation of considerable particulate sulfate compounds (H. Zhang et al., 2012), which can change the radiation

balance by scattering or absorbing solar radiation and thermal radiation from the earth's surface (Andreae & Crutzen, 1997).

4.1.5 The mass concentration of water-soluble inorganic ionic species size distribution and sources in Beijing

Detected ion water-soluble inorganic ionic species (WSIIs), an important of atmospheric particulate matters, which can be used to infer the chemical properties and origin of aerosols (Weiqian Wang et al., 2020) (Jingjing Zhang et al., 2018). Fig 30 illustrated the size distribution of Cl^-, NO_3^-, NO_2^- , SO_4^{2-}, NH_4^+, Na^+, K^+, Ca^{2+} and Mg^{2+} detected in winter. The percentage （%） of water-soluble inorganic ionic species for size fraction mass concentrations in Beijing were provided in Fig 31. The ratio of NO_3^-/ SO_4^{2-}, Cl^-/Na^+, Cl^-/ K^+ and Cl^-/NO_3^- in different size- that secondary pollution in the atmosphere in winter was strong. SO_4^{2-} showed a slightly bimodal size distribution, with fine＜1.1 μm, thus demonstrating a unimodal distribution of fine particles. Most of the SO_4^{2-}, $NO_3^-$and NH_4^+ mass concentration were concentrated in fine particles (＜1.1 μm) ,which is consistent with previous studies (Do et al., 2021) (X. Wu et al., 2020) (Q. Yao et al., 2020). The average mass concentration of NO_3^- in the fine particles accounted for 74.94% of the total nitrate mass, while that for NH_4^+ was 71.85 % and that for SO_4^{2-} was 61.70 % in winter in Beijing. Na^+ and Mg^{2+} were bimodal, the major peak in the size range of ＜1.1 μm while the minor peak in the size range of ＞7 μm, meanwhile Ca^{2+} was unimodal, peaking at ＞7 μm. The size distribution of K^+, Cl- and NO_2^- were bimodal, with fine particles peaking at ＜1.1 μm and coarse particles peaking at ＞7 μm.

It was well known that that SO_2 and NO_2, which are the gaseous precursors of SO_4^{2-} and NO_3^-,so the ratio of NO_3^-/ SO_4^{2-} could be used to compare the contribution of stationary (such as coal burning) and mobile source (such as motor vehicle exhausts) of SO_2 and NO_2 (Lv et al., 2019). NO_2^- concentration is very low, and it is unstable due to being easily oxidized by ozone, hydroxyl radicals, and hydrogen peroxide, so put NO_2^- and NO_3^- together to discuss. According to the previous studies show that the higher (NO_2^- + NO_3^-) / SO_4^{2-} values to mobile source over the stationary source of atmospheric pollutants. The average mass ration of (NO_2^- + NO_3^-) / SO_4^{2-} was 1.68. Compared to the previous results, which reported the measured ratio of 0.71 during 2001- 2003 (Ying Wang et al., 2005) ,1.03 in 2012 (Yongjie Yang et al., 2015), between 1.31-1.16 during 2014-2015 (X. Wu et al., 2020) 3.12 in 2017 (Che et al., 2021) ,indicating that air pollution during the research period was mainly from the mobile source in Beijing in winter.

Most of Na^+, Ca^{2+} and Mg^{2+} in coarse particles were found to be high, which are mainly from crustal source, such as re-suspended road dust, soil dust and building dust (Weiqian Wang et al., 2020). K^+ in

fine particles is known as an inorganic tracer of biomass burning emissions (Do et al., 2021). The results show that the distribution of mass concentration of Na^+, Ca^{2+} and Mg^{2+} were consistent with the distribution of mass concentration of Na, Mg and Ca. The dominant source of Cl^- was generally considered from coal burning, biomass burning and vehicle exhaustion fine fraction and from sea water in coarse fraction (X. Wu et al., 2020). The linear relationship between K^+ and Cl^- was strong (R>0.98), meanwhile, the liner relationship between Na^+ and Cl^- was weak (R<0.20). The average mass ratio of Cl^-/Na^+, Cl^-/K^+ and $Cl^-/(NO_2^- + NO_3^-)$ were 6.58 ,6.18 and 0.57, respectively. From the above discussion, which indicated that the major contributor of Cl^- was coal burning and the minor contributor of Cl^- was biomass burning and vehicle exhaustion in Beijing during the winter.

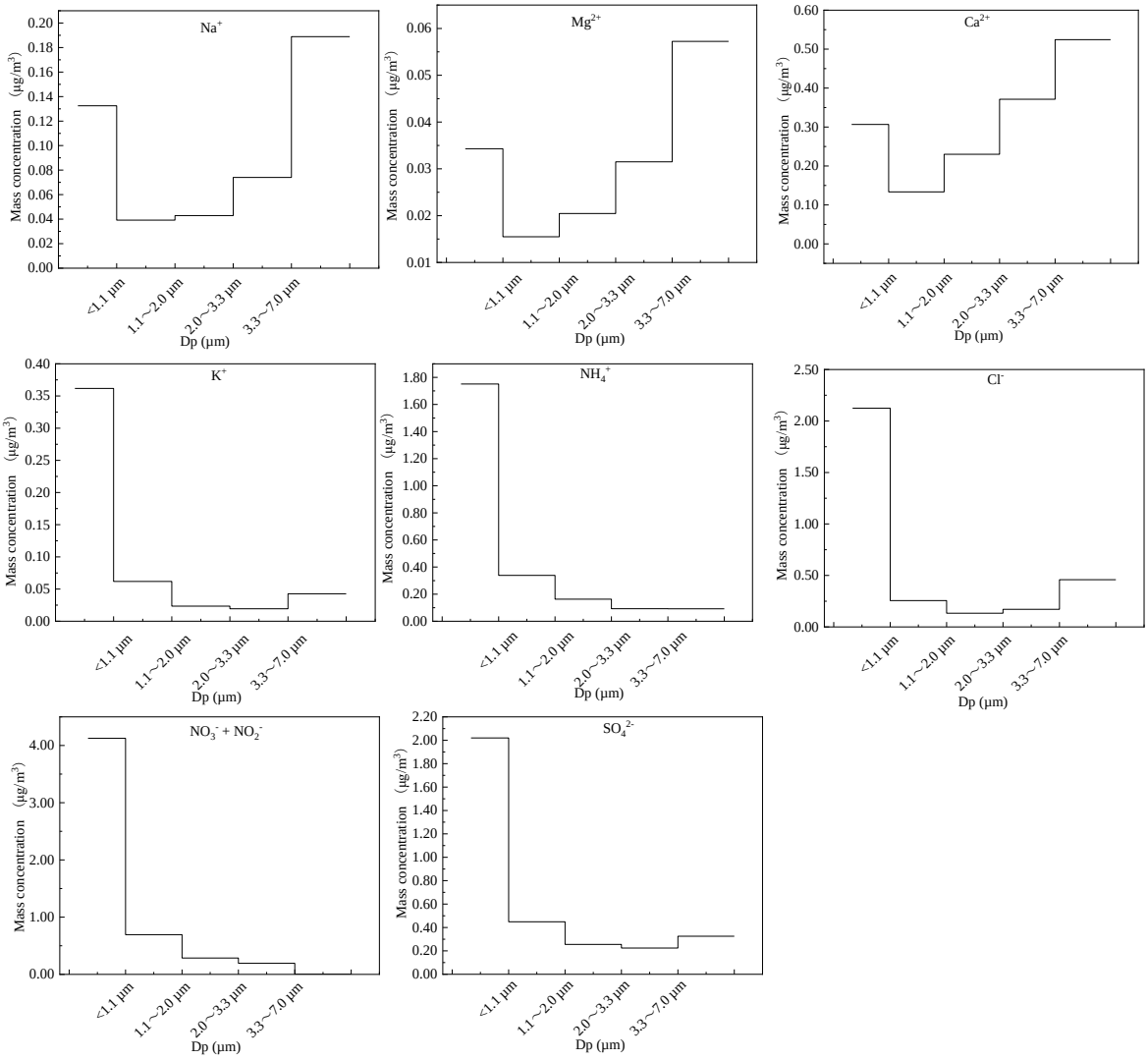

Fig. 30. Size distribution of water-soluble inorganic ionic species in Beijing

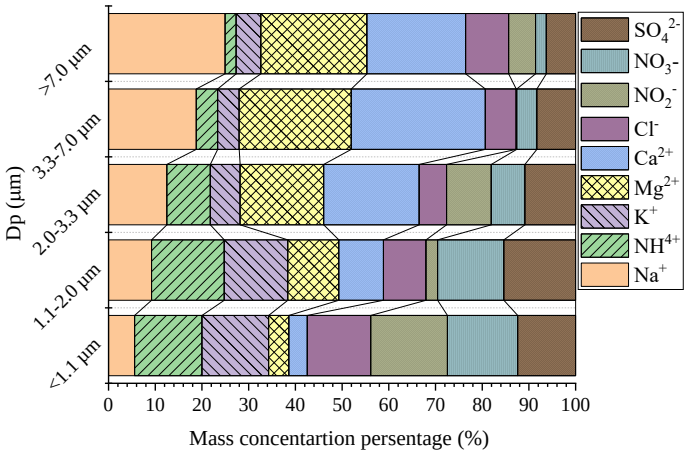

Fig. 31. The percentage（%）of water-soluble inorganic ionic species for size fraction mass concentrations in Beijing.

4.2 Water-Soluble Potentially Toxic Metals

Generally, PM is produced due to weathering and soil suspension, construction, coal, oil burning and resuspension of industrial dust (Shanshan Wang et al., 2019) (Y. Hu & Cheng, 2016). Potential toxic metals are considered to be an important ingredient in inducing respiratory diseases and cancer due to their toxicity (G. Shi et al., 2011) (Jin Zhang et al., 2017) (Al-Humour et al., 2019) (WHO, 2017). Thus, determining the types and sources of heavy metals is a direct and effective way to control potential toxic metals pollution.

4.2.1 The mass concentration of potential toxic metals size distribution APMs in Xuanwei

Size distributions of the WSPTMs within $PM_{1.1}$, $PM_{1.1\text{-}2.0}$, $PM_{2.0\text{-}3.3}$, $PM_{3.3\text{-}7.0}$, and $PM_{>7.0}$ are shown in Fig. 32 , Fig. 33 and Table 19. In this study, 19 WSPTMs were detected (Al, As, Ba, Ca, Cr, Cu, Fe, K, Li, Mg, Mn, Na, Ni, Pb, Ti, V and Zn), of which Al, Ca, Na, and Mg are the most abundant chemical components and altogether account for more than 93.93% of the total WSPTMs. The highest concentrations of WSPTMs were generally located within the coarse PM (>7.0 μm) and fine (< 1.1 μm),

respectively.

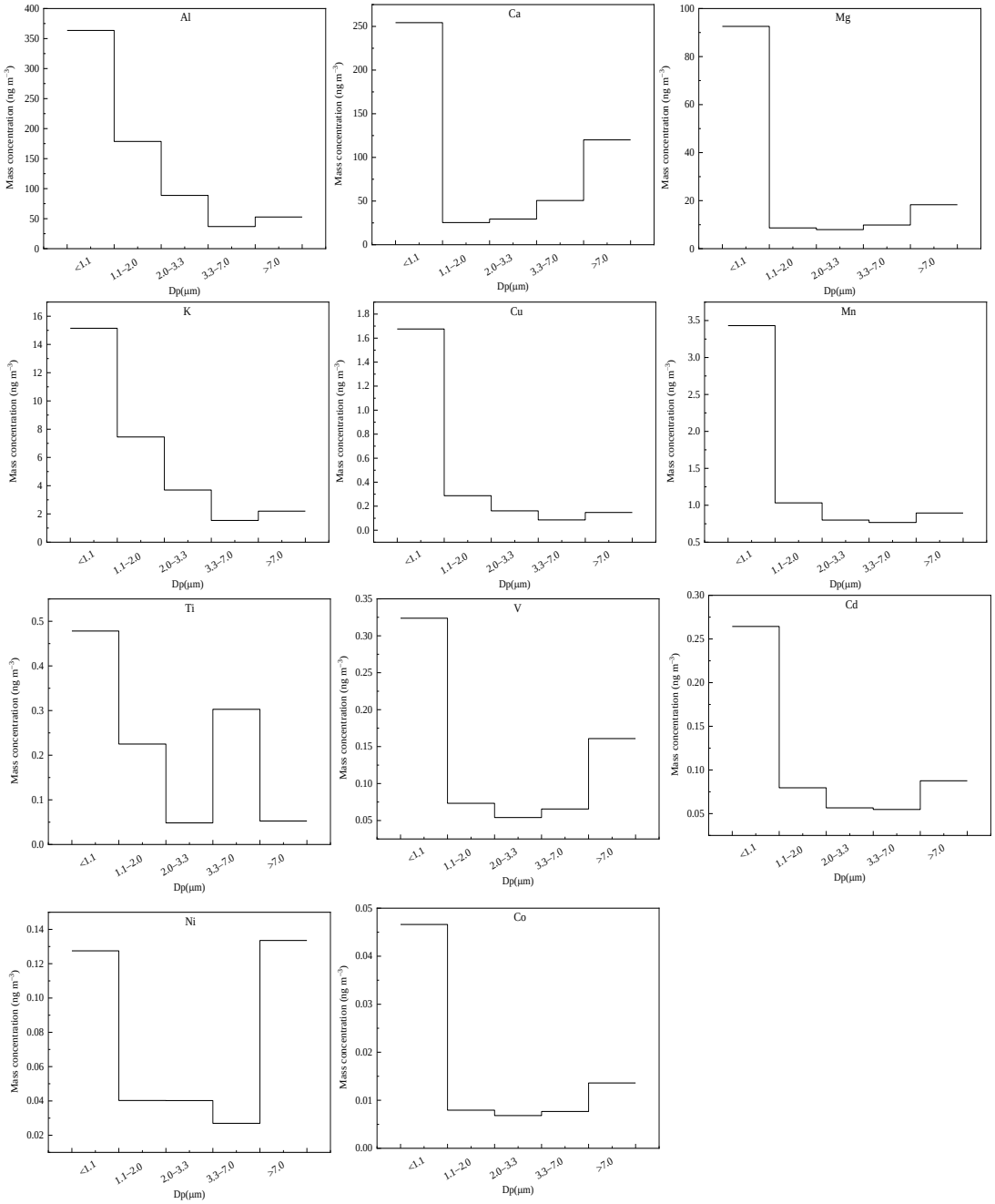

Fig.32. Water soluble potentially toxic metals with particle size-bimodal distribution during the sampling period in Xuanwei.

According to the average mass size distribution, 19 elements could be divided into 2 groups: bimodal, unimodal. Al, Ca, Mg, K, Cu, Mn, Ti, V, Cd Ni, and Co were bimodal (Fig.32 and Table 19), the major peak in the size range sizes of < 1.1μm, the minor peak in the size range of >7.0 μm, except for Ti which minor peak in the size range sizes of 3.3-7.0 μm and Ni which major peak in the size range

sizes of >7.0 μm. (The corresponding percentage of TSP were 50.45%, 53.00%, 67.41%, 50.44%,71.07%, 49.53%, 43.19%, 31.33%, 47.79%, 48.69%, 36.25%, 56.39% vs. 7.32%, 25.01%, 13.33%, 7.32%, 6.25%, 12.92%, 27.35%, 23.74%, 16.13%, 34.61%, 16.45%). Na, Zn, Ba, Fe, As, Se, Cr, and Pb were unimodal, the major peak in the size range sizes of <1.1μm, the concentration increased with the decrease of particle size (Fig.33 and Table 19). (The corresponding percentage of TSP were 48.93%, 73.58%, 52.78%, 48.80%, 65.82%, 90.96%, 68.73%, and 59.04%). In summary, the mass concentrations of WSPTMs in APMs in the Xuanwei area were mainly concentrated within $PM_{1.1}$, especially Se (90.96%). This indicates that fine particulate matter in Xuanwei is potentially the most harmful to humans.

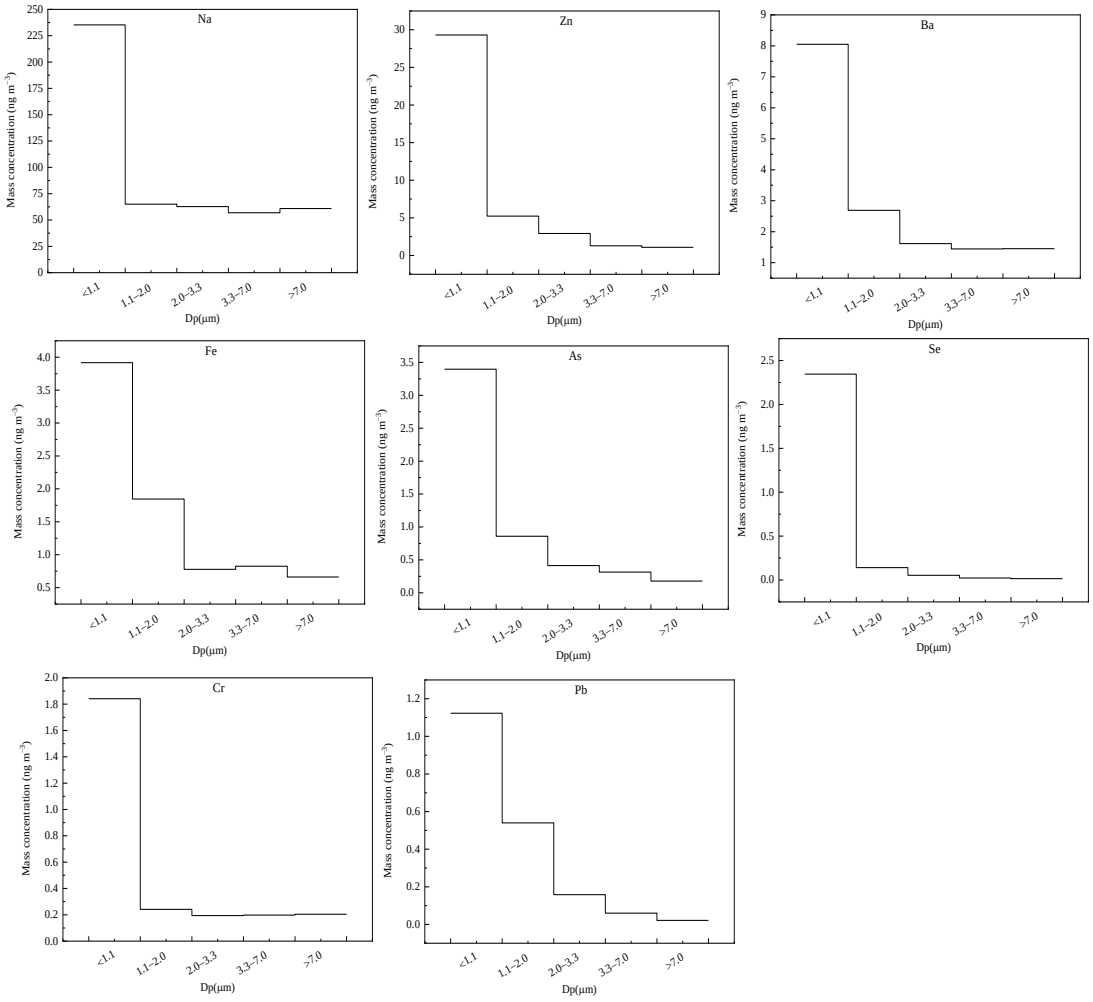

Fig.33. Water soluble potentially toxic metals with particle size-unimodal distribution during the sampling period in Xuanwei.

Table 19. Mass concentration of size-segregated in WSPTMs (μg/m^3) and Percentage distribution of mass concentration to TSP (%) during the sampling period.

WSP	Mass concentration (μg/m^3)					Percentage distribution (%)				
TMs	<1.1	1.1-2.0	2.0-3.3	3.3-7.0	>7.0	<1.1	1.1-2.0	2.0-3.3	3.3-7.0	>7.0
Na	235.29	65.03	62.70	56.87	60.92	48.94	13.52	13.04	11.83	12.67
Mg	92.57	8.65	7.93	9.85	18.31	67.42	6.30	5.78	7.17	13.33
K	15.15	7.45	3.70	1.54	2.20	50.44	24.81	12.31	5.12	7.32
Ca	254.35	25.36	29.43	50.66	120.04	53.01	5.29	6.13	10.56	25.02
Zn	29.31	5.23	2.92	1.28	1.09	73.58	13.14	7.33	3.22	2.73
Al	363.50	178.65	88.72	36.91	52.72	50.45	24.80	12.31	5.12	7.32
Ti	0.48	0.23	0.05	0.30	0.05	43.19	20.33	4.37	27.35	4.76
V	0.32	0.07	0.05	0.07	0.16	47.78	10.82	7.98	9.68	23.74
Cr	1.84	0.24	0.19	0.20	0.20	68.74	9.01	7.24	7.39	7.62
Mn	3.43	1.03	0.80	0.77	0.90	49.54	14.91	11.54	11.08	12.93
Fe	3.92	1.84	0.78	0.82	0.66	48.81	22.99	9.69	10.28	8.24
Co	0.05	0.01	0.01	0.01	0.01	56.40	9.61	8.25	9.28	16.47
Ni	0.13	0.04	0.04	0.03	0.13	34.61	10.93	10.91	7.31	36.25
Cu	1.68	0.29	0.16	0.09	0.15	71.08	12.19	6.84	3.64	6.25
As	3.40	0.86	0.41	0.31	0.18	65.82	16.63	8.01	6.09	3.44
Se	2.35	0.14	0.05	0.02	0.02	90.96	5.46	2.09	0.89	0.60
Cd	0.26	0.08	0.06	0.05	0.09	48.69	14.66	10.43	10.09	16.13
Ba	8.05	2.69	1.62	1.44	1.45	52.78	17.64	10.59	9.47	9.52
Pb	1.12	0.54	0.16	0.06	0.02	59.04	28.38	8.31	3.16	1.12

4.2.2 The mass concentration of potential toxic metals size distribution in Beijing

Mass concentrations of the total 21 elements (Na, Mg, Al, K, Ca, Ti, V, Cr, Mn, Fe, Co, Ni, Cu, Zn, As, Se, Sr, Cd, Sb, Ba, Pb) in multi-size PM samples were determined by using ICP-MS. Although the mass concentration of some potential toxic metals is very low, some of these potential toxic metals adsorbed on PM are harmful to public health and therefore cannot be ignored. The size distribution of potential toxic metals for Beijing samples during the winter were illustrated in Figure 34, Figure 35, and Figure 36.

According to their mean mass size distribution, 21 elements could be divided into three groups: bimodal, unimodal, irregular. Group I were classified into two situations (Fig.34), the first case I a: Na, Mg, Ca, Al, Ti, Fe, Ni, Cu, Mn, Sr and V were bimodal, the highest peak in the size range of > 7 μm, however, the lowest peak in the size range of < 1.1 μm. (The corresponding mass concentration

ratio of aggregate particle size were 50.45 %, 48.56 %, 47.12 %, 46.59 %, 49.38 %, 45.20 %, 34.61 %, 31.33 %, 37.44 %, 48.76 %, 51.70 % VS 26.57 %, 17.42 %, 16.41 %, 22.53 %, 17.80 %, 15.77 %, 23.31 %, 20.75 %, 24.53 %,18.18 %,16.25 %). Another case I b: Sb Zn and K were also bimodal, hoverer, the maximum average mass concentration aggregate particle size and the minimum aggregate particle size are opposite to the first case. (The corresponding mass concentration ratio of aggregate particle size were 38.07 %, 39.02 %, 38.10 % VS 19.24 %, 33.99 %, 21.84 %). Fig 35 is show that the potential toxic metals with particle size- unimodal distribution. Metals in group II a: the mean mass concentration of Ba, Co showed an unimodal size distribution, with coarse particles peaking at > 7 μm while Cd, As, Se and Pb (group II b) were accumulated on < 1.1 μm. The elements of Ba, Co appeared to have most of their mass portion in the coarser size-range > 7 μm, with more than 44% of the TSP. The mean mass concentration of Cd, As, Se and Pb in < 1.1 μm contributed about 67.98 % ,52.15%,78.73%,70.95% to the total corresponding metal in TSP, respectively. Fig 36 shows that the metal elements with particle size- irregular distribution Group III: the major of Cr was localized on > 7 μm, the minor was accumulated on 2.0-3.3 μm. Total concentrations of Na, Mg, Al, Ca and Fe in winter contributed about 80.24 % and 69.15 % to the total TSP and $PM_{2.0}$ element concentrations respectively, indicating that Na, Mg, Al, Ca and Fe would be more likely originated from dusts storm and road dust related sources and occurred mostly in coarse particles. While the total mass concentrations of As, Cd, Pb and Se were accounted for 0.69 % and 1.95 % of the whole element's concentrations for TSP and $PM_{2.0,}$ respectively, which indicated that As, Cd, Pb, and Se could be mainly associated with fuel combustion sources and existed largely in fine particles. This is in well accordance with the previous study (H. Tian et al., 2012), indicating that coal consumption of residential and other sectors for supplying heat in winter would increase emissions of Cd, Cr and Pb. The northern, west and southwest of our study area were surrounded by mountains and largely covered by forest and scenery protection zone. while the southern plain east regions were not only densely populated, but also were vulnerable affected by the pollutant's diffusion and trans-boundary transportation from surrounding regions, such as Tianjin, Hebei, Shandong.

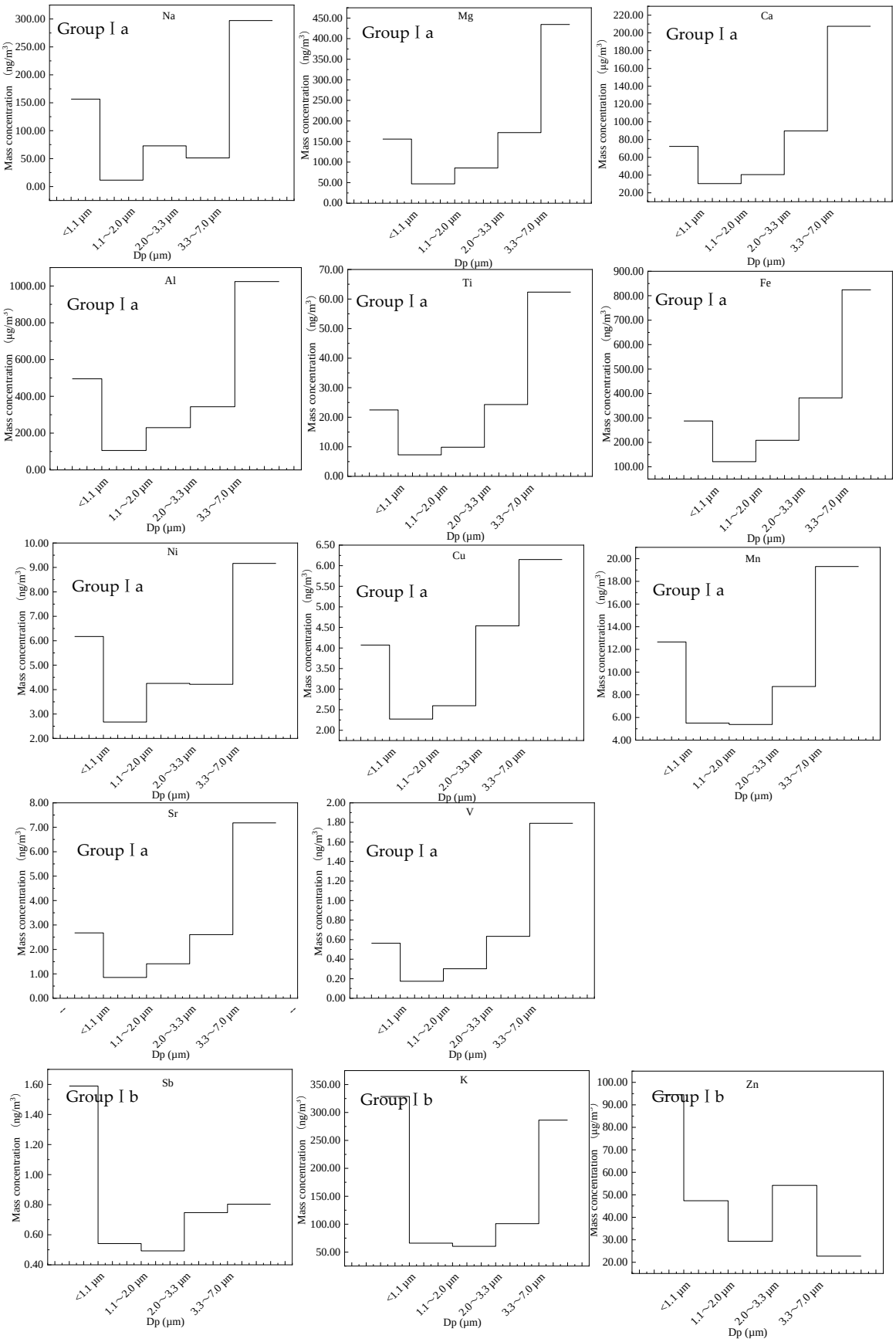

Fig. 34. Potential toxic metals with particle size-bimodal distribution. Group I a is the mass concentration mainly concentrated in $PM_{>7.0}$. Group I a is the mass concentration mainly concentrated in $PM_{<1.1}$.

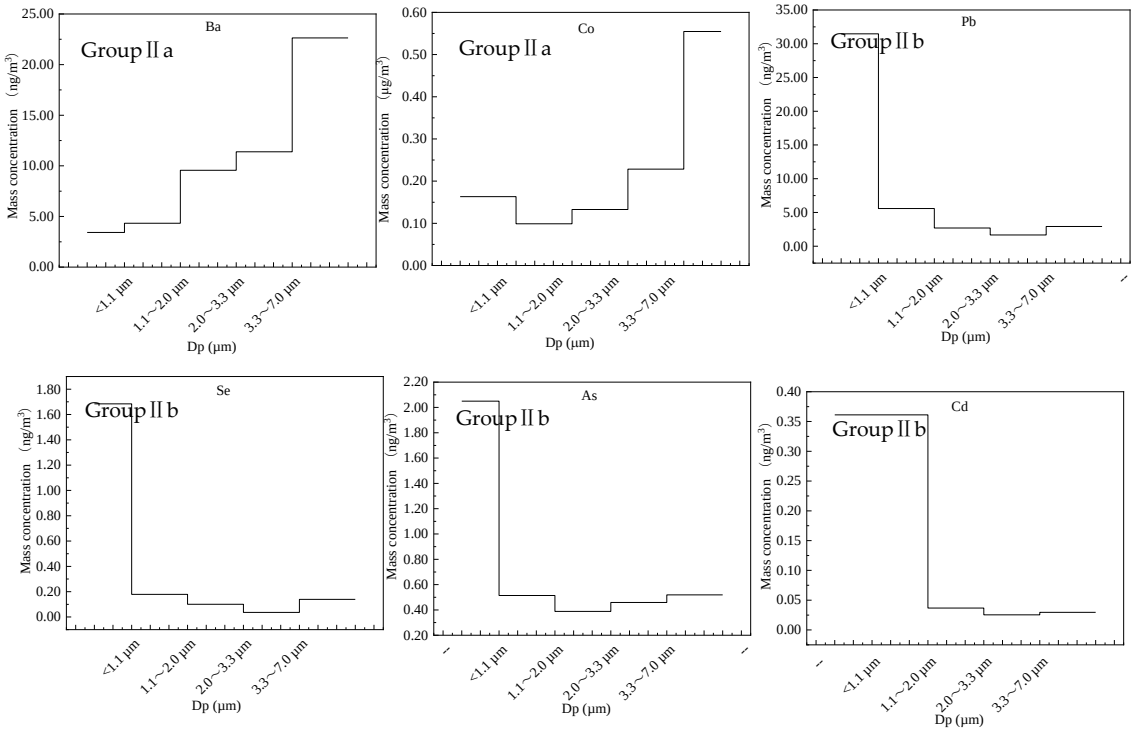

Fig. 35. Potential toxic metals with particle size-unimodal distribution. Group II a is the mass concentration mainly concentrated in $PM_{>7.0}$; Group II b is the mass concentration mainly concentrated in $PM_{<1.1.}$

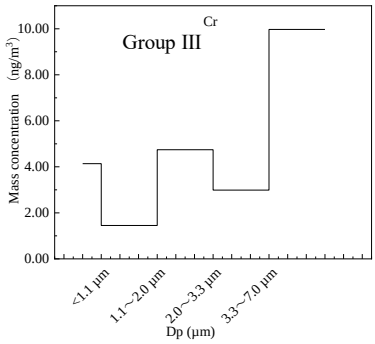

Fig. 36. Potential toxic metals with particle size- irregular distribution.

4.3 Source-apportionment of heavy metals by crustal enrichment factors (CEFs)

To assess the contribution of anthropogenic sources and crustal origin of various trace elements in multi-size PM. In this study, the crustal enrichment factors (CEFs) of all elements were calculated by dividing the relative abundance in the PM sample by the average abundance in the upper continental

crust. (CEFs) were calculated by equation (4):(Rovelli et al., 2020)

CEFs= （Eatm / Ratm） / （Ecrust / Rcrust） (4)

Where E and R represent the investigated element and reference element for crust material, respectively. （Eatm/Ratm） is the concentration ratio of E to R in PM sample while （Ecrust /Rcrust） is the concentration ratio of E to R from earth upper continental crust (Rudnick & Gao, 2013).

4.3.1 Source-apportionment of heavy metals by crustal enrichment factors of APMs in Xuanwei

The higher CEFs, the more it is influenced by anthropogenic sources, conversely, the less it is influenced by natural sources. It is generally accepted that if CEF value below 2, it is indicating significant contributions from earth crust; while CEF value between 2 and 10 reveals the elements are slightly enriched , meanwhile ,mainly affected by anthropogenic emissions and slightly come from the earth crust; whereas CEF value above 10 reveals the elements severely enriched and obviously affected by anthropogenic emissions (Y. C. Lin et al., 2016) (Tsai et al., 2020). The average CEFs of each WSPTMs calculated for $PM_{1.1}$, $PM_{1.1\text{-}2.0}$, $PM_{2.0\text{-}3.3}$, $PM_{3.3\text{-}7.0}$, and $PM_{>7.0}$ during the sampling period using Al as the reference element are depicted in Fig 37.

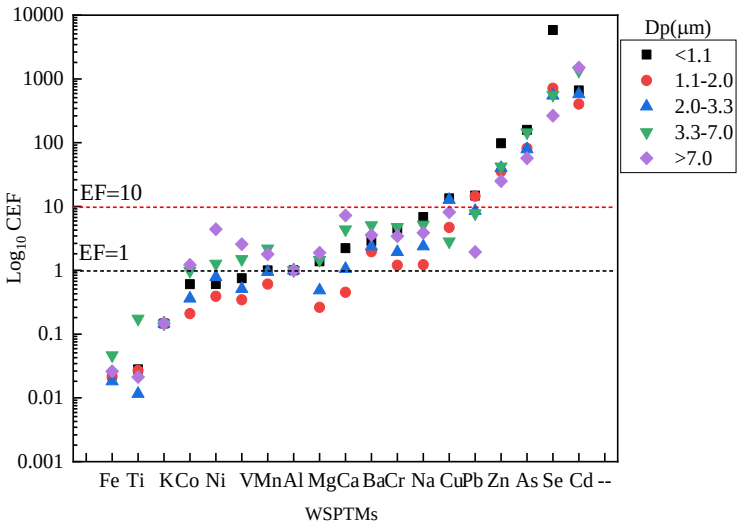

Fig.37. Water soluble potentially toxic metals with particle size-unimodal distribution during the sampling period.

As our sampling sites were in more remote rural areas, traffic pollution is almost negligible. Ni, V and Co are widely used as markers, mainly related to the combustion of fuel oil (Becagli et al., 2012) (Rovelli et al., 2020). Fe and Ti are typical crustal elements (Rovelli et al., 2020) and As and Se have

been widely used as tracers of coal combustion (Y. C. Lin et al., 2020). The lowest CEF values were calculated for Fe, Ti, K, Ni, V, and Co always near or below unity within $PM_{2.0}$, which were typically characterized as originating from crustal source (X. Duan et al., 2020). Mg, Ca, Ba, Cr, Na, Cu, and Pb had the CEF values between 2 and 10, suggesting mainly affected by anthropogenic emissions and slightly come from the earth crust. Coarse PM are much more influenced by Human activities. while Zn, As, Se and Cd were identified as the most enriched (CEF >10) WSPTMs in all PM sizes, were predominantly from anthropogenic emissions (Jianwei Liu et al., 2018)(Q. L. Dai et al., 2015), suggesting that coal combustion could be the important contributor of PM-bound WSPTMs in this study area.

4.3.2 Source-apportionment of heavy metals by crustal enrichment factors of APMs in Beijing

To facilitate interpretation, classification of EF follows: similar to crust(CEFs < 1),the elements almost all originated from the crust ; low enrichment (CEFs 1-10) ,the element mainly contributed by natural sources while slightly contributed by anthropogenic emissions; moderate enrichment (CEFs 10-100), the elements released from human activities and highly enrichment (CEFs > 100),the elements affected by human activities in most of the studies (Fomba et al., 2018)(Malandrino et al., 2016)(Gharaibeh et al., 2010). In the present study Al, high abundance in the Earth's crust composition, was selected as the reference element (Weiqian Wang et al., 2020).

The crustal enrichment factors (CEFs) of each element of size-segregated particles in Beijing were illustrated in Fig 33. In this study, the CEFs values of Na, Ti, V, Ca in five stages of all PM size and K in the range of particle size <3.3 μm were close to 1,fine PM suggested that these elements would be more likely originated from natural sources (including re-suspended road dust, soil dust and building dust) (Dall'Osto et al., 2013)(Tao et al., 2014) and had no obvious enrichment in aerosols.

Most elements in $PM_{1.1}$ and $PM_{1.1\text{-}2.0}$ revealed higher CEFs than those in PM > 7 , when the CEFs values between 1 and 10 ,reflecting that the metals in the smaller particles were significantly contributed by anthropogenic emissions, well consistent with previous research results (Shao et al., 2018). The CEFs values of Mg, Ba, Co, Mn, Sr and Fe in all particle size ranges were between 1 and 10, low enrichment, indicate a mixed contribution of metals majorly from natural sources and minorly from anthropogenic sources. Fe and Mn were speculated to be released from lubricating oil (Mugica-Álvarez et al., 2012)(Taghvaee et al., 2018). Fe, Mn, Ba can be released from the wear of rails or braking systems, or from diesel engines from vehicles (Amato et al., 2011), while it is an important part of the crustal

elements. Here, the mean CEFs of Cu, Ni, Pb, Cr and As were normally below 100, indicating these elements originated mainly from anthropogenic sources and had moderate enrichment in the PM. Cu was the metal with the moderate enrichment (17.48-80.05), major emitted from exhaust emissions and tire wear. The crustal enrichment factors for As and Pb were 8.39-123.39 and 13.37-551.65, respectively, they mainly came from coal combustion in metallurgy, thermal power and other industries (Xia Zhang et al., 2020). Leaded gasoline was eliminated more than ten years ago, but as this research shows, lead is still ubiquitous in the environment. Cr is widely used in the electroplating and leather tanning industries (Jianwei Liu et al., 2019), and a large number of leather industries and metal electroplating industries were found near Beijing (Jianwei Liu et al., 2018), which verified that the interpretation of this source was reasonable. The CEFs values of Sb, Se, Zn ,Cd were greater than 100 in all PM size, suggested that these elements were highly enrichment and significantly affected by vehicle emissions and industrial sources or coal combustion, including metal smelting and incineration emissions (Taghvaee et al., 2018)(Christian et al., 2010). From Figure 38, we conclude that when CEFs>10, the CEFs values increased with increasing aerosol particle size, reflecting those metals in coarse particles were mainly contributed by human activities.

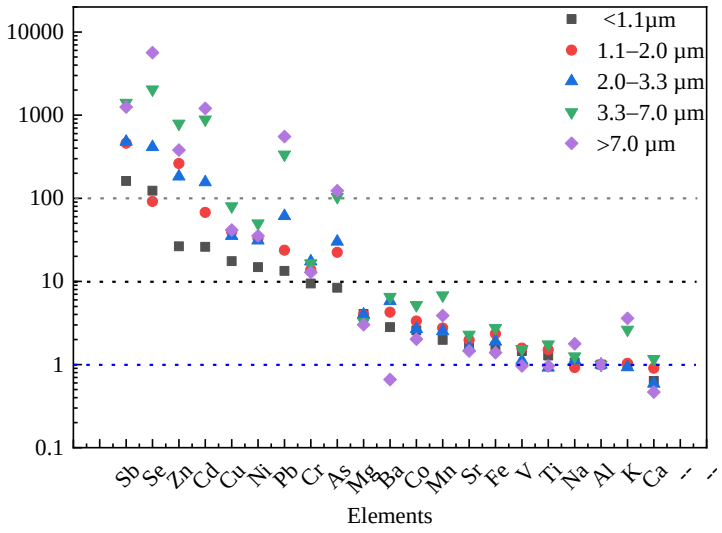

Fig. 38. The crustal enrichment factors (CEFs) of each element of size-segregated particles in Beijing (The blue dashed line indicates that CEFs are less than 1; the black dashed line indicates that CEFs are less than 10; the green dashed line indicates that CEFs are less than 100.)

4.4 Health Risk Assessment of Water-Soluble Potentially Toxic Metals

In this study, based on the US-EPA Integrated Risk Information System (IRIS) and International

Agency for Research on Cancer (IARC), the metals can be divided into carcinogens and non-carcinogens. Group 1 (carcinogenic to humans): As, Cd, Cr(VI) and Ni; Group 2A (probably carcinogenic to humans); Group 2B (possibly carcinogenic to humans): Co, V, and Pb. The concentration of Cr(VI) was presumed to be 1/7 of the total concentration of Cr when calculating the Cr health risk. According to US-EPA Region RSL (Regional Screening Levels), the Cr(VI) to Cr(III) ratio is 1:6 (C. R. Chen et al., 2021)(X. Duan et al., 2020). We analyzed the health risks of these seven toxic metal elements （As, Cd, Cr(VI), Ni, Co, V and Pb）.

To determine the probability of non-carcinogenic and carcinogenic risks (CR) to the public due to PM-bound metals, the risk to human health should be assessed. Fine particles matter through inhalation would deposit into the alveolar region. However, the alveolar region does not have protective mucus layers, particles deposited into this region are difficult to eliminate, causing considerable health risks for humans (L. C. Chen & Lippmann, 2009). Moreover, the alveolar area is difficult to eliminate particles deposited in this area, it can be posing a considerable health risk to the human body (Y. C. Lin et al., 2020).Thus, particles deposited in the alveolar region via inhalation route are considered to play the most important role in threatening human health (Betha et al., 2014).

The methodology has been used in previous studies (Men et al., 2018) (K. Xiao, Qin, et al., 2021). Sensitive local residents were divided into two groups (i.e., children and adults). Thus, inhalation exposure concentration (EC), hazard quotient (HQ) for non-carcinogenic risk, and carcinogenic risks (CR) of WSPTMs in RCC PM were calculated following Eqs (5-10):

$$ECn=\frac{Ci\times ET\times EF\times ED}{ATn} \quad 5)$$

$$ECc=\frac{Ci\times ET\times EF\times ED}{ATc} \quad 6)$$

$$HQi=\frac{ECn}{RfC\times 1000\ \mu g\ mg^{-1}} \quad 7)$$ (i= As, Cd, Co, Cr (VI), Mn, Ni , V, Zn, Ba and, Ba)

$$CRi=IUR\times ECc \quad 8)$$ (i= V, As, Cd, Cr (VI), Ni, Co, and Pb)

$$TCR=\Sigma CRi \quad 9)$$

$$HI=\Sigma HQi \quad 10)$$

The exposure concentration (EC) is each element through inhalation (μg m^{-3}). where Ci is the average concentration of individual WSPTMs of PM size i, where ECn is used to calculated the values of HQ, where ECc is used to calculated the values of CR, TCR is the total carcinogenic risks of all the WSPTMs, HI is the total hazard quotient of all the WSPTMs, where AT, ED, EF and ET are average lifetime (hours), exposure duration (year), exposure frequency (days $year^{-1}$), and exposure time (h day^{-1}).

The values of all the parameters and explanations are listed in Table 21. The parameter of Inhalation unit risk (IUR) and Inhalation reference dose (RfC) value of Water-Soluble Potentially Toxic Metals are shown in Table 20. The CR value between 1×10^{-6} and 1×10^{-4} indicates acceptable or tolerable carcinogenic risk. If the value is higher than 11×10^{-4}, it means the risk is unacceptable. CR value lower than 1×10^{-6} indicates no significant health hazards.

Table 20. RfCi and IUR values for different Water-Soluble Potentially Toxic Metals. (Jianwei Liu et al., 2018)

WSPTMs	Inhalation Unit Risk (IUR) ($\mu g\ m^{-3}$)$^{-1}$	References	RfC ($mg\ m^{-3}$)
V	8.3×10^{-3}	PPRTVs [a]	1.0×10^{-4}
Cr(VI)	1.2×10^{-2}	RAIS [b]	1.0×10^{-4}
Co	9.0×10^{-3}	PPRTVs [a]	6.0×10^{-6}
Ni	2.4×10^{-4}	RAIS [b]	1.4×10^{-5}
As	4.3×10^{-3}	RAIS [b]	1.5×10^{-5}
Cd	1.8×10^{-3}	RAIS [b]	1.0×10^{-5}
Pb	1.2×10^{-5}	CALEPA[c]	
Se	2.0×10^{-2}	USEPA[e]	
Zn		(Xiao et al., 2021) (Fu et al., 2021)	3.01×10^{-1}
Ba		(Xiao et al., 2021) (Fu et al., 2021)	5.00×10^{-4}
Mn		(Xiao et al., 2021) (Fu et al., 2021)	5.00×10^{-5}
Al		(Fu et al., 2021)	5.00×10^{-3}

a PPRTVs: Provisional Peer-Reviewed Toxicity Values (n.d.). Accessed 15 August 2020, from https://www.epa.gov/pprtv/provisional-peer-reviewed-toxicity-values-pprtvs-assessments.

b RAIS: The Risk Assessment Information System. (n.d.). Accessed 15 August 2020, from https://rais.ornl.gov/cgi-bin/tools/TOX_search?select=chemtox.

c CALEPA: California Environmental Protection Agency. (n.d.). Accessed 15 August 2020, from https://calepa.ca.gov/.

d USEPA : United States Environmental Protection Agency. (n.d.). Accessed 15 August 2020, from https://www.epa.gov/iris.

e USEPA. 2021. User's guide/technical background document for US EPA region 9's RSLs tables. Accessed 15 August 2020, from https://www.epa.gov/risk/regional-screening-levels-rsls-generic-tables

Table 21. Exposure parameters of health risk assessment (J. J. Xie et al., 2020)

Exposure parameter	Value for children	Vale for adults
EF (exposure frequency)	350 day·year^{-1}	350 day·year^{-1}
ET (exposure time)	24h·day^{-1}	24h·day^{-1}
ED (exposure duration)	6 years	24 years
ATn (average time for non-carcinogenic)	ED×365days·year^{-1}×24h·day^{-1}	ED×365days·year^{-1}×24h·day^{-1}
ATc (average time for carcinogenic)	74.83 year×365 days·year^{-1}×24 h·day^{-1}	74.83 year×365 days·year^{-1}×24 h·day^{-1}

China's Sixth National Census Shows Average Life Expectancy Reaches 74.83 Years. (National Bureau of Statistics of the People's Republic of China; http://www.stats.gov.cn/tjsj/ndsj/ ; accessed on 13 Jun 2021)

4.4.1 Health Risk Assessment of Water-Soluble Potentially Toxic Metals in APMs in Xuanwei

We divided the participants into three groups: boys (age: < 12), girls (age: < 12) (Xing Li et al., 2022), and adult (average 30) (USEPA, 2004). For carcinogenic risk of WSPTMs via inhalation exposure for boys, girls and adults, the CR and TCR within $PM_{1.1}$, $PM_{1.1–2.0}$, $PM_{2.0–3.3}$, $PM_{3.3–7.0}$, and $PM_{>7.0}$ during the sampling period were list in the Table 22. As expected, the total WSPTMs exhibited high TCR values (9.98×10^{-6}, 1.06×10^{-5} ,and 1.19×10^{-5} for girls, Boys and adults, respectively) in the smaller particles (<1.1 μm) because of their high deposition efficiencies (U.S. EPA, 2015).

We compared the difference of carcinogenic risk of WSPTMs for boys, girls and adults, and found that the TCR caused via inhalation of $PM_{2.0}$ in order: adults > girls > boys. Compared with the results of other cities in China, the carcinogenic values for children (boys and girls) were higher than Ningbo (6.24×10^{-6}) (Y. Wu et al., 2019), Wuhan (5.94×10^{-6}) (Weiqian Wang et al., 2020), but for adults were lower than that of Chengdu (5.76×10^{-4}) (Y. Li et al., 2016), Tanshan (1.48×10^{-4}) (Fang et al., 2021), Linfen City (7.75×10^{-5}) (Y. C. Lin et al., 2020), Ningbo (2.50×10^{-5}) (Y. Wu et al., 2019), Wuhan (4.65×10^{-5}) (Weiqian Wang et al., 2020).

The order of carcinogenic risk by the ingestion route for boys, girls and adults were Se > Cr (VI) > As > Cd > Co > V > Ni > Pb, with Se and Cr (VI) values were lower than 1×10^{-4} but higher than 1×10^{-6} for boys, girls and adults having the greater effect. The indicated that the carcinogenic risk of Se and Cr (VI) via inhalation is tolerable, indicating that we should pay more attention to these toxic elements (Do et al., 2021). This implied that control of Cr (VI) and Se emissions were a crucial way to decrease

the cancer risk in Xuanwei.

Table 22. The carcinogenic risk of WSPTMs for boys, girls and adults in Xuanwei

Groups	Carcinogenic risk（CR）							
	Dp(μm)							
	WSPTMs	<1.1	1.1-2.0	2.0-3.3	3.3-7.0	>7.0	<2.0	>2.0
Boys	V	5.34×10^{-8}	1.21×10^{-8}	8.91×10^{-9}	1.08×10^{-8}	2.68×10^{-8}	6.54×10^{-8}	4.62×10^{-8}
	Cr(VI)	3.07×10^{-6}	4.03×10^{-7}	3.24×10^{-7}	3.30×10^{-7}	3.40×10^{-7}	3.47×10^{-6}	9.94×10^{-7}
	Co	5.83×10^{-8}	9.94×10^{-9}	8.53×10^{-9}	9.59×10^{-9}	1.70×10^{-8}	6.82×10^{-8}	3.51×10^{-8}
	Ni	4.29×10^{-9}	1.34×10^{-9}	1.34×10^{-9}	8.98×10^{-10}	4.45×10^{-9}	5.60×10^{-9}	6.69×10^{-9}
	As	2.03×10^{-7}	5.13×10^{-8}	2.47×10^{-8}	1.88×10^{-8}	1.06×10^{-8}	2.54×10^{-7}	5.41×10^{-8}
	Se	6.52×10^{-6}	3.91×10^{-7}	1.50×10^{-7}	6.37×10^{-8}	4.28×10^{-8}	6.91×10^{-6}	2.56×10^{-7}
	Cd	6.61×10^{-8}	1.99×10^{-8}	1.42×10^{-8}	1.37×10^{-8}	2.19×10^{-8}	8.60×10^{-8}	4.98×10^{-8}
	Pb	1.87×10^{-9}	9.00×10^{-10}	2.64×10^{-10}	1.00×10^{-10}	3.55×10^{-11}	2.77×10^{-9}	3.99×10^{-10}
	TCR	9.98×10^{-6}	8.90×10^{-7}	5.31×10^{-7}	4.48×10^{-7}	4.64×10^{-7}	1.09×10^{-5}	1.44×10^{-6}
Girls	V	5.65×10^{-8}	1.23×10^{-8}	9.44×10^{-9}	1.15×10^{-8}	2.81×10^{-8}	6.93×10^{-8}	4.90×10^{-8}
	Cr(VI)	3.25×10^{-6}	4.27×10^{-7}	3.43×10^{-7}	3.50×10^{-7}	3.61×10^{-7}	3.68×10^{-6}	1.05×10^{-6}
	Co	6.18×10^{-8}	1.05×10^{-8}	9.03×10^{-9}	1.01×10^{-8}	1.80×10^{-8}	7.23×10^{-8}	3.72×10^{-8}
	Ni	4.51×10^{-9}	1.42×10^{-9}	1.42×10^{-9}	9.51×10^{-10}	4.72×10^{-9}	5.93×10^{-9}	7.09×10^{-9}
	As	2.15×10^{-7}	5.43×10^{-8}	2.62×10^{-8}	1.99×10^{-8}	1.12×10^{-8}	2.69×10^{-7}	5.73×10^{-8}
	Se	6.91×10^{-6}	4.15×10^{-7}	1.59×10^{-7}	6.75×10^{-8}	4.53×10^{-8}	7.32×10^{-6}	2.72×10^{-7}
	Cd	7.01×10^{-8}	2.11×10^{-8}	1.50×10^{-8}	1.45×10^{-8}	2.32×10^{-8}	9.12×10^{-8}	5.27×10^{-8}
	Pb	1.98×10^{-9}	9.54×10^{-10}	2.79×10^{-10}	1.06×10^{-10}	3.76×10^{-11}	2.94×10^{-9}	4.23×10^{-10}
	TCR	1.06×10^{-5}	9.43×10^{-7}	5.63×10^{-7}	4.74×10^{-7}	4.91×10^{-7}	1.51×10^{-5}	1.53×10^{-6}
Adults	V	6.35×10^{-8}	1.44×10^{-8}	1.06×10^{-8}	1.29×10^{-8}	3.16×10^{-8}	7.79×10^{-8}	5.50×10^{-8}
	Cr(VI)	3.66×10^{-6}	4.79×10^{-7}	3.85×10^{-7}	3.93×10^{-7}	4.05×10^{-7}	4.13×10^{-6}	1.18×10^{-6}
	Co	6.94×10^{-8}	1.18×10^{-8}	1.02×10^{-8}	1.14×10^{-8}	2.03×10^{-8}	8.12×10^{-8}	4.18×10^{-8}
	Ni	5.06×10^{-9}	1.60×10^{-9}	1.60×10^{-9}	1.07×10^{-9}	5.30×10^{-9}	6.66×10^{-9}	7.97×10^{-9}
	As	2.42×10^{-7}	6.11×10^{-8}	2.94×10^{-8}	2.24×10^{-8}	1.26×10^{-8}	3.03×10^{-7}	6.44×10^{-8}
	Se	7.76×10^{-6}	4.66×10^{-7}	1.78×10^{-7}	7.59×10^{-8}	5.09×10^{-8}	8.23×10^{-6}	3.05×10^{-7}
	Cd	7.87×10^{-8}	2.37×10^{-8}	1.69×10^{-8}	1.63×10^{-8}	2.61×10^{-8}	1.02×10^{-7}	5.92×10^{-8}
	Pb	2.23×10^{-9}	1.07×10^{-9}	3.14×10^{-10}	1.19×10^{-10}	2.42×10^{-11}	3.30×10^{-9}	4.75×10^{-10}
	TCR	1.19×10^{-5}	1.06×10^{-6}	6.33×10^{-7}	5.33×10^{-7}	5.52×10^{-7}	1.29×10^{-5}	1.72×10^{-6}

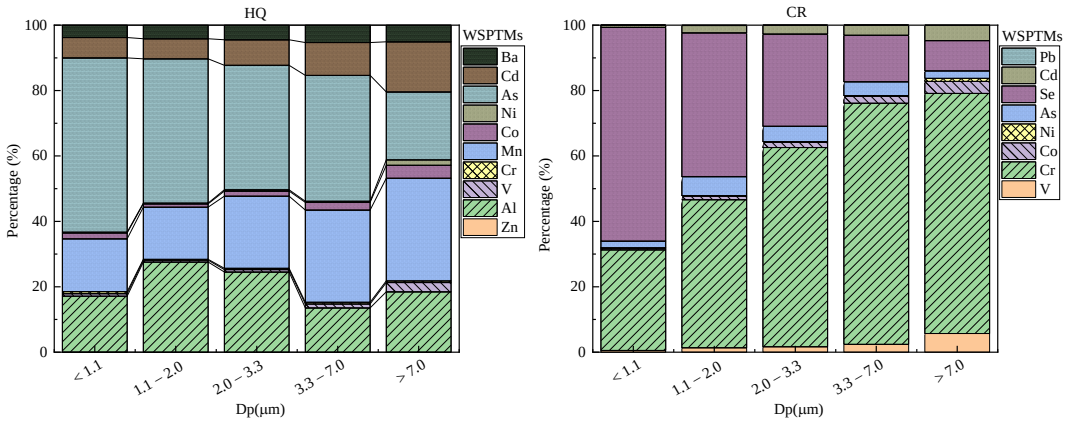

Fig.39. The relative portions of CR and HQ of WSPTMs within $PM_{1.1}$, $PM_{1.1\text{-}2.0}$, $PM_{2.0\text{-}3.3}$, $PM_{3.3\text{-}7.0}$, and $PM_{>7.0}$ fraction in Xuanwei during the sampling period.

Our data indicated the HI (Table 23) values for boys, girls and adults were all lower than the safe level (=1) (USEPA, 1989). indicating no non-carcinogenic risk from inhalation for people living in the rural areas of Xuanwei. Fig.39 shows the relative portions of CR and HQ of WSPTMs within $PM_{1.1}$, $PM_{1.1\text{-}2.0}$, $PM_{2.0\text{-}3.3}$, $PM_{3.3\text{-}7.0}$, and $PM_{>7.0}$ fraction in Xuanwei during the sampling period. Se make a major contribution (63.60%), followed by Cr (VI) (31.96%) of CR in $PM_{2.0}$, Cr (VI) make a major contribution (68.90%), followed by Se (17.77%) of CR in $PM_{2.0}$. According our result, the contribution of V, Cr (VI), Co, Ni, and Cd for CR, were increased with the PM size increase, while the contribution of Se for CR, were decreased with the PM size increase. This result is cross-validated with section 4.3.1.1, Se was identified as the most enriched WSPTMs. As, Mn and Al were the major contributor for non-carcinogenic risk.

Table 23. The non-carcinogenic risk of WSPTMs for boys, girls and adults in Xuanwei.

Groups	Non carcinogenic risk (HQ)							
	Dp(μm) / WSPTMs	<1.1	1.1-2.0	2.0-3.3	3.3-7.0	>7.0	<2.0	>2.0
Boys	Zn	0.0001	0.0000	0.0000	0.0000	0.0000	0.0001	0.0000
	Al	0.0586	0.0288	0.0143	0.0059	0.0085	0.0873	0.0287
	V	0.0026	0.0006	0.0004	0.0005	0.0013	0.0032	0.0023
	Cr(VI)	0.0021	0.0003	0.0002	0.0002	0.0002	0.0024	0.0007
	Mn	0.0553	0.0166	0.0129	0.0124	0.0144	0.0719	0.0397
	Co	0.0063	0.0011	0.0009	0.0010	0.0018	0.0073	0.0038
	Ni	0.0007	0.0002	0.0002	0.0002	0.0008	0.0010	0.0012
	As	0.1824	0.0461	0.0222	0.0169	0.0095	0.2285	0.0486
	Cd	0.0213	0.0064	0.0046	0.0044	0.0071	0.0277	0.0160
	Ba	0.0130	0.0043	0.0026	0.0023	0.0023	0.0173	0.0073
	HI	0.3423	0.1044	0.0584	0.0439	0.0460	0.4467	0.1482
Girls	Zn	0.0001	0.0000	0.0000	0.0000	0.0000	0.0001	0.0000
	Al	0.0620	0.0305	0.0151	0.0063	0.0090	0.0925	0.0304
	V	0.0028	0.0006	0.0005	0.0006	0.0014	0.0034	0.0024
	Cr(VI)	0.0022	0.0003	0.0002	0.0002	0.0002	0.0025	0.0007
	Mn	0.0586	0.0176	0.0136	0.0131	0.0153	0.0762	0.0420
	Co	0.0066	0.0011	0.0010	0.0011	0.0019	0.0078	0.0040
	Ni	0.0008	0.0002	0.0002	0.0002	0.0008	0.0010	0.0012
	As	0.1933	0.0488	0.0235	0.0179	0.0101	0.2421	0.0515
	Cd	0.0226	0.0068	0.0048	0.0047	0.0075	0.0293	0.0170
	Ba	0.0137	0.0046	0.0028	0.0025	0.0025	0.0183	0.0077
	HI	0.3627	0.1106	0.0618	0.0465	0.0487	0.4733	0.1570
Adults	Zn	0.0001	0.0000	0.0000	0.0000	0.0000	0.0001	0.0000
	Al	0.0697	0.0343	0.0170	0.0071	0.0101	0.1040	0.0342
	V	0.0031	0.0007	0.0005	0.0006	0.0015	0.0038	0.0027
	Cr(VI)	0.0025	0.0003	0.0003	0.0003	0.0003	0.0029	0.0008
	Mn	0.0658	0.0198	0.0153	0.0147	0.0172	0.0856	0.0472
	Co	0.0074	0.0013	0.0011	0.0012	0.0022	0.0087	0.0045
	Ni	0.0009	0.0003	0.0003	0.0002	0.0009	0.0011	0.0014
	As	0.2172	0.0549	0.0264	0.0201	0.0114	0.2720	0.0579
	Cd	0.0253	0.0076	0.0054	0.0052	0.0084	0.0330	0.0191
	Ba	0.0154	0.0052	0.0031	0.0028	0.0028	0.0206	0.0087
	HI	0.4075	0.1243	0.0695	0.0522	0.0547	0.5318	0.1764

4.4.2 Health Risk Assessment of Water-Soluble Potentially Toxic Metals in APMs in Beijing

Our sampling site is the largest residential area in Asia, with about 600,000 people, and the traffic volume is very heavy in the morning and evening rush hours. Residents living in this area are potential receptors for metals in the air. Fine and coarse atmospheric particulate matter has an important impact on human health and inhalation is the typical main route of direct exposure of toxic elements bound to PM in the atmosphere (Rovelli et al., 2020).

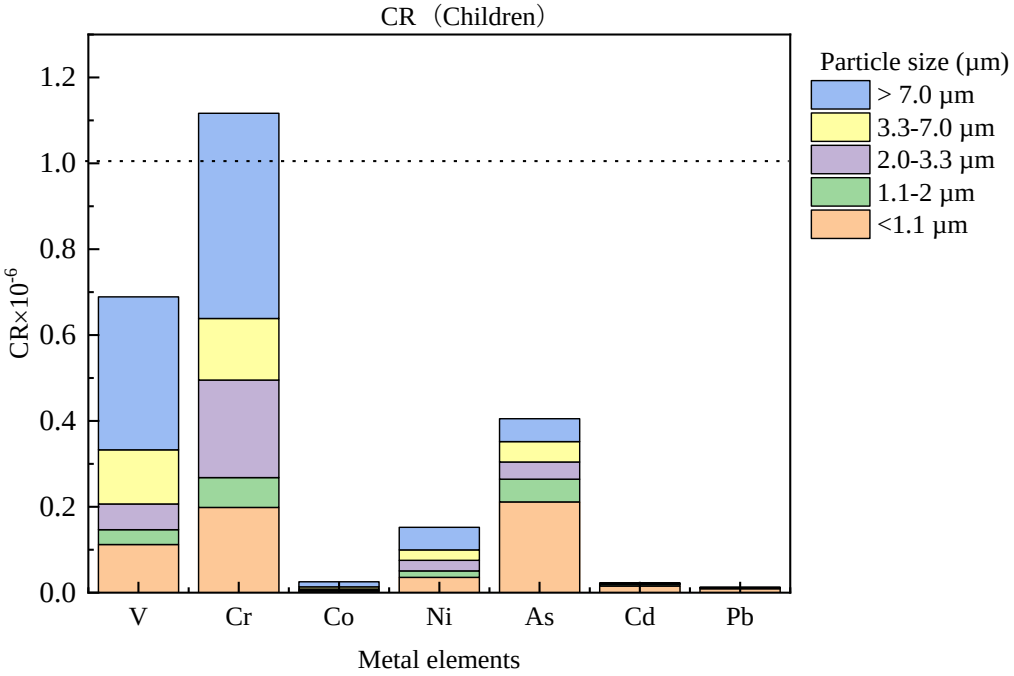

Fig. 40. The carcinogenic risks of toxic elements within $PM_{1.1}$, $PM_{1.1\text{-}2.0}$, $PM_{2.0\text{-}3.3}$, $PM_{3.3\text{-}7.0}$, $PM_{>7.0}$ in Beijing for children during the sampling period.

Figure 40, Figure 41, Figure 42, and Figure 43 show the carcinogenic and non- carcinogenic risks of each toxic elements for children and adults within $PM_{1.1}$, $PM_{1.1\text{-}2.0}$, $PM_{2.0\text{-}3.3}$, $PM_{3.3\text{-}7.0}$ and $PM_{>7.0}$ in Beijing during the sampling period. As expected, most of the toxic metals exhibited high CR values in the smaller particles (<1.1 μm) because of their high deposition efficiencies (Y. C. Lin et al., 2020) .The total CR values (reached 2.42×10^{-6} for children and 66.71×10^{-6} for adults , respectively) were exceeded the acceptable level (1×10^{-6}), indicating that we should pay more attention to these toxic elements (USEPA, 1989). Compared with previous studies, carcinogenic risks for children and adults is lower than those carcinogenic risks in Nanjing (2.57×10^{-5} for children and 4.59×10^{-5} for adults) (Yuanyuan Sun et al., 2014), in Linfen (2.91×10^{-5} for children and 7.75×10^{-5} for adults) (Y. C. Lin et al., 2020), In

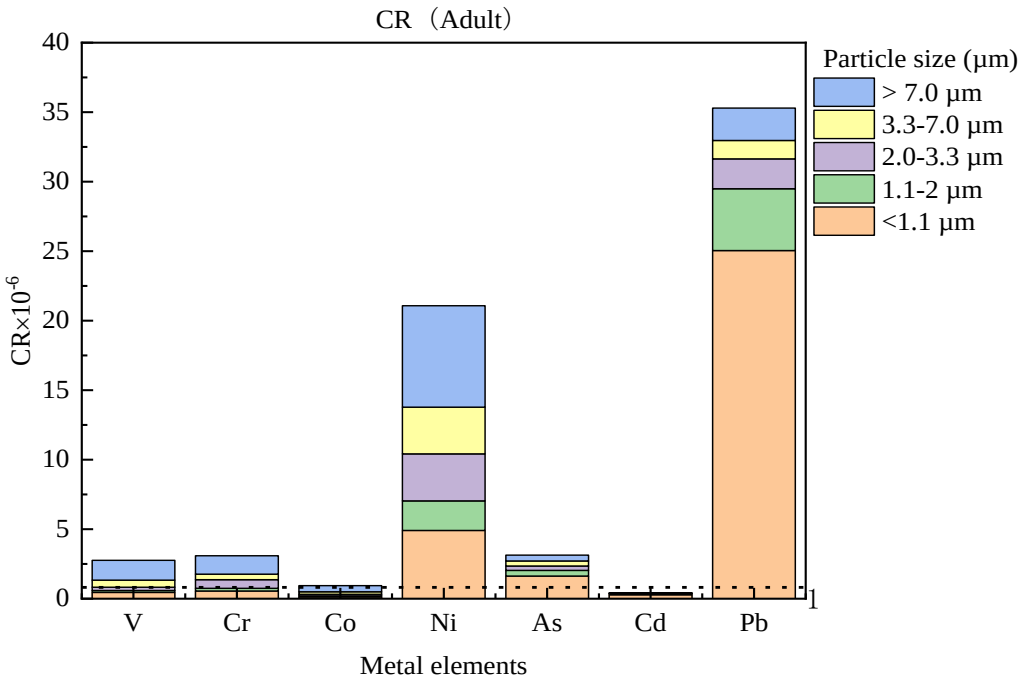

Fig. 41. The carcinogenic and non- carcinogenic risks of toxic elements within $PM_{1.1}$, $PM_{1.1\text{-}2.0}$, $PM_{2.0\text{-}3.3}$, $PM_{3.3\text{-}7.0}$, $PM_{>7.0}$ in Beijing for adults during the sampling period.

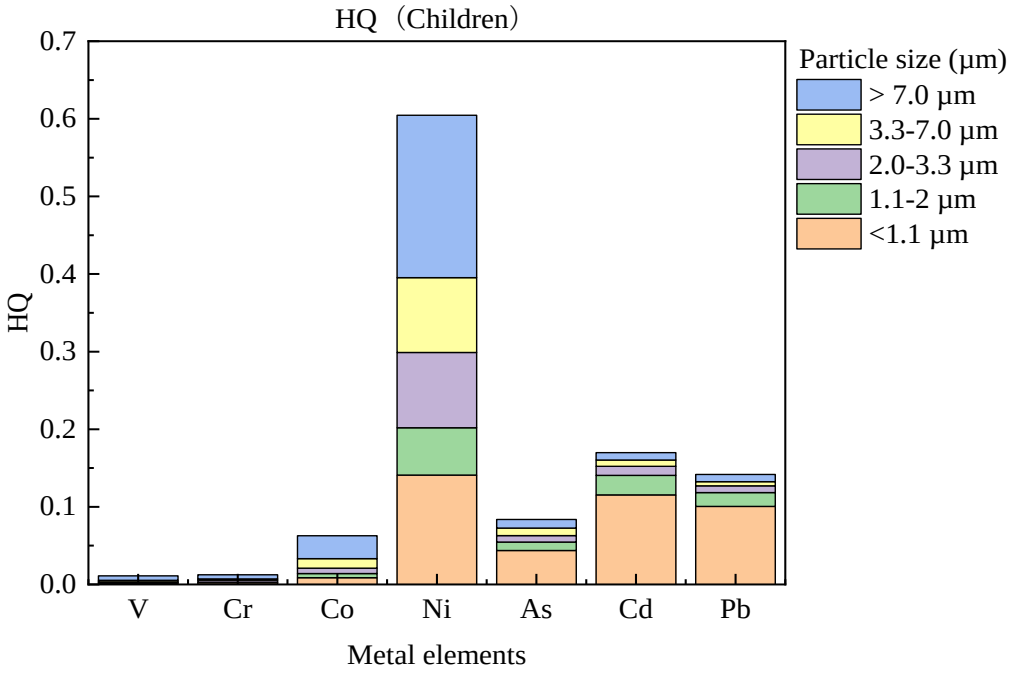

Fig. 42. The non- carcinogenic risks of toxic elements within $PM_{1.1}$, $PM_{1.1\text{-}2.0}$, $PM_{2.0\text{-}3.3}$, $PM_{3.3\text{-}7.0}$, $PM_{>7.0}$ in Beijing for children during the sampling period.

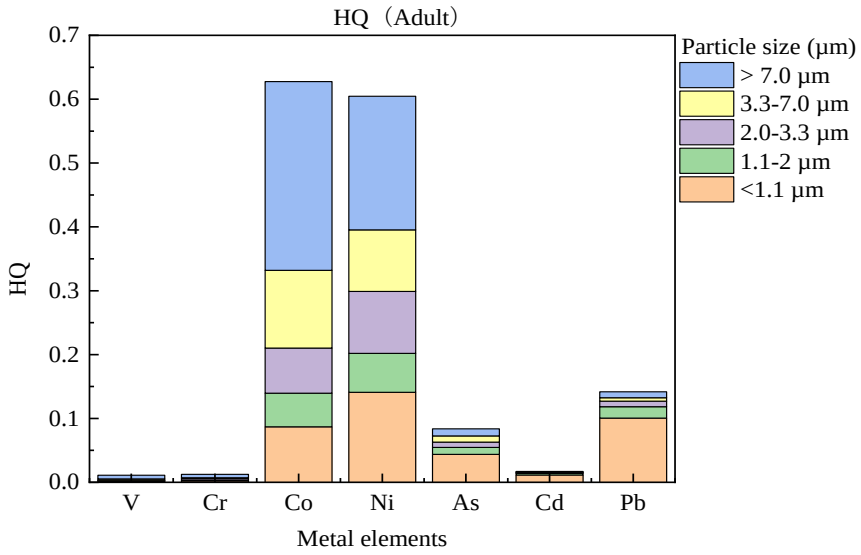

Fig. 43. The non- carcinogenic risks of toxic elements within $PM_{1.1}$, $PM_{1.1\text{-}2.0}$, $PM_{2.0\text{-}3.3}$, $PM_{3.3\text{-}7.0}$, $PM_{>7.0}$ in Beijing for adults during the sampling period.

Changzhi (2.58×10^{-6} for children and 10.31×10^{-6} for adults) (X. Duan et al., 2020), in Kanpur (1.60×10^{-5} for children and 3.99×10^{-6} for adults) (Can-Terzi et al., 2021) , in Ningbo (6.24×10^{-6} for children and 2.50×10^{-5} for adults) (Y. Wu et al., 2019).

Figure 44, Figure 45, Figure 46, and Figure 47 show that the relative portions of carcinogenic and non- carcinogenic risks of toxic elements within $PM_{1.1}$, $PM_{1.1\text{-}2.0}$, $PM_{2.0\text{-}3.3}$, $PM_{3.3\text{-}7.0}$ and $PM_{>7.0}$ in Beijing during the sampling period. $PM_{1.1}$ was the major contributor of Pb, Cd and As for CR and HQ (Table 24), it was indicated that $PM_{1.1}$ is more harmful than coarse PM. The toxic elements of Cr^{6+} (1.12×10^{-6}), V (0.69×10^{-6}) and As (0.41×10^{-6}) were caused higher CR for children than Ni, Cd, Co, Pb, meanwhile, Pb (35.30×10^{-6}) and Ni (21.07×10^{-6}) caused higher CR for adults than As, Cr^{6+}, V, Co, Cd, especially $PM_{1.1}$ (Table 25). It was indicated that V, Cr^{6+} and As may be more dangerous for children, Pb and Ni may be more dangerous for adults. The toxic element of Ni had the highest HQ for children and adults.

With respect to children and adults non-carcinogenic risk, the corresponding contributions of elements to the HQ were ranked in the following order: Cr(VI) (46.06 %) > V (28.42 %) > As (16.71 %) > Ni (6.28 %) > Co (1.05 %) > Cd (0.95 %) > Pb (0.53 %) and Pb (52.92 %) > V (31.59 %) > As (4.69 %) > Cr(VI) (4.63 %) > V (4.13 %) > Co (1.41 %) > Cd (0.63 %). The HQ values for As, Cd, Co, Cr(VI), Ni and V via inhalation exposure for both children and adults were all lower than the safe level (= 1), indicating no non-carcinogenic risks from the inhalation exposure for each toxic elements (USEPA, 1989).

$PM_{1.1}$ was the major contributor of Pb, Cd and As for CR and HQ in APMs in Beijing. The potential toxic metals of Cr(VI), V and As caused higher CR for children than Ni, Cd, Co, Pb, meanwhile, Pb and Ni were cause higher CR for adults than As, Cr(VI), V, Co, Cd, especially in $PM_{1.1}$ in APMs in Beijing.

TCR values were exceeded the acceptable level (1×10^{-6}), indicating that we should pay more attention to these PTMs in APMs particles. Both children and adults, the CR of As were the highest followed by Cr (VI) and Pb had the lowest CR in APMs.

Table 24. The non- carcinogenic risks of toxic elements for children and adult by inhalation route

WSPTMs	HQ									
	$PM_{1.1}$		$PM_{1.1-2.0}$		$PM_{2.0-3.3}$		$PM_{3.3-7.0}$		$PM_{>7.0}$	
	CH	AD	CH	AD	CH	AD	CH	AD	CH	AD
V	1.80E-03	1.8E-03	5.57E-04	5.5E-04	9.64E-04	9.6E-04	2.03E-03	2.03E-03	5.7E-03	5.7E-03
Cr (VI)	2.20E-03	2.20E-03	7.73E-04	7.73E-04	2.53E-03	2.53E-03	1.59E-03	1.59E-03	5.31E-03	5.31E-03
Co	8.70E-03	8.70E-02	5.26E-03	5.26E-02	7.07E-03	7.07E-02	1.22E-02	1.22E-02	2.96E-02	2.96E-01
Ni	1.41E-01	1.41E-01	6.10E-02	6.10E-02	9.71E-02	9.71E-02	9.63E-02	9.63E-02	2.09E-01	2.09E-01
As	4.37E-02	4.37E-02	1.10E-02	1.10E-02	8.28E-03	8.28E-03	9.78E-03	9.78E-03	1.11E-02	1.11E-02
Cd	1.15E-01	1.15E-02	2.51E-02	2.51E-03	1.18E-02	1.18E-03	8.10E-03	8.10E-03	9.45E-03	9.45E-04
Pb	1.01E-01	1.01E-01	1.78E-02	1.78E-02	8.64E-03	8.64E-03	5.35E-03	5.35E-03	9.36E-03	9.36E-03

CH: Children, AD: Adult

Table. 25. The carcinogenic risks of toxic elements for children and adult by inhalation route in Beijing

Element	CR									
	$PM_{1.1}$		$PM_{1.1-2.0}$		$PM_{2.0-3.3}$		$PM_{3.3-7.0}$		$PM_{>7.0}$	
	CH	AD	CH	AD	CH	AD	CH	AD	CH	AD
V	1.12E-07	4.4804E-07	3.4683E-08	1.38734E-07	6.004E-08	2.4E-07	1.2606E-07	5.043E-07	3.562E-07	1.4251E-06
Cr^{6+}	1.98E-07	5.4879E-07	6.9561E-08	1.92454E-07	2.274E-07	6.29E-07	1.4330E-07	3.965E-07	4.780E-07	1.3226E-06
Co	3.52E-09	1.2994E-07	2.1312E-09	7.86185E-08	2.865E-09	1.06E-07	4.9274E-09	1.818E-07	1.196E-08	4.4151E-07
Ni	3.55E-08	4.9121E-06	1.5368E-08	2.12599E-06	2.447E-08	3.39E-06	2.4257E-08	3.356E-06	5.273E-08	7.2946E-06
As	2.11E-07	1.6315E-06	5.3007E-08	4.09268E-07	4.006E-08	3.09E-07	4.7323E-08	3.654E-07	5.348E-08	4.1292E-07
Cd	1.56E-08	2.8739E-07	3.3845E-09	6.24264E-08	1.586E-09	2.93E-08	1.0932E-09	2.016E-08	1.275E-09	2.3518E-08
Pb	9.05E-09	2.5044E-05	1.6054E-09	4.44163E-06	7.772E-10	2.15E-06	4.8162E-10	1.332E-06	8.422E-10	2.3302E-06

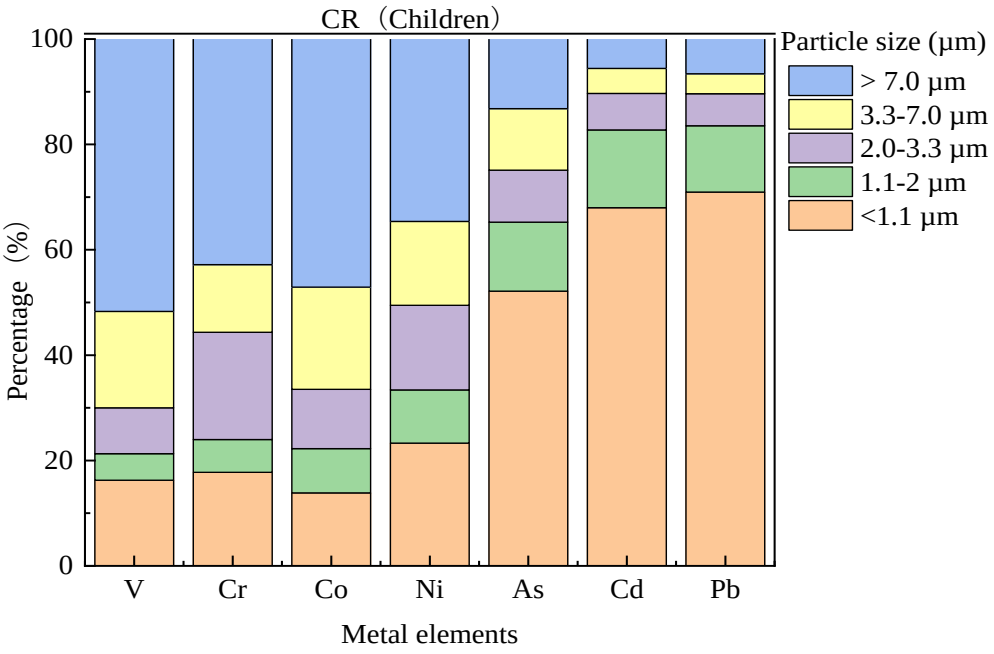

Fig. 44. The relative portions of carcinogenic risks of toxic elements within $PM_{1.1}$, $PM_{1.1\text{-}2.0}$, $PM_{2.0\text{-}3.3}$, $PM_{3.3\text{-}7.0}$ and $PM_{>7.0}$ in Beijing for children during the sampling period.

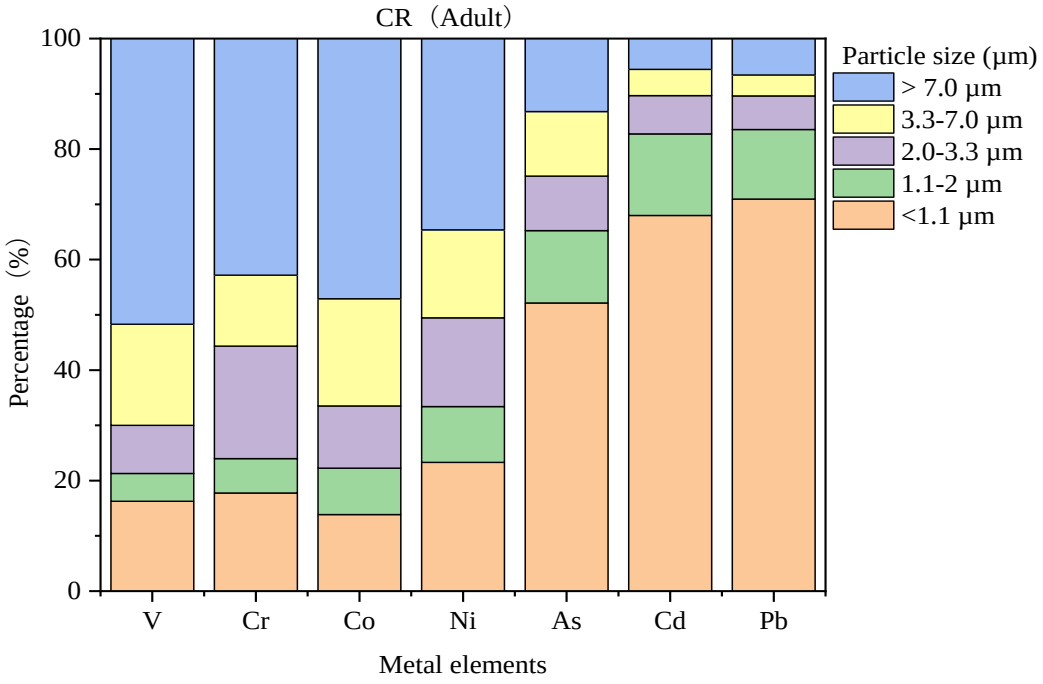

Fig. 45. The relative portions of carcinogenic risks of toxic elements within $PM_{1.1}$, $PM_{1.1\text{-}2.0}$, $PM_{2.0\text{-}3.3}$, $PM_{3.3\text{-}7.0}$ and $PM_{>7.0}$ in Beijing for adults during the sampling period.

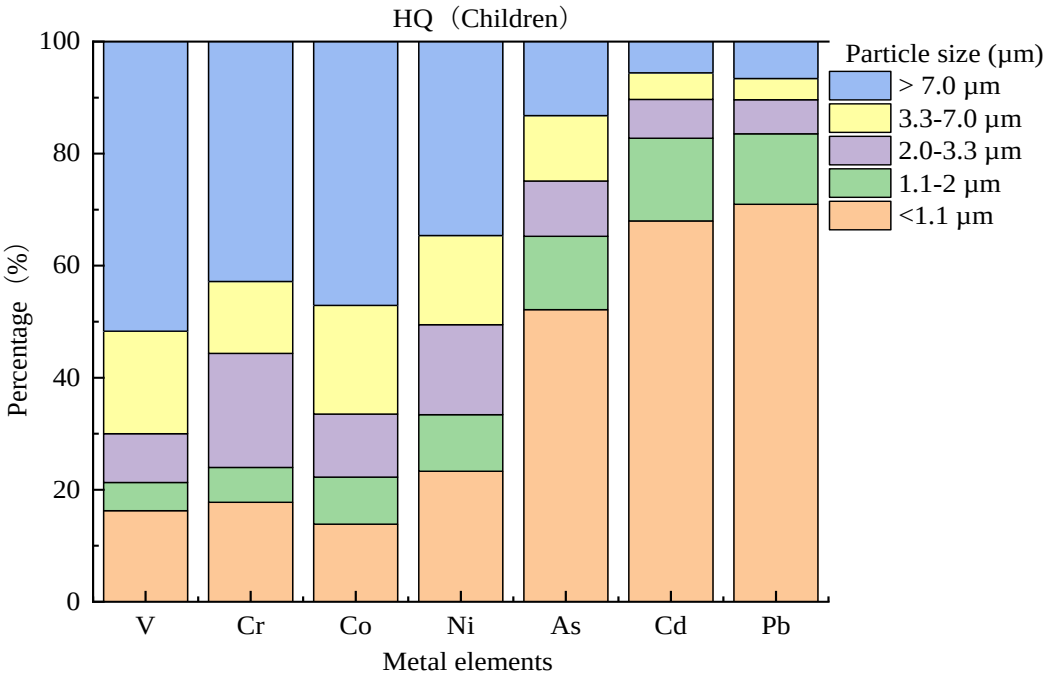

Fig. 46. The relative portions of non- carcinogenic risks of toxic elements within $PM_{1.1}$, $PM_{1.1\text{-}2.0}$, $PM_{2.0\text{-}3.3}$, $PM_{3.3\text{-}7.0}$ and $PM_{>7.0}$ in Beijing for children during the sampling period.

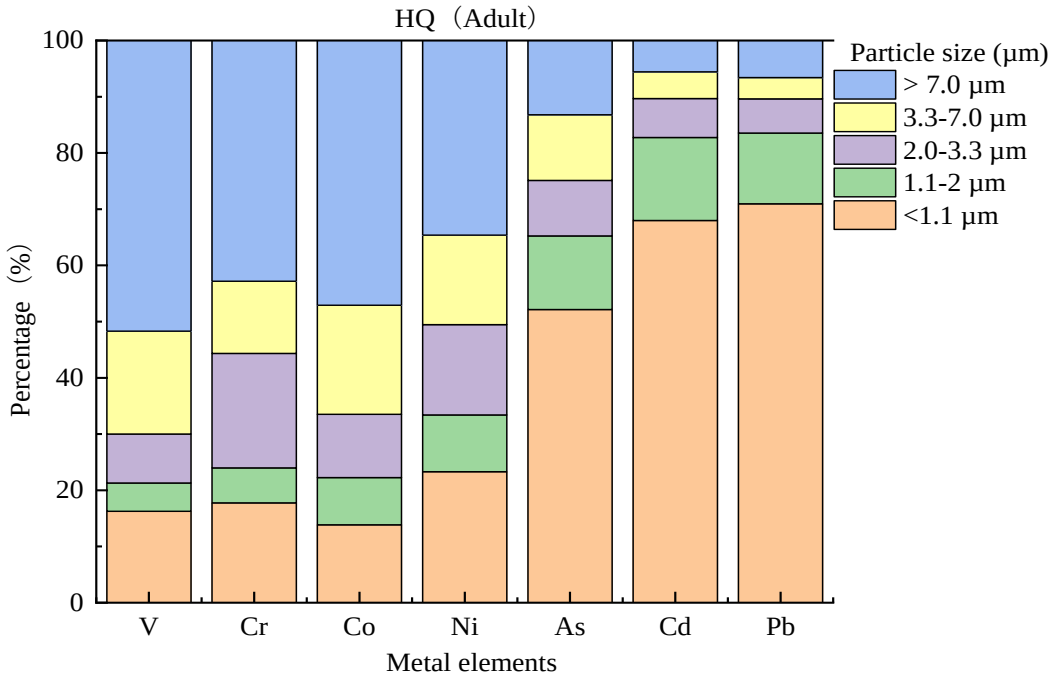

Fig. 47. The relative portions of non- carcinogenic risks of toxic elements within $PM_{1.1}$, $PM_{1.1\text{-}2.0}$, $PM_{2.0\text{-}3.3}$, $PM_{3.3\text{-}7.0}$ and $PM_{>7.0}$ in Beijing for adults during the sampling period.

4.4.3 Health Risk Assessment of Water-Soluble Potentially Toxic Metals in RCC Particles

HULIS chelates transition metals in atmospheric particulate matter and participates in the redox cycle (S. Lu et al., 2019), such as Copper (Cu) and Iron (Fe)) may cause oxidation potential in lung fluid (M. Lin & Yu, 2021). In the HULIS-Fe (II) system, the ROS generation capacity depends on the mixing time of HULIS-C with Fe (II), and the Fe (II)-induced Fenton reaction plays a role in cell mortality(S. Lu et al., 2019). Cu, Ni, Fe, Cr (VI), Co, As, Mn, V, and Zn could support electron exchange (Sen et al., 2016) and induce the formation of reactive oxygen species in the lungs (Verma et al., 2014), causing damage of oxidative DNA and inflammation of respiratory tracts (Distefano et al., 2009).

The HQ of V Cr (VI) Co As Cd Zn Mn and Ba within $PM_{1.1}$, $PM_{1.1–2.0}$, $PM_{2.0–3.3}$, $PM_{3.3–7.0}$, and $PM_{>7.0}$ in RCC particles were estimated (Table 26). Among these WSPTMs Ba, As, and Mn had the greatest contributions to HI, with risk (contributions) of $3.66\times10^{0} \pm 3.28\times10^{0}$ (78.39 ± 19.53%), $2.34\times10^{-2} \pm 2.34\times10^{-2} \pm 8.61\times10^{-2}$ (11.89 ± 10.20%), and $6.38\times10^{-2} \pm 1.84\times10^{-2}$ (2.57 ± 1.39%) in TSP, respectively. The HI of PTMs in descending order was Ba > As > Mn > Ni > Co > Cd > V > Cr (VI) in $PM_{1.1}$. The HQ values of WSPTMs were all below 1 within $PM_{1.1–2.0}$, $PM_{2.0–3.3}$, $PM_{3.3–7.0}$, and $PM_{>7.0}$, were higher than 1 in $PM_{1.1}$, indicating that there were noncancer risk in $PM_{1.1}$ of RCC particles (USEPA, 1989). The noncancer risk of Ba account for 91.28 %, 71.39 %, 78.74 %, 82.38 %, and 84.95 % within $PM_{1.1}$, $PM_{1.1–2.0}$, $PM_{2.0–3.3}$, $PM_{3.3–7.0}$, and $PM_{>7.0}$. It indicates that the non-carcinogenic risk of WSPTMs in RCC particles, mainly Ba, followed by As and the non-carcinogenic risk is highest within $PM_{1.1}$.

Figure 48, Figure 49, Figure 50, and Figure 51 show the carcinogenic and non-carcinogenic risks of each toxic elements for children and adults within $PM_{1.1}$, $PM_{1.1\text{-}2.0}$, $PM_{2.0\text{-}3.3}$, $PM_{3.3\text{-}7.0}$ and $PM_{>7.0}$ in RCC particles. The CR of V Cr (VI) Co As Cd and Pb for children and adults within $PM_{1.1}$, $PM_{1.1–2.0}$, $PM_{2.0–3.3}$, $PM_{3.3–7.0}$, and $PM_{>7.0}$ in RCC particles were estimated (Table 27). TCR values for As, Cd and Co decreased with increasing PM particle size (for adults and children), indicating that As, Cd and Co had the highest in $PM_{1.1}$. Interestingly, the TCR values for Cr (VI) were stable across PM particle sizes with no variability (adults and children), and the TCR for lead was negligible. Notably, the TCR values for V showed a bimodal distribution, with the major peak in the particle size <1.1 μm while the minor peak in the size range of > 7 μm. The TCR of PTMs for adults and children in the smaller particles (<1.1 μm) contributed 42.95 ± 8.49% and 42.01 ± 8.72% to the TSP, respectively. Among both children and adults, the CR of As were the highest ($1.40\times10^{-6} \pm 5.16\times10^{-7}$ for children, $5.60\times10^{-6} \pm 2.06\times10^{-6}$ for adults), followed by Cr (VI) ($1.40\times10^{-6} \pm 3.53\times10^{-6}$ for children, $5.60\times10^{-6} \pm 1.41\times10^{-6}$ for adults) in TSP. Pb had

Table 26. Non-carcinogenic health risk of WSPTMs in RCC particles

Samples	Size μm	V		Cr(VI)		Co		As		Cd		Zn		Mn		Ba		HI
		EC	HQ	EC	HQ	EC	HQ	EC	HQ	EC	HQ	EC	HQ	EC	HQ	EC	HQ	
LM	>7	8.74E-04	2.19E-03	2.62E-04	6.56E-04	7.58E-05	1.26E-02	2.20E-04	1.47E-02	2.36E-05	2.36E-03	1.12E-01	3.73E-05	4.92E-03	9.84E-03	4.88E-03	9.75E-02	1.40E-01
	3.3-7.0	2.94E-04	7.34E-04	3.46E-04	8.64E-04	2.21E-05	3.69E-03	1.76E-04	1.17E-02	1.50E-05	1.50E-03	6.16E-02	2.05E-05	4.19E-03	8.38E-03	5.05E-03	1.01E-01	1.28E-01
	2.0-3.3	9.26E-05	2.32E-04	2.79E-04	6.98E-04	9.52E-06	1.59E-03	2.68E-04	1.79E-02			5.31E-02	1.76E-05	5.23E-03	1.05E-02	1.44E-02	2.88E-01	3.19E-01
	1.1-2.0	7.54E-05	1.89E-04	3.66E-04	9.14E-04	3.00E-05	5.00E-03	3.42E-04	2.28E-02			9.43E-02	3.13E-05	6.36E-03	1.27E-02	1.32E-02	2.64E-01	3.06E-01
	<1.1	1.99E-04	4.97E-04	9.65E-05	2.41E-04	2.93E-04	4.89E-02	3.93E-03	2.62E-01	3.87E-05	3.87E-03	7.48E-01	2.48E-04	2.14E-02	4.29E-02	4.33E-01	8.66E+00	9.02E+00
BL	>7	1.70E-04	4.24E-04	3.55E-04	8.86E-04	4.91E-05	8.19E-03	1.79E-04	1.19E-02			4.29E-02	1.43E-05	3.33E-03	6.66E-03	1.35E-02	2.69E-01	2.98E-01
	3.3-7.0	8.45E-05	2.11E-04	5.53E-04	1.38E-03	4.00E-05	6.67E-03	2.54E-04	1.69E-02			4.31E-02	1.43E-05	1.98E-03	3.96E-03	1.31E-02	2.61E-01	2.90E-01
	2.0-3.3	2.61E-05	6.51E-05	3.11E-04	7.77E-04	1.12E-04	1.86E-02	5.39E-04	3.59E-02	9.97E-05	9.97E-03	9.39E-02	3.12E-05	4.63E-03	9.26E-03	4.63E-03	9.26E-02	1.67E-01
	1.1-2.0	2.74E-05	6.85E-05	3.56E-04	8.89E-04	1.12E-04	1.86E-02	6.30E-04	4.20E-02	1.30E-04	1.30E-02	1.06E-01	3.53E-05	1.48E-03	2.96E-03	4.28E-03	8.56E-02	1.63E-01
	<1.1	1.89E-04	4.72E-04	3.01E-04	7.51E-04	3.97E-04	6.62E-02	2.85E-03	1.90E-01	3.67E-04	3.67E-02	2.91E-01	9.68E-05	1.94E-02	3.89E-02	5.91E-02	1.18E+00	1.51E+00
SF	>7	1.16E-03	2.91E-03	2.32E-04	5.80E-04	6.97E-05	1.16E-02	1.58E-04	1.05E-02			1.06E-01	3.54E-05	2.49E-03	4.99E-03	5.20E-03	1.04E-01	1.35E-01
	3.3-7.0	2.50E-04	6.26E-04	1.15E-04	2.88E-04	3.67E-05	6.11E-03	2.27E-04	1.51E-02	1.50E-05	1.50E-03	3.87E-02	1.29E-05	3.15E-03	6.29E-03	1.53E-03	3.06E-02	6.05E-02
	2.0-3.3	8.74E-05	2.19E-04	1.85E-04	4.61E-04	1.20E-05	2.00E-03	1.55E-04	1.03E-02			7.12E-02	2.37E-05	4.83E-03	9.65E-03	1.15E-02	2.29E-01	2.52E-01
	1.1-2.0	2.91E-05	7.28E-05	7.60E-05	1.90E-04	9.09E-06	1.51E-03	1.83E-04	1.22E-02	2.67E-05	2.67E-03	8.68E-02	2.89E-05	6.81E-03	1.36E-02	1.34E-02	2.67E-01	2.98E-01
	<1.1	1.85E-04	4.64E-04	2.63E-04	6.57E-04	7.55E-05	1.26E-02	1.14E-03	7.60E-02	3.86E-05	3.86E-03	9.13E-01	3.03E-04	1.32E-02	2.64E-02	2.97E-01	5.94E+00	6.06E+00
LJW	>7	2.48E-04	6.19E-04	2.29E-04	5.73E-04	3.04E-05	5.07E-03	1.61E-04	1.08E-02			6.16E-02	2.05E-05	3.39E-03	6.78E-03	1.67E-02	3.33E-01	3.57E-01
	3.3-7.0	9.25E-05	2.31E-04	4.63E-04	1.16E-03	3.33E-06	5.55E-04	1.39E-04	9.26E-03			5.88E-02	1.95E-05	9.84E-04	1.97E-03	4.10E-03	8.20E-02	9.52E-02
	2.0-3.3	6.89E-05	1.72E-04	2.42E-04	6.05E-04	9.83E-06	1.64E-03	1.58E-04	1.05E-02			5.38E-02	1.79E-05	1.41E-03	2.82E-03	1.35E-03	2.71E-02	4.29E-02
	1.1-2.0	1.71E-06	4.28E-06	1.98E-04	4.96E-04	1.67E-05	2.78E-03	1.46E-04	9.71E-03			7.43E-02	2.47E-05	5.53E-03	1.11E-02	5.92E-03	1.18E-01	1.42E-01
	<1.1	1.62E-04	4.06E-04	1.16E-04	2.91E-04	9.13E-05	1.52E-02	2.14E-03	1.43E-01	6.76E-05	6.76E-03	3.93E-01	1.31E-04	6.79E-03	1.36E-02	6.02E-03	1.20E-01	3.00E-01
GM	>7	2.73E-04	6.82E-04	1.82E-04	4.55E-04	6.02E-05	1.00E-02	1.44E-04	9.62E-03			4.37E-02	1.45E-05	5.53E-03	1.11E-02	1.07E-02	2.13E-01	2.45E-01
	3.3-7.0	1.38E-04	3.46E-04	1.86E-04	4.65E-04	4.51E-05	7.52E-03	9.83E-05	6.55E-03			4.25E-02	1.41E-05	2.62E-03	5.23E-03	8.66E-03	1.73E-01	1.93E-01
	2.0-3.3	1.11E-04	2.78E-04	1.27E-04	3.17E-04	7.68E-06	1.28E-03	1.10E-04	7.33E-03			4.26E-02	1.42E-05	1.00E-03	2.00E-03	8.91E-03	1.78E-01	1.89E-01
	1.1-2.0	1.26E-04	3.14E-04	2.25E-04	5.64E-04	5.88E-05	9.80E-03	3.29E-04	2.19E-02			7.98E-02	2.65E-05	3.60E-03	7.21E-03	2.25E-03	4.51E-02	8.49E-02
	<1.1	6.59E-04	1.65E-03	3.05E-04	7.63E-04	2.48E-04	4.13E-02	1.47E-03	9.82E-02	5.02E-04	5.02E-02	3.23E-01	1.07E-04	3.20E-02	6.39E-02	1.18E-01	2.35E+00	2.61E+00
ZF	>7	2.00E-04	5.01E-04	2.41E-04	6.02E-04	7.68E-06	1.28E-03	2.09E-04	1.40E-02			4.28E-02	1.42E-05	1.72E-03	3.44E-03	2.37E-03	4.74E-02	6.72E-02
	3.3-7.0	1.09E-04	2.71E-04	3.08E-04	7.70E-04	2.61E-05	4.34E-03	1.97E-04	1.31E-02			4.93E-02	1.64E-05	1.48E-03	2.97E-03	1.92E-03	3.83E-02	5.98E-02
	2.0-3.3	4.57E-05	1.14E-04	2.60E-04	6.50E-04			2.40E-04	1.60E-02			2.20E-02	7.29E-06	1.73E-03	3.47E-03	1.92E-03	3.83E-02	5.86E-02
	1.1-2.0	6.23E-05	1.56E-04	1.47E-04	3.68E-04	7.88E-06	1.31E-03	5.73E-04	3.82E-02	3.38E-04	3.38E-02	4.71E-02	1.56E-05	3.80E-03	7.59E-03	3.97E-03	7.95E-02	1.61E-01
	<1.1	5.43E-04	1.36E-03	2.08E-04	5.19E-04	3.69E-05	6.15E-03	3.69E-03	2.46E-01	2.30E-03	2.30E-01	1.87E-01	6.22E-05	1.62E-02	3.25E-02	1.11E-02	2.22E-01	7.39E-01

Table 27. Carcinogenic health risk of WSPTMs in RCC particles

Sample	Size (μm)	V		Cr(VI)		Co		As		Cd		Pb		TCR	
		Child	Adult	Child	Adult	Child	Adult	Child	Adult	Child	Adult	Child	Adult	Child	Adult
LM	>7	6.74E-07	2.70E-06	2.92E-07	1.17E-06	6.34E-08	2.54E-08	8.77E-08	3.51E-07	3.95E-09	1.58E-08	1.51E-10	6.04E-10	1.12E-06	4.26E-06
	3.3-7.0	2.26E-07	9.05E-07	3.85E-07	1.54E-06	1.85E-08	7.39E-09	7.03E-08	2.81E-07	2.51E-09	1.00E-08	1.41E-10	5.64E-10	7.03E-07	2.75E-06
	2.0-3.3	7.14E-08	2.86E-07	3.11E-07	1.24E-06	7.95E-09	3.18E-09	1.07E-07	4.28E-07			1.14E-10	4.54E-10	4.98E-07	1.96E-06
	1.1-2.0	5.81E-08	2.32E-07	4.07E-07	1.63E-06	2.51E-08	1.00E-08	1.37E-07	5.46E-07			1.36E-10	5.44E-10	6.27E-07	2.42E-06
	<1.1	1.53E-07	6.12E-07	1.08E-07	4.30E-07	2.45E-07	9.80E-08	1.57E-06	6.27E-06	6.46E-09	2.58E-08	3.07E-09	1.23E-08	2.08E-06	7.45E-06
	TSP	1.18E-06	4.73E-06	1.50E-06	6.01E-06	3.60E-07	1.44E-07	1.97E-06	7.88E-06	1.29E-08	5.17E-08	3.61E-09	1.44E-08	5.03E-06	1.88E-05
BL	>7	1.31E-07	5.23E-07	3.95E-07	1.58E-06	4.11E-08	1.64E-08	7.13E-08	2.85E-07			3.95E-11	1.58E-10	6.38E-07	2.40E-06
	3.3-7.0	6.51E-08	2.61E-07	6.16E-07	2.46E-06	3.34E-08	1.34E-08	1.01E-07	4.06E-07			5.74E-11	2.30E-10	8.16E-07	3.14E-06
	2.0-3.3	2.01E-08	8.03E-08	3.46E-07	1.39E-06	9.34E-08	3.74E-08	2.15E-07	8.61E-07	1.67E-08	6.66E-08	1.54E-10	6.16E-10	6.92E-07	2.43E-06
	1.1-2.0	2.11E-08	8.45E-08	3.96E-07	1.58E-06	9.34E-08	3.74E-08	2.52E-07	1.01E-06	2.17E-08	8.69E-08	1.26E-10	5.02E-10	7.84E-07	2.80E-06
	<1.1	1.45E-07	5.82E-07	3.35E-07	1.34E-06	3.32E-07	1.33E-07	1.14E-06	4.55E-06	6.14E-08	2.45E-07	4.39E-10	1.76E-09	2.01E-06	6.85E-06
	TSP	3.83E-07	1.53E-06	2.09E-06	8.35E-06	5.93E-07	2.37E-07	1.78E-06	7.11E-06	9.97E-08	3.99E-07	8.15E-10	3.26E-09	4.94E-06	1.76E-05
SF	>7	8.96E-07	3.58E-06	2.58E-07	1.03E-06	5.82E-08	2.33E-08	6.31E-08	2.52E-07			4.41E-12	1.76E-11	1.28E-06	4.89E-06
	3.3-7.0	1.93E-07	7.71E-07	1.28E-07	5.14E-07	3.06E-08	1.23E-08	9.06E-08	3.63E-07	2.51E-09	1.00E-08			4.45E-07	1.67E-06
	2.0-3.3	6.74E-08	2.69E-07	2.06E-07	8.23E-07	1.00E-08	4.00E-09	6.17E-08	2.47E-07					3.45E-07	1.34E-06
	1.1-2.0	2.24E-08	8.98E-08	8.47E-08	3.39E-07	7.59E-09	3.04E-09	7.30E-08	2.92E-07	4.46E-09	1.78E-08	3.07E-10	1.23E-09	1.93E-07	7.43E-07
	<1.1	1.43E-07	5.72E-07	2.93E-07	1.17E-06	6.31E-08	2.52E-08	4.55E-07	1.82E-06	6.46E-09	2.58E-08	5.55E-10	2.22E-09	9.61E-07	3.62E-06
	TSP	1.32E-06	5.28E-06	9.70E-07	3.88E-06	1.70E-07	6.78E-08	7.43E-07	2.97E-06	1.34E-08	5.37E-08	8.66E-10	3.46E-09	3.22E-06	1.23E-05
LJW	>7	1.91E-07	7.64E-07	2.56E-07	1.02E-06	2.54E-08	1.02E-08	6.44E-08	2.58E-07					5.36E-07	2.05E-06
	3.3-7.0	7.13E-08	2.85E-07	5.16E-07	2.06E-06	2.78E-09	1.11E-09	5.55E-08	2.22E-07					6.45E-07	2.57E-06
	2.0-3.3	5.31E-08	2.12E-07	2.70E-07	1.08E-06	8.21E-09	3.28E-09	6.31E-08	2.52E-07					3.94E-07	1.55E-06
	1.1-2.0	1.32E-09	5.28E-09	2.21E-07	8.84E-07	1.39E-08	5.57E-09	5.82E-08	2.33E-07					2.94E-07	1.13E-06
	<1.1	1.25E-07	5.00E-07	1.30E-07	5.19E-07	7.63E-08	3.05E-08	8.55E-07	3.42E-06	1.13E-08	4.52E-08	1.73E-10	6.91E-10	1.20E-06	4.51E-06
	TSP	4.42E-07	1.77E-06	1.39E-06	5.57E-06	1.27E-07	5.07E-08	1.10E-06	4.38E-06	1.13E-08	4.52E-08	1.73E-10	6.91E-10	3.07E-06	1.18E-05
GM	>7	2.10E-07	8.41E-07	2.03E-07	8.11E-07	5.03E-08	2.01E-08	5.76E-08	2.30E-07					5.21E-07	1.90E-06
	3.3-7.0	1.07E-07	4.26E-07	2.07E-07	8.30E-07	3.77E-08	1.51E-08	3.92E-08	1.57E-07					3.91E-07	1.43E-06
	2.0-3.3	8.57E-08	3.43E-07	1.41E-07	5.64E-07	6.41E-09	2.57E-09	4.39E-08	1.75E-07					2.77E-07	1.08E-06
	1.1-2.0	9.68E-08	3.87E-07	2.51E-07	1.00E-06	4.91E-08	1.96E-08	1.31E-07	5.25E-07			4.87E-11	1.95E-10	5.28E-07	1.94E-06
	<1.1	5.08E-07	2.03E-06	3.40E-07	1.36E-06	2.07E-07	8.28E-08	5.88E-07	2.35E-06	8.40E-08	3.36E-07	0.00E+00	0.00E+00	1.73E-06	6.16E-06
	TSP	1.01E-06	4.03E-06	1.14E-06	4.57E-06	3.50E-07	1.40E-07	8.60E-07	3.44E-06	8.40E-08	3.36E-07	4.87E-11	1.95E-10	3.44E-06	1.25E-05
ZF	>7	1.54E-07	6.17E-07	2.68E-07	1.07E-06	6.41E-09	2.57E-09	8.36E-08	3.35E-07					5.13E-07	2.03E-06
	3.3-7.0	8.36E-08	3.35E-07	3.43E-07	1.37E-06	2.18E-08	8.71E-09	7.85E-08	3.14E-07					5.27E-07	2.03E-06
	2.0-3.3	3.52E-08	1.41E-07	2.90E-07	1.16E-06			9.60E-08	3.84E-07					4.21E-07	1.68E-06
	1.1-2.0	4.80E-08	1.92E-07	1.64E-07	6.55E-07	6.58E-09	2.63E-09	2.29E-07	9.14E-07	5.65E-08	2.26E-07	1.27E-09	5.07E-09	5.05E-07	2.00E-06
	<1.1	4.19E-07	1.67E-06	2.31E-07	9.25E-07	3.08E-08	1.23E-08	1.47E-06	5.90E-06	3.84E-07	1.54E-06	2.41E-08	9.65E-08	2.56E-06	1.01E-05
	TSP	7.40E-07	2.96E-06	1.30E-06	5.19E-06	6.56E-08	2.62E-08	1.96E-06	7.84E-06	4.41E-07	1.76E-06	2.54E-08	1.02E-07	4.53E-06	1.79E-05

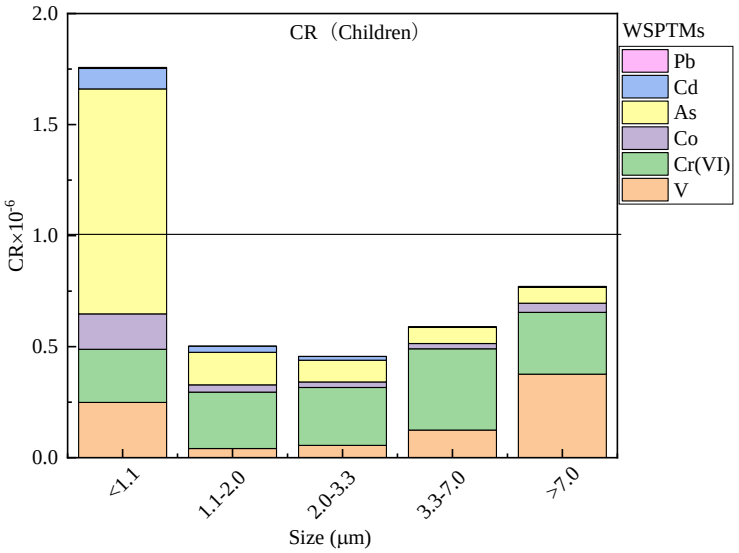

Fig. 48. The carcinogenic risks of toxic elements within $PM_{1.1}$, $PM_{1.1\text{-}2.0}$, $PM_{2.0\text{-}3.3}$, $PM_{3.3\text{-}7.0}$, $PM_{>7.0}$ for children in RCC particles.

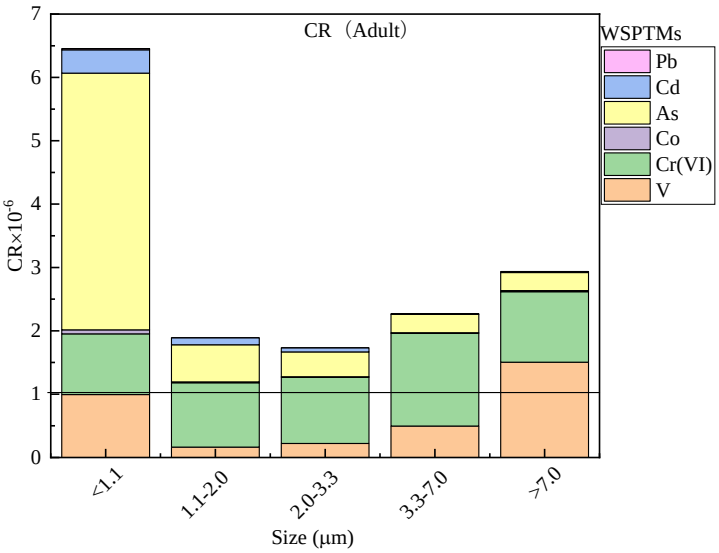

Fig. 49. The carcinogenic risks of toxic elements within $PM_{1.1}$, $PM_{1.1\text{-}2.0}$, $PM_{2.0\text{-}3.3}$, $PM_{3.3\text{-}7.0}$, $PM_{>7.0}$ for adults in RCC particles.

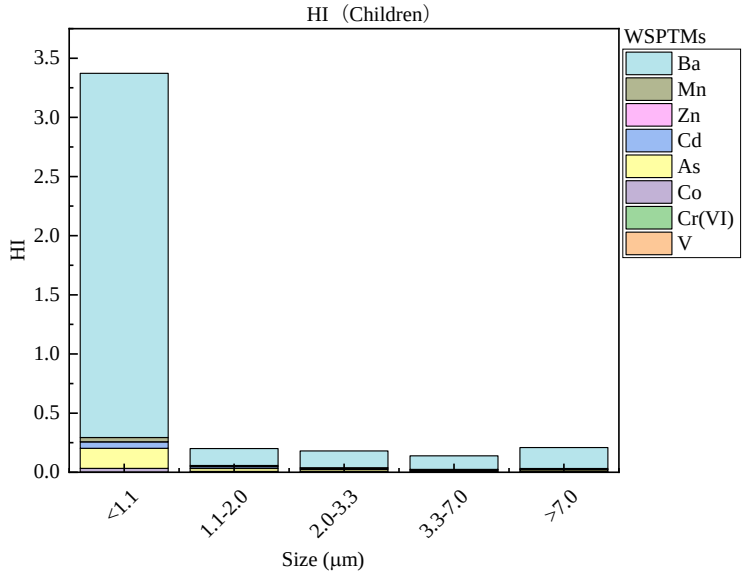

Fig. 50. The non- carcinogenic risks of toxic elements within $PM_{1.1}$, $PM_{1.1\text{-}2.0}$, $PM_{2.0\text{-}3.3}$, $PM_{3.3\text{-}7.0}$, $PM_{>7.0}$ for children in RCC particles.

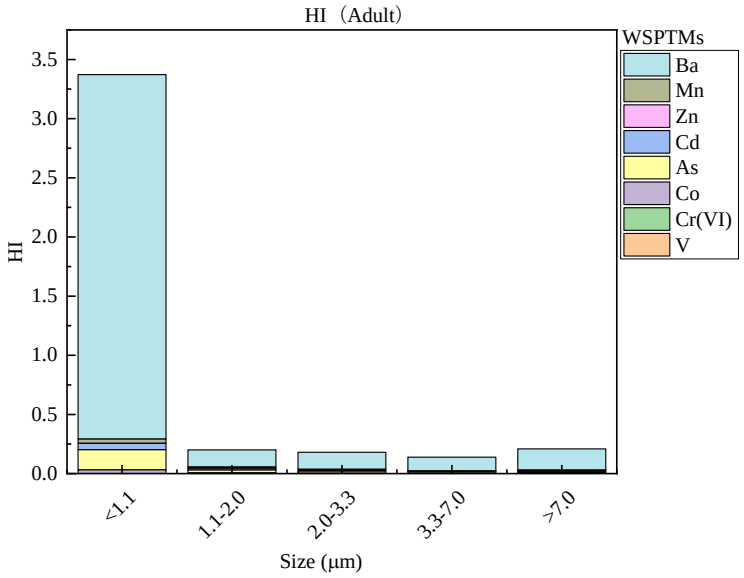

Fig. 51. The non- carcinogenic risks of toxic elements within $PM_{1.1}$, $PM_{1.1\text{-}2.0}$, $PM_{2.0\text{-}3.3}$, $PM_{3.3\text{-}7.0}$, $PM_{>7.0}$ for adults in RCC particles.

the lowest CR, which was approximately 1.47×10^{-2} times for children and 7.21×10^{-1} for adults of that of As in TSP. The TCR values (reached $4.04\times10^{-7} \pm 8.18\times10^{-6}$ for children and $1.52\times10^{-5} \pm 2.99\times10^{-6}$ for adults) were exceeded the acceptable level (1×10^{-6}), indicating that we should pay more attention to these WSPTMs.

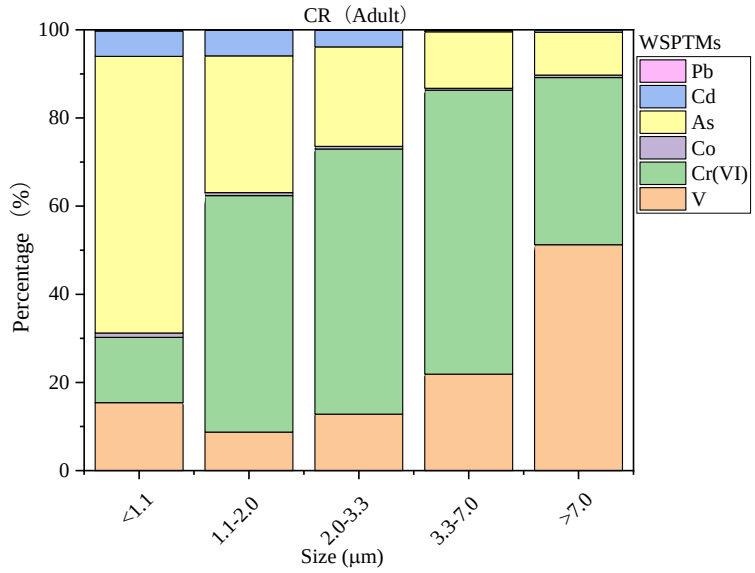

Fig. 52. The relative portions of carcinogenic of toxic elements within $PM_{1.1}$, $PM_{1.1\text{-}2.0}$, $PM_{2.0\text{-}3.3}$, $PM_{3.3\text{-}7.0}$ and $PM_{>7.0}$ for adults in RCC particles.

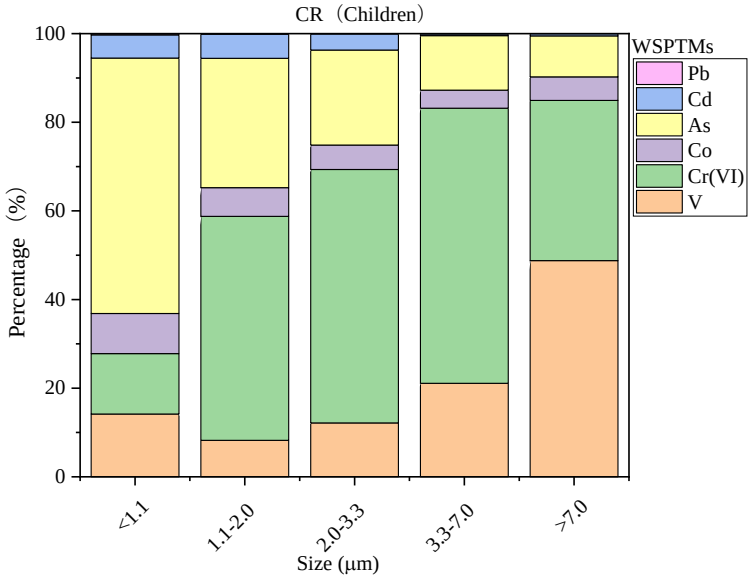

Fig. 53. The relative portions of carcinogenic risks of toxic elements within $PM_{1.1}$, $PM_{1.1\text{-}2.0}$, $PM_{2.0\text{-}3.3}$, $PM_{3.3\text{-}7.0}$ and $PM_{>7.0}$ for children in RCC particles.

Figure 52 and 53 show that the relative portions of carcinogenic risks of toxic elements within $PM_{1.1}$, $PM_{1.1\text{-}2.0}$, $PM_{2.0\text{-}3.3}$, $PM_{3.3\text{-}7.0}$ and $PM_{>7.0}$ in RCC particles. With respect to children and adults non-carcinogenic risk, the corresponding contributions of elements to the HQ were ranked in the following order: Ba (81.75 %) > As (8.14 %) > Cd (3.52 %) > Co (2.86 %) > Mn (3.20 %) > Cr(VI) (0.30 %) > V (0.21 %) and Zn (0.01 %)). The HQ values for As, Cd, Co, Cr(VI), Ni and V via inhalation exposure for both children and adults were all lower than the safe level (= 1), indicating no non-carcinogenic risks from the inhalation exposure for each toxic elements (USEPA, 1989).

The of WSPTMs for both children and adults were exceeded the acceptable level (1×10^{-6}) in $PM_{1.1}$, indicating that we should pay more attention to these WSPTMs. Compare with the TCR of RCC particles in Xuanwei and APMs, we find that CR of Water-Soluble Potentially Toxic Metals in APMs particles is higher than RCC. This indicates that the carcinogenic risk of Water-Soluble Potentially Toxic Metals in APMs is much greater than the carcinogenic risk of Water-Soluble Potentially Toxic Metals in RCC particulate matter. Our results suggest that WSPTMs contained in particulate matter emitted from coal combustion are an important component of Xuanwei APMs, but there are other sources that require further investigation. Potentially toxic metals are not the main cause of the high incidence of lung cancer in Xuanwei, so we have studied them in depth.

4.3.4 Briefly Summary

In Xuanwei:

APMs: The order of carcinogenic risk by the ingestion route for boys, girls and adults were Se > Cr (VI) > As > Cd > Co > V > Ni > Pb, with Se and Cr (VI) values were lower than 1×10^{-4} but higher than 1×10^{-6} for boys, girls and adults having the greater effect. The contribution of V, Cr (VI), Co, Ni, and Cd for CR, were increased with the PM size increase, while the contribution of Se for CR, were decreased with the PM size increase. Se was identified as the most enriched WSPTMs. As, Mn and Al were the major contributor for non-carcinogenic risk.

RBC: Our result show that all PMs, the TCR was higher than 1 for adults and lower than 1 for children, except for $PM_{1.1}$. TCR values for As, Cd and Co decreased with increasing PM particle size (for adults and children), indicating that As, Cd and Co had the highest in $PM_{1.1}$. Interestingly, the TCR values for Cr (VI) were stable across PM particle sizes with no variability (adults and children), and the TCR for lead was negligible. Notably, the TCR values for V showed a bimodal distribution, with the major peak in the particle size <1.1 μm while the minor peak in the size range of > 7 μm. The noncancer risk of Ba account for 91.28 %, 71.39 %, 78.74 %, 82.38 %, and 84.95 % within $PM_{1.1}$, $PM_{1.1–2.0}$, $PM_{2.0–3.3}$, $PM_{3.3–7.0}$, and $PM_{>7.0}$. It indicates that the non-carcinogenic risk of WSPTMs in RCC particles, mainly Ba, followed by As and the non-carcinogenic risk is highest within $PM_{1.1}$.

In Beijing: $PM_{1.1}$ was the major contributor of Pb, Cd and As for CR and HQ in APMs in Beijing. The potential toxic metals of Cr(VI), V and As caused higher CR for children than Ni, Cd, Co, Pb, meanwhile, Pb and Ni were cause higher CR for adults than As, Cr(VI), V, Co, Cd, especially in $PM_{1.1}$ in APMs in Beijing. TCR values were exceeded the acceptable level (1×10^{-6}), indicating that we should pay more attention to these PTMs in RCC particles. Both children and adults, the CR of As were the highest followed by Cr (VI) and Pb had the lowest CR in RCC particles.

Compare with the TCR of RCC particles in Xuanwei and APMs, we find that CR of Water-Soluble Potentially Toxic Metals in APMs particles is higher than RCC. This indicates that the carcinogenic risk of Water-Soluble Potentially Toxic Metals in APMs is much greater than the carcinogenic risk of Water-Soluble Potentially Toxic Metals in RCC particulate matter. Our results suggest that WSPTMs contained in particulate matter emitted from coal combustion are an important component of Xuanwei APMs, but there are other sources that require further investigation. Potentially toxic metals are not the main cause of the high incidence of lung cancer in Xuanwei, so we have studied them in depth.

4.5 The characteristics of EC, OC, WSOC, and HULIS-C in RCC particles

WSOC is a significant portion of OC, which account for 10~90 %, depending on source location, source, and meteorological conditions(Wen et al., 2018). HULIS-C are important hydrophobic compound of WSOC in ambient aerosols.

4.5.1 Abundance of EC, OC, WSOC, and HULIS-C in RCC particles.

Researcher based on Community Multiscale Air Quality (CMAQ) model (version 5.0.1) shows that RCC was the important sources of HULIS, accounting for 15.1 % in Beijing (Xinghua Li, Han, et al., 2019). Mass concentrations of OCx, ECx, WSOCx and HULIS-C in coarse and fine PM from RCC particles are shown in Table 28. The average values of WSOC, HULIS-C, OC, and EC were 234.72 ± 149.04 μg·m^{-3}, 117.65 ± 53.90 μg C m^{-3}, 3250.99 ± 2126.65 μg·m^{-3}, and 643.19 ± 263.94 μg·m^{-3} in $PM_{2.0}$, while, were 82.37 ± 46.82 μg·m^{-3}, 40.23 ± 19.17 μg C m^{-3}, 822.86 ± 522.48 μg·m^{-3}, and 30.11 ± 35.62 μg·m^{-3} in $PM_{2.0\sim7.0}$. There has similar contribution of HULIS-C to the PM were 2.09 %~5.65 % for $PM_{2.0}$ and 2.68%~5.62% for $PM_{2.0\sim7.0}$, respectively. This result was consistent with previous research HULIS account for 3.5 ± 0.4 % of $PM_{2.5}$ emitted from coal combustion (X. Fan, Wei, et al., 2016), but lower than the reported WSOC results (14%~56%) for biomass burning $PM_{2.5}$, which was significantly lower than that (22.6 ± 3.7 %) in ambient $PM_{2.5}$ (X. Fan, Wei, et al., 2016).

Table 28. Mass concentrations of OCx, WSOCx and HULIS-C in $PM_{2.0}$ and $PM_{2.0\sim7.0}$ from RCC particles

Samples	Size μm	OC	EC	TC	PM	HULIS-C	WSOC
BL	$PM_{2.0}$	1556.00	749.35	2305.35	3651.35	137.78	206.40
LM		2385.33	851.68	3237.01	7854.83	168.63	275.95
SF		4490.54	353.95	4844.49	10303.30	137.19	215.44
LJW		6983.05	1056.47	8039.52	11833.04	174.01	531.67
GM		3649.02	503.15	4152.17	4185.81	38.76	90.00
ZF		442.01	344.56	786.57	1810.95	49.52	88.85
Average		3250.99	643.19	3894.18	6606.55	117.65	234.72
TSD		2126.65	263.94	2264.47	3654.48	53.90	149.04
BL	$PM_{2.0\text{-}7.0}$	1000.09	108.73	1108.82	2492.64	71.85	108.53
LM		1023.89	18.13	1042.02	2391.05	44.02	72.80
SF		959.05	22.78	981.82	2314.49	45.92	135.41
LJW		1632.95	16.60	1649.55	3492.34	46.40	131.92
GM		244.74	6.04	250.78	1311.84	17.84	21.69
ZF		76.47	8.35	84.82	1143.99	15.35	23.86
Average		822.86	30.11	852.97	2191.06	40.23	82.37
TSD		522.48	35.62	533.08	786.23	19.17	46.82

Fig. 54 show the mass concentration (μg m^{-3}) and standard deviation (STD) of OC, EC, WSOC, and HULIS-C (Coal, N=6) in RCC particles. The mass concentrations of HULIS are in the following order: 1.1 μm > 1.1~2.0 μm > 2.0~3.3 μm > 3.3~7.0 μm. The mass concentration of HULIS-C in our research far exceeded HULIS-C in the ambient is in the average range of 0.8~15.9 μg·m^{-3} (M. Zhao et al., 2016) (M. Zhao et al., 2015)(Win et al., 2018)(Zheng et al., 2013)(X. Fan, Song, et al., 2016)(Win et al., 2020).

The variability in mass concentration can be explained by the independent and closed sampling system. It is also related to the type and maturity of the coal. Relatively little water-soluble brown carbon was found in particles produced by burning middle-maturity coal in residential stoves, while significant amounts were found in low maturity bituminous coal and anthracite (M. Li, Fan, et al., 2019). Unlike general atmospheric particulate sampling, we collect high concentrations of RCC particulate matter directly with our sampling system. In the future, a comprehensive investigation of coal combustion HULIS-C emissions under different stove types, combustion conditions and combustion stages are necessary to better understand the distribution pattern of HULIS-C.

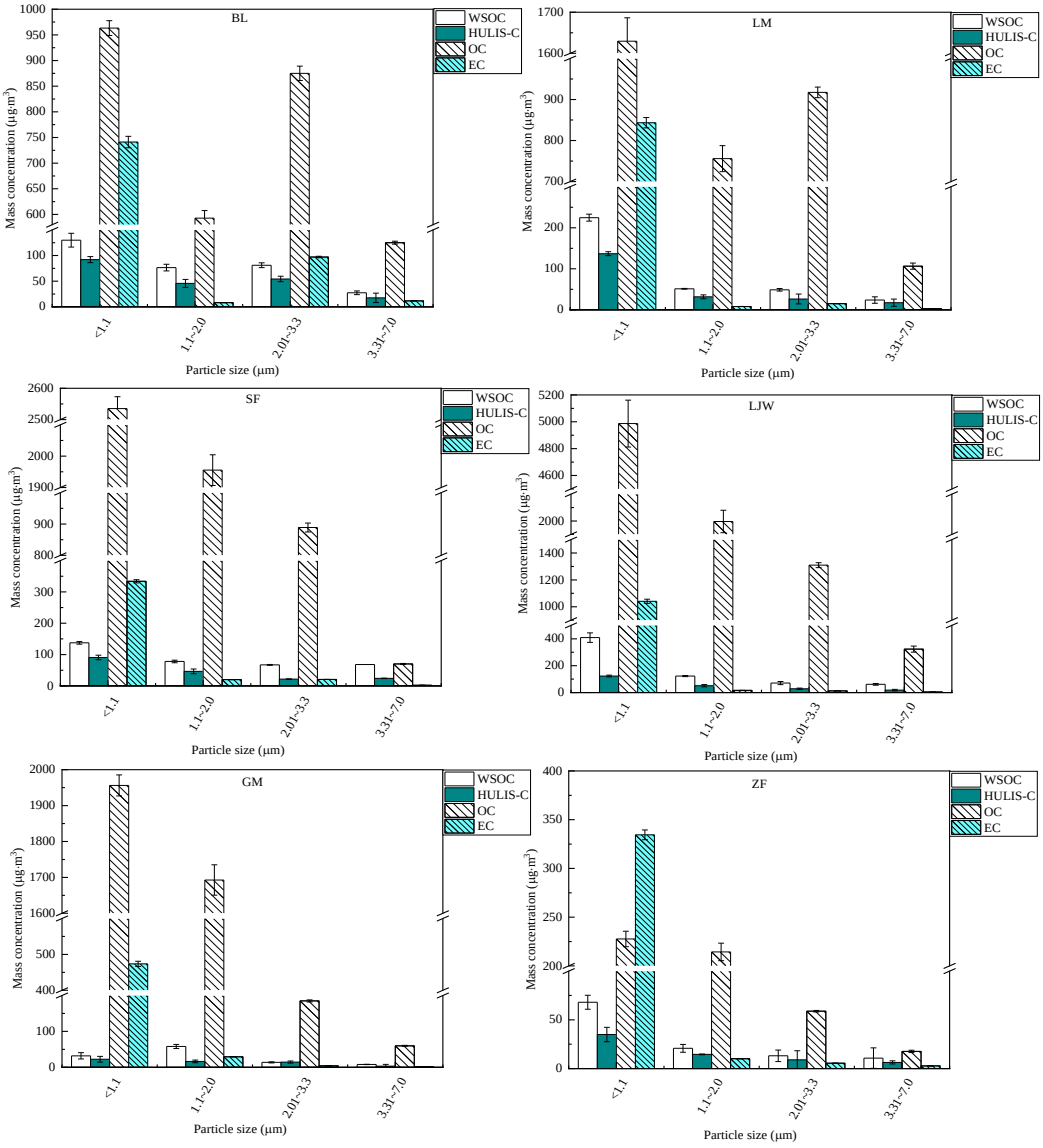

Fig. 54. Mass concentration (μg m^{-3}) and standard deviation (STD) of OC, EC, WSOC, and HULIS-C (Coal, N=6) in RCC particles.

4.5.2 Size distribution of HULIS-C in RCC particles.

HULIS-C accounts for a large proportion of WSOC in RCC particles and have received much attention in recent years (M. Li, Fan, et al., 2019). The percentage of OCx, ECx, WSOCx to WSOC and HULIS-C in coarse and fine PM from RCC particles is show in Table 29. In our study, the HULIS-Cx /WSOCx (%) values in RCC particles are 32.73 %~63.76 % (Average 53.85 ± 12.12 %) for $PM_{2.0}$ and 33.91%~82.67 % (Average 57.06 ± 17.32 %) for $PM_{2.0\sim7.0}$, respectively.

Table 29. The percentage of OCx, ECx, WSOCx to WSOC and HULIS-C in $PM_{2.0}$ and $PM_{2.0\sim7.0}$ from RCC particles

Samples	Size μm	HULIS-Cx/WSOCx	OCx/PMx	ECx/PMx	WSOCx/TCx	HULIS-Cx/TCx	OCx/ECx	HULIS-Cx/PMx	WSOCx/PMx	HULIS-Cx/HULIS-Ct
BL	$PM_{2.0}$	66.76	42.61	20.52	8.95	5.98	2.08	3.77	5.65	65.73
LM		61.11	30.37	10.84	8.52	5.21	2.80	2.15	3.51	79.30
SF		63.68	43.58	3.44	4.45	2.83	12.69	1.33	2.09	74.92
LJW		32.73	59.01	8.93	6.61	2.16	6.61	1.47	4.49	78.95
GM		43.07	87.18	12.02	2.17	0.93	7.25	0.93	2.15	68.48
ZF		55.73	24.41	19.03	11.30	6.30	1.28	2.73	4.91	76.34
Average		53.85	47.86	12.46	7.00	3.90	5.45	2.06	3.80	73.95
TSD		12.12	20.70	5.84	3.02	2.03	3.93	0.96	1.35	5.13
BL	$PM_{2.0\sim7.0}$	66.20	40.12	4.36	9.79	6.48	9.20	2.88	4.35	34.27
LM		60.47	42.82	0.76	6.99	4.22	56.46	1.84	3.04	20.70
SF		33.91	41.44	0.98	13.79	4.68	42.11	1.98	5.85	25.08
LJW		35.17	46.76	0.48	8.00	2.81	98.36	1.33	3.78	21.05
GM		82.27	18.66	0.46	8.65	7.12	40.53	1.36	1.65	31.52
ZF		64.35	6.68	0.73	28.13	18.10	9.16	1.34	2.09	23.66
Average		57.06	32.75	1.30	12.56	7.23	42.64	1.79	3.46	26.05
TSD		17.32	14.75	1.38	7.29	5.06	30.39	0.55	1.41	5.13

This suggests that HULIS-C is the main component of WSOC in RCC particles. Despite the large variance of HULIS-C concentrations, the abundance of HULIS-C in WSOC was relatively stable. Interestingly, the HULIS-Cx/HULIS-Ct (%) values in RCC particles are 68.48 %~79.30 % (average 73.95 ± 5.13%) for $PM_{2.0}$ and 20.70 %~34.27 (average 26.05 ± 5.13 %) for $PM_{2.0\sim7.0}$, respectively. The first study about HULIS percentage contributions in particles in the Pearl River Delta region in China report the similar results that HULIS made the highest percentage contribution (81 %) in $PM_{0.63\sim0.87}$, and the lowest percentage contribution (7 %) in $PM_{4.0\sim5.7}$ during biomass burning seasons (P. Lin et al., 2010). Our conclusion indicated that the HULIS-C emitted from RCC is mainly concentrated in fine particles, and the mass concentration of HULIS-C and WSOC are inversely proportional to the particle size (Pearson correlation coefficients 0.92 ± 0.16) in our research (Table 30).

OC to EC ratio is commonly regarded as secondary organic aerosol indicator, when the OC/EC ratio exceeds 2.8 (Renjian Zhang et al., 2009). The OC/EC ratio decreases gradually with increasing particle size in the range of >1.1 μm particle size. However, when the particle size <1.1 μm, the OC/EC ratio suddenly decreases to a minimum of 0.68. This phenomenon can be explained by the fact that due to insufficient combustion of coal in the initial stage of combustion (Wen et al., 2018), a large amount of black smoke is released, resulting in a lower ratio of OC/EC in <1.1 μm particles smaller than other

particle sizes. The average contribution of WSOC and HULIS-C to the TC of RCC particles were 2.54 %~12.93 % and 1.29 %~7.44 % in $PM_{7.0}$.

Table 30. Pearson correlation coefficients between HULIS-C and WSOC

Samples	Size (μm)	WSOC (μg m^{-3})	HULIS-C (C μg m^{-3})	Pearson correlation coefficients
BL	<1.1	129.93	92.02	0.99
	1.1-2.0	76.47	45.76	
	2.0-3.3	81.08	54.33	
	3.3-7.0	27.44	17.52	
LM	<1.1	224.58	136.86	1.00
	1.1-2.0	51.37	31.77	
	2.0-3.3	48.88	26.50	
	3.3-7.0	23.91	17.52	
SF	<1.1	137.40	90.78	0.98
	1.1-2.0	78.04	46.41	
	2.0-3.3	67.17	21.86	
	3.3-7.0	68.24	24.06	
LJW	<1.1	408.91	123.02	0.99
	1.1-2.0	122.76	50.99	
	2.0-3.3	70.75	28.36	
	3.3-7.0	61.18	18.04	
GM	<1.1	31.96	22.42	0.57
	1.1-2.0	58.04	16.34	
	2.0-3.3	13.74	14.58	
	3.3-7.0	7.95	3.27	
ZF	<1.1	68.07	34.94	0.99
	1.1-2.0	20.78	14.58	
	2.0-3.3	13.11	9.01	
	3.3-7.0	10.75	6.34	
			Average	0.92
			TSD	0.16

4.5.3 Correlation of HULIS-C and WSOC with other species in RCC particles

HULIS-C and WSOC can be produced from both primary emissions and secondary formation. Table 31 shows the correlation between HULIS-C and WSOC with water-soluble ion species. During our measurements, the concentrations of HULIS-C and WSOC were significantly correlated with SIA (SO_4^{2-},

NO_3^-, and NH_4^+), K^+ and, Mg^{2+} in RCC particles.

NO_3^-, SO_4^{2-} and, NH_4^+ are usually referred to as secondary water-soluble ions (X. Fan, Song, et al., 2016). In this study, both HULIS-C and WSOC were strongly correlated with secondary water-soluble ions such as NH_4^+ (r = 0.89 ± 0.10), NO_3^- (r = 0.88 ± 0.14), and SO_4^{2-} (r = 0.86 ± 0.11) for HULIS-C and NH_4^+ (r = 0.80 ± 0.30), NO_3^- (r = 0.81 ± 0.33), and SO_4^{2-} (r = 0.83 ± 0.18) for WSOC were observed as shown in Table 31. Cl^-, NO_2^-, Na^+, and Ca^{2+} exhibited a relatively weak link with HULIS-C and WSOC. During simulated RCC with high relative humidity (79 ± 2.09 %) (Table 32), in this situation, heterogeneous reactions of SO_2 and NOx were more easily happened (S. F. Kong et al., 2015).

This finding may indicate that HULIS-C and WSOC was subject to a similar formation process as SIA through secondary formation processes (Ni et al., 2021)(An et al., 2019). Relevant studies have shown that HULIS may result from primary emission sources and secondary formation involving newly formed sulfate particles. (Song et al., 2012) (N. Wang & Yu, 2017).

Our result show that HULIS-C to the PM were 2.09%~5.65% for $PM_{2.0}$ and 2.68%~5.62% for $PM_{2.0\text{-}7.0}$, respectively. HULIS-C emitted from RCC is mainly concentrated in $PM_{2.0}$ (68.48 %~79.30 %). During our measurements, the concentrations of HULIS-C and WSOC were significantly correlated with SO_4^{2-}, NO_3^-, and NH_4^+ in RCC particles.

Table 31. The correlation between HULIS-C and WSOC and water-soluble ions in RCC particles size

	BL		LM		SF		LJW		GM		ZF	
Samples	HULIS-C	WSOC	HULIS-C	WSOC	HULIS-C	WSOC	HULIS-C	WSOC	HULIS-C	WSOC	HULIS-C	WSOC
Cl^-	0.66	0.71	0.42	0.44	0.06	0.14	0.76	0.80	-0.74	-0.77	0.13	0.19
NO_2^-	0.06	0.14	0.15	0.20	0.94	0.99	0.63	0.72	-0.19	-0.72	-0.26	-0.21
NO_3^-	0.84	0.83	1.00	0.99	0.94	0.99	0.95	0.99	0.58	0.07	0.94	0.98
SO_4^{2-}	0.74	0.72	0.97	0.97	0.81	0.85	0.95	0.99	0.72	0.49	0.98	0.99
Na^+	0.89	0.80		0.99	0.96	0.99		-0.28	0.73	-0.29	0.97	0.99
NH_4^+	0.89	0.92			0.96	1.00			0.73	0.27	0.97	0.99
K^+	0.83	0.82	0.90	0.89	0.95	0.99	0.93	0.95	0.69	0.30	0.97	0.99
Mg^{2+}	0.78	0.76	1.00	0.99	0.93	0.98	0.93	0.96	0.80	0.38	0.98	0.99
Ca^{2+}	0.78	0.76	-0.14	-0.09	-0.34	-0.46	-0.49	-0.48	0.29	0.90	0.98	0.99

Table 32. Simulated combustion conditions

Samples	Date	period	Volume L/min	Pump, Volume m^3/min	Temperature℃	Humidity%
BL	2017.8.08	9：52-11:52	566	50	25.7	75
LM	2017.8.15	10:10-12：10	566	50	33	81
SF	2017.8.16	16：36-18：36	566	50	36	78
LJW	2017.8.16	10:12-12:12	566	50	35	79
GM	2017.8.20	14：10-16:10	566	50	28	81
ZF	2017.8.20	16：55-18:55	566	50	38	80
Average					32.62	79.00
SD					4.39	2.08

In the future, a comprehensive investigation of coal combustion HULIS-C emissions under different stove types, combustion conditions and combustion stages are necessary to better understand HULIS-C. Unfortunately, HULIS-C as a powerful sequestering agent in atmospheric particulate matter, there is a lack of information on the ROS generated (P. Lin & Yu, 2011) (Win et al., 2018) by the HULIS-metal combination through the cellular matrices and tissue. Some attempts should be done in cell-free and cell-based experiments to obtain well-characterized information about the ROS generated by the HULIS-metal combination and to better address the health effects of HULIS-C.

4.6 The characteristics of EPFRs in RCC particles

4.6.1 EPFRs exposure evaluation

To date, there is no internationally accepted method to assess the health risk of EPFRs in PM. According to my knowledge, several methods have been used to assess the health risks of EPFRs (Q. Chen, Sun, Mu, et al., 2019) (Q. Chen et al., 2020) (Y. Xu et al., 2020) (J. Zhao et al., 2021), however, all of them evaluate EPFRs inhalation risk for adult except child. In our study, the equivalent number of cigarettes to evaluate the potential health risks of EPFRs in PM for Xunawei residents (Gehling & Dellinger, 2013).The EPFRs exposure level is given in equation (11-12) :

$$Inh_{PM} = RC_{PM} \times F \times Fr \times PC_{PM} \times Rinhalation \quad (11)$$

$$N_{cig} = 365 \times Inh_{PM} / RC_{cig} \times C_{tar} \quad (12)$$

where Inh_{PM} is the daily EPFRs exposure from inhaled PM (spins/g/day); F is the conversion from *g* to micrograms (1×10^{-6}) (Gehling & Dellinger, 2013), Fr is the alveolar fraction retained in the lung (0.75). PC_{PM} is the concentration of PM (μg/m^3) and R inhalation represents the daily amount of air inhaled (20 m^3/day for adult (Grevatt, 1998), 7.6 m^3 / day for child) (https://www.epa.gov/risk/risk-assessment-guidance-superfund-rags-part; accessed on 24 September 2021). N_{cig} represents the number of cigarettes (person/year), 30 represents 30 days per monthly. RCcig (4.75×10^{16} spins/g) (Q. Chen, Sun, Mu, et al., 2019) indicates the concentration of free radicals in cigarette tar, and Ctar (0.013 g/cig) indicates the amount of tar per cigarette (Gehling & Dellinger, 2013).

4.6.2 EPFRs and PM concentrations in atmospheric particulate matter and solid fuel combustion particles

4.6.2.1 EPFRs and PM concentrations in biomass combustion particles

The concentration distributions of EPFRs and PM in simulated particulate matter emitted from biomass combustion (corncobs, pine, poplar) were given in Fig 55 and Table 33. The concentrations of EPFEs and PM emitted from the three-biomass combustion were significantly different in the particle size ranges <1.1, 1.1-2.0 and 2.0-3.3. Both the EPFRs and the PM concentration reach their maximum at <1.1 μm, while the lowest concentration is found at particle size 2.0-3.3 μm. The atmospheric concentrations of EPFRs percentage mean value of $PM_{1.1}$, $PM_{1.1–2.0}$, and $PM_{2.0–3.3}$ were 76.25 ± 4.14%, 13.69 ± 3.95%, and 10.06 ± 0.23%, which corresponded to PM mass concentrations were 2948.77 ± 1438.66 μg/m^3, 1415.44 ± 712.85 μg/m^3 and 1087.57 ± 504.44 μg/m^3, respectively (Table 34).

Table 33. EPFRs and PM concentrations in biomass combustion particles.

Samples	1.1			1.1-2.0			2.0-3.3		
	Spins/m^3	Spins/g	μg/m^3	Spins/m^3	Spins/g	μg/m^3	Spins/m^3	Spins/g	μg/m^3
Corncob	4.51E+17	3.11E+15	1781.82	1.04E+17	1.30E+15	985.86	6.19E+16	9.28E+14	820.20
Pine	4.27E+17	3.37E+15	2088.89	4.22E+16	8.29E+14	840.40	5.09E+16	1.29E+15	648.48
Poplar	3.26E+17	1.08E+15	4975.61	7.13E+16	4.86E+14	2420.05	4.59E+16	4.22E+14	1794.04
Average	4.01E+17	2.52E+15	2948.77	7.25E+16	8.72E+14	1415.44	5.29E+16	8.80E+14	1087.57
Min	3.26E+17	1.08E+15	1781.82	4.22E+16	4.86E+14	840.40	4.59E+16	4.22E+14	648.48
Max	4.51E+17	3.37E+15	4975.61	1.04E+17	1.30E+15	2420.05	6.19E+16	1.29E+15	1794.04
STD	5.42E+16	1.02E+15	1438.66	2.52E+16	3.34E+14	712.85	6.68E+15	3.56E+14	504.44

Table 34. Size distribution of EPFRs and PM in simulated biomass combustion particles from Xuanwei (%)

Sample groups	$PM_{1.1}/PM_{3.3}$ (%)			$PM_{1.1\text{-}2.0}/PM_{3.3}$ (%)			$PM_{2.0\text{-}3.3}/PM_{3.3}$ (%)		
	Spins/m^3	Spins/g	μg/m^3	Spins/m^3	Spins/g	μg/m^3	Spins/m^3	Spins/g	μg/m^3
Corncob	73.11	58.26	49.66	16.86	24.35	27.48	10.03	17.38	22.86
Pine	82.10	61.40	58.39	8.11	15.10	23.49	9.79	23.50	18.13
Poplar	73.56	54.33	54.14	16.09	24.45	26.33	10.36	21.23	19.52
Average	76.25	57.99	54.06	13.69	21.30	25.77	10.06	20.70	20.17
Min	73.11	54.33	49.66	8.11	15.10	23.49	9.79	17.38	18.13
Max	82.10	61.40	58.39	16.86	24.45	27.48	10.36	23.50	22.86
STD	4.14	2.89	3.56	3.95	4.38	1.68	0.23	2.52	1.99

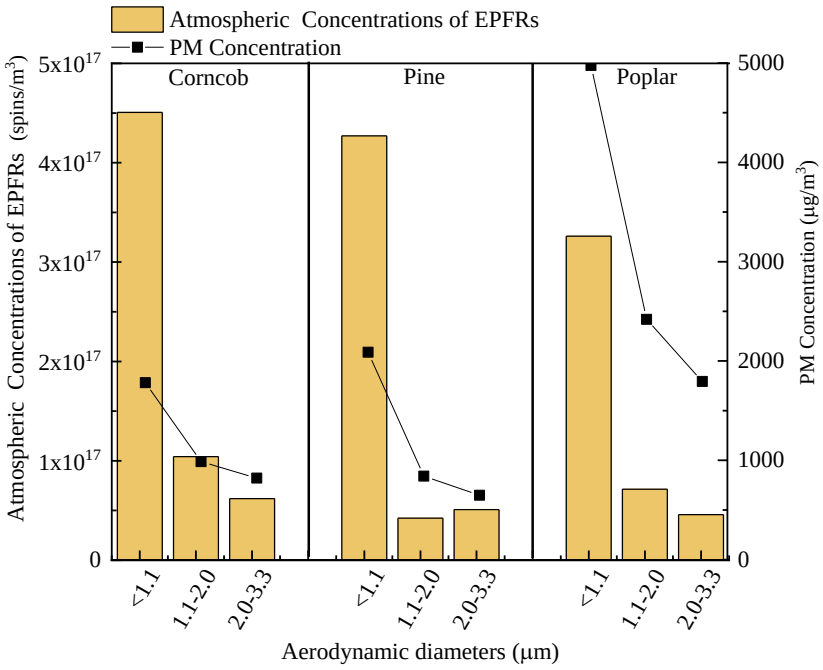

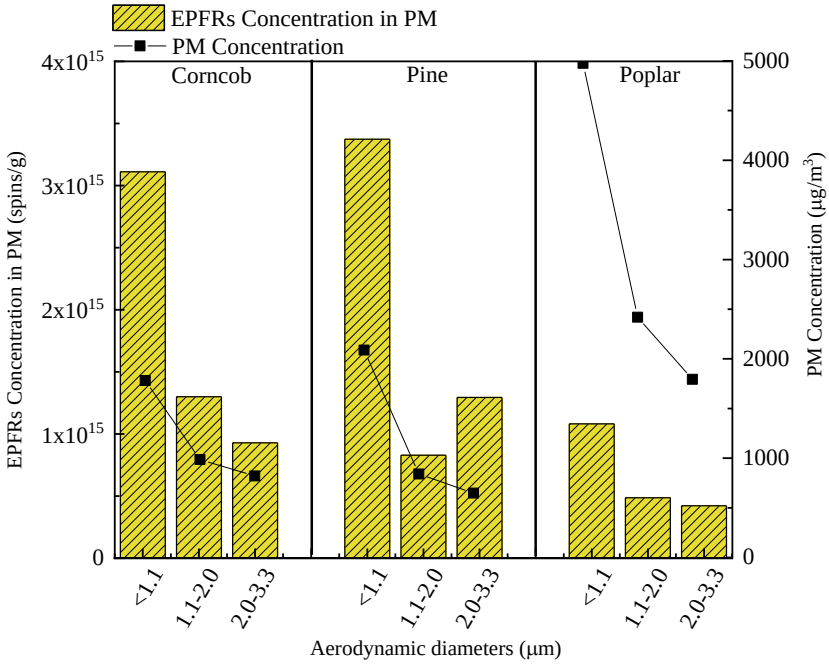

Fig. 55. EPFRs and PM concentrations in biomass combustion particles from Xuanwei. (The left: the atmospheric EPFRs concentrations; the right: EPFRs concentrations in PM)

The atmospheric concentrations of EPFRs in the $PM_{1.1}$ were 4.51×10^{17}, 4.27×10^{17} and 3.26×10^{17} spins/m^3 for corncob, pine and poplar, respectively, while the mean atmospheric concentrations in $PM_{1.1}$ were found to be several times than $PM_{1.1\text{-}2.0}$ (6.34 ± 2.67) and $PM_{2.0\text{-}3.3}$ (7.60± 0.57). The EPFR concentrations in the $PM_{1.1}$ at the three sites were 3.11×10^{15}, 3.37×10^{15} and 1.08×10^{15} spins/g for corncob, pine and poplar, respectively (shown in Table 33). It has been reported that the EPFR concentrations in $PM_{2.5}$ from the corn straw, rice straw, jujube wood, and pine wood (four biomass, purchased from Jiangsu province) were in the range of 0.9×10^{19} spins/g to 6.1×10^{19} spins/g (J. Zhao et al., 2021), the average radical intensities in PM emissions from fatwood, pine wood were 1.2×10^{18}, and 9.1×10^{17} spins/gram, respectively (L. Tian et al., 2009). Compared with previous studies, the EPFR concentrations in $PM_{3.3}$ (the range of 1.99×10^{15} spins/g to 5.50×10^{15} spins/g) which were 2-4 orders of magnitude lower than those reported in a previous study. EPFRs were mainly concentrated in the size range of <1.1 μm, which accounted for 76.25 ± 4.15% of $PM_{3.3}$, indicating that the $PM_{1.1}$ emitted biomass combustion is more harmful to human body than $PM_{2.0\text{-}3.3}$ and $PM_{2.0\text{-}3.3}$, therefore, deserves more in-depth study.

4.6.2.2 EPFRs and PM concentrations in coal combustion particles

Table 35 lists the size distribution of EPFRs and PM in simulated coal combustion particles (%). Fig 56 shows the EPFRs and PM concentrations in coal combustion particles. The atmospheric EPFRs concentrations in $PM_{1.1}$, $PM_{2.0\text{-}3.3}$ and $PM_{2.0\text{-}3.3}$ make the contribution to $PM_{3.3}$ were 74.85± 10.76%, 13.10 ± 7.66%, and 12.05 ± 7.25%, respectively. The average atmospheric concentrations in $PM_{1.1}$ were found to be several times than $PM_{1.1\text{-}2.0}$ (8.81 ± 6.70) and $PM_{2.0\text{-}3.3}$ (8.07 ± 3.68). The concentration distribution of EPFRs and PM in coal combustion emission particulate matter is similar to that of biomass combustion particulate matter, both mainly concentrated in the <1.1um particle size.

Table 35. Size distribution of EPFRs and PM in simulated coal combustion particles from Xuanwei (%)

Sample	$PM_{1.1}/PM_{3.3}$ (%)			$PM_{1.1\text{-}2.0}/PM_{3.3}$ (%)			$PM_{2.0\text{-}3.3}/PM_{3.3}$ (%)		
groups	Spins/m^3	Spins/g	μg/m^3	Spins/m^3	Spins/g	μg/m^3	Spins/m^3	Spins/g	μg/m^3
BL	58.15	51.66	40.00	14.00	18.72	26.58	27.85	29.61	33.42
LM	63.74	52.12	46.46	28.09	28.37	37.62	8.17	19.51	15.92
SF	81.77	56.06	56.29	7.07	8.66	31.50	11.16	35.27	12.21
LJW	89.86	81.85	43.81	4.03	4.14	38.77	6.12	14.01	17.43
GM	78.85	71.34	42.23	10.76	12.24	33.60	10.39	16.42	24.17
ZF	76.76	58.53	50.35	14.64	15.16	37.10	8.60	26.31	12.55
Average	74.85	61.93	46.52	13.10	14.55	34.19	12.05	23.52	19.28
Min	58.15	51.66	40.00	4.03	4.14	26.58	6.12	14.01	12.21
Max	89.86	81.85	56.29	28.09	28.37	38.77	27.85	35.27	33.42
STD	10.76	11.05	5.45	7.66	7.71	4.22	7.25	7.53	7.46

STD: Standard Deviation

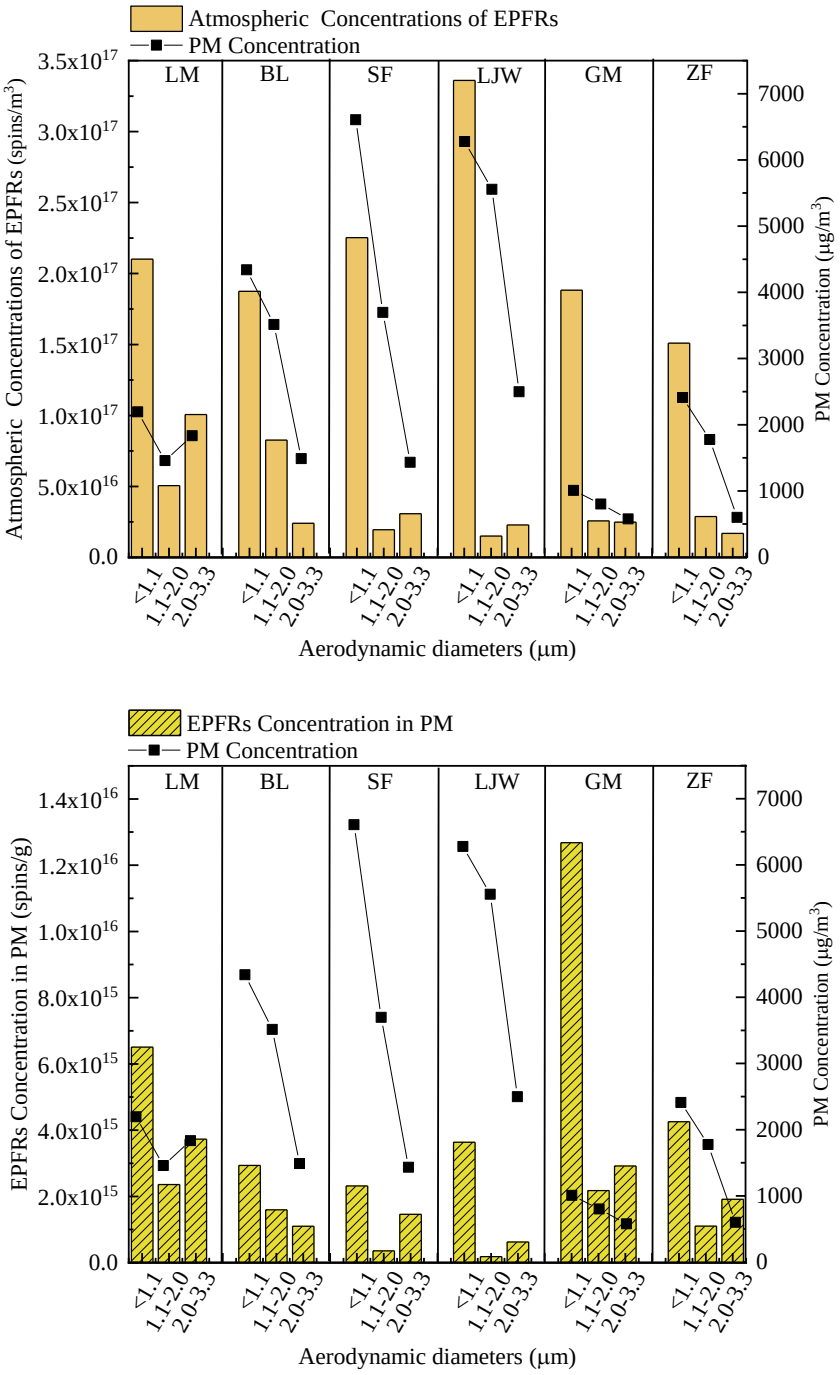

Fig. 56. EPFRs and PM concentrations in coal combustion particles from Xuanwei. (The left: the atmospheric EPFRs concentrations; the right: EPFRs concentrations in PM)

The mean atmospheric concentrations of EPFRs in the $PM_{1.1}$, $PM_{2.0\text{-}3.3}$ and $PM_{2.0\text{-}3.3}$ were $2.16 \times 10^{17} \pm 5.82 \times 10^{16}$ spins/m^3, $3.70 \times 10^{16} \pm 2.32 \times 10^{16}$ spins/m^3 and $3.67 \times 10^{16} \pm 2.89 \times 10^{16}$ spins/m^3, which corresponded to PM mass concentrations were 3806.19 ± 2105.99 μg/m^3, 1537.84 ± 565.64 μg/m^3 and 1404.60 ± 672.75 μg/m^3, respectively (shown in Table 36). Compared with previous studies, the EPFR concentrations in $PM_{3.3}$ (the range of 4.13×10^{15} spins/g to 1.78×10^{16} spins/g) which were 1-4 orders of

magnitude lower than those reported in a previous study for the total particular matter from bituminous coal (4.4×10^{17} spins/g), anthracite (2.3×10^{17} spins/g) (L. Tian et al., 2009) and bituminous (10^{19} spins/g) which purchased from Henan province than those reported in a previous studies.

Table 36. EPFRs and PM concentrations in coal combustion particles.

Samples	1.1			1.1-2.0			2.0-3.3		
	Spins/m^3	Spins/g	μg/m^3	Spins/m^3	Spins/g	μg/m^3	Spins/m^3	Spins/g	μg/m^3
BL	2.10E+17	6.51E+15	2193.76	5.06E+16	2.36E+15	1457.60	1.01E+17	3.73E+15	1833.04
LM	1.87E+17	2.93E+15	4340.40	8.26E+16	1.60E+15	3514.43	2.40E+16	1.10E+15	1487.04
SF	2.25E+17	2.32E+15	6606.30	1.95E+16	3.58E+14	3697.00	3.07E+16	1.46E+15	1432.57
LJW	3.36E+17	3.64E+15	6277.97	1.51E+16	1.84E+14	5555.06	2.29E+16	6.22E+14	2497.06
GM	1.88E+17	1.27E+16	1008.54	2.57E+16	2.18E+15	802.41	2.48E+16	2.92E+15	577.15
ZF	1.51E+17	4.25E+15	2410.19	2.88E+16	1.10E+15	1775.62	1.69E+16	1.91E+15	600.71
Average	2.16E+17	5.39E+15	3806.19	3.70E+16	1.30E+15	2800.35	3.67E+16	1.96E+15	1404.60
Min	1.51E+17	2.32E+15	1008.54	1.51E+16	1.84E+14	802.41	1.69E+16	6.22E+14	577.15
Max	3.36E+17	1.27E+16	6606.30	8.26E+16	2.36E+15	5555.06	1.01E+17	3.73E+15	2497.06
STD	5.82E+16	3.52E+15	2105.99	2.33E+16	8.31E+14	1620.04	2.89E+16	1.07E+15	672.75

4.6.2.3 EPFRs and PM concentrations in atmospheric particulate matters

The mass concentrations of three PM fractions classified as $PM_{<1.1}$, $PM_{1.1–2.0}$, and $PM_{2.0–3.3}$, were 42.92 ± 16.50 μg/m^3, 26.33 ± 5.66 μg/m^3, and 20.42 ± 2.68μg/m^3, respectively (shown in Figure 57 and Table 37). As shown in Table 38, the $PM_{1.1}$ fraction contributed 46.56% ± 9.67% of the $PM_{3.3}$ mass, which indicated that much more PM in the atmosphere was present in smaller size fractions.

Table 37. EPFRs and PM concentrations in atmospheric particulate matters.

Samples	1.1			1.1-2.0			2.0-3.3		
	Spins/m^3	Spins/g	μg/m^3	Spins/m^3	Spins/g	μg/m^3	Spins/m^3	Spins/g	μg/m^3
A	8.5E+15	2.23E+17	62.08	1.24E+15	8.72E+16	23.25	1.34E+15	1.10E+17	19.94
B	6.61E+15	1.55E+17	69.69	8.71E+14	5.90E+16	24.06	7.08E+14	4.88E+16	23.62
C	3.14E+15	1.63E+17	31.41	4.95E+14	5.16E+16	20.8	4.95E+14	5.16E+16	15.64
D	1.79E+16	4.26E+17	34.23	1.16E+15	4.17E+16	22.82	1.16E+15	4.17E+16	22.58
E	2.86E+15	1.44E+17	32.39	7.39E+14	3.21E+16	37.48	6.99E+14	5.19E+16	21.96
F	3.17E+15	1.86E+17	27.73	9.24E+14	5.09E+16	29.57	6.07E+14	5.27E+16	18.77
Average	7.03E+15	2.16E+17	42.92	9.05E+14	5.38E+16	26.33	8.35E+14	5.95E+16	20.42
Min	2.86E+15	1.44E+17	27.73	4.95E+14	3.21E+16	20.80	4.95E+14	4.17E+16	15.64
Max	1.79E+16	4.26E+17	69.69	1.24E+15	8.72E+16	37.48	1.34E+15	1.10E+17	23.62
STD	5.29E+15	9.73E+16	16.50	2.50E+14	1.72E+16	5.66	3.06E+14	2.29E+16	2.68

The mean atmospheric concentrations of EPFRs in $PM_{1.1}$, $PM_{1.1–2.0}$, and $PM_{2.0–3.3}$ were $7.03 \times 10^{15} \pm 5.29 \times 10^{15}$ spins/m^3, $9.05 \times 10^{14} \pm 2.50 \times 10^{14}$ spins/m^3, and $8.35 \times 10^{15} \pm 3.06 \times 10^{15}$ spins/m^3, respectively, while the mean concentrations in PM were in the range of $2.16 \times 10^{17} \pm 9.73 \times 10^{16}$ spins/g,

$5.38 \times 10^{16} \pm 1.72 \times 10^{16}$ spins/m^3, and $8.35 \times 10^{14} \pm$ to 3.06×10^{14} spins/m^3, respectively.

Table 38. Size distribution of EPFRs and PM in atmospheric particulate matters from Xuanwei (%)

Sample groups	$PM_{1.1}/PM_{3.3}$ (%)			$PM_{1.1\text{-}2.0}/PM_{3.3}$ (%)			$PM_{2.0\text{-}3.3}/PM_{3.3}$ (%)		
	Spins/m^3	Spins/g	μg/m^3	Spins/m^3	Spins/g	μg/m^3	Spins/m^3	Spins/g	μg/m^3
A	76.71	53.07	58.97	11.19	20.75	22.09	12.09	26.18	18.94
B	80.72	58.98	59.38	10.64	22.45	20.50	8.65	18.57	20.12
C	70.31	58.26	46.29	18.61	23.30	30.66	11.08	18.44	23.05
D	89.67	85.22	42.99	4.51	6.44	28.66	5.81	8.34	28.36
E	66.54	63.16	35.27	17.19	14.08	40.81	16.26	22.76	23.91
F	67.43	64.23	36.45	19.66	17.58	38.87	12.91	18.20	24.67
Average	75.23	63.82	46.56	13.63	17.43	30.26	11.14	18.75	23.18
Min	66.54	53.07	35.27	4.51	6.44	20.50	5.81	8.34	18.94
Max	89.67	85.22	59.38	19.66	23.30	40.81	16.26	26.18	28.36
STD	8.18	10.23	9.67	5.35	5.81	7.64	3.29	5.48	3.08

STD: Standard Deviation

Several other studies have reported EPFR concentrations in atmospheric particulate matter, in $PM_{2.5}$ in Taif, Saudi Arabia, Saudi Arabia ranged from 1.6×10^{16} to 5.8×10^{16} spins/m^3 (Shaltout et al., 2015), and in $PM_{2.5}$ in Xuanwei, China ranged from 3.20×10^{17} to 3.10×10^{19} spins/g (P. Wang et al., 2018), in $PM_{2.5}$ in Xi'an ranged from 9.8×10^{11} to 6.9×10^{14} spins/m^3 (Q. Chen, Sun, Mu, et al., 2019), in $PM_{2.5}$ samples from Baton Rouge, ranged from 2.46×10^{16} to 2.79×10^{17} spins/g (Gehling & Dellinger, 2013), respectively. The concentrations of EPFRs were lower. The level of EPFR concentration in PM in Xuanwei is several times smaller than that in previous studies. However, in our study, the levels of EPFRs in the PM were dozens of times lower than previous reported EPFR concentrations. EPFRs were mostly present in the $PM_{1.1}$ fraction, in which the EPFR concentration was 3.43–19.85 times higher than that in $PM_{1.1–2.0}$ and 4.09–15.47 times higher than that in $PM_{2.0\text{-}3.3,}$ which were in agreement with previous research (L. Yang et al., 2017). In addition, it is worth noting that $PM_{2.0}$ can enter the lungs and even the bloodstream more deeply than coarse particles, which may induce harmful reactive oxygen species (ROS) and DNA damage (Valavanidis et al., 2006).

In our study, the simulated combustion experiments with raw coal and biomass were carried out in a relatively closed room, so the mass concentrations of collected particulate matter were much higher than those collected in open areas. Our results indicate that EPFRs attach more readily to fine particles, which may be due to the fact that fine particles have larger surface areas and more porous surfaces,

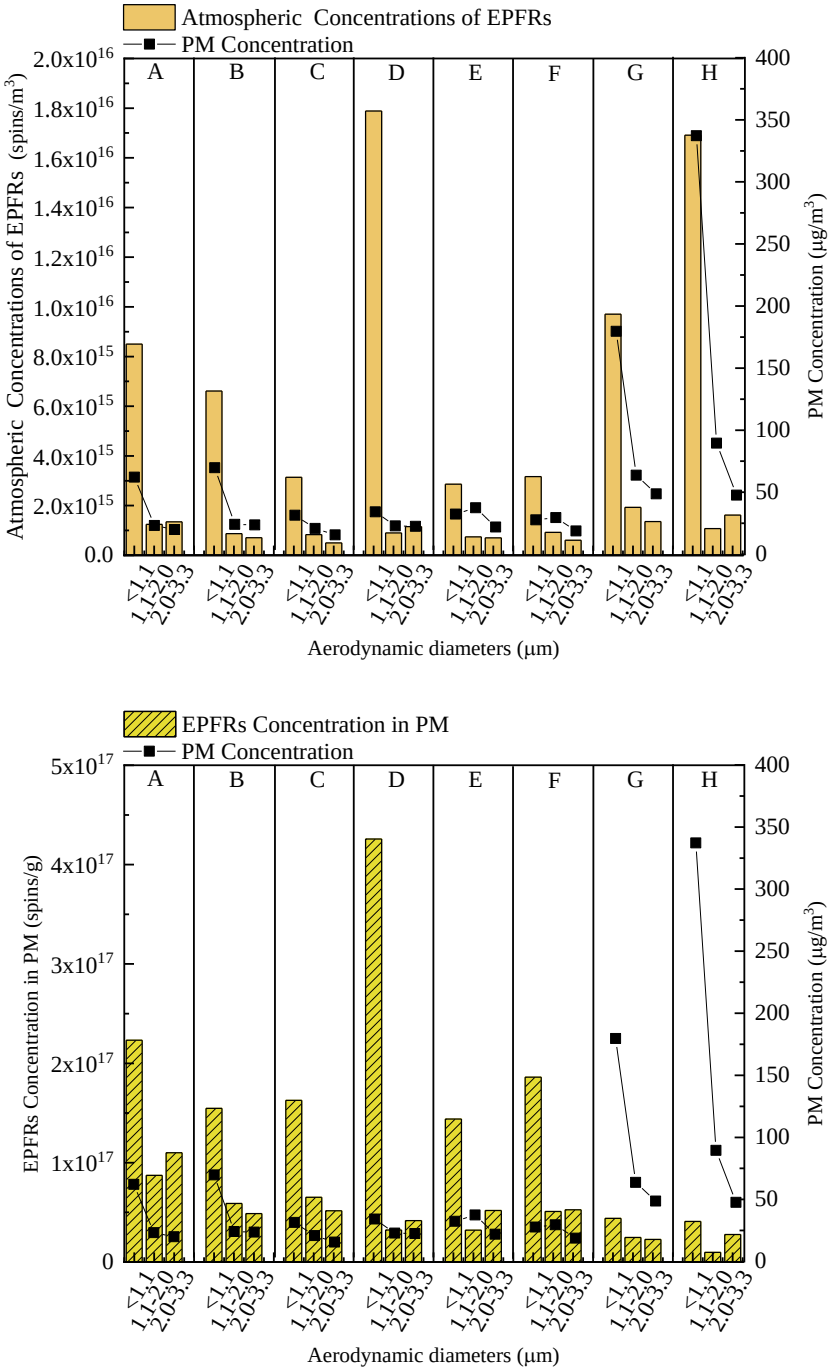

Fig .57. EPFRs and PM concentrations in atmospheric particulate matters from Xuanwei. (The left: the atmospheric EPFRs concentrations; the right: EPFRs concentrations in PM)

to higher adsorption and retention of EPFRs (B. Dellinger et al., 2001) (Arangio et al., 2016)(L. Yang et al., 2017). The distribution pattern in Figure 55, Figure 56, and Figure 57 showed that EPFR concentrations in each PM fraction increased as the particle size decreased. The main reason for the low concentration of EPFRs in our samples may be that our samples have been stored for too long, resulting

in partial degradation. The above results suggest that the concentration of EPFRs in atmospheric particulate matter varies across regions and different combustion sources. However, to the best of our knowledge, the current studies on the concentrations of EPFRs in atmospheric particulate matter are still limited to a few regions and a limited number of samples. In addition, more studies on EPFRs concentrations in atmospheric particulate matter samples from different regions, particle sizes, and sources are still needed.

4.6.3 EPFRs species characteristics

Table 39. g- values and ΔH_{p-p} of the EPFRs produced by different PM from Xuanwei

Sample type	Sample groups	<1.1 (μm)		1.1-2.0 (μm)		2.0-3.3 (μm)	
		g-factors	ΔHp-p (Gauss)	g-factors	ΔHp-p (Gauss)	g-factors	ΔHp-p (Gauss)
Coal	BL	2.0041	5.6404	2.0039	5.6647	2.0039	5.8357
	LM	2.0041	5.5670	2.0039	5.4205	2.0039	5.5670
	SF	2.0041	6.2996	2.0039	6.5193	2.0040	5.9333
	LJW	2.0038	5.4694	2.0039	5.9089	2.0039	5.9333
	GM	2.0041	6.5193	2.0043	6.2996	2.0041	6.5682
	ZF	2.0041	5.6648	2.0016	5.5182	2.0041	5.2741
	Average	2.0040	5.8601	2.0036	5.8885	2.0040	5.8519
	STD	0.0001	0.3985	0.0009	0.4028	0.0001	0.3962
Biomass	Poplar	2.0042	3.8335	2.0043	2.2219	2.0042	6.1043
	Pine	2.0039	8.4239	2.0040	4.8590	2.0039	8.6680
	Corncob	2.0039	6.0554	2.0041	4.2730	2.0039	6.0798
	Average	2.0040	6.1043	2.0041	3.7846	2.0040	6.9507
	STD	0.0001	1.8743	0.0001	1.1306	0.0001	1.2144
APMs	A	2.0046	6.8612	2.0048	4.6148	2.0046	9.0098
	B	2.0044	8.1064	2.0041	6.0554	2.0044	9.3517
	C	2.0039	4.8834	2.0043	5.3474	2.0041	1.7581
	D	2.0039	16.0420	2.0039	6.7635	2.0039	9.3029
	E	2.0042	11.0853	2.0042	6.1042	2.0044	9.4738
	F	2.0042	5.5915	2.0044	4.9811	2.0042	3.4672
	Average	2.0042	8.7616	2.0043	5.6444	2.0043	7.0606
	STD	0.0002	3.8196	0.0003	0.7327	0.0002	3.1867

STD: Standard Deviation

The g-factor and peak width (referred to as ΔHp-p, Gauss) were important parameter for identifying

the type of free radicals (Shaltout et al., 2015) (Arangio et al., 2016), the average ΔHp-p is calculated was finding the distance between the maximum and minimum y-axis values on the x-axis (Runberg et al., 2020). According to previous reports, carbon-centered radicals is generally less than 2.003, oxygen-centered radicals is generally greater than 2.0040, and *g* factors in the range of 2.0030–2.0040 are believed to correspond to a mixture of carbon- and oxygen-centered radicals (Barry Dellinger et al., 2007)(Ruan et al., 2019)(Y. Huang et al., 2020).

Comparison of the EPR spectra of EPFRs in different PMs (as shown in Fig. 58) indicates that the g-factors in PMs were different and the signal intensity of EPFRs is also different. The mean g factor and ΔHp-p of the EPFRs (Table 39) were ranged from 2.0036 to 2.0040 and 5.8519 to 5.8885 G for PM from coal combustion, ranged from 2.0040 to 2.0041 and 3.7846 to 6.9807 G for PM from biomass combustion, and ranged from 2.0042 to 2.0043 and 5.6444 to 8.7616 G for APMs, indicating that the samples were mainly oxygen-centered radicals (phenoxyl and semiquinone radicals) in Xuanwei. In addition, the small ΔH p-p variability of EPFRs in biomass combustion particulate matter, raw coal combustion particulate matter, and APMs also indicates that EPFRs are of the same type, but contains various organic species or organometallic combinations (Feld-Cook et al., 2017)(Gehling et al., 2014).

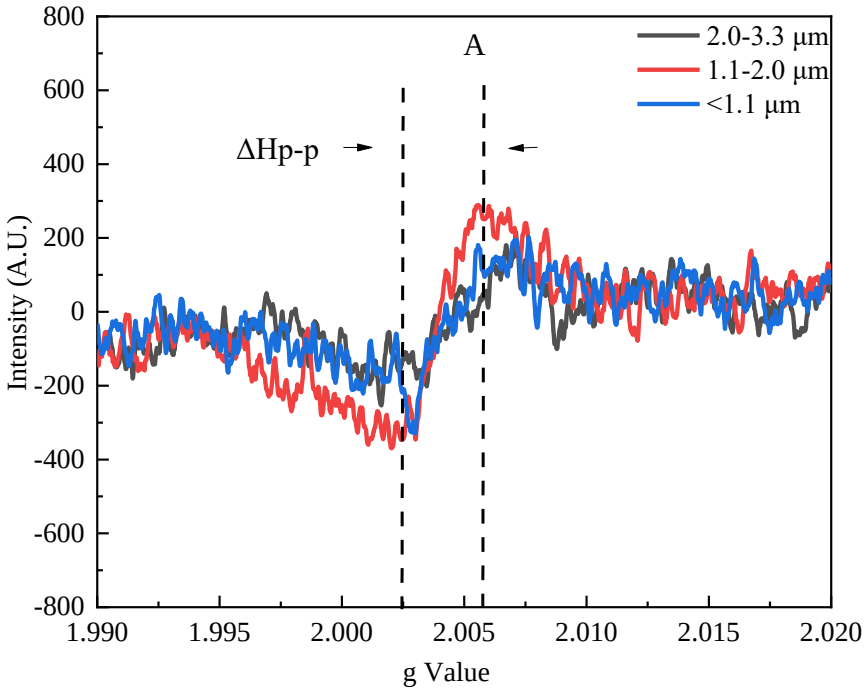

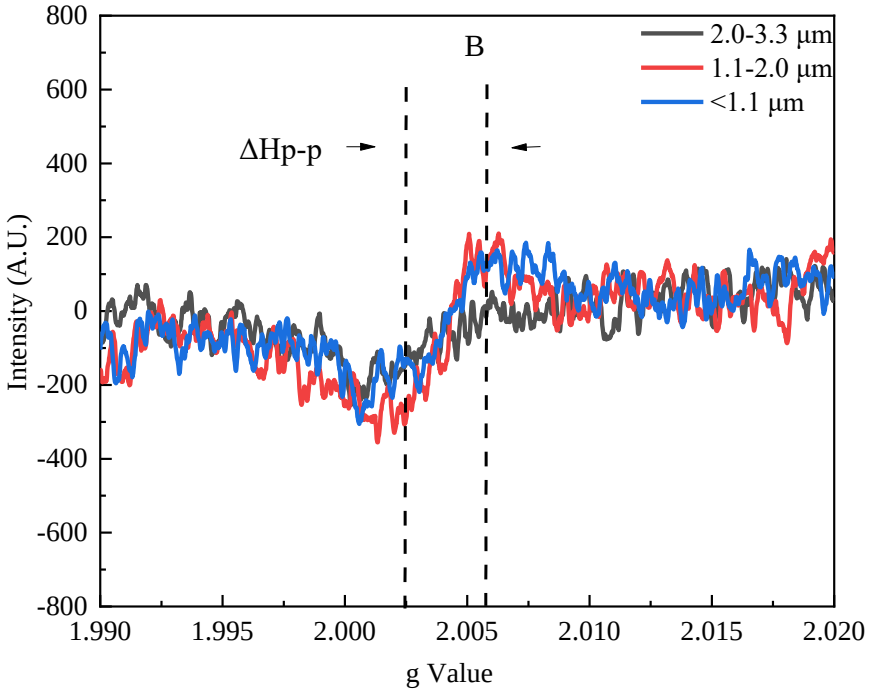
B
2.0-3.3 μm
1.1-2.0 μm
<1.1 μm
ΔHp-p
Intensity (A.U.)
800
600
400
200
0
-200
-400
-600
-800
1.990
1.995
2.000
2.005
2.010
2.015
2.020
g Value

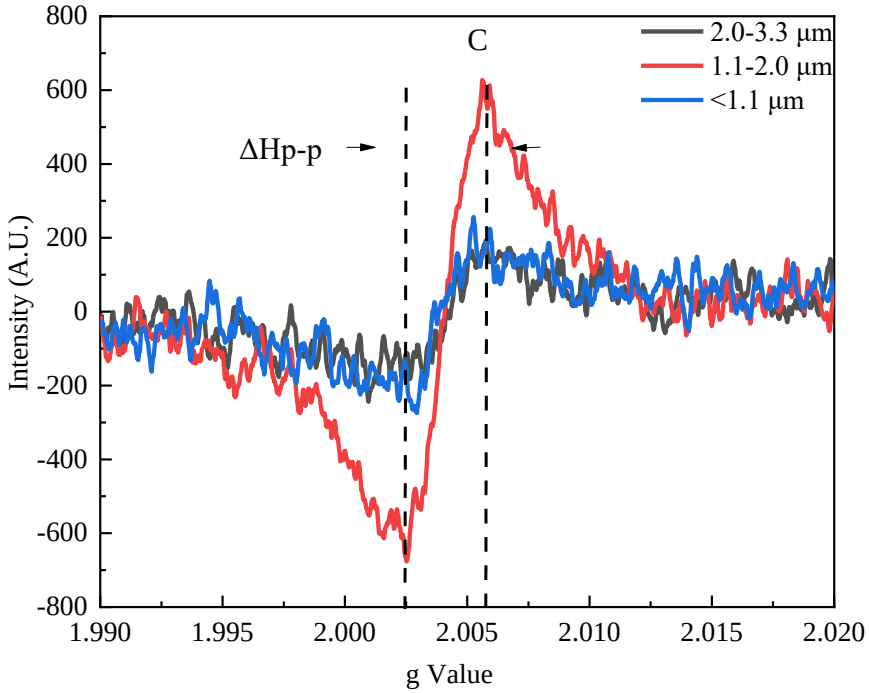
C
2.0-3.3 μm
1.1-2.0 μm
<1.1 μm
ΔHp-p
Intensity (A.U.)
800
600
400
200
0
-200
-400
-600
-800
1.990
1.995
2.000
2.005
2.010
2.015
2.020
g Value

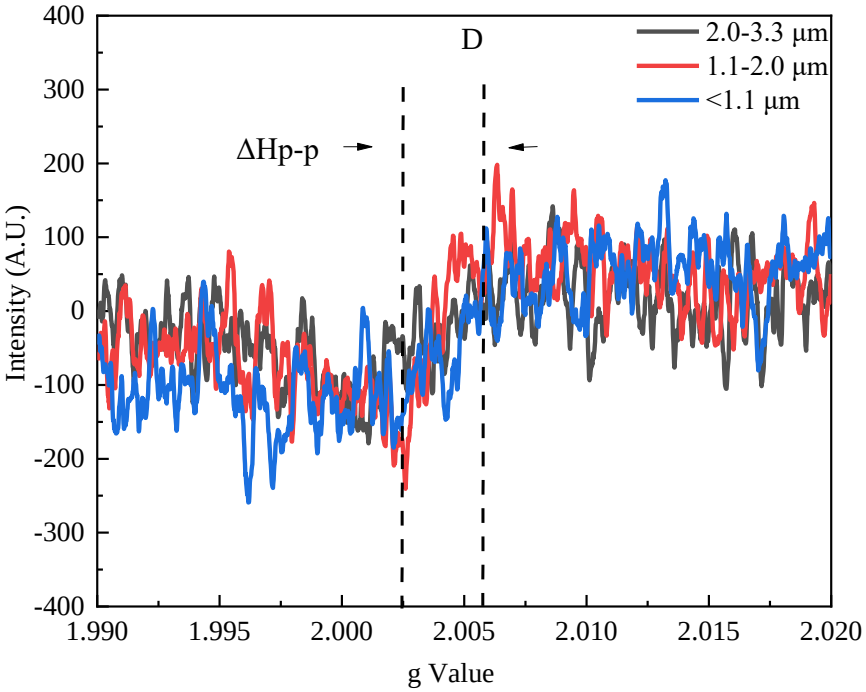
D
2.0-3.3 μm
1.1-2.0 μm
<1.1 μm
ΔHp-p
Intensity (A.U.)
g Value
400
300
200
100
0
-100
-200
-300
-400
1.990
1.995
2.000
2.005
2.010
2.015
2.020

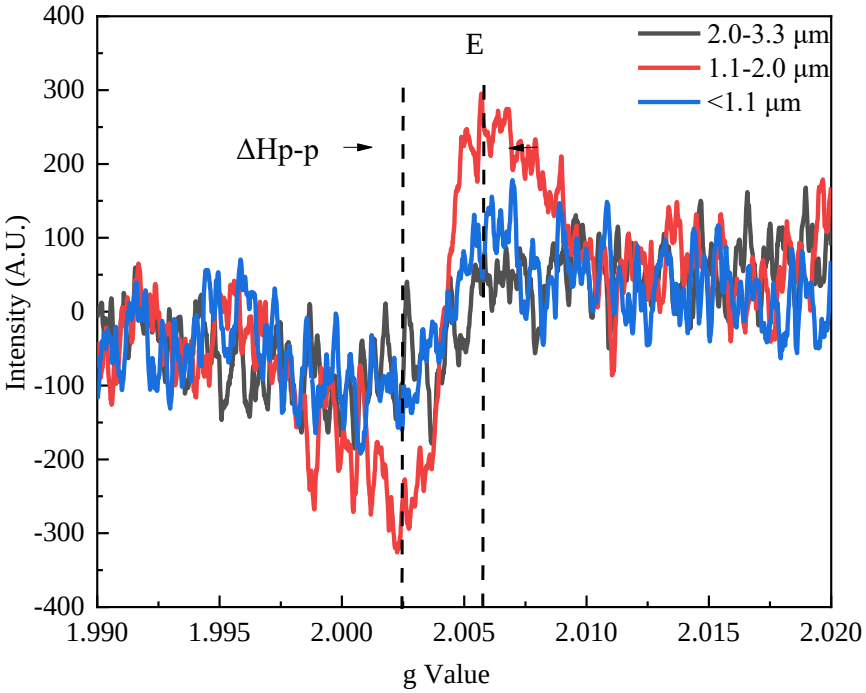
E
2.0-3.3 μm
1.1-2.0 μm
<1.1 μm
ΔHp-p
Intensity (A.U.)
g Value
400
300
200
100
0
-100
-200
-300
-400
1.990
1.995
2.000
2.005
2.010
2.015
2.020

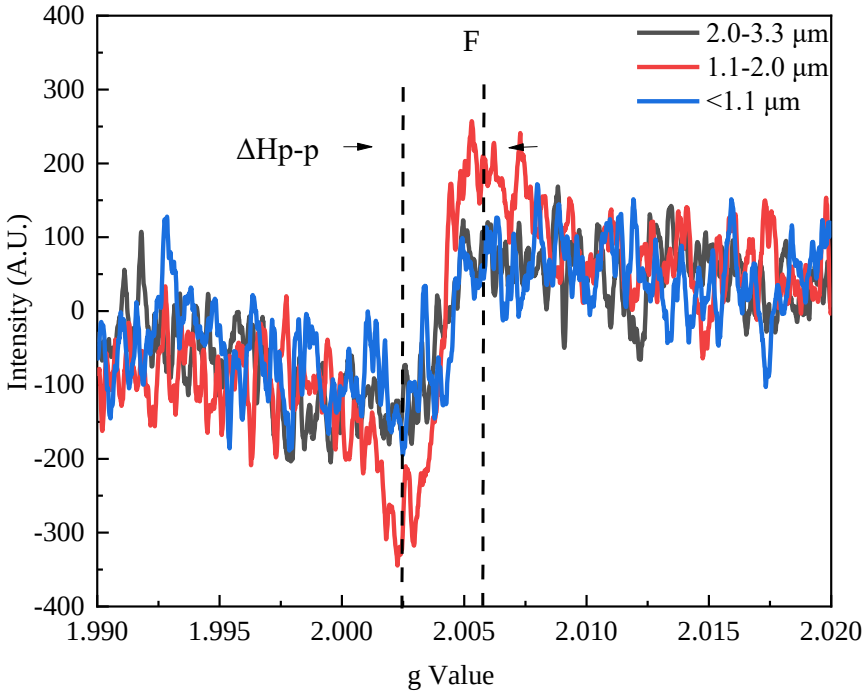
F
2.0-3.3 μm
1.1-2.0 μm
<1.1 μm
ΔHp-p
Intensity (A.U.)
g Value

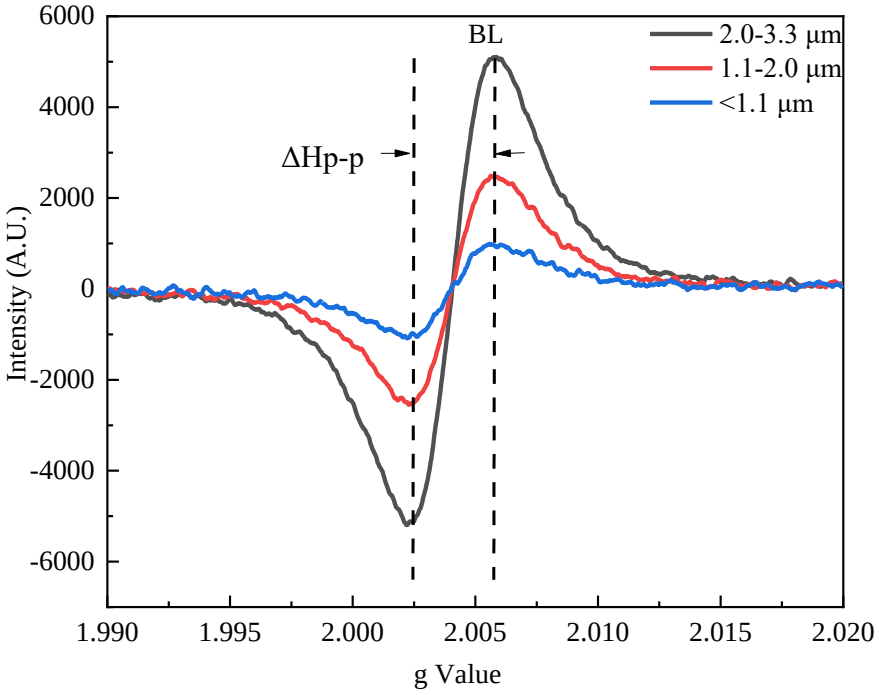
BL
2.0-3.3 μm
1.1-2.0 μm
<1.1 μm
ΔHp-p
Intensity (A.U.)
g Value

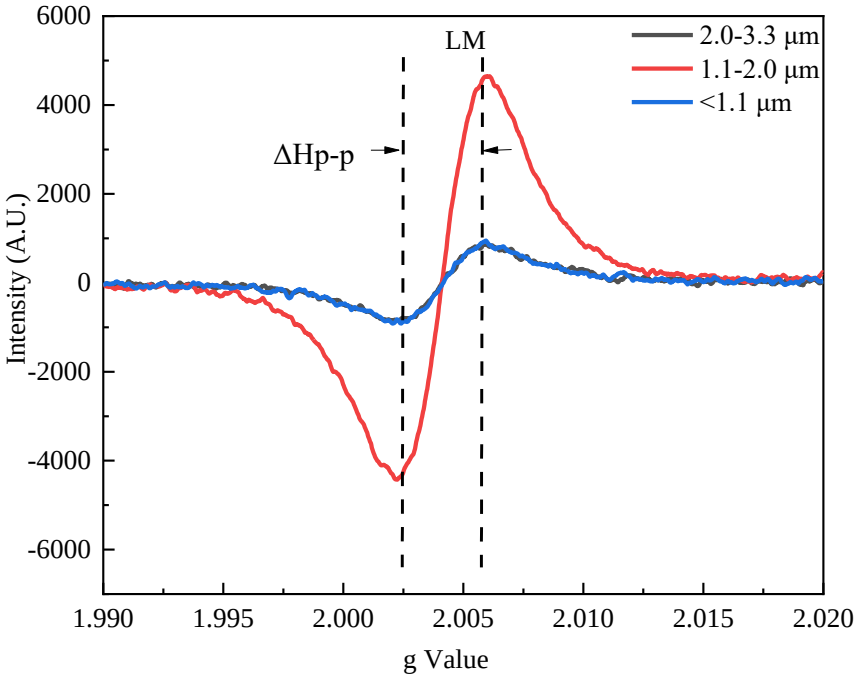
LM
ΔHp-p
2.0-3.3 μm
1.1-2.0 μm
<1.1 μm
Intensity (A.U.)
g Value

2

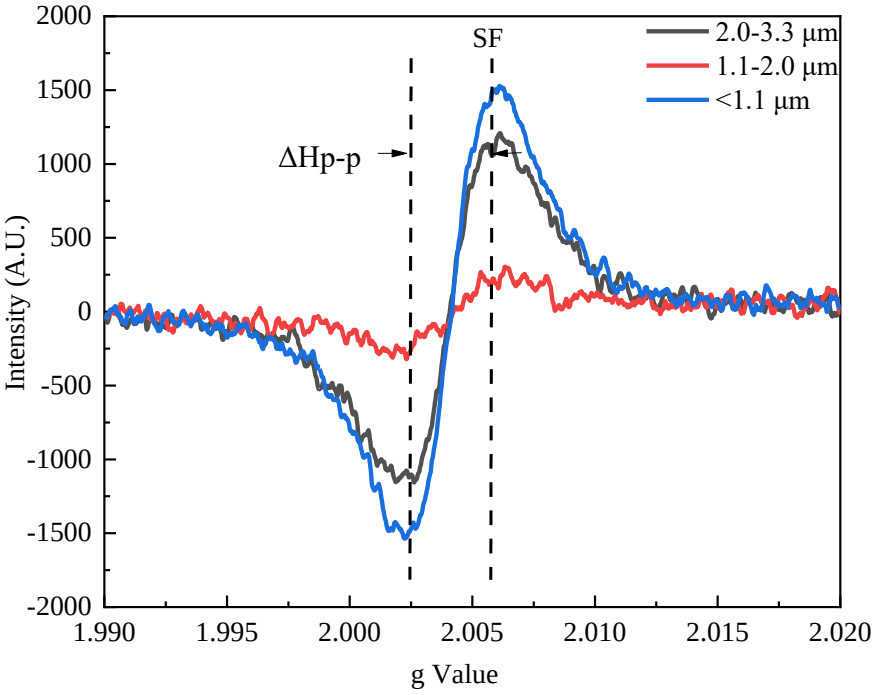
SF
ΔHp-p
2.0-3.3 μm
1.1-2.0 μm
<1.1 μm
Intensity (A.U.)
g Value

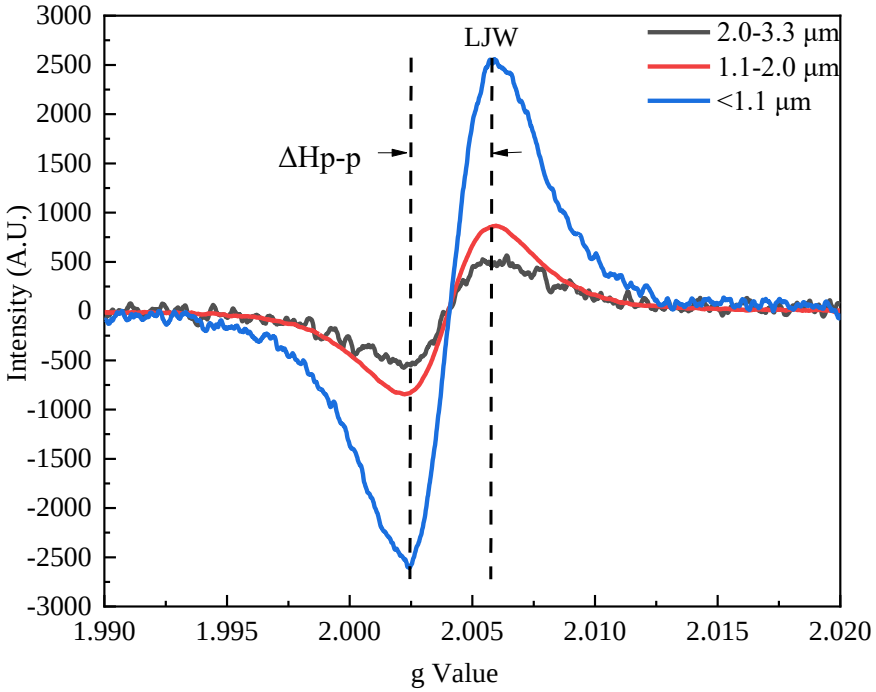
LJW
ΔHp-p
2.0-3.3 μm
1.1-2.0 μm
<1.1 μm
Intensity (A.U.)
g Value

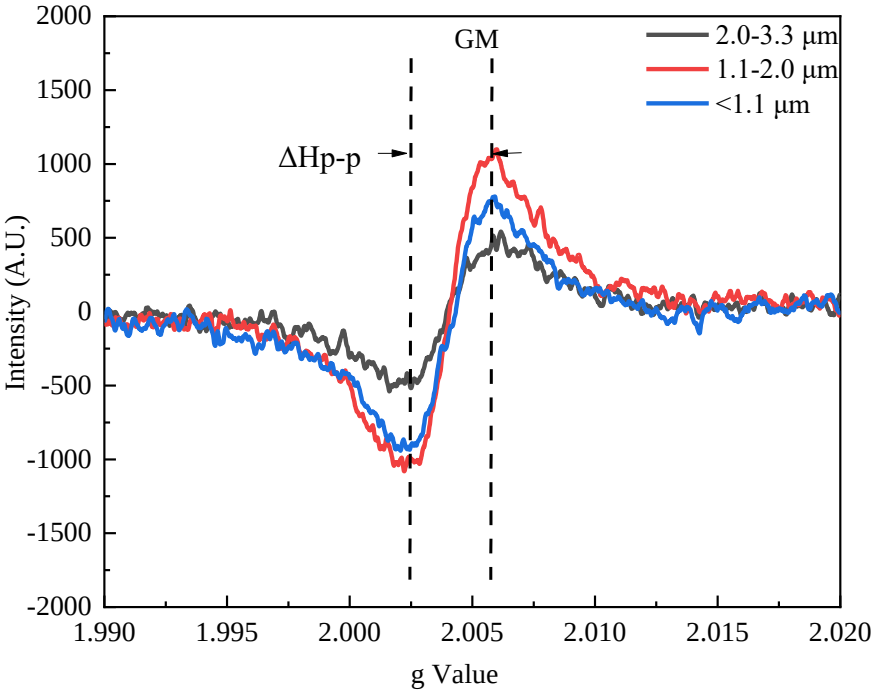
GM
ΔHp-p
2.0-3.3 μm
1.1-2.0 μm
<1.1 μm
Intensity (A.U.)
g Value

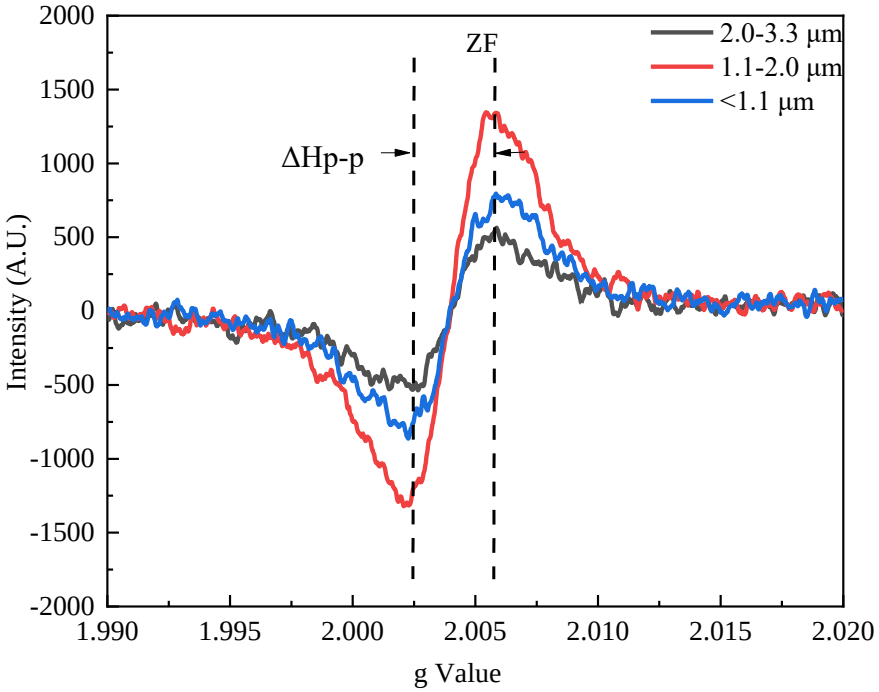
ZF
ΔHp-p
2.0-3.3 μm
1.1-2.0 μm
<1.1 μm
Intensity (A.U.)
g Value

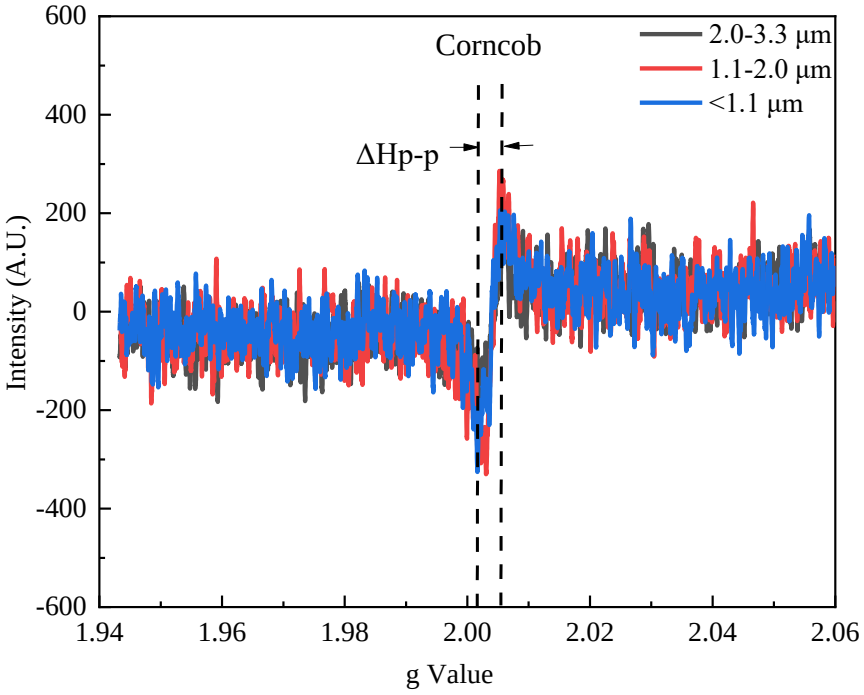
Corncob
ΔHp-p
2.0-3.3 μm
1.1-2.0 μm
<1.1 μm
Intensity (A.U.)
g Value

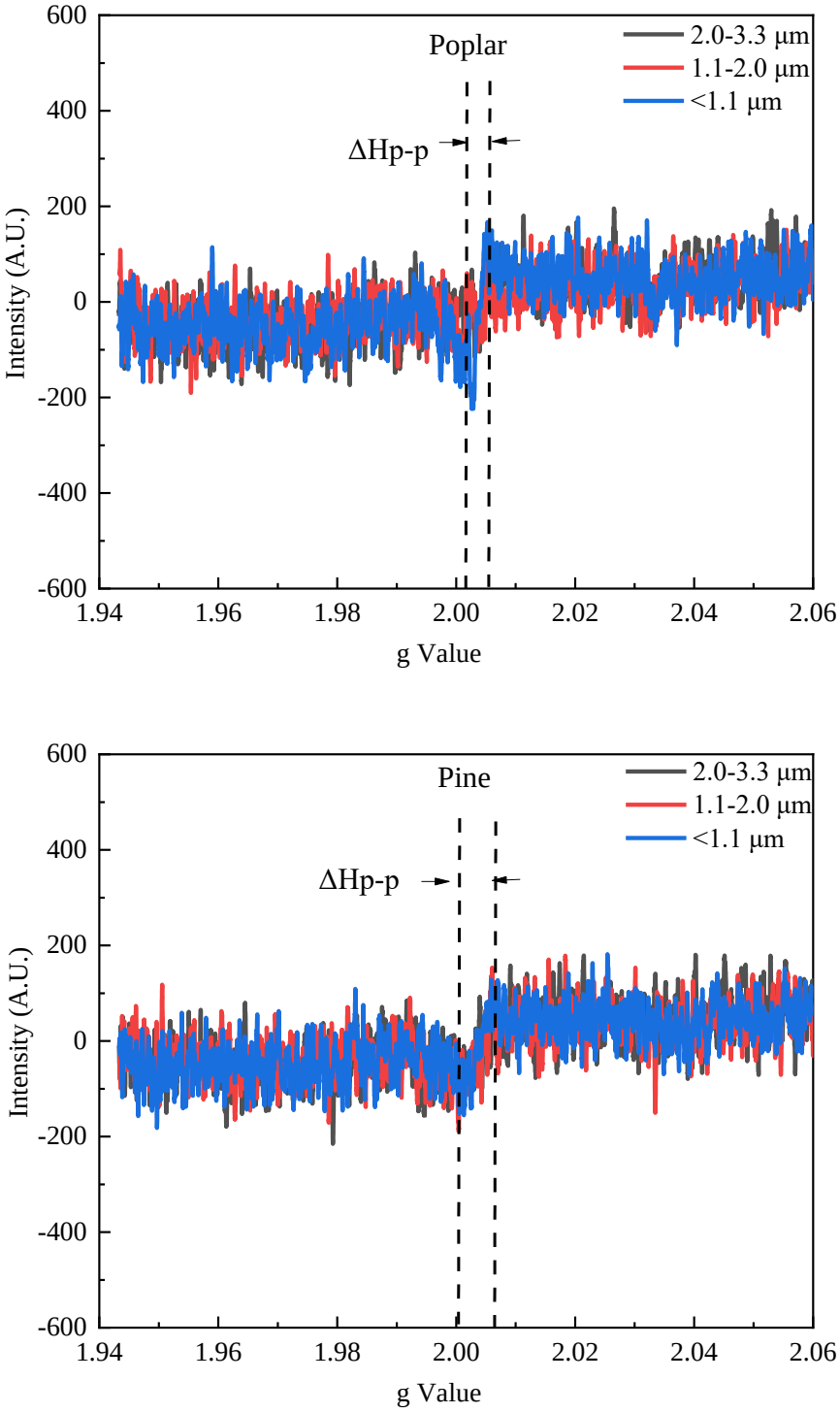

Fig. 58. The mean g factor and ΔHp-p of the EPFRs.

Research found that coal has a high *g*-value of 2.0046 in Xuanwei (P. Wang et al., 2018), and the g-factors of EPFRs in atmospheric particles vary from 2.0030 to 2.0047 and $\Delta H_{p\text{-}p}$ of 4.7–7.9 G (Gehling et al., 2014), which are typical of oxygen-centered or oxygen-containing EPFRs, for example, phenoxyl and semiquinone radicals (L. Yang et al., 2017)(P. Wang et al., 2018)(Q. Chen et al., 2018). In general, both oxygen-centered and carbon-centered radicals are present in atmospheric particulate matter, as

oxygen-centered radicals tend to adhere to fine particles, while carbon-centered radicals mostly adhere to coarse particles. For fine particles, more of the porous structure is exposed, thus providing more available active and adsorption sites for EPFRs (Jiaxun Liu et al., 2015).

Moreover, the presence of semiquinone and phenoxy radicals may lead to activated species in fine particulate matter in the environment (Lyu et al., 2018)(McFerrin et al., 2008).Thus, oxygen-centered radicals appear to be more toxic with fine particles because of their direct effects on the human body; carbon-centered radicals on coarse particles should also be emphasized because of their environmental impact(L. Yang et al., 2017)(Jiaxun Liu et al., 2015).

4.6.4 Potential health risk of EPFRs

In our study, the main types of EPFRs in PM were phenoxyl and semiquinone radicals. The spectral characteristics of EPFRs compared to that of cigarette tar, both of them were similar to semiquinone radicals, and identified as semiquinone radicals (Church & Pryor, 1985)(Dugas et al., 2016), which associated with a quinone/hydroquinone redox cycle capable of producing reactive oxygen species (ROS), to be involved in the carcinogenicity (Y. Xu et al., 2020).

In this study, to assess the potential health risk of EPFRs in biomass combustion particulate matter, coal combustion particulate matter and APMs for Xuanwei residents, we used the equivalent of cigarettes to represent the potential health risk of EPFRs for adults and child per person per year (Table 40).

Our results showed that the average amount of EPFRs exposure were equivalent to 130.31 ± 35.06 cigarettes for adult, 49.52 ± 13.32 cigarettes for child in $PM_{1.1}$, 42.97 ± 43.51 cigarettes for adult, 16.33 ± 16.54 cigarettes for child in $PM_{1.1\text{-}2.0}$, and 22.09 ± 17.40 cigarettes for adult, 8.39 ± 6.61 cigarettes for child in $PM_{2.0\text{-}3.3}$ from coal combustion, respectively. The exposure levels in $PM_{1.1}$ were 1.00-22.32 times higher than in $PM_{1.1\text{-}2.0}$, and 2.09-14.69 times higher than in $PM_{2.0\text{-}3.3}$ for both adult and child, which indicates that EPFRs in $PM_{1.1}$ are the most harmful to humans. Meanwhile, the estimated results of EPFRs emission biomass combustion showed that the average EPFRs exposure were equivalent to 53.11 ± 6.65 cigarettes for adult, 20.18 ± 2.53 cigarettes for child in $PM_{1.1}$, 9.33 ± 2.26 cigarettes for adult, 3.54 ± 0.86 cigarettes for child in $PM_{1.1\text{-}2.0}$, and 6.97 ± 0.34 cigarettes for adult, 2.65 ± 0.13 cigarettes for child in $PM_{2.0\text{-}3.3}$ per year, respectively. In contrast, the average EPFRs exposure in APMs were equivalent to 80.02 ± 37.37 cigarettes for adult, 30.41 ± 14.20 cigarettes for child in $PM_{1.1}$, 31.57 ± 31.27 cigarettes for adult, 12.00 ± 11.88 cigarettes for child in $PM_{1.1\text{-}2.0}$, and 11.44 ± 4.06 cigarettes for adult, 4.35 ± 1.54 cigarettes for child in $PM_{2.0\text{-}3.3}$ per day, respectively. Previous studies have shown that EPFRs inhaled from $PM_{2.5}$ can cause human health risk comparable to 0.4–0.9 cigarettes per day (Gehling & Dellinger,

2013), 5.0 cigarettes in $PM_{2.5}$ per person per day in Xi'an in 2017 (Q. Chen, Sun, Mu, et al., 2019), 46 cigarettes in $PM_{2.5}$ per day in airborne particulate matter in Beijing (Y. Xu et al., 2021), 2.3-6.8 cigarettes per capita per day in Wanzhou, China (Qian et al., 2020). The above results indicate that the potential health risks of EPFRs in PM varies from region to region and from one combustion source to another.

Table 40. The potential health risk of EPFRs for adults and child per year

Sample type	Sample groups	<1.1 (μm)		1.1-2.0 (μm)		2.0-3.3 (μm)		3.3 (μm)	
		EQ(Adult)	EQ(child)	EQ(Adult)	EQ(child)	EQ(Adult)	EQ(child)	EQ(Adult)	EQ(child)
Coal	BL	126.57	48.10	30.48	11.58	60.62	23.04	217.68	82.72
	LM	112.90	42.90	49.75	18.91	14.48	5.50	177.13	67.31
	SF	135.69	51.56	135.69	51.56	18.51	7.03	165.94	63.06
	LJW	202.37	76.90	9.07	3.45	13.78	5.24	225.21	85.58
	GM	113.39	43.09	15.47	5.88	14.94	5.68	143.80	54.64
	ZF	90.91	34.55	17.35	6.59	10.18	3.87	118.44	45.01
	Average	130.31	49.52	42.97	16.33	22.09	8.39	174.70	66.39
	Min	90.91	34.55	9.07	3.45	10.18	3.87	118.44	45.01
	Max	202.37	76.90	135.69	51.56	60.62	23.04	225.21	85.58
	STD	35.06	13.32	43.51	16.54	17.40	6.61	37.86	14.39
Biomass	Poplar	49.15	18.68	11.37	4.32	6.75	2.57	67.27	25.56
	Pine	62.48	23.74	6.18	2.35	7.44	2.83	76.10	28.92
	Corncob	47.71	18.13	10.44	3.97	6.71	2.55	64.86	24.65
	Average	53.11	20.18	9.33	3.54	6.97	2.65	69.41	26.37
	Min	47.71	18.13	6.18	2.35	6.71	2.55	64.86	24.65
	Max	62.48	23.74	11.37	4.32	7.44	2.83	76.10	28.92
	STD	6.65	2.53	2.26	0.86	0.34	0.13	4.83	1.84
APMs	A	122.91	46.70	17.97	6.83	19.44	7.39	160.31	60.92
	B	95.56	36.31	95.56	36.31	10.23	3.89	118.38	44.98
	C	45.34	17.23	45.34	17.23	7.16	2.72	64.52	24.52
	D	129.24	49.11	6.51	2.47	8.35	3.17	144.11	54.76
	E	41.33	15.70	10.68	4.06	10.10	3.84	62.11	23.60
	F	45.76	17.39	13.35	5.07	13.35	5.07	67.88	25.79
	Average	80.02	30.41	31.57	12.00	11.44	4.35	102.88	39.10
	Min	41.33	15.70	6.51	2.47	7.16	2.72	62.11	23.60
	Max	129.24	49.11	95.56	36.31	19.44	7.39	160.31	60.92
	STD	37.37	14.20	31.27	11.88	4.06	1.54	39.99	15.20

Min: Minimum value, Max: Maximum value, STD: Standard Deviation

The results of this study suggest that the health risk of EPFRs is significantly increased when the particle size distribution of EPFRs is taken into account, and RCC particulate matter is more hazardous

to humans than APMs, followed by RBC particulate matter.

4.6.5 Brief summary

To the best of our knowledge, coal combustion, biomass burning and APMs are considered to be important sources of EPFRs (Y. Wang et al., 2019) (Zhao et al., 2021), and in addition, there is little information on individual exposure levels of inhaled EPFRs in the high lung cancer prevalence area of Xuanwei, China. However, the most important thing is that the mechanism of the high lung incidence is still not clear. In this study, we conducted simulated combustion experiments (six kinds of coal, three kinds of biomass), and six groups of atmospheric particulate matter were collected to explore the content and particle size distribution pattern of EPFRs and potential health risk of EPFRs for adult and child, providing new perspectives and evidence to reveal the high incidence of lung cancer in Xuanwei.

(1) The contribution of EPFRs for biomass combustion, coal combustion and APMs were mainly distributed in the size range of <1.1 μm, which accounted for 76.15 ± 4.14%, 74.85 ± 10.76%, and 75.23 ± 8.18 % of $PM_{3.3}$, respectively.

(2) The mean g factors were ranged from 2.0016 to 2.0043, 2.0039 to 2.0043 and 2.0039 to 2.0046 for biomass combustion, coal combustion and APMs, respectively, indicating that the samples were mainly oxygen-centered radicals (phenoxyl and semiquinone radicals) in Xuanwei

(3) The potential health risks of EPFRs for adult and child in $PM_{1.1}$ were equivalent to 130.31 ± 35.06, 49.52 ± 13.32 cigarettes in coal combustion particles, 53.11 ± 6.65, 20.18 ± 2.53 cigarettes in biomass combustion particles, and 80.02 ± 37.37, 30.41 ± 14.20 cigarettes in APMs, respectively.The results suggest that the health risk of EPFRs is significantly increased when the particle size distribution of EPFRs is taken into account, and RCC particulate matter is more hazardous to humans than APMs, followed by RBC particulate matter.

Chapter 5 Summary, limitation and future work

5.1 Summary of PM Concentration

We collected six groups of atmospheric particulate matter, three types of biomasses, and six types of raw coal in Xuanwei, Yunnan, an area with a high incidence of lung cancer and eight sets of atmospheric particulate matter samples were collected in Beijing. Comparing the different type particulate matter, we found that the mass concentration of particulate matter emitted from solid fuel combustion was mainly concentrated in particle size < 2.0 μm (58.17 ± 3.59 % for RBC particles, 67.02 ± 9.06 % for RCC particles), while the mass concentrations of atmospheric particulate matter were mainly concentrated in the particle size < 2.0 μm (49.74 ± 2.15 %) and >7.0 μm (20.28 ± 3.29 %). It indicates that the emission of fine particulate matter from raw coal combustion is more than that from biomass combustion, and the health risk is not negligible as the ambient atmosphere is dominated by fine particulate matter. We found that the mass of atmospheric particles showed a bimodal distribution, with the major peak in the range of particle size <1.1 μm and the minor peak in the range of size >7 μm. In contrast, the concentration of particulate matter emitted from solid fuel combustion is mainly concentrated in the range of particle size <1.1 μm. Xuanwei area, there are no large sources of pollution in the vicinity of the sampling site, and its pollution may be caused by solid fuel combustion, road transport, dust from construction sites, exhaust emissions from cars or mining in the county, and long-distance transport of pollution from surrounding cities. Beijing area, it is generally acknowledged that primary source like road dust and soil as the main emission source of coarse particulate matter, while fine atmospheric particulate matters are emitted from both primary source and secondary formation due to complex chemical processes in the atmosphere. Predominantly, high PM in the winter in Beijing was mainly attributed to the adverse meteorological conditions like low temperature and lower boundary layer height, less precipitation and weaker wind and solid fuel (coal) combustion for indoor heating. another reason may be that probably due to the transport of polluted air masses from urban areas.

The results show that the particulate matter pollution in Xuanwei is not serious and is at a medium level in the country, indicating that the mass concentration of particulate matter is not the main factor of lung cancer in Xuanwei, which may be due to the possibility that the local particulate matter in Xuanwei contains some special components or the content of certain pollutants exceeds the standard.

5.2 Summary of APMs

5.2.1 Summary of APMs in Beijing:

Airborne particulate matter (APM) pollution often occurs in the wintertime in northern China, posing a potential threat to human health. To date, there are limited studies about the metals and inorganic ions to link source apportionments and health risk assessments in the different size-segregated PM samples. In this study our samples were collected by a high-volume air sampler from December 26, 2018 to January 11, 2019 in a high population residential area (Beijing). Water-soluble inorganic ions, metal elements in the different size-segregated PM samples were determined for health risk assessments by inhalation of PM.

(1), The mass concentration of SO_4^{2-} and NO_3^-, NH_4^+ have demonstrated a unimodal distribution of fine particles (< 1.1 μm). The average mass ratio of (NO_3^- + NO_2^-) / SO_4^{2-} , Cl^-/Na^+, Cl^-/ K^+ and Cl^- / (NO_3^- + NO_2^-) were1.68 6.58 ,6.18 and 0.57, respectively. Combined with higher CEFs, it showed that coal combustion and vehicle emissions were the main anthropogenic sources of PM in Beijing in winter.

(2), $PM_{1.1}$ was the major contributor of Pb, Cd and As for CR and HQ. The potential toxic metals of Cr(VI), V and As caused higher CR for children than Ni, Cd, Co, Pb, meanwhile, Pb and Ni were cause higher CR for adults than As, Cr(VI), V, Co , Cd , especially in $PM_{1.1}$.

Our results can help stakeholders and policy makers recognize the characteristics of anthropogenic particles and their impact on air quality in the region, and initiate strategies to further control emissions to improve public health. We recommend continuing efforts in controlling coal burning throughout the year and also to include the surrounding areas.

5.2.2 Summary of APMs in Xuamwei:

In the current work, the results show that the particulate matter pollution in Xuanwei is not serious and is at a medium level in the country, indicating that the mass concentration of particulate matter is not a major factor of lung cancer in Xuanwei, but it is possible that the local particulate matter in Xuanwei contains some special components or the contents of certain pollutants, which are significant health risks to the human body. For example, in our previous study (K. Xiao, Yichun L, et al., 2021), we selected six groups of coal in Xuanwei rural areas, then conducted simulated combustion experiments to explore the environmentally persistent free radicals, the result show that the average amount of environmentally persistent free radicals exposure were equivalent to 130.31 ± 35.06 cigarettes for an adult, 49.52 ± 13.32

cigarettes for children in $PM_{1.1}$.

The average ratio of NO_3^-/SO_4^{2-} in all particulate were 0.22, 0.18, 0.15, 0.34 and 0.36, it indicating that stationary industrial and combustion sources contributed to PM were more significant. The ANE / CAE < 1 in all particulate indicate that the APMs was alkaline. SO_4^{2-} prefers to combine with NH_4^+ to form $(NH_4)_2SO_4$, which hinders the formation of NH_4NO_3, the remaining SO_4^{2-} and NO_3^- to neutralize the K^+, KNO_3 was formed at all particulate. However, K_2SO_4 can only be formed in the particle size less than 3.3 μm. As and Se were identified as the most enriched (EF >10) WSPTMs in all PM sizes, were predominantly from anthropogenic emissions, suggesting that coal combustion could be the important contributor of PM-bound WSPTMs in this study area. Total WSPTMs exhibited high TCR values (9.98×10^{-6}, 1.06×10^{-5}, and 1.19×10^{-5} for girls, boys and adults, respectively) in the smaller particles (<1.1 μm). Se make a major contribution (63.60%) CR in $PM_{2.0}$, furthermore decreased with the PM size increase and should be of more concern.

5.3 Xuanwei:

5.3.1 Summary of WSPTMs

Our result show that all PMs, the TCR was higher than 1 for adults and lower than 1 for children, except for $PM_{1.1}$. TCR values for As, Cd and Co decreased with increasing PM particle size (for adults and children), indicating that As, Cd and Co had the highest in $PM_{1.1}$. Interestingly, the TCR values for Cr (VI) were stable across PM particle sizes with no variability (adults and children), and the TCR for lead was negligible. Notably, the TCR values for V showed a bimodal distribution, with the major peak in the particle size <1.1 μm while the minor peak in the size range of > 7 μm. The noncancer risk of Ba account for 91.28 %, 71.39 %, 78.74 %, 82.38 %, and 84.95 % within $PM_{1.1}$, $PM_{1.1–2.0}$, $PM_{2.0–3.3}$, $PM_{3.3–7.0}$, and $PM_{>7.0}$. It indicates that the non-carcinogenic risk of WSPTMs in RCC particles, mainly Ba, followed by As and the non-carcinogenic risk is highest within $PM_{1.1}$.

Compare with the TCR of RCC particles in Xuanwei and APMs in Beijing, we find that CR of Water-Soluble Potentially Toxic Metals in RCC particles is higher than APMs. This indicates that the carcinogenic risk of Water-Soluble Potentially Toxic Metals in particulate matter emitted from coal combustion is much greater than the carcinogenic risk of Water-Soluble Potentially Toxic Metals in atmospheric particulate matter.

5.3.2 Summary of HULIS:

Lung cancer has unique epidemiological characteristics due to the toxicity of indoor RCC particles in Xuanwei, which suggests that there may be unique molecular mechanisms for the development of lung cancer in Xuanwei. However, mechanism of the high lung incidence is still not clear. In this study, we selected six types of coal and conducted simulated combustion experiments to explore the content and particle size distribution pattern of HULIS-C in particulate matter produced by RCC, providing new perspectives and evidence to reveal the high incidence of lung cancer in Xuanwei

(1) HULIS-C to the PM were 2.09 %~5.65 % for $PM_{2.0}$ and 2.68 %~5.62 % for $PM_{2.0\sim7.0}$, respectively. HULIS-C emitted from RCC is mainly concentrated in $PM_{2.0}$ (68.48 %~79.30 %)

(2) During our measurements, the concentrations of HULIS-C and WSOC were significantly correlated with SO_4^{2-}, NO_3^-, and NH_4^+ in RCC particles.

(3) HULIS-Cx to HULIS-Ct (%) values in RCC particles are 68.48 %–79.30 % (average 73.95 ± 5.13%) for $PM_{2.0}$ and 20.70 %~34.27 (average 26.05 ± 5.13%) for $PM_{2.0\text{-}7.0}$, respectively. The HULIS-Cx to WSOCx (%) values in RCC particles are 32.73 %–63.76 % (average 53.85 ± 12.12%) for $PM_{2.0}$ and 33.91%~82.67% (average 57.06 ± 17.32%) for $PM_{2.0\sim7.0}$, respectively.

5.3.3 Summary of EPFRs:

To the best of our knowledge, coal combustion, biomass burning and APMs are considered to be important sources of EPFRs (Y. Wang et al., 2019) (Zhao et al., 2021), and in addition, there is little information on individual exposure levels of inhaled EPFRs in the high lung cancer prevalence area of Xuanwei, China. However, the most important thing is that the mechanism of the high lung incidence is still not clear. In this study, we conducted simulated combustion experiments (six kinds of coal, three kinds of biomass), and six groups of atmospheric particulate matter were collected to explore the content and particle size distribution pattern of EPFRs and potential health risk of EPFRs for adult and child, providing new perspectives and evidence to reveal the high incidence of lung cancer in Xuanwei.

(1) The mean g factors were ranged from 2.0016 to 2.0043, 2.0039 to 2.0043 and 2.0039 to 2.0046 for biomass combustion, coal combustion and APMs, respectively, indicating that the samples were mainly oxygen-centered radicals (phenoxyl and semiquinone radicals) in Xuanwei

(2) The potential health risks of EPFRs for adult and child in PM1.1 were equivalent to 130.31 ± 35.06, 49.52 ± 13.32 cigarettes in coal combustion particles, 53.11 ± 6.65, 20.18 ± 2.53 cigarettes in

biomass combustion particles, and 80.02 ± 37.37, 30.41 ± 14.20 cigarettes in APMs, respectively. The results suggest that the health risk of EPFRs is significantly increased when the particle size distribution of EPFRs is taken into account, and RCC particulate matter is more hazardous to humans than APMs, followed by RBC particulate matter.

5.4 Limitations of the study

There is a lack of information on the ROS generated by the EPFRs (and HULIS-C)- transition metal oxide combination through the cellular matrices and tissue. Some attempts should be done in cell-free and cell-based experiments to obtain well-characterized information about the ROS generated by the EPFRs (and HULIS-C)- transition metal oxide combination and to better address the health effects of EPFRs and HULIS-C.

5.5 Policy Implications

The following policy suggestions can be drawn based on the findings in our study.

(a) The government should increase awareness of environmental protection in rural areas, for example installation air purifier with a filter membrane that reduces $PM_{1.1}$ in the kitchen or bedroom.

(b) The government should improve the structure of houses and fireplaces in the area.

(c) In order to effectively mitigate the severe $PM_{1.1}$ pollution and promote environmental equity, a differentiated carbon policy should be considered. The local government should better adjust the structure of domestic energy, reduce the use of coal and biomass, and promote the use of environmentally friendly sources in Xuanwei area.

5.6 Future work

EPFRs are emerging and ubiquitous contaminants in the environment, and they have significant toxic effects. Therefore, systematic work is needed to assess and predict their fate and risk. Due to the mixing of various EPFRs in the environment, the first challenge in investigating the fate of EPFRs is to identify their sources. For this purpose, additional parameters should be included in addition to the apparent g-value and bandwidth. Therefore, the first challenge is the need to incorporate analytical methods from EPFR studies. Unlike common pollutants, where multimedia behavior can be described by their physiochemical properties, there is no theory to quantify the interfacial and kinetic behavior of EPFR. Combining certain colloid-based techniques or theories may greatly facilitate the study of the fate

of these particle-associated EPFRs.

Based on the current studies, EPFRs may or may not form with the help of transition metals. What properties of the transition metals determine the formation of EPFRs (including strength and stability) are inconclusive at this time. At this stage of EPFR studies, we suggest a systematic consideration of the properties of particles (e.g., particle size and surface area) and transition metals (e.g., electron transfer and redox activity).

Frequently reported precursor molecules for EPFRs include quinones, phenols, chlorinated/hydroxybenzenes, and polycyclic aromatic hydrocarbons. However, no relationship linking the properties of precursors and EPFRs has been proposed. It is common for various radicals to coexist in a single system. However, except for mathematical peak splitting and deconvolution, no in situ measurements were performed to examine the type and structure of the stable radicals. Apart from the EPR intensity, the lifetime and activity of EPFRs related to the properties of the precursors have not been investigated. Environmental factors, such as oxygen, light, humidity, and humic substances, play an important role in the production and stabilization of EPFRs. All these factors are environmentally relevant, so this line of research will provide valuable information for understanding the mechanism of EPFRs generation and their fate.

EPFR-embedded particles have been reported to have significant toxicity. However, no well-designed experiments have been conducted to separate the toxicity caused by the precursor chemicals, their degradation by-products and EPFRs. More importantly, the relationship between EPFR signal intensity and their activity is unclear. Any indirect measurement of EPFR activity and thus of their toxicity will contribute to their risk assessment.

For precursor chemicals interacting with transition metals, the production of EPFRs may alter their degradation pathways. In addition, other co-occurring organic pollutants may interact with EPFRs or their active species. Both processes are important in the behavior of organic pollutants, but have not been properly considered in previous studies on their multimedia environmental fate.

In the future, a comprehensive investigation of coal combustion HULIS-C and EPFRs emissions under different stove types, combustion conditions and combustion stages are necessary to better understand HULIS-C. we should pay more attention to mechanism on the ROS generated by the HULIS and EPFRs through the cellular matrices and tissue. Some attempts should be done in cell-free and cell-based experiments to obtain well-characterized information about the ROS generated by the HULIS and EPFRs combination and to better address the health effects of HULIS and EPFRs.

Acknowledgments

Finally, I have written here. At this point, the first thing that flashes in my mind is the feeling of stepping into this campus for the first time, a little apprehension, a little excitement, a little excitement, and a little nervousness and anxiety. Three years passed in a flash, and its summer again, goodbye to some people and farewell to some other ones. Some people or things that will be fixed in my mind.

First and foremost, I would like to express deepest gratitude and appreciation to my supervisor, Professor Qingyue Wang, Graduate School of Science and Engineering, Saitama University, Japan, who provide a great opportunity to me for the pursue of Ph.D. study. During the PhD, the professional knowledge, rigorous academic attitude, and excellent work style made me feel like a spring. Someone who I admire and inspires me to move forward.

Particularly important, I received careful guidance from Professor Qingyue Wang from the selection of the topic, the development of the experimental protocol, the analysis of the experimental results and the writing of the thesis. Every time, my supervisor was able to make meaningful suggestions and encourage me to find solutions to my problems.

Secondly, I would like to thank Professor Senlin Lv from School of Environmental and Chemical Engineering in Shanghai University. He provided valuable suggestions in article writing. Thanks to Qin Ao for his work on Beijing samples, collection and testing of metals and ions.. I would also like to thank Dr. Shinich Yonemochi form the Center for Environmental Science in Saitama for his help with the metal experiments, and Rongfang Shen from Shanghai Institute of Applied Physics in Chinese Academy of Sciences. Meanwhile, I want to say thanks to my whole family for their kind understanding, support, and love.

I also grateful to all lab members at the pollution control laboratory, Saitana University, Japan, and well-wishers for their sincere co-operation and encouragement during the study period.

Abbreviations and symbols

Atmospheric Particulate Matters	APMs
An Aerodynamic Diameter Less Than 0.1 MM	$PM_{0.1}$
An Aerodynamic Diameter Less Than 10 MM	PM_{1}
An Aerodynamic Diameter Less Than 2.5 MM	$PM_{1.1}$
An Aerodynamic Diameter Between 1.1 And 2.0 MM	$PM_{1.1\text{-}2.0}$
An Aerodynamic Diameter Less Than 2.5 MM	$PM_{2.5}$
An Aerodynamic Diameter Between 2.0 And 3.3 MM	$PM_{2.0\text{-}3.3}$
An Aerodynamic Diameter Between 3.3 And 7.0 MM	$PM_{3.3\text{-}7.0}$
An Aerodynamic Diameter More 7.0 MM	$PM_{7.0}$
An Aerodynamic Diameter Between 2.0 And 3.3 MM	$PM_{2.0\text{-}3.3}$
An Aerodynamic Diameter Less Than 10 MM	PM_{10}
Alkoxyl	RO•
Air Quality Guideline	AQG
Average Time for Non-Carcinogenic	ATn
Average Time for Carcinogenic	ATc
Beijing-Tianjin-Hebei	BTH
Black Carbon	BC
Bole Coal	BL
Carcinogenic Risks	CR
Chinese National Ambient Air Quality Standards	CNAAQS
Center For Environmental Science in Saitama	CESS
Chronic Obstructive Pulmonary Disease	COPD
Environmental Persistent Free Radicals	EPFRs
Electron Spin Resonance	ESR
Exposure Concentration	EC
Hazard Quotient	HQ
Exposure Frequency	EF
Exposure Time	ET
Exposure Duration	ED

Fraction Retained	Fr
Guangming Coal	GM
High-Volume Air Sampler	HV-RW
Humic Substances	HULIS
Ion Chromatography	IC
Inductively Coupled Plasma Mass Spectrometry	ICP-MS
Integrated Risk Information System	IRIS
International Agency for Research On Cancer	IARC
Inhalation Unit Risk	IUR
Inhalation Reference Dose	RfC
Luomu Coal	LM
Lijiawu Coal	LJW
Organic Carbon	OC
Polytetrafluoroethylene	PTFE
Peroxyl	RO_2•
Potentially Toxic Metals	PTMs
Reactive Oxygen Species	ROS
Residential Coal Combustion	RCC
Relative Humidity	RH
Secondary Inorganic Aerosol	SIA
Standard Deviation	STD
SO_4^{2-}, NO_3^-, And NH_4^+	SNA
Shunfa Coal	SF
The Daily EPFRs Exposure from Inhaled PM	Inh_{PM}
The Concentration of PM	PC_{PM}
The Daily Amount of Air Inhaled	R
The Number of Cigarettes	N_{cig}
Temperature	T
Total Suspended Particulate Matter	TSP
Ultrafine Particles	UFPs
World Health Organization	WHO
Water-Soluble Organic Carbon	WSOC

Water-Soluble Inorganic Ionic Species	WSIIs
Wind Speed	WS
Water-Soluble Potentially Toxic Metals	WSPTMs
Zongfan Coal	ZF

List of Figures

List of Tables

Published List During PH.D period

1. **Kai Xiao**, **Qingyue Wang***, Yichun Lin, Weiqian Wang, Senlin Lu*, and Shinich Yonemochi, "Approval Research for Carcinogen Humic-Like Substances (HULIS) Emitted from Residential Coal Combustion in High Lung Cancer Incidence Areas of China." *Processes* 9.7 (2021): 1254.
2. **Kai Xiao**, Ao Qin, Weiqian Wang, Senlin Lu and **Qingyue Wang***, "Study on the Characteristics of Size-Segregated Particulate Water-Soluble Inorganic Ions and Potentially Toxic Metals during Wintertime in a High Population Residential Area in Beijing, China." *Processes* 9.3 (2021): 552.
3. **Kai Xiao,** Yichun Lin, **Qingyue Wang, ***, Senlin Lu, *, Weiqian Wang, Tanzin Chowdhury, Enyoh Christian Ebere and Mominul Haque Rabin. "Characteristics and Potential Inhalation Exposure Risks of Environmentally Persistent Free Radicals in Atmospheric Particulate Matter and Solid Fuel Combustion Particles in High Lung Cancer Incidence Area, China." *Atmosphere* 12.11 (2021): 1467.4.
4. Weiqian Wang, **Qingyue Wang*,** Daisuke Nakajima, Senlin Lu, **Kai Xiao,** Tanzin Chowdhury Risha, Miho Suzuki, Fenwu Liu, "Industrial Source Contributions and Health Risk Assessment of Fine Particle-Bound Polycyclic Aromatic Hydrocarbons (PAHs) during Spring and Late Summer in the Baoshan Area, Shanghai." *Processes* 9.11 (2021): 2016.
5. Wang Xingzi, Zhou Shumin, Lu Senlin, Zhang Lu, Ma Teng, Liu Xinchun, Zhang Wei, Li Shuijun, **Xiao Kai**, Wang Weqian and **Wang Qingyue**, "Comparison of the characterization of allergenic protein 3 (Pla a3) released from Platanus pollen grains collected in Shanghai during the spring of 2019 and 2020." Aerobiologia (2021): 1-11.**,**
6. Christian Ebere Enyoh*, **Qingyue Wang*,** Tanzin Chowdhury, Weiqian Wang, Senlin Lu, **Kai Xiao** and Md. Akhter Hossain Chowdhury, "New Analytical Approaches for Effective Quantification and Identification of Nanoplastics in Environmental Samples." *Processes* 9.11 (2021): 2086.,
7. **Xiao Kai,** Peng Jiaxian, Xie Tingting, Zeng Junyang, Yao Chuanhe, Myat Sandar Win, Lu Senlin, **Qingyue Wang,** Yonemochi Shinich, Physicochemical characterization of ambient particulate matter emitted from solid fuel combustion in high lung cancer incidence areas in Xuanwei, Yunnan, Journal of Shanghai University (Natural Science Edition), Vol.27(2), 388-399 (2021)(in Chinese) ;
8. Lanfang Rao, Luying Zhang, Xingzi Wang, Tingting Xie, Shumin Zhou, Senlin Lu, **Kai Xiao**, Weqian Wang, **Qingyue Wang***, Oxidative Potential induced by ambient particulatematters with acellular assays: a review, Processes , Vol.8(11), 1410; 22 pages (2020) https://doi.org/10.3390/pr8111410.

Reference

Agarwal, A. K., Gupta, T., Bothra, P., & Shukla, P. C. (2015). Emission profiling of diesel and gasoline cars at a city traffic junction. *Particuology*, *18*. https://doi.org/10.1016/j.partic.2014.06.008

Al-Hemoud, A., Gasana, J., Al-Dabbous, A., Alajeel, A., Al-Shatti, A., Behbehani, W., & Malak, M. (2019). Exposure levels of air pollution (PM2.5) and associated health risk in Kuwait. *Environmental Research*, *179*. https://doi.org/10.1016/j.envres.2019.108730

Amato, F., Viana, M., Richard, A., Furger, M., Prévôt, A. S. H., Nava, S., Lucarelli, F., Bukowiecki, N., Alastuey, A., Reche, C., Moreno, T., Pandolfi, M., Pey, J., & Querol, X. (2011). Size and time-resolved roadside enrichment of atmospheric particulate pollutants. *Atmospheric Chemistry and Physics*, *11*(6). https://doi.org/10.5194/acp-11-2917-2011

Amodio, M., Andriani, E., de Gennaro, G., di Gilio, A., Ielpo, P., Placentino, C. M., & Tutino, M. (2013). How a steel plant affects air quality of a nearby urban area: A study on metals and PAH concentrations. *Aerosol and Air Quality Research*, *13*(2). https://doi.org/10.4209/aaqr.2012.09.0254

An, Z., Huang, R. J., Zhang, R., Tie, X., Li, G., Cao, J., Zhou, W., Shi, Z., Han, Y., Gu, Z., & Ji, Y. (2019). Severe haze in northern China: A synergy of anthropogenic emissions and atmospheric processes. *Proceedings of the National Academy of Sciences of the United States of America*, *116*(18). https://doi.org/10.1073/pnas.1900125116

Andreae, M. O., & Crutzen, P. J. (1997). Atmospheric aerosols: Biogeochemical sources and role in atmospheric chemistry. *Science*, *276*(5315). https://doi.org/10.1126/science.276.5315.1052

Arangio, A. M., Tong, H., Socorro, J., Pöschl, U., & Shiraiwa, M. (2016). Quantification of environmentally persistent free radicals and reactive oxygen species in atmospheric aerosol particles. *Atmospheric Chemistry and Physics*, *16*(20). https://doi.org/10.5194/acp-16-13105-2016

Balakrishna, S., Saravia, J., Thevenot, P., Ahlert, T., Lominiki, S., Dellinger, B., & Cormier, S. A. (2011). Environmentally persistent free radicals induce airway hyperresponsiveness in neonatal rat lungs. *Particle and Fibre Toxicology*, *8*. https://doi.org/10.1186/1743-8977-8-11

Baltrenaite, E., Baltrenas, P., Lietuvninkas, A., Šerevičiene, V., & Zuokaite, E. (2014). Integrated evaluation of aerogenic pollution by air-transported heavy metals (Pb, Cd, Ni, Zn, Mn and Cu) in the analysis of the main deposit media. *Environmental Science and Pollution Research*, *21*(1). https://doi.org/10.1007/s11356-013-2046-6

Barone-Adesi, F., Chapman, R. S., Silverman, D. T., He, X., Hu, W., Vermeulen, R., Ning, B., Fraumeni, J. F., Rothman, N., & Lan, Q. (2012). Risk of lung cancer associated with domestic use of coal in Xuanwei, China: Retrospective cohort study. *BMJ (Online)*, *345*(7874). https://doi.org/10.1136/bmj.e5414

Becagli, S., Sferlazzo, D. M., Pace, G., Di Sarra, A., Bommarito, C., Calzolai, G., Ghedini, C., Lucarelli, F., Meloni, D., Monteleone, F., Severi, M., Traversi, R., & Udisti, R. (2012). Evidence for heavy fuel oil combustion aerosols from chemical analyses at the island of Lampedusa: A

possible large role of ships emissions in the Mediterranean. *Atmospheric Chemistry and Physics*, *12*(7). https://doi.org/10.5194/acp-12-3479-2012

Bellouin, N., Boucher, O., Haywood, J., & Reddy, M. S. (2005). Global estimate of aerosol direct radiative forcing from satellite measurements. *Nature*, *438*(7071). https://doi.org/10.1038/nature04348

Betha, R., Behera, S. N., & Balasubramanian, R. (2014). 2013 Southeast Asian smoke haze: Fractionation of particulate-bound elements and associated health risk. *Environmental Science and Technology*, *48*(8). https://doi.org/10.1021/es405533d

Birdwell, J. E., & Valsaraj, K. T. (2010). Characterization of dissolved organic matter in fogwater by excitation-emission matrix fluorescence spectroscopy. *Atmospheric Environment*, *44*(27). https://doi.org/10.1016/j.atmosenv.2010.05.055

Bodlet, A., Maury, G., Jamart, J., & Dahlqvist, C. (2013). Influence of radiological emphysema on lung function test in idiopathic pulmonary fibrosis. *Respiratory Medicine*, *107*(11). https://doi.org/10.1016/j.rmed.2013.08.039

Bonner, J. C. (2007). Lung Fibrotic Responses to Particle Exposure. *Toxicologic Pathology*, *35*(1). https://doi.org/10.1080/01926230601060009

Bray, F., Ferlay, J., Soerjomataram, I., Siegel, R. L., Torre, L. A., & Jemal, A. (2018). Global cancer statistics 2018: GLOBOCAN estimates of incidence and mortality worldwide for 36 cancers in 185 countries. *CA: A Cancer Journal for Clinicians*, *68*(6). https://doi.org/10.3322/caac.21492

Cai, T., Zhang, H., Li, Z., Rahman, A. F. M. M., & Qiu, H. (2016). A new nano-on-micro stationary phase based on nanodiamond bonded on silica for hydrophilic interaction chromatography. *RSC Advances*, *6*(39). https://doi.org/10.1039/c6ra04824b

Can-Terzi, B., Ficici, M., Tecer, L. H., & Sofuoglu, S. C. (2021). Fine and coarse particulate matter, trace element content, and associated health risks considering respiratory deposition for Ergene Basin, Thrace. *Science of the Total Environment*, *754*. https://doi.org/10.1016/j.scitotenv.2020.142026

Cao, C., Jiang, W., Wang, B., Fang, J., Lang, J., Tian, G., Jiang, J., & Zhu, T. F. (2014). Inhalable microorganisms in Beijing's PM2.5 and PM10 pollutants during a severe smog event. *Environmental Science and Technology*, *48*(3). https://doi.org/10.1021/es4048472

Che, Y., Zhang, J., Zhao, C., Fang, W., Xue, W., Yang, W., Ji, D., Dang, J., Duan, J., Sun, J., Shen, X., & Zhou, X. (2021). A study on the characteristics of ice nucleating particles concentration and aerosols and their relationship in spring in Beijing. *Atmospheric Research*, *247*. https://doi.org/10.1016/j.atmosres.2020.105196

Chen, C. R., Lai, H. C., Liao, M. I., Hsiao, M. C., & Ma, H. wen. (2021). Health risk assessment of trace elements of ambient PM2.5 under monsoon patterns. *Chemosphere*, *264*. https://doi.org/10.1016/j.chemosphere.2020.128462

Chen, G., Sun, X., Ren, H., Wan, X., Huang, H., Ma, X., Ning, B., Zou, X., Hu, W., & Yang, G. (2015). The mortality patterns of lung cancer between 1990 and 2013 in Xuanwei, China. *Lung Cancer*, *90*(2). https://doi.org/10.1016/j.lungcan.2015.08.006

Chen, L. C., & Lippmann, M. (2009). Effects of metals within ambient air particulate matter (PM) on

human health. In *Inhalation Toxicology* (Vol. 21, Issue 1). https://doi.org/10.1080/08958370802105405

Chen, Q., Sun, H., Mu, Z., Wang, Y., Li, Y., Zhang, L., Wang, M., & Zhang, Z. (2019). Characteristics of environmentally persistent free radicals in PM2.5: Concentrations, species and sources in Xi'an, Northwestern China. *Environmental Pollution*, *247*. https://doi.org/10.1016/j.envpol.2019.01.015

Chen, Q., Sun, H., Song, W., Cao, F., Tian, C., & Zhang, Y. L. (2020). Size-resolved exposure risk of persistent free radicals (PFRs) in atmospheric aerosols and their potential sources. *Atmospheric Chemistry and Physics*, *20*(22). https://doi.org/10.5194/acp-20-14407-2020

Chen, Q., Sun, H., Wang, J., Shan, M., Yang, X., Deng, M., Wang, Y., & Zhang, L. (2019). Long-life type — The dominant fraction of EPFRs in combustion sources and ambient fine particles in Xi'an. *Atmospheric Environment*, *219*. https://doi.org/10.1016/j.atmosenv.2019.117059

Chen, Q., Sun, H., Wang, M., Mu, Z., Wang, Y., Li, Y., Wang, Y., Zhang, L., & Zhang, Z. (2018). Dominant Fraction of EPFRs from Nonsolvent-Extractable Organic Matter in Fine Particulates over Xi'an, China. *Environmental Science and Technology*, *52*(17). https://doi.org/10.1021/acs.est.8b01980

Chen, W., Zheng, R., Zeng, H., & Zhang, S. (2015). Epidemiology of lung cancer in China. *Thoracic Cancer*, *6*(2). https://doi.org/10.1111/1759-7714.12169

Chen, Yan, Hou, C., Zhao, L. X., Cai, Q. C., Zhang, Y., Li, D. L., Tang, Y., Liu, H. Y., Liu, Y. Y., Zhang, Y. Y., Yang, Y. K., Gao, C. W., Yao, Q., Zhu, Q. S., & Cao, C. H. (2021). The Association of microRNA-34a With High Incidence and Metastasis of Lung Cancer in Gejiu and Xuanwei Yunnan. *Frontiers in Oncology*, *11*. https://doi.org/10.3389/fonc.2021.619346

Chen, Yang, Xiao, Y., Yang, Y., Duan, J., & Xu, W. (2015). Decomposing contribution of age and non-age factors to rapid growth of lung cancer in Xuanwei over past 30 years. *BMC Public Health*, *15*(1). https://doi.org/10.1186/s12889-015-2482-y

Christian, T. J., Yokelson, R. J., Cárdenas, B., Molina, L. T., Engling, G., & Hsu, S. C. (2010). Trace gas and particle emissions from domestic and industrial biofuel use and garbage burning in central Mexico. *Atmospheric Chemistry and Physics*, *10*(2). https://doi.org/10.5194/acp-10-565-2010

Church, D. F., & Pryor, W. A. (1985). Free-radical chemistry of cigarette smoke and its toxicological implications. *Environmental Health Perspectives*, *VOL. 64*. https://doi.org/10.1289/ehp.8564111

Clark, M. L., Peel, J. L., Balakrishnan, K., Breysse, P. N., Chillrud, S. N., Naeher, L. P., Rodes, C. E., Vette, A. F., & Balbus, J. M. (2013). Health and household air pollution from solid fuel use: The need for improved exposure assessment. In *Environmental Health Perspectives* (Vol. 121, Issue 10). https://doi.org/10.1289/ehp.1206429

Cruz, A. L. N. D., Cook, R. L., Lomnicki, S. M., & Dellinger, B. (2012). Effect of low temperature thermal treatment on soils contaminated with pentachlorophenol and environmentally persistent free radicals. *Environmental Science and Technology*, *46*(11). https://doi.org/10.1021/es300362k

Cui, Y., Ji, D., He, J., Kong, S., & Wang, Y. (2020). In situ continuous observation of hourly elements in PM2.5 in urban beijing, China: Occurrence levels, temporal variation, potential source regions

and health risks. *Atmospheric Environment*, *222*. https://doi.org/10.1016/j.atmosenv.2019.117164

Dai, Q., Bi, X., Liu, B., Li, L., Ding, J., Song, W., Bi, S., Schulze, B. C., Song, C., Wu, J., Zhang, Y., Feng, Y., & Hopke, P. K. (2018). Chemical nature of PM2.5 and PM10 in Xi'an, China: Insights into primary emissions and secondary particle formation. *Environmental Pollution*, *240*. https://doi.org/10.1016/j.envpol.2018.04.111

Dai, Q. L., Bi, X. H., Wu, J. H., Zhang, Y. F., Wang, J., Xu, H., Yao, L., Jiao, L., & Feng, Y. C. (2015). Characterization and source identification of heavy metals in ambient PM10 and PM2.5 in an integrated Iron and Steel industry zone compared with a background site. *Aerosol and Air Quality Research*, *15*(3). https://doi.org/10.4209/aaqr.2014.09.0226

Dai, S., Tian, L., Chou, C. L., Zhou, Y., Zhang, M., Zhao, L., Wang, J., Yang, Z., Cao, H., & Ren, D. (2008). Mineralogical and compositional characteristics of Late Permian coals from an area of high lung cancer rate in Xuan Wei, Yunnan, China: Occurrence and origin of quartz and chamosite. *International Journal of Coal Geology*, *76*(4). https://doi.org/10.1016/j.coal.2008.09.001

Dall'Osto, M., Querol, X., Amato, F., Karanasiou, A., Lucarelli, F., Nava, S., Calzolai, G., & Chiari, M. (2013). Hourly elemental concentrations in PM2.5 aerosols sampled simultaneously at urban background and road site during SAPUSS -diurnal variations and PMF receptor modelling. *Atmospheric Chemistry and Physics*, *13*(8). https://doi.org/10.5194/acp-13-4375-2013

Dao, X., Lin, Y. C., Cao, F., Di, S. Y., Hong, Y., Xing, G., Li, J. J., Fu, P., & Zhang, Y. L. (2019). Introduction to the national aerosol chemical composition monitoring network of China objectives, current status, and outlook. *Bulletin of the American Meteorological Society*, *100*(12). https://doi.org/10.1175/BAMS-D-18-0325.1

Dellinger, B., Pryor, W. A., Cueto, R., Squadrito, G. L., Hegde, V., & Deutsch, W. A. (2001). Role of free radicals in the toxicity of airborne fine particulate matter. *Chemical Research in Toxicology*, *14*(10). https://doi.org/10.1021/tx010050x

Dellinger, Barry, Lomnicki, S., Khachatryan, L., Maskos, Z., Hall, R. W., Adounkpe, J., McFerrin, C., & Truong, H. (2007). Formation and stabilization of persistent free radicals. *Proceedings of the Combustion Institute*, *31 I*(1). https://doi.org/10.1016/j.proci.2006.07.172

Delmastro, C., Lavagno, E., & Mutani, G. (2015). Chinese residential energy demand: Scenarios to 2030 and policies implication. *Energy and Buildings*, *89*. https://doi.org/10.1016/j.enbuild.2014.12.004

Distefano, E., Eiguren-Fernandez, A., Delfino, R. J., Sioutas, C., Froines, J. R., & Cho, A. K. (2009). Determination of metal-based hydroxyl radical generating capacity of ambient and diesel exhaust particles. *Inhalation Toxicology*, *21*(9). https://doi.org/10.1080/08958370802491433

Do, T. Van, Vuong, Q. T., & Choi, S. D. (2021). Day–night variation and size distribution of water-soluble inorganic ions in particulate matter in Ulsan, South Korea. *Atmospheric Research*, *247*. https://doi.org/10.1016/j.atmosres.2020.105145

Downward, G. S., Hu, W., Rothman, N., Reiss, B., Wu, G., Wei, F., Chapman, R. S., Portengen, L., Qing, L., & Vermeulen, R. (2014). Polycyclic aromatic hydrocarbon exposure in household air pollution from solid fuel combustion among the female population of Xuanwei and Fuyuan counties, China. *Environmental Science and Technology*, *48*(24).

https://doi.org/10.1021/es504102z

Duan, J., Tan, J., Hao, J., & Chai, F. (2014). Size distribution, characteristics and sources of heavy metals in haze episod in Beijing. *Journal of Environmental Sciences (China)*, *26*(1). https://doi.org/10.1016/S1001-0742(13)60397-6

Duan, X., Yan, Y., Li, R., Deng, M., Hu, D., & Peng, L. (2020). Seasonal variations, source apportionment, and health risk assessment of trace metals in PM2.5 in the typical industrial city of changzhi, China. *Atmospheric Pollution Research*. https://doi.org/10.1016/j.apr.2020.09.017

Dugas, T. R., Lomnicki, S., Cormier, S. A., Dellinger, B., & Reams, M. (2016). Addressing emerging risks: Scientific and regulatory challenges associated with environmentally persistent free radicals. In *International Journal of Environmental Research and Public Health* (Vol. 13, Issue 6). https://doi.org/10.3390/ijerph13060573

Dunea, D., Iordache, S., Liu, H. Y., Bøhler, T., Pohoata, A., & Radulescu, C. (2016). Quantifying the impact of PM2.5 and associated heavy metals on respiratory health of children near metallurgical facilities. *Environmental Science and Pollution Research*, *23*(15). https://doi.org/10.1007/s11356-016-6734-x

Edgerton, S. A., Bian, X., Doran, J. C., Fast, J. D., Hubbe, J. M., Malone, E. L., Shaw, W. J., Whiteman, C. D., Zhong, S., Arriaga, J. L., Ortiz, E., Ruiz, M., Sosa, G., Vega, E., Limón, T., Guzman, F., Archuleta, J., Bossert, J. E., Elliot, S. M., … Petty, R. (1999). Particulate Air Pollution in Mexico City: A Collaborative Research Project. *Journal of the Air and Waste Management Association*, *49*(10). https://doi.org/10.1080/10473289.1999.10463915

Fan, J., Shang, Y., Zhang, X., Wu, X., Zhang, M., Cao, J., Luo, B., Zhang, X., Wang, S., Li, S., Liu, H., & Wu, P. (2020). Joint pollution and source apportionment of PM2.5 among three different urban environments in Sichuan Basin, China. *Science of the Total Environment*, *714*. https://doi.org/10.1016/j.scitotenv.2019.136305

Fan, X., Song, J., & Peng, P. (2016). Temporal variations of the abundance and optical properties of water soluble Humic-Like Substances (HULIS) in PM2.5 at Guangzhou, China. *Atmospheric Research*, *172–173*. https://doi.org/10.1016/j.atmosres.2015.12.024

Fan, X., Wei, S., Zhu, M., Song, J., & Peng, P. (2016). Comprehensive characterization of humic-like substances in smoke PM2.5 emitted from the combustion of biomass materials and fossil fuels. *Atmospheric Chemistry and Physics*, *16*(20). https://doi.org/10.5194/acp-16-13321-2016

Fang, B., Zeng, H., Zhang, L., Wang, H., Liu, J., Hao, K., Zheng, G., Wang, M., Wang, Q., & Yang, W. (2021). Toxic metals in outdoor/indoor airborne PM2.5 in port city of Northern, China: Characteristics, sources, and personal exposure risk assessment. *Environmental Pollution*, *279*. https://doi.org/10.1016/j.envpol.2021.116937

Feld-Cook, E. E., Bovenkamp-Langlois, L., & Lomnicki, S. M. (2017). Effect of Particulate Matter Mineral Composition on Environmentally Persistent Free Radical (EPFR) Formation. *Environmental Science and Technology*, *51*(18). https://doi.org/10.1021/acs.est.7b01521

Feng, H., Ye, X., Liu, Y., Wang, Z., Gao, T., Cheng, A., Wang, X., & Chen, J. (2020). Simultaneous determination of nine atmospheric amines and six inorganic ions by non-suppressed ion chromatography using acetonitrile and 18-crown-6 as eluent additive. *Journal of Chromatography A*, *1624*. https://doi.org/10.1016/j.chroma.2020.461234

Feng, X., Shao, L., Xi, C., Jones, T., Zhang, D., & BéruBé, K. (2020). Particle-induced oxidative damage by indoor size-segregated particulate matter from coal-burning homes in the Xuanwei lung cancer epidemic area, Yunnan Province, China. *Chemosphere*, *256*. https://doi.org/10.1016/j.chemosphere.2020.127058

Finkelman, R. B., & Tian, L. (2018). The health impacts of coal use in China. In *International Geology Review* (Vol. 60, Issues 5–6). https://doi.org/10.1080/00206814.2017.1335624

Fomba, K. W., van Pinxteren, D., Müller, K., Spindler, G., & Herrmann, H. (2018). Assessment of trace metal levels in size-resolved particulate matter in the area of Leipzig. *Atmospheric Environment*, *176*. https://doi.org/10.1016/j.atmosenv.2017.12.024

Gasparini, M., Angelone, B., & Ferretti, E. (2020). Glyphosate and other highly polar pesticides in fruit, vegetables and honey using ion chromatography coupled with high resolution mass spectrometry: Method validation and its applicability in an official laboratory. *Journal of Mass Spectrometry*, *55*(11). https://doi.org/10.1002/jms.4624

Gehling, W., & Dellinger, B. (2013). Environmentally persistent free radicals and their lifetimes in PM 2.5. *Environmental Science and Technology*, *47*(15). https://doi.org/10.1021/es401767m

Gehling, W., Khachatryan, L., & Dellinger, B. (2014). Hydroxyl radical generation from environmentally persistent free radicals (EPFRs) in PM2.5. *Environmental Science and Technology*, *48*(8). https://doi.org/10.1021/es401770y

Georgakakou, S., Gourgoulianis, K., Daniil, Z., & Bontozoglou, V. (2016). Prediction of particle deposition in the lungs based on simple modeling of alveolar mixing. *Respiratory Physiology and Neurobiology*, *225*. https://doi.org/10.1016/j.resp.2015.12.009

Gharaibeh, A. A., El-Rjoob, A. W. O., & Harb, M. K. (2010). Determination of selected heavy metals in air samples from the northern part of Jordan. *Environmental Monitoring and Assessment*, *160*(1–4). https://doi.org/10.1007/s10661-008-0706-7

Ghio, A. J., Stonehuerner, J., Dailey, L. A., & Carter, J. D. (1999). Metals associated with both the water-soluble and insoluble fractions of an ambient air pollution particle catalyze an oxidative stress. *Inhalation Toxicology*, *11*(1). https://doi.org/10.1080/089583799197258

Gou, H., Lu, J., Li, S., Tong, Y., Xie, C., & Zheng, X. (2016). Assessment of microbial communities in PM1 and PM10 of Urumqi during winter. *Environmental Pollution*, *214*. https://doi.org/10.1016/j.envpol.2016.03.073

Grevatt, P. C. (1998). Toxicological Review Of Trivalent Chromium. In *Toxicological Review Of Trivalent Chromium (CAS No. 16065-83-1) - In Support of Summary Information on the Integrated Risk Information System (IRIS)*.

Guenther, A. B., Jiang, X., Heald, C. L., Sakulyanontvittaya, T., Duhl, T., Emmons, L. K., & Wang, X. (2012). The model of emissions of gases and aerosols from nature version 2.1 (MEGAN2.1): An extended and updated framework for modeling biogenic emissions. *Geoscientific Model Development*, *5*(6). https://doi.org/10.5194/gmd-5-1471-2012

Guo, X., Zhang, N., Hu, X., Huang, Y., Ding, Z., Chen, Y., & Lian, H. zhen. (2020). Characteristics and potential inhalation exposure risks of PM2.5–bound environmental persistent free radicals in Nanjing, a mega–city in China. *Atmospheric Environment*, *224*.

https://doi.org/10.1016/j.atmosenv.2020.117355

Hao, Y., Meng, X., Yu, X., Lei, M., Li, W., Yang, W., Shi, F., & Xie, S. (2020). Quantification of primary and secondary sources to PM2.5 using an improved source regional apportionment method in an industrial city, China. *Science of the Total Environment, 706*. https://doi.org/10.1016/j.scitotenv.2019.135715

He, H., Wang, Y., Ma, Q., Ma, J., Chu, B., Ji, D., Tang, G., Liu, C., Zhang, H., & Hao, J. (2014). Erratum: Mineral dust and NOx promote the conversion of SO2 to sulfate in heavy pollution days (Scientific Reports (2014) 4 (4172) DOI: 10.1038/srep04172). In *Scientific Reports* (Vol. 4). https://doi.org/10.1038/srep06092

Henschel, S., Atkinson, R., Zeka, A., Tertre, A., Analitis, A., Katsouyanni, K., Chanel, O., Pascal, M., Forsberg, B., Medina, S., & Goodman, P. G. (2012). Air pollution interventions and their impact on public health. In *International Journal of Public Health* (Vol. 57, Issue 5). https://doi.org/10.1007/s00038-012-0369-6

Hirner, A. V. (2006). Speciation of alkylated metals and metalloids in the environment. In *Analytical and Bioanalytical Chemistry* (Vol. 385, Issue 3). https://doi.org/10.1007/s00216-006-0368-7

Hofmann, J. N., Liao, L. M., Strickland, P. T., Shu, X. O., Yang, G., Ji, B. T., Li, H. L., Rothman, N., Kamangar, F., Gao, Y. T., Zheng, W., & Chow, W. H. (2013). Polycyclic aromatic hydrocarbons: Determinants of urinary 1-hydroxypyrene glucuronide concentration and risk of colorectal cancer in the Shanghai Women's Health Study. *BMC Cancer*, *13*. https://doi.org/10.1186/1471-2407-13-282

Hosgood, H. D., Sapkota, A. R., Rothman, N., Rohan, T., Hu, W., Xu, J., Vermeulen, R., He, X., White, J. R., Wu, G., Wei, F., Mongodin, E. F., & Lan, Q. (2014). The potential role of lung microbiota in lung cancer attributed to household coal burning exposures. *Environmental and Molecular Mutagenesis*, *55*(8). https://doi.org/10.1002/em.21878

Hu, X., Zhang, Y., Ding, Z., Wang, T., Lian, H., Sun, Y., & Wu, J. (2012). Bioaccessibility and health risk of arsenic and heavy metals (Cd, Co, Cr, Cu, Ni, Pb, Zn and Mn) in TSP and PM2.5 in Nanjing, China. *Atmospheric Environment*, *57*. https://doi.org/10.1016/j.atmosenv.2012.04.056

Hu, Y., & Cheng, H. (2016). A method for apportionment of natural and anthropogenic contributions to heavy metal loadings in the surface soils across large-scale regions. *Environmental Pollution*, *214*. https://doi.org/10.1016/j.envpol.2016.04.028

Hu, Z., Shi, Y., Niu, H., & Cai, Y. (2012). Synthetic musk fragrances and heavy metals in snow samples of Beijing urban area, China. *Atmospheric Research*, *104–105*. https://doi.org/10.1016/j.atmosres.2011.09.002

Huang, J., Hu, X., Zhang, J., Li, K., Yan, Y., & Xu, X. (2006). The application of inductively coupled plasma mass spectrometry in pharmaceutical and biomedical analysis. In *Journal of Pharmaceutical and Biomedical Analysis* (Vol. 40, Issue 2). https://doi.org/10.1016/j.jpba.2005.11.014

Huang, X., Liu, Z., Zhang, J., Wen, T., Ji, D., & Wang, Y. (2016). Seasonal variation and secondary formation of size-segregated aerosol water-soluble inorganic ions during pollution episodes in Beijing. *Atmospheric Research*, *168*. https://doi.org/10.1016/j.atmosres.2015.08.021

Huang, Y., Guo, X., Ding, Z., Chen, Y., & Hu, X. (2020). Environmentally persistent free radicals in biochar derived from Laminaria japonica grown in different habitats. *Journal of Analytical and Applied Pyrolysis*, *151*. https://doi.org/10.1016/j.jaap.2020.104941

Huo, Y., Wang, Y., Qi, W., Jiang, M., & Li, M. (2021). Comprehensive characterizations of HULIS in fresh and secondary emissions of crop straw burning. *Atmospheric Environment*, *248*. https://doi.org/10.1016/j.atmosenv.2021.118220

Jenke, D. (2011). Application of Ion chromatography in pharmaceutical and drug analysis. *Journal of Chromatographic Science*, *49*(7). https://doi.org/10.1093/chrsci/49.7.524

Ji, W., Wang, Y., & Zhuang, D. (2019). Spatial distribution differences in PM2.5 concentration between heating and non-heating seasons in Beijing, China. *Environmental Pollution*, *248*. https://doi.org/10.1016/j.envpol.2019.01.002

Johnston, F. H., Borchers-Arriagada, N., Morgan, G. G., Jalaludin, B., Palmer, A. J., Williamson, G. J., & Bowman, D. M. J. S. (2021). Unprecedented health costs of smoke-related PM2.5 from the 2019–20 Australian megafires. *Nature Sustainability*, *4*(1). https://doi.org/10.1038/s41893-020-00610-5

Kelley, M. A., Hebert, V. Y., Thibeaux, T. M., Orchard, M. A., Hasan, F., Cormier, S. A., Thevenot, P. T., Lomnicki, S. M., Varner, K. J., Dellinger, B., Latimer, B. M., & Dugas, T. R. (2013). Model combustion-generated particulate matter containing persistent free radicals redox cycle to produce reactive oxygen species. *Chemical Research in Toxicology*, *26*(12). https://doi.org/10.1021/tx400227s

Kim, C., Chapman, R. S., Hu, W., He, X., Hosgood, H. D., Liu, L. Z., Lai, H., Chen, W., Silverman, D. T., Vermeulen, R., Tian, L., Bassig, B., Shen, M., Zhang, Y., Ma, S., Rothman, N., & Lan, Q. (2014). Smoky coal, tobacco smoking, and lung cancer risk in Xuanwei, China. *Lung Cancer*, *84*(1). https://doi.org/10.1016/j.lungcan.2014.01.004

Knaapen, A. M., Shi, T., Borm, P. J. A., & Schins, R. P. F. (2002). Soluble metals as well as the insoluble particle fraction are involved in cellular DNA damage induced by particulate matter. *Molecular and Cellular Biochemistry*, *234–235*. https://doi.org/10.1023/A:1015970023889

Kong, S. F., Li, L., Li, X. X., Yin, Y., Chen, K., Liu, D. T., Yuan, L., Zhang, Y. J., Shan, Y. P., & Ji, Y. Q. (2015). The impacts of firework burning at the Chinese Spring Festival on air quality: Insights of tracers, source evolution and aging processes. *Atmospheric Chemistry and Physics*, *15*(4). https://doi.org/10.5194/acp-15-2167-2015

Kong, S., Wen, B., Chen, K., Yin, Y., Li, L., Li, Q., Yuan, L., Li, X., & Sun, X. (2014). Ion chemistry for atmospheric size-segregated aerosol and depositions at an offshore site of Yangtze River Delta region, China. *Atmospheric Research*, *147–148*. https://doi.org/10.1016/j.atmosres.2014.05.018

Kristensen, T. B., Prisle, N. L., & Bilde, M. (2014). Cloud droplet activation of mixed model HULIS and NaCl particles: Experimental results and κ-Köhler theory. *Atmospheric Research*, *137*. https://doi.org/10.1016/j.atmosres.2013.09.017

Kuang, B. Y., Lin, P., Huang, X. H. H., & Yu, J. Z. (2015). Sources of humic-like substances in the Pearl River Delta, China: Positive matrix factorization analysis of PM2.5 major components and source markers. *Atmospheric Chemistry and Physics*, *15*(4). https://doi.org/10.5194/acp-15-1995-

2015

Kulhánová, I., Forman, D., Vignat, J., Espina, C., Brenner, H., Storm, H. H., Bauld, L., & Soerjomataram, I. (2020). Tobacco-related cancers in Europe: The scale of the epidemic in 2018. *European Journal of Cancer*, *139*. https://doi.org/10.1016/j.ejca.2020.07.024

Large, D. J., Kelly, S., Spiro, B., Tian, L., Shao, L., Finkelman, R., Zhang, M., Somerfield, C., Plint, S., Yasmin, A. L. I., & Zhou, Y. (2009). Silica - Volatile interaction and the geological cause of the Xuan Wei lung cancer epidemic. *Environmental Science and Technology*, *43*(23). https://doi.org/10.1021/es902033j

Lelieveld, J., Evans, J. S., Fnais, M., Giannadaki, D., & Pozzer, A. (2015). The contribution of outdoor air pollution sources to premature mortality on a global scale. *Nature*, *525*(7569). https://doi.org/10.1038/nature15371

Li, C., Ma, Z., Chen, J., Wang, X., Ye, X., Wang, L., Yang, X., Kan, H., Donaldson, D. J., & Mellouki, A. (2015). Evolution of biomass burning smoke particles in the dark. *Atmospheric Environment*, *120*. https://doi.org/10.1016/j.atmosenv.2015.09.003

Li, G., Yang, J., Zhao, G., Shen, Z., Yang, K., Tian, L., Zhou, Q., Chen, Y., & Huang, Y. (2021). Dysregulation of ferroptosis may involve in the development of non-small-cell lung cancer in Xuanwei area. *Journal of Cellular and Molecular Medicine*, *25*(6). https://doi.org/10.1111/jcmm.16318

Li, Jia, Pósfai, M., Hobbs, P. V., & Buseck, P. R. (2003). Individual aerosol particles from biomass burning in southern Africa: 2. Compositions and aging of inorganic particles. *Journal of Geophysical Research: Atmospheres*, *108*(13). https://doi.org/10.1029/2002jd002310

Li, Jingyi, Li, J., Zhang, H., Ying, Q., Wu, Z., Wu, Z., Zhang, Y., Zhang, Y., Wang, X., Wang, X., Wang, X., Li, X., Sun, Y., Hu, M., Hu, M., Zhang, Y., Zhang, Y., Hu, J., & Hu, J. (2020). Impacts of water partitioning and polarity of organic compounds on secondary organic aerosol over eastern China. *Atmospheric Chemistry and Physics*, *20*(12). https://doi.org/10.5194/acp-20-7291-2020

Li, Jinhui, Guo, W., Ran, J., Tang, R., Lin, H., Chen, X., Ning, B., Li, J., Zhou, Y., Chen, L. C., Tian, L., & Huang, Y. (2019). Five-year lung cancer mortality risk analysis and topography in Xuan Wei: A spatiotemporal correlation analysis. *BMC Public Health*, *19*(1). https://doi.org/10.1186/s12889-019-6490-1

Li, Jinhui, Ran, J., Chen, L. chi, Costa, M., Huang, Y., Chen, X., & Tian, L. (2019). Bituminous coal combustion and Xuan Wei Lung cancer: a review of the epidemiology, intervention, carcinogens, and carcinogenesis. In *Archives of Toxicology* (Vol. 93, Issue 3). https://doi.org/10.1007/s00204-019-02392-y

Li, M., Fan, X., Zhu, M., Zou, C., Song, J., Wei, S., Jia, W., & Peng, P. (2019). Abundance and Light Absorption Properties of Brown Carbon Emitted from Residential Coal Combustion in China. *Environmental Science and Technology*, *53*(2). https://doi.org/10.1021/acs.est.8b05630

Li, R., Liu, Y., Wang, T., Tang, J., Xie, L., Yao, Z., Li, K., Liao, Y., Zhou, L., Geng, Z., Huang, Z., Yang, Z., & Han, L. (2019). The characteristics of lung cancer in Xuanwei County: A review of differentially expressed genes and noncoding RNAs on cell proliferation and migration. In *Biomedicine and Pharmacotherapy* (Vol. 119). https://doi.org/10.1016/j.biopha.2019.109312

Li, Xing, Yan, C., Wang, C., Ma, J., Li, W., Liu, J., & Liu, Y. (2022). PM2.5-bound elements in Hebei Province, China: Pollution levels, source apportionment and health risks. *Science of the Total Environment*, *806*. https://doi.org/10.1016/j.scitotenv.2021.150440

Li, Xinghua, Han, J., Hopke, P. K., Hu, J., Shu, Q., Chang, Q., & Ying, Q. (2019). Quantifying primary and secondary humic-like substances in urban aerosol based on emission source characterization and a source-oriented air quality model. *Atmospheric Chemistry and Physics*, *19*(4). https://doi.org/10.5194/acp-19-2327-2019

Li, Xinghua, He, K., Li, C., Yang, F., Zhao, Q., Ma, Y., Cheng, Y., Ouyang, W., & Chen, G. (2013). PM2.5 mass, chemical composition, and light extinction before and during the 2008 Beijing Olympics. *Journal of Geophysical Research Atmospheres*, *118*(21). https://doi.org/10.1002/2013JD020106

Li, Xingru, Wang, L., Ji, D., Wen, T., Pan, Y., Sun, Y., & Wang, Y. (2013). Characterization of the size-segregated water-soluble inorganic ions in the Jing-Jin-Ji urban agglomeration: Spatial/temporal variability, size distribution and sources. *Atmospheric Environment*, *77*. https://doi.org/10.1016/j.atmosenv.2013.03.042

Li, Y. R., Feng, L. T., Chen, B. Y., Kim, H., Yi, S. M., Guo, Y. L., & Wu, C. F. (2016). Association of urban particle numbers and sources with lung function among children with asthma or allergies. *Science of the Total Environment*, *542*. https://doi.org/10.1016/j.scitotenv.2015.10.098

Li, Y., Zhang, Z., Liu, H., Zhou, H., Fan, Z., Lin, M., Wu, D., & Xia, B. (2016). Characteristics, sources and health risk assessment of toxic heavy metals in PM2.5 at a megacity of southwest China. *Environmental Geochemistry and Health*, *38*(2). https://doi.org/10.1007/s10653-015-9722-z

Lin, H., Ning, B., Li, J., Zhao, G., Huang, Y., & Tian, L. (2015). Temporal trend of mortality from major cancers in Xuanwei, China. *Frontiers of Medicine*, *9*(4). https://doi.org/10.1007/s11684-015-0413-z

Lin, M., & Yu, J. Z. (2021). Assessment of oxidative potential by hydrophilic and hydrophobic fractions of water-soluble PM2.5 and their mixture effects. *Environmental Pollution*, *275*. https://doi.org/10.1016/j.envpol.2021.116616

Lin, P., Huang, X. F., He, L. Y., & Zhen Yu, J. (2010). Abundance and size distribution of HULIS in ambient aerosols at a rural site in South China. *Journal of Aerosol Science*, *41*(1). https://doi.org/10.1016/j.jaerosci.2009.09.001

Lin, P., & Yu, J. Z. (2011). Generation of reactive oxygen species mediated by Humic-like substances in atmospheric aerosols. *Environmental Science and Technology*, *45*(24). https://doi.org/10.1021/es2028229

Lin, Y. C., Hsu, S. C., Chou, C. C. K., Zhang, R., Wu, Y., Kao, S. J., Luo, L., Huang, C. H., Lin, S. H., & Huang, Y. T. (2016). Wintertime haze deterioration in Beijing by industrial pollution deduced from trace metal fingerprints and enhanced health risk by heavy metals. *Environmental Pollution*, *208*. https://doi.org/10.1016/j.envpol.2015.07.044

Lin, Y. C., Zhang, Y. L., Song, W., Yang, X., & Fan, M. Y. (2020). Specific sources of health risks caused by size-resolved PM-bound metals in a typical coal-burning city of northern China during the winter haze event. *Science of the Total Environment*, *734*.

https://doi.org/10.1016/j.scitotenv.2020.138651

Liu, Jianwei, Chen, Y., Cao, H., & Zhang, A. (2019). Burden of typical diseases attributed to the sources of PM2.5-bound toxic metals in Beijing: An integrated approach to source apportionment and QALYs. *Environment International*, *131*. https://doi.org/10.1016/j.envint.2019.105041

Liu, Jianwei, Chen, Y., Chao, S., Cao, H., Zhang, A., & Yang, Y. (2018). Emission control priority of PM2.5-bound heavy metals in different seasons: A comprehensive analysis from health risk perspective. *Science of the Total Environment*, *644*. https://doi.org/10.1016/j.scitotenv.2018.06.226

Liu, Jiaxun, Jiang, X., Shen, J., & Zhang, H. (2015). Influences of particle size, ultraviolet irradiation and pyrolysis temperature on stable free radicals in coal. *Powder Technology*, *272*. https://doi.org/10.1016/j.powtec.2014.11.017

Liu, X., Wang, Y., Cong, H., Shen, Y., & Yu, B. (2021). A review of the design of packing materials for ion chromatography. In *Journal of Chromatography A* (Vol. 1653). https://doi.org/10.1016/j.chroma.2021.462313

Liu, Z., Hu, B., Ji, D., Cheng, M., Gao, W., Shi, S., Xie, Y., Yang, S., Gao, M., Fu, H., Chen, J., & Wang, Y. (2019). Characteristics of fine particle explosive growth events in Beijing, China: Seasonal variation, chemical evolution pattern and formation mechanism. *Science of the Total Environment*, *687*. https://doi.org/10.1016/j.scitotenv.2019.06.068

Lu, S., Hao, X., Liu, D., Wang, Q., Zhang, W., Liu, P., Zhang, R., Yu, S., Pan, R., Wu, M., Yonemochi, S., & Wang, Q. (2016). Mineralogical characterization of ambient fine/ultrafine particles emitted from Xuanwei C1 coal combustion. *Atmospheric Research*, *169*. https://doi.org/10.1016/j.atmosres.2015.09.020

Lu, S., Tan, Z., Liu, P., Zhao, H., Liu, D., Yu, S., Cheng, P., Win, M. S., Hu, J., Tian, L., Wu, M., Yonemochi, S., & Wang, Q. (2017). Single particle aerosol mass spectrometry of coal combustion particles associated with high lung cancer rates in Xuanwei and Fuyuan, China. *Chemosphere*, *186*. https://doi.org/10.1016/j.chemosphere.2017.07.161

Lu, S., Win, M. S., Zeng, J., Yao, C., Zhao, M., Xiu, G., Lin, Y., Xie, T., Dai, Y., Rao, L., Zhang, L., Yonemochi, S., & Wang, Q. (2019). A characterization of HULIS-C and the oxidative potential of HULIS and HULIS-Fe(II) mixture in PM2.5 during hazy and non-hazy days in Shanghai. *Atmospheric Environment*, *219*. https://doi.org/10.1016/j.atmosenv.2019.117058

Lu, S., Yi, F., Hao, X., Yu, S., Ren, J., Wu, M., Jialiang, F., Yonemochi, S., & Wang, Q. (2014). Physicochemical properties and ability to generate free radicals of ambient coarse, fine, and ultrafine particles in the atmosphere of Xuanwei, China, an area of high lung cancer incidence. *Atmospheric Environment*, *97*. https://doi.org/10.1016/j.atmosenv.2013.11.047

Lu, Y., Zhao, L., Lin, S., Zhang, F., & Yang, B. (2019). Fabrication of a two-membrane configured electrodialytic methanesulfonic acid generator for ion chromatography. *Analyst*, *144*(7). https://doi.org/10.1039/c9an00010k

Lubick, N. (2008). Persistent free radicals: Discovery and mechanisms for health impacts. In *Environmental Science and Technology* (Vol. 42, Issue 22). https://doi.org/10.1021/es802580c

Lui, K. H., Bandowe, B. A. M., Tian, L., Chan, C. S., Cao, J. J., Ning, Z., Lee, S. C., & Ho, K. F.

(2017). Cancer risk from polycyclic aromatic compounds in fine particulate matter generated from household coal combustion in Xuanwei, China. *Chemosphere*, *169*. https://doi.org/10.1016/j.chemosphere.2016.11.112

Lui, Ka Hei, Dai, W. T., Chan, C. S., Tian, L., Ning, B. F., Zhou, Y., Song, X., Wang, B., Li, J., Cao, J. J., Lee, S. C., & Ho, K. F. (2017). Cancer risk from gaseous carbonyl compounds in indoor environment generated from household coal combustion in Xuanwei, China. *Environmental Science and Pollution Research*, *24*(21). https://doi.org/10.1007/s11356-017-9223-y

Lung cancer in radon-exposed miners and estimation of risk from indoor exposure. (1995). *Lung Cancer*, *13*(2). https://doi.org/10.1016/0169-5002(95)90522-7

Lv, D., Chen, Y., Zhu, T., Li, T., Shen, F., Li, X., & Mehmood, T. (2019). The pollution characteristics of PM10 and PM2.5 during summer and winter in Beijing, Suning and Islamabad. *Atmospheric Pollution Research*, *10*(4). https://doi.org/10.1016/j.apr.2019.01.021

Lyu, Y., Guo, H., Cheng, T., & Li, X. (2018). Particle Size Distributions of Oxidative Potential of Lung-Deposited Particles: Assessing Contributions from Quinones and Water-Soluble Metals. *Environmental Science and Technology*, *52*(11). https://doi.org/10.1021/acs.est.7b06686

Ma, Y., Cheng, Y., Qiu, X., Cao, G., Fang, Y., Wang, J., Zhu, T., Yu, J., & Hu, D. (2018). Sources and oxidative potential of water-soluble humic-like substances (HULISWS) in fine particulate matter (PM2.5) in Beijing. *Atmospheric Chemistry and Physics*, *18*(8). https://doi.org/10.5194/acp-18-5607-2018

Malandrino, M., Casazza, M., Abollino, O., Minero, C., & Maurino, V. (2016). Size resolved metal distribution in the PM matter of the city of Turin (Italy). *Chemosphere*, *147*. https://doi.org/10.1016/j.chemosphere.2015.12.089

Manalis, N., Grivas, G., Protonotarios, V., Moutsatsou, A., Samara, C., & Chaloulakou, A. (2005). Toxic metal content of particulate matter (PM10), within the Greater Area of Athens. *Chemosphere*, *60*(4). https://doi.org/10.1016/j.chemosphere.2005.01.003

Marocco, P., Sundseth, K., Aarhaug, T., Lanzini, A., Santarelli, M., Barnett, A. O., & Thomassen, M. (2021). Online measurements of fluoride ions in proton exchange membrane water electrolysis through ion chromatography. *Journal of Power Sources*, *483*. https://doi.org/10.1016/j.jpowsour.2020.229179

McFerrin, C. A., Hall, R. W., & Dellinger, B. (2008). Ab initio study of the formation and degradation reactions of semiquinone and phenoxyl radicals. *Journal of Molecular Structure: THEOCHEM*, *848*(1–3). https://doi.org/10.1016/j.theochem.2007.09.005

Mehra, D., Geraghty, P. M., Hardigan, A. A., & Foronjy, R. (2012). A Comparison of the Inflammatory and Proteolytic Effects of Dung Biomass and Cigarette Smoke Exposure in the Lung. *PLoS ONE*, *7*(12). https://doi.org/10.1371/journal.pone.0052889

Men, C., Liu, R., Xu, F., Wang, Q., Guo, L., & Shen, Z. (2018). Pollution characteristics, risk assessment, and source apportionment of heavy metals in road dust in Beijing, China. *Science of the Total Environment*, *612*. https://doi.org/10.1016/j.scitotenv.2017.08.123

Meng, C. C., Wang, L. T., Zhang, F. F., Wei, Z., Ma, S. M., Ma, X., & Yang, J. (2016). Characteristics of concentrations and water-soluble inorganic ions in PM2.5 in Handan City, Hebei province,

China. *Atmospheric Research*, *171*. https://doi.org/10.1016/j.atmosres.2015.12.013

Meng, W., Zhong, Q., Chen, Y., Shen, H., Yun, X., Smith, K. R., Li, B., Liu, J., Wang, X., Ma, J., Cheng, H., Zeng, E. Y., Guan, D., Russell, A. G., & Tao, S. (2019). Energy and air pollution benefits of household fuel policies in northern China. *Proceedings of the National Academy of Sciences of the United States of America*, *116*(34). https://doi.org/10.1073/pnas.1904182116

Mohanraj, R., Azeez, P. A., & Priscilla, T. (2004). Heavy metals in airborne particulate matter of urban Coimbatore. *Archives of Environmental Contamination and Toxicology*, *47*(2). https://doi.org/10.1007/s00244-004-3054-9

Mölter, A., Simpson, A., Berdel, D., Brunekreef, B., Custovic, A., Cyrys, J., De Jongste, J., De Vocht, F., Fuertes, E., Gehring, U., Gruzieva, O., Heinrich, J., Hoek, G., Hoffmann, B., Klümper, C., Korek, M., Kuhlbusch, T. A. J., Lindley, S., Postma, D., … Agius, R. (2015). A multicentre study of air pollution exposure and childhood asthma prevalence: The ESCAPE project. *European Respiratory Journal*, *45*(3). https://doi.org/10.1183/09031936.00083614

Mosonik, B. C., Kibet, J. K., Ngari, S. M., & Nyamori, V. O. (2018). Environmentally persistent free radicals and particulate emissions from the thermal degradation of Croton megalocarpus biodiesel. *Environmental Science and Pollution Research*, *25*(25). https://doi.org/10.1007/s11356-018-2546-5

Mugica-Álvarez, V., Figueroa-Lara, J., Romero-Romo, M., Sepúlvea-Sánchez, J., & López-Moreno, T. (2012). Concentrations and properties of airborne particles in the Mexico City subway system. *Atmospheric Environment*, *49*. https://doi.org/10.1016/j.atmosenv.2011.11.038

Mumford, J. L., He, X. Z., Chapman, R. S., Cao, S. R., Harris, D. B., Li, X. M., Xian, Y. L., Jiang, W. Z., Xu, C. W., Chuang, J. C., Wilson, W. E., & Cooke, M. (1987). Lung cancer and indoor air pollution in Xuan Wei, China. *Science*, *235*(4785). https://doi.org/10.1126/science.3798109

National Bureau of Statistics. (2016). China Energy Statistical Yearbook 2016. In *China Statistics Press, Beijing, China*.

Neuberger, M., Schimek, M. G., Horak, F., Moshammer, H., Kundi, M., Frischer, T., Gomiscek, B., Puxbaum, H., & Hauck, H. (2004). Acute effects of particulate matter on respiratory diseases, symptoms and functions: Epidemiological results of the Austrian Project on Health Effects of Particulate Matter (AUPHEP). *Atmospheric Environment*, *38*(24). https://doi.org/10.1016/j.atmosenv.2003.12.044

Ni, X., Pan, Y., Shao, P., Tian, S., Zong, Z., Gu, M., Liu, B., Liu, J., Cao, J., Sun, Q., Wang, Y., & Jiang, C. (2021). Size distribution and formation processes of aerosol water-soluble organic carbon during winter and summer in urban Beijing. *Atmospheric Environment*, *244*. https://doi.org/10.1016/j.atmosenv.2020.117983

Nie, D., Chen, M., Wu, Y., Ge, X., Hu, J., Zhang, K., & Ge, P. (2018). Characterization of fine particulate matter and associated health burden in Nanjing. *International Journal of Environmental Research and Public Health*, *15*(4). https://doi.org/10.3390/ijerph15040602

Oberdörster, G. (2000). Pulmonary effects of inhaled ultrafine particles. In *International Archives of Occupational and Environmental Health* (Vol. 74, Issue 1). https://doi.org/10.1007/s004200000185

Olsen, Y., Karottki, D. G., Jensen, D. M., Bekö, G., Kjeldsen, B. U., Clausen, G., Hersoug, L. G., Holst, G. J., Wierzbicka, A., Sigsgaard, T., Linneberg, A., Møller, P., & Loft, S. (2014). Vascular and lung function related to ultrafine and fine particles exposure assessed by personal and indoor monitoring: A cross-sectional study. *Environmental Health: A Global Access Science Source*, *13*(1). https://doi.org/10.1186/1476-069X-13-112

Onder, S., & Dursun, S. (2006). Air borne heavy metal pollution of Cedrus libani (A. Rich.) in the city centre of Konya (Turkey). *Atmospheric Environment*, *40*(6). https://doi.org/10.1016/j.atmosenv.2005.11.006

Oros, D. R., & Simoneit, B. R. T. (2000). Identification and emission rates of molecular tracers in coal smoke particulate matter. *Fuel*, *79*(5). https://doi.org/10.1016/S0016-2361(99)00153-2

Park, S. S., & Yu, J. (2016). Chemical and light absorption properties of humic-like substances from biomass burning emissions under controlled combustion experiments. *Atmospheric Environment*, *136*. https://doi.org/10.1016/j.atmosenv.2016.04.022

Parsons, P. J., & Barbosa, F. (2007). Atomic spectrometry and trends in clinical laboratory medicine. In *Spectrochimica Acta - Part B Atomic Spectroscopy* (Vol. 62, Issue 9). https://doi.org/10.1016/j.sab.2007.03.007

Pathak, R. K., Wu, W. S., & Wang, T. (2009). Summertime PM2.5 ionic species in four major cities of China: Nitrate formation in an ammonia-deficient atmosphere. *Atmospheric Chemistry and Physics*, *9*(5). https://doi.org/10.5194/acp-9-1711-2009

Pope, C. A., & Dockery, D. W. (2006). Health effects of fine particulate air pollution: Lines that connect. *Journal of the Air and Waste Management Association*, *56*(6). https://doi.org/10.1080/10473289.2006.10464485

Pöschl, U., & Shiraiwa, M. (2015). Multiphase Chemistry at the Atmosphere-Biosphere Interface Influencing Climate and Public Health in the Anthropocene. In *Chemical Reviews* (Vol. 115, Issue 10). https://doi.org/10.1021/cr500487s

Qian, R., Zhang, S., Peng, C., Zhang, L., Yang, F., Tian, M., Huang, R., Wang, Q., Chen, Q., Yao, X., & Chen, Y. (2020). Characteristics and potential exposure risks of environmentally persistent free radicals in PM2.5 in the three gorges reservoir area, Southwestern China. *Chemosphere*, *252*. https://doi.org/10.1016/j.chemosphere.2020.126425

Qiao, B., Chen, Y., Tian, M., Wang, H., Yang, F., Shi, G., Zhang, L., Peng, C., Luo, Q., & Ding, S. (2019). Characterization of water soluble inorganic ions and their evolution processes during PM2.5 pollution episodes in a small city in southwest China. *Science of the Total Environment*, *650*. https://doi.org/10.1016/j.scitotenv.2018.09.376

Qiu, H., Zhu, X., Wang, L., Pan, J., Pu, X., Zeng, X., Zhang, L., Peng, Z., & Zhou, L. (2019). Attributable risk of hospital admissions for overall and specific mental disorders due to particulate matter pollution: A time-series study in Chengdu, China. *Environmental Research*, *170*. https://doi.org/10.1016/j.envres.2018.12.019

Qiu, P., Huang, C., Dong, G., Chen, F., Zhao, F., Yu, Y., Liu, X., Li, Z., & Wang, Y. (2021). Plasmonic gold nanocrystals simulated efficient photocatalytic nitrogen fixation over Mo doped W18O49nanowires. *Journal of Materials Chemistry A*, *9*(25). https://doi.org/10.1039/d1ta03339e

Querol, X., Viana, M., Alastuey, A., Amato, F., Moreno, T., Castillo, S., Pey, J., de la Rosa, J., Sánchez de la Campa, A., Artíñano, B., Salvador, P., García Dos Santos, S., Fernández-Patier, R., Moreno-Grau, S., Negral, L., Minguillón, M. C., Monfort, E., Gil, J. I., Inza, A., … Zabalza, J. (2007). Source origin of trace elements in PM from regional background, urban and industrial sites of Spain. *Atmospheric Environment*, *41*(34). https://doi.org/10.1016/j.atmosenv.2007.05.022

Radulescu, C., Iordache, S., Dunea, D., Stihi, C., & Dulama, I. D. (2015). Risks assessment of heavy metals on public health associated with atmospheric exposure to PM2.5 in urban area. *Romanian Journal of Physics*, *60*(7–8).

Rohra, H., Tiwari, R., Khandelwal, N., & Taneja, A. (2018). Mass distribution and health risk assessment of size segregated particulate in varied indoor microenvironments of Agra, India - A case study. *Urban Climate*, *24*. https://doi.org/10.1016/j.uclim.2018.01.002

Rovelli, S., Cattaneo, A., Nischkauer, W., Borghi, F., Spinazzè, A., Keller, M., Campagnolo, D., Limbeck, A., & Cavallo, D. M. (2020). Toxic trace metals in size-segregated fine particulate matter: Mass concentration, respiratory deposition, and risk assessment. *Environmental Pollution*, *266*. https://doi.org/10.1016/j.envpol.2020.115242

Ruan, X., Sun, Y., Du, W., Tang, Y., Liu, Q., Zhang, Z., Doherty, W., Frost, R. L., Qian, G., & Tsang, D. C. W. (2019). Formation, characteristics, and applications of environmentally persistent free radicals in biochars: A review. In *Bioresource Technology* (Vol. 281). https://doi.org/10.1016/j.biortech.2019.02.105

Rudnick, R. L., & Gao, S. (2013). Composition of the Continental Crust. In *Treatise on Geochemistry: Second Edition* (Vol. 4). https://doi.org/10.1016/B978-0-08-095975-7.00301-6

Runberg, H. L., Mitchell, D. G., Eaton, S. S., Eaton, G. R., & Majestic, B. J. (2020). Stability of environmentally persistent free radicals (EPFR) in atmospheric particulate matter and combustion particles. *Atmospheric Environment*, *240*. https://doi.org/10.1016/j.atmosenv.2020.117809

Samet, J. M., Avila-Tang, E., Boffetta, P., Hannan, L. M., Olivo-Marston, S., Thun, M. J., & Rudin, C. M. (2009). Lung cancer in never smokers: Clinical epidemiology and environmental risk factors. In *Clinical Cancer Research* (Vol. 15, Issue 18). https://doi.org/10.1158/1078-0432.CCR-09-0376

Santos, P. S. M., Santos, E. B. H., & Duarte, A. C. (2012). First spectroscopic study on the structural features of dissolved organic matter isolated from rainwater in different seasons. *Science of the Total Environment*, *426*. https://doi.org/10.1016/j.scitotenv.2012.03.023

Sen, I. S., Bizimis, M., Tripathi, S. N., & Paul, D. (2016). Lead isotopic fingerprinting of aerosols to characterize the sources of atmospheric lead in an industrial city of India. *Atmospheric Environment*, *129*. https://doi.org/10.1016/j.atmosenv.2016.01.005

Seow, W. J., Hu, W., Vermeulen, R., Dean Hosgood, H., Downward, G. S., Chapman, R. S., He, X., Bassig, B. A., Kim, C., Wen, C., Rothman, N., & Lan, Q. (2014). Household air pollution and lung cancer in China: A review of studies in Xuanwei. In *Chinese Journal of Cancer* (Vol. 33, Issue 10). https://doi.org/10.5732/cjc.014.10132

Shaltout, A. A., Boman, J., Shehadeh, Z. F., Al-Malawi, D. allah R., Hemeda, O. M., & Morsy, M. M. (2015). Spectroscopic investigation of PM2.5 collected at industrial, residential and traffic sites

in Taif, Saudi Arabia. *Journal of Aerosol Science*, *79*. https://doi.org/10.1016/j.jaerosci.2014.09.004

Shao, P., Tian, H., Sun, Y., Liu, H., Wu, B., Liu, S., Liu, X., Wu, Y., Liang, W., Wang, Y., Gao, J., Xue, Y., Bai, X., Liu, W., Lin, S., & Hu, G. (2018). Characterizing remarkable changes of severe haze events and chemical compositions in multi-size airborne particles (PM1, PM2.5 and PM10) from January 2013 to 2016–2017 winter in Beijing, China. *Atmospheric Environment*, *189*. https://doi.org/10.1016/j.atmosenv.2018.06.038

Shen, G., Tao, S., Chen, Y., Zhang, Y., Wei, S., Xue, M., Wang, B., Wang, R., Lu, Y., Li, W., Shen, H., Huang, Y., & Chen, H. (2013). Emission characteristics for polycyclic aromatic hydrocarbons from solid fuels burned in domestic stoves in rural China. *Environmental Science and Technology*, *47*(24). https://doi.org/10.1021/es403110b

Shen, G., Wang, W., Yang, Y., Zhu, C., Min, Y., Xue, M., Ding, J., Li, W., Wang, B., Shen, H., Wang, R., Wang, X., & Tao, S. (2010). Emission factors and particulate matter size distribution of polycyclic aromatic hydrocarbons from residential coal combustions in rural Northern China. *Atmospheric Environment*, *44*(39). https://doi.org/10.1016/j.atmosenv.2010.08.042

Shen, M., Tu, M., Zhang, W., Zou, J., Zhang, M., Cao, Z., & Zou, B. (2020). Ion chromatography as candidate reference method for the determination of chloride in human serum. *Journal of Clinical Laboratory Analysis*, *34*(8). https://doi.org/10.1002/jcla.23296

Sheng, L., Tu, J. W., Tian, J. H., Chen, H. J., Pan, C. L., & Zhou, R. Z. (2018). A meta-analysis of the relationship between environmental tobacco smoke and lung cancer risk of nonsmoker in China. In *Medicine (United States)* (Vol. 97, Issue 28). https://doi.org/10.1097/MD.0000000000011389

Shi, G., Chen, Z., Bi, C., Wang, L., Teng, J., Li, Y., & Xu, S. (2011). A comparative study of health risk of potentially toxic metals in urban and suburban road dust in the most populated city of China. *Atmospheric Environment*, *45*(3). https://doi.org/10.1016/j.atmosenv.2010.08.039

Shi, T., Knaapen, A. M., Begerow, J., Birmili, W., Borm, P. J. A., & Schins, R. P. F. (2003). Temporal variation of hydroxyl radical generation and 8-hydroxy-2′-deoxyguanosine formation by coarse and fine particulate matter. *Occupational and Environmental Medicine*, *60*(5). https://doi.org/10.1136/oem.60.5.315

Shi, Tingming, Schins, R. P. F., Knaapen, A. M., Kuhlbusch, T., Pitz, M., Heinrich, J., & Borm, P. J. A. (2003). Hydroxyl radical generation by electron paramagnetic resonance as a new method to monitor ambient particulate matter composition. *Journal of Environmental Monitoring*, *5*(4). https://doi.org/10.1039/b303928p

Silverman, D. T., Samanic, C. M., Lubin, J. H., Blair, A. E., Stewart, P. A., Vermeulen, R., Coble, J. B., Rothman, N., Schleiff, P. L., Travis, W. D., Ziegler, R. G., Wacholder, S., & Attfield, M. D. (2012). The diesel exhaust in miners study: A nested case-control study of lung cancer and diesel exhaust. *Journal of the National Cancer Institute*, *104*(11). https://doi.org/10.1093/jnci/djs034

Singh, N., Banerjee, T., Murari, V., Deboudt, K., Khan, M. F., Singh, R. S., & Latif, M. T. (2021). Insights into size-segregated particulate chemistry and sources in urban environment over central Indo-Gangetic Plain. *Chemosphere*, *263*. https://doi.org/10.1016/j.chemosphere.2020.128030

Smith, S., Cheng, Y. S., & Yeh, H. C. (2001). Deposition of ultrafine particles in human tracheobronchial airways of adults and children. *Aerosol Science and Technology*, *35*(3).

https://doi.org/10.1080/02786820152546743

Song, J., He, L., Peng, P., Zhao, J., & Ma, S. (2012). Chemical and isotopic composition of humic-like substances (HULIS) in ambient aerosols in Guangzhou, South China. *Aerosol Science and Technology*, *46*(5). https://doi.org/10.1080/02786826.2011.645956

Spengler, J. D., Brauer, M., & Koutrakis, P. (1990). Acid air and health. *Environmental Science and Technology*, *24*(7). https://doi.org/10.1021/es00077a002

Squizzato, S., Masiol, M., Brunelli, A., Pistollato, S., Tarabotti, E., Rampazzo, G., & Pavoni, B. (2013). Factors determining the formation of secondary inorganic aerosol: A case study in the Po Valley (Italy). *Atmospheric Chemistry and Physics*, *13*(4). https://doi.org/10.5194/acp-13-1927-2013

Srivastava, D., Tomaz, S., Favez, O., Lanzafame, G. M., Golly, B., Besombes, J. L., Alleman, L. Y., Jaffrezo, J. L., Jacob, V., Perraudin, E., Villenave, E., & Albinet, A. (2018). Speciation of organic fraction does matter for source apportionment. Part 1: A one-year campaign in Grenoble (France). *Science of the Total Environment*, *624*. https://doi.org/10.1016/j.scitotenv.2017.12.135

Stanaway, J. D., Afshin, A., Gakidou, E., Lim, S. S., Abate, D., Abate, K. H., Abbafati, C., Abbasi, N., Abbastabar, H., Abd-Allah, F., Abdela, J., Abdelalim, A., Abdollahpour, I., Abdulkader, R. S., Abebe, M., Abebe, Z., Abera, S. F., Abil, O. Z., Abraha, H. N., … Murray, C. J. L. (2018). Global, regional, and national comparative risk assessment of 84 behavioural, environmental and occupational, and metabolic risks or clusters of risks for 195 countries and territories, 1990-2017: A systematic analysis for the Global Burden of Disease Study 2017. *The Lancet*, *392*(10159). https://doi.org/10.1016/S0140-6736(18)32225-6

Steinfeld, J. I. (1998). Atmospheric Chemistry and Physics: From Air Pollution to Climate Change. *Environment: Science and Policy for Sustainable Development*, *40*(7). https://doi.org/10.1080/00139157.1999.10544295

Sudheer, A. K., Rengarajan, R., Deka, D., Bhushan, R., Singh, S. K., & Aslam, M. Y. (2014). Diurnal and seasonal characteristics of aerosol ionic constituents over an urban location in Western India: Secondary aerosol formation and meteorological influence. *Aerosol and Air Quality Research*, *14*(6). https://doi.org/10.4209/aaqr.2013.09.0288

Sun, H., Li, X., Zhu, C., Huo, Y., Zhu, Z., Wei, Y., Yao, L., Xiao, H., & Chen, J. (2021). Molecular composition and optical property of humic-like substances (HULIS) in winter-time PM2.5 in the rural area of North China Plain. *Atmospheric Environment*, *252*. https://doi.org/10.1016/j.atmosenv.2021.118316

Sun, S., Schiller, J. H., & Gazdar, A. F. (2007). Lung cancer in never smokers - A different disease. In *Nature Reviews Cancer* (Vol. 7, Issue 10). https://doi.org/10.1038/nrc2190

Sun, Yele, Wang, Z., Fu, P., Jiang, Q., Yang, T., Li, J., & Ge, X. (2013). The impact of relative humidity on aerosol composition and evolution processes during wintertime in Beijing, China. *Atmospheric Environment*, *77*. https://doi.org/10.1016/j.atmosenv.2013.06.019

Sun, Yele, Zhuang, G., Zhang, W., Wang, Y., & Zhuang, Y. (2006). Characteristics and sources of lead pollution after phasing out leaded gasoline in Beijing. *Atmospheric Environment*, *40*(16). https://doi.org/10.1016/j.atmosenv.2005.12.032

Sun, Yuanyuan, Hu, X., Wu, J., Lian, H., & Chen, Y. (2014). Fractionation and health risks of atmospheric particle-bound As and heavy metals in summer and winter. *Science of the Total Environment*, *493*. https://doi.org/10.1016/j.scitotenv.2014.06.017

Taghvaee, S., Sowlat, M. H., Mousavi, A., Hassanvand, M. S., Yunesian, M., Naddafi, K., & Sioutas, C. (2018). Source apportionment of ambient PM2.5 in two locations in central Tehran using the Positive Matrix Factorization (PMF) model. *Science of the Total Environment*, *628–629*. https://doi.org/10.1016/j.scitotenv.2018.02.096

Tan, J., Xiang, P., Zhou, X., Duan, J., Ma, Y., He, K., Cheng, Y., Yu, J., & Querol, X. (2016). Chemical characterization of humic-like substances (HULIS) in PM2.5 in Lanzhou, China. *Science of the Total Environment*, *573*. https://doi.org/10.1016/j.scitotenv.2016.08.025

Tao, J., Gao, J., Zhang, L., Zhang, R., Che, H., Zhang, Z., Lin, Z., Jing, J., Cao, J., & Hsu, S. C. (2014). PM2.5 pollution in a megacity of Southwest China: Source apportionment and implication. *Atmospheric Chemistry and Physics*, *14*(16). https://doi.org/10.5194/acp-14-8679-2014

Thomas, R. (2002). Beginner's guide to ICP-MS. *Spectroscopy (Santa Monica)*, *17*(11).

Tian, H., Cheng, K., Wang, Y., Zhao, D., Lu, L., Jia, W., & Hao, J. (2012). Temporal and spatial variation characteristics of atmospheric emissions of Cd, Cr, and Pb from coal in China. *Atmospheric Environment*, *50*. https://doi.org/10.1016/j.atmosenv.2011.12.045

Tian, L., Koshland, C. P., Yano, J., Yachandra, V. K., Yu, I. T. S., Lee, S. C., & Lucas, D. (2009). Carbon-centered free radicals in participate matter emissions from wood and coal combustion. *Energy and Fuels*, *23*(5). https://doi.org/10.1021/ef8010096

Tian, L., Lucas, D., Fischer, S. L., Lee, S. C., Hammond, S. K., & Koshland, C. P. (2008). Particle and gas emissions from a simulated coal-burning household fire pit. *Environmental Science and Technology*, *42*(7). https://doi.org/10.1021/es0716610

Tian, X., Xiao, L., Shen, Y., Luo, L., Zhang, G., Zhang, Q., Li, D., Wu, J., Wu, Z., Zhang, Z., & Tian, Y. (2019). A combination of super-resolution fluorescence and magnetic resonance imaging using a Mn(ii) compound. *Inorganic Chemistry Frontiers*, *6*(10). https://doi.org/10.1039/c9qi00895k

Tiede, K., Boxall, A. B. A., Tiede, D., Tear, S. P., David, H., & Lewis, J. (2009). A robust size-characterisation methodology for studying nanoparticle behaviour in "real" environmental samples, using hydrodynamic chromatography coupled to ICP-MS. *Journal of Analytical Atomic Spectrometry*, *24*(7). https://doi.org/10.1039/b822409a

Tsai, P. J., Young, L. H., Hwang, B. F., Lin, M. Y., Chen, Y. C., & Hsu, H. T. (2020). Source and health risk apportionment for PM2.5 collected in Sha-Lu area, Taiwan. *Atmospheric Pollution Research*, *11*(5). https://doi.org/10.1016/j.apr.2020.01.013

U.S. EPA. (2015). Exposure Factors Handbook 2011 Edition (Final Report). *U.S. Environmental Protection Agency, September*.

USEPA. (1989). Risk Assessment Guidance for Superfund (RAGS): Part A. *United States Environmental Protection Agency*.

USEPA. (2004). Risk assessment guidance for superfund (RAGS). Volume I. Human health evaluation manual (HHEM). Part E. Supplemental guidance for dermal risk assessment. *Us Epa*,

1(540/R/99/005). https://doi.org/EPA/540/1-89/002

Valavanidis, A., Fiotakis, K., & Vlachogianni, T. (2008). Airborne particulate matter and human health: Toxicological assessment and importance of size and composition of particles for oxidative damage and carcinogenic mechanisms. In *Journal of Environmental Science and Health - Part C Environmental Carcinogenesis and Ecotoxicology Reviews* (Vol. 26, Issue 4). https://doi.org/10.1080/10590500802494538

Valavanidis, A., Fiotakis, K., Vlahogianni, T., Papadimitriou, V., & Pantikaki, V. (2006). Determination of selective quinones and quinoid radicals in airborne particulate matter and vehicular exhaust particles. *Environmental Chemistry*, *3*(3). https://doi.org/10.1071/EN05089

Vega, E., Ruiz, H., Escalona, S., Cervantes, A., Lopez-Veneroni, D., Gonzalez-Avalos, E., & Sanchez-Reyna, G. (2011). Chemical composition of fine particles in Mexico City during 2003-2004. *Atmospheric Pollution Research*, *2*(4). https://doi.org/10.5094/APR.2011.054

Verma, V., Fang, T., Guo, H., King, L., Bates, J. T., Peltier, R. E., Edgerton, E., Russell, A. J., & Weber, R. J. (2014). Reactive oxygen species associated with water-soluble PM_{2.5} in the southeastern United States: spatiotemporal trends and source apportionment. *Atmospheric Chemistry and Physics Discussions*, *14*(13). https://doi.org/10.5194/acpd-14-19625-2014

Vermeulen, R., Downward, G. S., Zhang, J., Hu, W., Portengen, L., Bassig, B. A., Hammond, S. K., Wong, J. Y. Y., Li, J., Reiss, B., He, J., Tian, L., Yang, K., Seow, W. J., Xu, J., Anderson, K., Ji, B. T., Silverman, D., Chanock, S., … Lan, Q. (2019). Constituents of household air pollution and risk of lung cancer among never-smoking women in Xuanwei and Fuyuan, China. *Environmental Health Perspectives*, *127*(9). https://doi.org/10.1289/EHP4913

Wang, B., Jin, L., Ren, A., Yuan, Y., Liu, J., Li, Z., Zhang, L., Yi, D., Wang, L. L., Zhang, Y., Wang, X., Tao, S., & Finnell, R. H. (2015). Levels of polycyclic aromatic hydrocarbons in maternal serum and risk of neural tube defects in offspring. *Environmental Science and Technology*, *49*(1). https://doi.org/10.1021/es503990v

Wang, C., Huang, Y., Zhang, Z., & Cai, Z. (2020). Levels, spatial distribution, and source identification of airborne environmentally persistent free radicals from tree leaves. *Environmental Pollution*, *257*. https://doi.org/10.1016/j.envpol.2019.113353

Wang, Dexiang, Hu, J., Xu, Y., Lv, D., Xie, X., Kleeman, M., Xing, J., Zhang, H., & Ying, Q. (2014). Source contributions to primary and secondary inorganic particulate matter during a severe wintertime PM2.5 pollution episode in Xi'an, China. *Atmospheric Environment*, *97*. https://doi.org/10.1016/j.atmosenv.2014.08.020

Wang, Dongbin, Pakbin, P., Shafer, M. M., Antkiewicz, D., Schauer, J. J., & Sioutas, C. (2013). Macrophage reactive oxygen species activity of water-soluble and water-insoluble fractions of ambient coarse, PM2.5 and ultrafine particulate matter (PM) in Los Angeles. *Atmospheric Environment*, *77*. https://doi.org/10.1016/j.atmosenv.2013.05.031

Wang, G., Zhang, R., Gomez, M. E., Yang, L., Zamora, M. L., Hu, M., Lin, Y., Peng, J., Guo, S., Meng, J., Li, J., Cheng, C., Hu, T., Ren, Y., Wang, Y., Gao, J., Cao, J., An, Z., Zhou, W., … Molina, M. J. (2016). Persistent sulfate formation from London Fog to Chinese haze. *Proceedings of the National Academy of Sciences of the United States of America*, *113*(48).

https://doi.org/10.1073/pnas.1616540113

Wang, N., & Yu, J. Z. (2017). Size distributions of hydrophilic and hydrophobic fractions of water-soluble organic carbon in an urban atmosphere in Hong Kong. *Atmospheric Environment*, *166*. https://doi.org/10.1016/j.atmosenv.2017.07.009

Wang, P., Pan, B., Li, H., Huang, Y., Dong, X., Ai, F., Liu, L., Wu, M., & Xing, B. (2018). The Overlooked Occurrence of Environmentally Persistent Free Radicals in an Area with Low-Rank Coal Burning, Xuanwei, China. *Environmental Science and Technology*, *52*(3). https://doi.org/10.1021/acs.est.7b05453

Wang, Q., Dong, Z., Guo, Y., Yu, F., Zhang, Z., & Zhang, R. (2020). Characterization of PM2.5-Bound Polycyclic Aromatic Hydrocarbons at Two Central China Cities: Seasonal Variation, Sources, and Health Risk Assessment. *Archives of Environmental Contamination and Toxicology*, *78*(1). https://doi.org/10.1007/s00244-019-00671-4

Wang, R., Huang, Q., Cai, J., & Wang, J. (2021). Seasonal variations of atmospheric polycyclic aromatic hydrocarbons (PAHs) surrounding Chaohu Lake, China: Source, partitioning behavior, and lung cancer risk. *Atmospheric Pollution Research*, *12*(5). https://doi.org/10.1016/j.apr.2021.101056

Wang, Shanshan, Hu, G., Yan, Y., Wang, S., Yu, R., & Cui, J. (2019). Source apportionment of metal elements in PM2.5 in a coastal city in Southeast China: Combined Pb-Sr-Nd isotopes with PMF method. *Atmospheric Environment*, *198*. https://doi.org/10.1016/j.atmosenv.2018.10.056

Wang, Shunqin, & Zhang, J. (2006). Blood lead levels in children, China. In *Environmental Research* (Vol. 101, Issue 3). https://doi.org/10.1016/j.envres.2005.11.007

Wang, Shuxiao, Wei, W., Li, D., Aunan, K., & Hao, J. (2010). Air pollutants in rural homes in Guizhou, China - Concentrations, speciation, and size distribution. *Atmospheric Environment*, *44*(36). https://doi.org/10.1016/j.atmosenv.2010.08.013

Wang, Weiqian, Zhang, W., Dong, S., Yonemachi, S., Lu, S., & Wang, Q. (2020). Characterization, pollution sources, and health risk of ionic and elemental constituents in PM2.5 of wuhan, central China. *Atmosphere*, *11*(7). https://doi.org/10.3390/ATMOS11070760

Wang, Wenhua, Shao, L., Li, J., Chang, L., Zhang, D., Zhang, C., & Jiang, J. (2019). Characteristics of individual particles emitted from an experimental burning chamber with coal from the lung cancer area of Xuanwei, China. *Aerosol and Air Quality Research*, *19*(2). https://doi.org/10.4209/aaqr.2018.05.0187

Wang, Ying, Zhuang, G., Tang, A., Yuan, H., Sun, Y., Chen, S., & Zheng, A. (2005). The ion chemistry and the source of PM2.5 aerosol in Beijing. *Atmospheric Environment*, *39*(21). https://doi.org/10.1016/j.atmosenv.2005.03.013

Wang, Yuqin, Li, S., Wang, M., Sun, H., Mu, Z., Zhang, L., Li, Y., & Chen, Q. (2019). Source apportionment of environmentally persistent free radicals (EPFRs) in PM2.5 over Xi'an, China. *Science of the Total Environment*, *689*. https://doi.org/10.1016/j.scitotenv.2019.06.424

Ward, D. J., & Ayres, J. G. (2004). Particulate air pollution and panel studies in children: a systematic review. In *Occupational and environmental medicine* (Vol. 61, Issue 4). https://doi.org/10.1136/oem.2003.007088

Wen, J., Shi, G., Tian, Y., Chen, G., Liu, J., Huang-Fu, Y., Ivey, C. E., & Feng, Y. (2018). Source contributions to water-soluble organic carbon and water-insoluble organic carbon in PM2.5 during Spring Festival, heating and non-heating seasons. *Ecotoxicology and Environmental Safety*, *164*. https://doi.org/10.1016/j.ecoenv.2018.08.002

WHO. (2017). *WHO | Air pollution and health: Summary*. Who.

Win, M. S., Tian, Z., Zhao, H., Xiao, K., Peng, J., Shang, Y., Wu, M., Xiu, G., Lu, S., Yonemochi, S., & Wang, Q. (2018). Atmospheric HULIS and its ability to mediate the reactive oxygen species (ROS): A review. In *Journal of Environmental Sciences (China)* (Vol. 71). https://doi.org/10.1016/j.jes.2017.12.004

Win, M. S., Zeng, J., Yao, C., Zhao, M., Xiu, G., Xie, T., Rao, L., Zhang, L., Lu, H., Liu, X., Wang, Q., & Lu, S. (2020). Sources of HULIS-C and its relationships with trace metals, ionic species in PM2.5 in suburban Shanghai during haze and non-haze days. *Journal of Atmospheric Chemistry*, *77*(3). https://doi.org/10.1007/s10874-020-09404-7

Wu, F., Liu, X., Wang, W., Man, Y. B., Chan, C. Y., Liu, W., Tao, S., & Wong, M. H. (2015). Characterization of particulate-bound PAHs in rural households using different types of domestic energy in Henan Province, China. *Science of the Total Environment*, *536*. https://doi.org/10.1016/j.scitotenv.2015.07.101

Wu, X., Chen, B., Wen, T., Habib, A., & Shi, G. (2020). Concentrations and chemical compositions of PM10 during hazy and non-hazy days in Beijing. *Journal of Environmental Sciences (China)*, *87*. https://doi.org/10.1016/j.jes.2019.03.021

Wu, Y., Lu, B., Zhu, X., Wang, A., Yang, M., Gu, S., Wang, X., Leng, P., Zierold, K. M., Li, X., Tang, K. K., Fang, L., Huang, R., Xu, G., & Chen, L. (2019). Seasonal variations, source apportionment, and health risk assessment of heavy metals in pm2.5 in Ningbo, China. *Aerosol and Air Quality Research*, *19*(9). https://doi.org/10.4209/aaqr.2018.12.0452

Xiang, P., Zhou, X., Duan, J., Tan, J., He, K., Yuan, C., Ma, Y., & Zhang, Y. (2017). Chemical characteristics of water-soluble organic compounds (WSOC) in PM2.5 in Beijing, China: 2011–2012. *Atmospheric Research*, *183*. https://doi.org/10.1016/j.atmosres.2016.08.020

Xiao, K., Qin, A., Wang, W., Lu, S., & Wang, Q. (2021). Study on the characteristics of size-segregated particulate water-soluble inorganic ions and potentially toxic metals during wintertime in a high population residential area in Beijing, China. *Processes*, *9*(3). https://doi.org/10.3390/pr9030552

Xiao, K., Wang, Q., Lin, Y., Wang, W., Lu, S., & Yonemochi, S. (2021). Approval research for carcinogen humic-like substances (Hulis) emitted from residential coal combustion in high lung cancer incidence areas of china. *Processes*, *9*(7). https://doi.org/10.3390/pr9071254

Xiao, Kai, et al. "Characteristics and Potential Inhalation Exposure Risks of Environmentally Persistent Free Radicals in Atmospheric Particulate Matter and Solid Fuel Combustion Particles in High Lung Cancer Incidence Area, China." Atmosphere 12.11 (2021): 1467.

Xiao, Y., Shao, Y., Yu, X., & Zhou, G. (2012). The epidemic status and risk factors of lung cancer in Xuanwei City, Yunnan Province, China. In *Frontiers of Medicine in China* (Vol. 6, Issue 4). https://doi.org/10.1007/s11684-012-0233-3

Xie, J. J., Yuan, C. G., Xie, J., Niu, X. D., & He, A. E. (2020). PM2.5-bound potentially toxic elements (PTEs) fractions, bioavailability and health risks before and after coal limiting. *Ecotoxicology and Environmental Safety*, *192*. https://doi.org/10.1016/j.ecoenv.2020.110249

Xie, Y., Liu, Z., Wen, T., Huang, X., Liu, J., Tang, G., Yang, Y., Li, X., Shen, R., Hu, B., & Wang, Y. (2019). Characteristics of chemical composition and seasonal variations of PM 2.5 in Shijiazhuang, China: Impact of primary emissions and secondary formation. *Science of the Total Environment*, *677*. https://doi.org/10.1016/j.scitotenv.2019.04.300

Xu, C., Wei, M., Chen, J., Wang, X., Zhu, C., Li, J., Zheng, L., Sui, G., Li, W., Wang, W., Zhang, Q., & Mellouki, A. (2017). Bacterial characterization in ambient submicron particles during severe haze episodes at Ji'nan, China. *Science of the Total Environment*, *580*. https://doi.org/10.1016/j.scitotenv.2016.11.145

Xu, W., Wen, Z., Shang, B., Dore, A. J., Tang, A., Xia, X., Zheng, A., Han, M., Zhang, L., Zhao, Y., Zhang, G., Feng, Z., Liu, X., & Zhang, F. (2020). Precipitation chemistry and atmospheric nitrogen deposition at a rural site in Beijing, China. *Atmospheric Environment*, *223*. https://doi.org/10.1016/j.atmosenv.2019.117253

Xu, X., Lu, X., Li, X., Liu, Y., Wang, X., Chen, H., Chen, J., Yang, X., Fu, T. M., Zhao, Q., & Fu, Q. (2020). ROS-generation potential of Humic-like substances (HULIS) in ambient PM2.5 in urban Shanghai: Association with HULIS concentration and light absorbance. *Chemosphere*, *256*. https://doi.org/10.1016/j.chemosphere.2020.127050

Xu, Y., Qin, L., Liu, G., Zheng, M., Li, D., & Yang, L. (2021). Assessment of personal exposure to environmentally persistent free radicals in airborne particulate matter. *Journal of Hazardous Materials*, *409*. https://doi.org/10.1016/j.jhazmat.2020.125014

Xu, Y., Yang, L., Wang, X., Zheng, M., Li, C., Zhang, A., Fu, J., Yang, Y., Qin, L., Liu, X., & Liu, G. (2020). Risk evaluation of environmentally persistent free radicals in airborne particulate matter and influence of atmospheric factors. *Ecotoxicology and Environmental Safety*, *196*. https://doi.org/10.1016/j.ecoenv.2020.110571

Yan, F., Zhu, F., Wang, Q., & Xiong, Y. (2016). Preliminary Study of PM2.5 Formation During Municipal Solid Waste Incineration. *Procedia Environmental Sciences*, *31*. https://doi.org/10.1016/j.proenv.2016.02.054

Yan, Q., Kong, S., Yan, Y., Liu, H., Wang, W., Chen, K., Yin, Y., Zheng, H., Wu, J., Yao, L., Zeng, X., Cheng, Y., Zheng, S., Wu, F., Niu, Z., Zhang, Y., Zheng, M., Zhao, D., Liu, D., & Qi, S. (2020). Emission and simulation of primary fine and submicron particles and water-soluble ions from domestic coal combustion in China. *Atmospheric Environment*, *224*. https://doi.org/10.1016/j.atmosenv.2020.117308

Yang, F., Liu, C., & Qian, H. (2021). Comparison of indoor and outdoor oxidative potential of PM2.5: pollution levels, temporal patterns, and key constituents. *Environment International*, *155*. https://doi.org/10.1016/j.envint.2021.106684

Yang, K., Li, Q., Yuan, M., Guo, M., Wang, Y., Li, S., Tian, C., Tang, J., Sun, J., Li, J., & Zhang, G. (2019). Temporal variations and potential sources of organophosphate esters in PM2.5 in Xinxiang, North China. *Chemosphere*, *215*. https://doi.org/10.1016/j.chemosphere.2018.10.063

Yang, L., Liu, G., Zheng, M., Jin, R., Zhu, Q., Zhao, Y., Wu, X., & Xu, Y. (2017). Highly Elevated

Levels and Particle-Size Distributions of Environmentally Persistent Free Radicals in Haze-Associated Atmosphere. *Environmental Science and Technology*, *51*(14). https://doi.org/10.1021/acs.est.7b01929

Yang, Yanrong, Qin, J., Qi, T., Zhou, X., Chen, R., Tan, J., Xiao, K., Ji, D., He, K., & Chen, X. (2020). Fluorescence characteristics of particulate water-soluble organic compounds emitted from coal-fired boilers. *Atmospheric Environment*, *223*. https://doi.org/10.1016/j.atmosenv.2020.117297

Yang, Yongjie, Zhou, R., Wu, J., Yu, Y., Ma, Z., Zhang, L., & Di, Y. (2015). Seasonal variations and size distributions of water-soluble ions in atmospheric aerosols in Beijing, 2012. *Journal of Environmental Sciences (China)*, *34*. https://doi.org/10.1016/j.jes.2015.01.025

Yao, L., Li, T., Xu, M., & Xu, Y. (2020). How the landscape features of urban green space impact seasonal land surface temperatures at a city-block-scale: An urban heat island study in Beijing, China. *Urban Forestry and Urban Greening*, *52*. https://doi.org/10.1016/j.ufug.2020.126704

Yao, Q., Liu, Z., Han, S., Cai, Z., Liu, J., Hao, T., Liu, J., Huang, X., & Wang, Y. (2020). Seasonal variation and secondary formation of size-segregated aerosol water-soluble inorganic ions in a coast megacity of North China Plain. *Environmental Science and Pollution Research*, *27*(21). https://doi.org/10.1007/s11356-020-09052-0

Ye, M., Nesterenko, P. N., Lu, Y., Huang, X., Jin, X., & Chen, M. (2021). Determination of trace bromate in drinking water with high chloride matrix by cyclic ion chromatography. *Journal of Chromatographic Science*, *59*(3). https://doi.org/10.1093/chromsci/bmaa095

Zanobetti, A., Austin, E., Coull, B. A., Schwartz, J., & Koutrakis, P. (2014). Health effects of multi-pollutant profiles. *Environment International*, *71*. https://doi.org/10.1016/j.envint.2014.05.023

Zhan, Y., Xie, M., Gao, D., Wang, T., Zhang, M., & An, F. (2021). Characterization and source analysis of water-soluble inorganic ionic species in PM2.5 during a wintertime particle pollution episode in Nanjing, China. *Atmospheric Research*, *262*. https://doi.org/10.1016/j.atmosres.2021.105769

Zhang, H., Wang, S., Hao, J., Wan, L., Jiang, J., Zhang, M., Mestl, H. E. S., Alnes, L. W. H., Aunan, K., & Mellouki, A. W. (2012). Chemical and size characterization of particles emitted from the burning of coal and wood in rural households in Guizhou, China. *Atmospheric Environment*, *51*. https://doi.org/10.1016/j.atmosenv.2012.01.042

Zhang, Jin, Hua, P., & Krebs, P. (2017). Influences of land use and antecedent dry-weather period on pollution level and ecological risk of heavy metals in road-deposited sediment. *Environmental Pollution*, *228*. https://doi.org/10.1016/j.envpol.2017.05.029

Zhang, Jingjing, Tong, L., Huang, Z., Zhang, H., He, M., Dai, X., Zheng, J., & Xiao, H. (2018). Seasonal variation and size distributions of water-soluble inorganic ions and carbonaceous aerosols at a coastal site in Ningbo, China. *Science of the Total Environment*, *639*. https://doi.org/10.1016/j.scitotenv.2018.05.183

Zhang, Mengyuan, Shao, L., Jones, T., Hu, Y., Adams, R., & BéruBé, K. (2021). Hemolysis of PM10 on RBCs in vitro: An indoor air study in a coal-burning lung cancer epidemic area. *Geoscience Frontiers*. https://doi.org/10.1016/j.gsf.2021.101176

Zhang, Ming, & Su, B. (2016). Assessing China's rural household energy sustainable development

using improved grouped principal component method. *Energy*, *113*. https://doi.org/10.1016/j.energy.2016.07.071

Zhang, R., Jing, J., Tao, J., Hsu, S. C., Wang, G., Cao, J., Lee, C. S. L., Zhu, L., Chen, Z., Zhao, Y., & Shen, Z. (2013). Chemical characterization and source apportionment of PM2.5 in Beijing: Seasonal perspective. In *Atmospheric Chemistry and Physics* (Vol. 13, Issue 14). https://doi.org/10.5194/acp-13-7053-2013

Zhang, Renjian, Ho, K. F., Cao, J., Han, Z., Zhang, M., Cheng, Y., & Lee, S. C. (2009). Organic carbon and elemental carbon associated with PM10 in Beijing during spring time. *Journal of Hazardous Materials*, *172*(2–3). https://doi.org/10.1016/j.jhazmat.2009.07.087

Zhang, Xia, Xu, Y., & Su, J. (2020). Temporal and spatial characteristics of particulate matters in metro stations of Shanghai, China. *Building and Environment*, *179*. https://doi.org/10.1016/j.buildenv.2020.106956

Zhang, Xin, Zhang, Z., Xiao, Z., Tang, G., Li, H., Gao, R., Dao, X., Wang, Y., & Wang, W. (2021). Heavy haze pollution during the COVID-19 lockdown in the Beijing-Tianjin-Hebei region, China. *Journal of Environmental Sciences*. https://doi.org/10.1016/j.jes.2021.08.030

Zhao, J., Shi, L., Duan, W., Li, H., Yi, P., Tao, W., Shen, G., Tao, S., Pan, B., & Xing, B. (2021). Emission factors of environmentally persistent free radicals in PM2.5 from rural residential solid fuels combusted in a traditional stove. *Science of the Total Environment*, *773*. https://doi.org/10.1016/j.scitotenv.2021.145151

Zhao, M., Huang, Z., Qiao, T., Zhang, Y., Xiu, G., & Yu, J. (2015). Chemical characterization, the transport pathways and potential sources of PM2.5 in Shanghai: Seasonal variations. *Atmospheric Research*, *158–159*. https://doi.org/10.1016/j.atmosres.2015.02.003

Zhao, M., Qiao, T., Li, Y., Tang, X., Xiu, G., & Yu, J. Z. (2016). Temporal variations and source apportionment of Hulis-C in PM2.5 in urban Shanghai. *Science of the Total Environment*, *571*. https://doi.org/10.1016/j.scitotenv.2016.07.127

Zhao, P. S., Dong, F., He, D., Zhao, X. J., Zhang, X. L., Zhang, W. Z., Yao, Q., & Liu, H. Y. (2013). Characteristics of concentrations and chemical compositions for PM2.5 in the region of Beijing, Tianjin, and Hebei, China. *Atmospheric Chemistry and Physics*, *13*(9). https://doi.org/10.5194/acp-13-4631-2013

Zheng, G., He, K., Duan, F., Cheng, Y., & Ma, Y. (2013). Measurement of humic-like substances in aerosols: A review. In *Environmental Pollution* (Vol. 181). https://doi.org/10.1016/j.envpol.2013.05.055

Zhou, J., Xing, Z., Deng, J., & Du, K. (2016). Characterizing and sourcing ambient PM2.5 over key emission regions in China I: Water-soluble ions and carbonaceous fractions. *Atmospheric Environment*, *135*. https://doi.org/10.1016/j.atmosenv.2016.03.054

Zhu, C., Tian, H., Hao, Y., Gao, J., Hao, J., Wang, Y., Hua, S., Wang, K., & Liu, H. (2018). A high-resolution emission inventory of anthropogenic trace elements in Beijing-Tianjin-Hebei (BTH) region of China. *Atmospheric Environment*, *191*. https://doi.org/10.1016/j.atmosenv.2018.08.035

Zhu, X., Yun, X., Meng, W., Xu, H., Du, W., Shen, G., Cheng, H., Ma, J., & Tao, S. (2019). Stacked Use and Transition Trends of Rural Household Energy in Mainland China. *Environmental*

Science and Technology, *53*(1). https://doi.org/10.1021/acs.est.8b04280